GEOLOGICA ULTRAIECTINA

Mededelingen van de
Faculteit Geowetenschappen
Universiteit Utrecht

No. 263

Investigating Lithologic Characteristics of Marine Magnetic Proxy Parameters

Christine Franke

The research described in this thesis was carried out at:

Department of Geosciences
Marine Geophysics
University of Bremen
Klagenfurter Straße
28359 Bremen
Germany

http://www.geophysik.uni-bremen.de

Department of Earth Sciences
Paleomagnetic Laboratory 'Fort Hoofddijk'
Utrecht University
Budapestlaan 17
3584 CD Utrecht
The Netherlands

http://www.geo.uu.nl/~forth/

ISBN-10: 90-5744-127-6
ISBN-13: 978-90-5744-127-1

Investigating Lithologic Characteristics of Marine Magnetic Proxy Parameters

Lithologische Eigenschappen Bepaald met Mariene Magnetische Proxy Parameters

(met een samenvatting in het Nederlands)

Untersuchung Lithologischer Merkmale von Marinen Magnetischen Proxy Parametern

(mit einer Zusammenfassung in deutscher Sprache)

Proefschrift

ter verkrijging van de graad van doctor aan de Universiteit Utrecht
op gezag van de Rector Magnificus, prof. dr. W.H. Gispen,
ingevolge het besluit van het college voor promoties
in het openbaar te verdedigen op

maandag 16 oktober 2006 des middags te 4.15 uur

door

Christine Franke

geboren op 11 januari 1974 te Bremerhaven, Duitsland

Promotoren: Prof. Dr. C.G. Langereis
Department of Earth Sciences
Paleomagnetic Laboratory 'Fort Hoofddijk'
Utrecht University
The Netherlands

Prof. Dr. T. von Dobeneck
Department of Geosciences
Marine Geophysics
University of Bremen
Germany

Co-promotoren: Dr. M.J. Dekkers
Department of Earth Sciences
Paleomagnetic Laboratory 'Fort Hoofddijk'
Utrecht University
The Netherlands

Dr. M.R. Drury
Department of Earth Sciences
Structural Geology and Tectonics
Utrecht University
The Netherlands

Dit proefschrift werd voornamelijk mogelijk gemaakt door financiële steun van de DFG via de European Graduate College EUROPROX.

Contents

Members of the dissertation committee:

Prof. Dr. P. Rochette
CEREGE
Université de Aix-Marseille III
France

Prof. Dr. B. A. Maher
Department of Geography
Lancaster University
United Kingdom

Prof. Dr. N. Petersen
Fachbereich für Geo- und Umweltwissenschaften
Ludwig-Maximilian-Universität München
Deutschland

Prof. Dr. C.J. Spiers
Department voor Aardwetenschappen
Universiteit Utrecht
Nederland

PD Dr. S. Kasten
Alfred-Wegener-Institut für Polar- und Meeresforschung
Bremerhaven
Deutschland

1. Prologue and Summary

In the framework of global marine research, the Equatorial and South Atlantic Ocean is an ideal 'natural laboratory' to study the past climate of the Earth, because it is influenced by a broad variety of climatically driven processes:

From North to South this ocean embraces vastly different climatic regions from the tropics to the polar zone, crossing the intertropical, subtropical and subantartic frontal systems and their high productivity belts, and exchanging water masses with Northern Atlantic and Southern Ocean. In the West and East, it is bounded by the South American and African continents from where large quantities of terrestrial sediment enter by the Saharan, Sahelian and Patagonian dust belts and major feeders like Amazon, Niger, Congo and Rio de la Plata. The Mid-Atlantic Ridge and its active ocean floor spreading divide the South Atlantic into the main western and eastern basins, which are themselves segmented by submarine rises like the Walvis Ridge and the Rio Grande Rise. The great variety of interrelated wind, current, river and productivity systems, seafloor morphology and water body stratification create a wealth of mutually merging sedimentary environments (e.g. *Ruddiman* 2001).

The Equatorial and South Atlantic sediments are a natural archive of the complex climatic and environmental history of this entire region. Various biological, chemical and physical sediment properties deliver useful information for reconstructing paleoenvironmental conditions such as surface water temperature, primary productivity, or wind strength. Many of these parameters are notoriously difficult to model based on first principles. In such cases so-called 'proxy' information is required. Proxy parameters are measurable, sediment-based descriptors for desired (but unobservable) environmental variables and their spatial and temporal variability. Proxies must have a close, if possible linear relationship to the environmental parameters, by which they are formed, and they must have a good preservation potential. A large number of paleoenvironmental and paleoclimatic proxy parameters have been developed during the last few decades, in particular for the marine realm. Numerous case studies (e.g. *Emiliani* 1955; *Imbrie & Kipp* 1971; *Shackleton & Opdyke* 1973; and South Atlantic case studies e.g. in *Fischer & Wefer* 1999) have been carried out to validate the applicability of proxy parameters and to develop complementary proxies to be able to verify obtained results independently.

The so-called rock-, mineral-, or environmental magnetic parameters, obtained from rock or sediment samples by physical measurements, constitute a specific set of proxies that complement the probably better-known geochemical or biological approaches. They are based on the diversity, concentration and grain-size of iron oxide and sulphide minerals and offer various information on the history of climate, sedimentation, diagenesis and the geomagnetic field. Magnetic proxies are well established as chronostratigraphic markers and cyclostratigraphic tools, but can also help to establish mass budgets and source-to-sink relationships (e.g. *Thompson & Oldfield* 1986; *Lund & Karlin* 1990, *Oldfield* 1991; *King & Channell* 1991; *Verosub & Roberts* 1995; *Dekkers* 1997; *Frederichs et al.* 1999; *Evans & Heller* 2003).

The formation of magnetic proxies is simple in theory, but complex in reality: marine sediments - including their magnetic mineral fractions - are composites of various oceanic and terrestrial sources, the contributions of which are modulated by changing tectonic, climatic, and oceanographic settings. These primary magnetic carriers can be modified by secondary, postdepositional processes driven mainly by the degradation of organic carbon. The spatial distribution of source- and process-specific magnetic mineral species within a

sediment time-slice is therefore a superimposed image of all the above described factors. For example, detrital river input reflects the geology (e.g. Fe/Ti ratio) and weathering conditions of the continental hinterland. Depending on humidity, the mineralogy of detrital iron oxide minerals can alternate between magnetite (Fe_3O_4), goethite (FeOOH) or hematite (Fe_2O_3) dominated states. Magnetic grain-sizes are controlled by source- and transport-related factors; eolian grain-sizes depend directly on wind strength and travel distance. The formation of authigenic fractions such as bacterial magnetofossils or the iron sulphides greigite (Fe_3S_4), pyrrhotite (Fe_7S_8) and pyrite (FeS_2) depend on Eh-pH conditions. The identification and quantitative description of these magnetic components can provide information on changes in mass flux and geochemical milieu related to environmental changes (e.g. *Frederichs et al.* 1999).

Mineral magnetic proxies have certain advantages to others: they usually do not require cumbersome sample preparation other than sample weighing. They are so sensitive that meaningful information can generally be obtained from bulk marine sediments. They usually require very small samples and are non-destructive so that valuable sample material can be used for further analyses. Most importantly, they offer grain-size information (particularly for the finest fractions) that is difficult to obtain with other techniques. Rock- and environmental magnetic parameters are divided into concentration, grain-size and magneto-mineral specific proxy parameters (e.g. *Thompson & Oldfield* 1986; *Butler* 1992; *Dunlop & Özdemir* 1997).

A specificity of magnetic parameters is the regional character of interpretational schemes and the multi-parameter approach used to circumvent non-uniqueness problems created by the physical principles of rock magnetism. Specific issues concerning magnetic proxy meaning have to be considered separately for each sedimentary system: why does magnetic susceptibility (a proxy for magnetic mineral concentration) correlate positively with $\delta^{18}O$ records (a global proxy for ice volume, thus climate) in some oceanic regions and negatively or not at all in others? Are variations in magnetic grain-size driven by weathering conditions, varying provenances or transport mechanisms? Why do sediment (relative) paleointensity records (a proxy for the Earth's magnetic field strength) sometimes correlate highly between different areas, and in other cases show nearly no correlation, even if diagenetic overprinting is not significant? Some of these issues have been resolved, while others are still open and subject of this thesis.

A promising, but experimentally demanding strategy to investigate magnetic proxies is to determine the lithologic characteristics of the magnetic carrier minerals and the surrounding sediment matrix. While for the latter standard methods in sedimentology are sufficient the first part is more complicated. To investigate the petrology of micro- and nanometer sized iron trace minerals, this thesis sets out to develop dedicated magnetic experimental techniques and novel extraction methods. Scanning and transmission electronic microscopy (SEM and TEM) are used to support and constrain magnetic proxy interpretations. Electron backscatter diffraction patterns in SEM serve to discriminate different Fe-Ti oxide phases. By scrutinising the magnetic mineral assemblage under various geochemical and sedimentologic aspects, conclusions can be drawn on the environmental magnetic implications of the magnetic petrology.

Chapter 2 deals with the so-called relative paleointensity (RPI); high-resolution records of the paleointensity of the Earth's magnetic field have been successfully obtained from many marine sediment sequences. These are determined by normalising the natural remanent magnetisation (NRM) intensity by the concentration of the magnetic carriers. The question is dealt with why some of the worldwide obtained RPI records show a

high correlation and others don't. Amongst other parameters the lithology of the sediment matrix appears to have an influence on the character of the RPI signal. In this chapter, such 'matrix effects' are explored by sediment analytical and statistical approaches. RPI data from deep-sea sediments sampled across the frontal systems of the subtropical and subantartic South Atlantic are compared. These sites are regionally fairly close to each other and thus have experienced the same magnetic paleofield history, but their lithologies are diverse. Differences in the RPI values should therefore reflect the influence of the sediment matrix on magnetic particle alignment. Extensive sedimentological investigations were performed to characterise the lithology and grain-size of the sediment matrix. Bi- and multivariate statistics were applied to test the hypothesis of a 'matrix effect'. While several parameters did not yield significant results, clay grain-size and chlorite content correlate weakly and opal, illite and kaolinite content correlate moderately with RPI. The most influential single sedimentological factor appeared to be the kaolinite/illite ratio with a Pearson's coefficient of 0.51 and 99.9% significance. It was found that matrix-related effects might possibly influence RPI signal dynamics to nearly the same extent as geomagnetic field intensity variations. The study also outlines strategies to correct for these lithology effects.

In **Chapter 3**, we test the efficiency of magnetic and heavy-liquid extraction techniques on marine sediments from the Equatorial Atlantic to improve the identification of magnetic minerals by means of low-temperature rock magnetic techniques. Enrichment is necessary because of the very low concentrations of magnetic particles (typically in the ppm range) and to remove the influence of the large paramagnetic contribution to the magnetic signal at low temperatures. The applied magnetic extraction technique is based on cycling suspended sediment nearby the strong magnetic gradient field a 'magnetic finger', to which magnetic particles attach. Heavy liquid separation is generally based on the specific density of the individual mineral components in the sediment. The heavy liquid solution chosen for this study, a sodium polytungstenate solution, is adequate for fine-grained marine sediments with a high clay mineral content due to its hydrophilic character. The density was set to 3 g cm^{-3} to separate the lighter non-magnetic minerals from the denser magnetically enriched fraction.

Subsequently, thermomagnetic data was obtained on both kinds of extracts from the same sample material to demonstrate the benefits and disadvantages of each technique. Low-temperature cycling of zero-field and field-cooled remanent magnetisation was performed together with cycling of room temperature isothermal remanent magnetisation to identify the magneto-mineralogical composition of the samples and to quantify the efficiency of the extractions. Both extraction techniques allowed identifying magnetic mineral phases such as magnetite, titanomagnetite, hemoilmenite, goethite and presumably also superparamagnetic ferrihydrite. Except goethite, which could also be detected in bulk measurements in the high-temperature range, all other magnetic phases were solely identified in the magnetic and heavy liquid concentrates. The heavy liquid method turned out to extract the magnetic fraction in a more efficient manner; weakly magnetic high coercivity minerals and very fine grains were extracted much better than by magnetic extraction.

Chapter 4 highlights the advantage of the electron backscatter diffraction (EBSD) technique in SEM to identify different magnetic iron-titanium oxide minerals. EBSD is particularly helpful in combination with element dispersive Xray spectroscopy (EDS) in samples which contain mineral phases of very similar elemental composition but of different crystallographic structure. On a set of synthetic and natural samples of various origins, the possibility to distinguish

between titanomagnetite [$Fe_{3-x}Ti_xO_4$] and hemolimenite [$Fe_{2-y}Ti_yO_3$] is demonstrated. Up to now, EBSD was mainly used on polished sections that have a smooth surface. In this chapter we show that it can be successfully applied as well to individual particles that are just carbon coated, so-called 'non-embedded' samples.

To further understand implications of magnetic proxy data, the magnetic micro- and nanoparticle inventories of marine sediments from the Equatorial Atlantic were identified by analytic SEM and transmission electron microscopy (TEM) on magnetic extracts, outlined in **Chapter 5**. All present detrital and authigenic magnetic species were classified according to their regional distribution, origin, transport, and preservation. The West-East transect under investigation offers a variety of detrital input pathways, such as fluvial detritus of the Amazon river, submarine weathering of mid-oceanic ridge basalts, and eolian contribution of Sahelian/Saharan dust, all traceable by examination with SEM. In addition authigenic sources of chemical precipitation, biomineralisation of bacterial magnetite, and different stages of presumably superparamagnetic to single domain goethite were identified by TEM. This information was used to establish source-to-sink relations and to constrain environmental magnetic proxy interpretations for this area.

At the western site (Ceará Rise; 3°49.9'N and 41°37.3'W), a 'component mixing system' was observed, where about 80% of the magnetic input consists of relatively coarse-grained magnetite from Amazon detritus. The remaining 20% are composed of basaltic titanomagnetite probably delivered from proximal sources, eolian input from the African continent and authigenic bacterial magnetite. The latter component was solely identified at this site. At the eastern site (Sierra Leone Rise; 4°50.7'N and 21°03.2'W), the input of magnetic components is mainly controlled by the climatic changes of the prevailing trade wind systems, resulting in magnetic 'grain-size sorting system' of the main eolian magnetic component (about 30 to 60%). The central site (Mid-Atlantic Ridge; 4°02.8'N and 33°26.3'W) comprised a magnetic assemblage which is explained by the combined mechanisms of grain-size sorting and component mixing. Climatically driven bottom current systems trigger the grain-size variations of the dominant submarine fragmental titanomagnetites, about 50% of the magnetic assemblage at the Mid-Atlantic Ridge. Additional detrital input of Amazonian material from the West and Saharan/Sahelian dust from the East complete the magnetic inventory, which together with the titanomagnetite component form a three-component magnetic assemblage. Hematite, goethite and possibly ferrihydrite particles coexist in all samples and could have high-coercive or superparamagnetic properties according to their partly ultra-fine grain-sizes. These two magnetic fractions are generally discussed as separate fractions, but could actually be genetically linked.

Chapter 6 investigates the strong influence by reductive diagenesis on the magnetic inventory of marine sediments originating from the Argentine continental slope near the Rio de la Plata estuary. All Fe-rich magnetic minerals were dissolved unless they were preserved as magnetic inclusions in silicate grains. Rock magnetic measurements using a magnetic property measurement system (MPMS) in the low-temperature range (between 300 and 5 K) were combined with SEM to characterise the remaining Ti-rich magnetic minerals. Since the dominant input source consists of volcanic particles from the Paraná Basin containing titanomagnetites and hemoilmenites, magnetic self-reversing during the low-temperature cooling measurements was observed, indicative of the nearly complete absence of Fe-rich magnetic mineral phases.

The identification of target minerals and related proxy parameters is of course not restricted to magnetic materials, but can also be applied to other non-magnetic

paleoceanographic tracers. In marine sediments barite is often used as a proxy parameter for paleoproductivity. However, the application of this proxy is limited by possible diagenetic overprints of the primary signal that can alter the original paleoproductivity information. Therefore it is important to investigate diagenetic processes in marine sediments. **Chapter 7** focuses on the influence of non-steady state diagenesis processes on primary geochemical signals. Sediments recovered from the eastern Cape Basin were used for this study. Geochemical pore water and solid phase analyses combined with numerical modelling as well as scanning electron microscopy were applied to identify and interpret the occurrence of diagenetic barite fronts at and below the sulfate methane transition (SMT). Barite fronts are formed authigenically by the reaction of upward diffusing barium with interstitial sulfate. In sulfate depleted sediments barite is supposed to be unstable. Thus, the occurrence of barite enrichments below the SMT is argued to be associated with a decelerated dissolution of barite, which is (among others) explained by high concentrations of dissolved barium in the pore water. An upward migration of the SMT leads to the establishment of a new active barite front. Occurrence of high amounts of buried organic matter below the SMT leads to an increase in the rate of methanogenesis followed by an upward flux of methane that caused the shift of the SMT. With such detailed geochemical investigations, misinterpretation of paleoenvironmental setting in terms of enhanced paleoproductivity can be avoided.

The work described in this thesis illustrates that magnetic proxy parameters need to be validated, ideally for every case study of an oceanic region. Some issues, such as the dependence of the relative paleointensity signal on matrix lithology, the identification of ubiquitous and regional magnetic carriers in the Equatorial and South Atlantic, and the reasons for magnetic grain-size variations, were solved or at least advanced. The influence of mild and pervasive diagenetic overprint was investigated at microscopic scale. Scrutinising environmental magnetic proxies by rock magnetic and 'non-magnetic' techniques has improved understanding of the underlying processes and evolved the level of interpretability. This subsequently enhances the possibilities of reconstructing the paleoceanigraphic history at a regional level.

References

Butler, R.F., 1992. Paleomagnetism: Magnetic Domains to Geological Terranes, Boston, Backwell Scientific Publications. http://www.geo.arizona.edu/Paleomag/book/

Dekkers, M.J., 1997. Environmental magnetism: an introduction, *Geologie en Mijnbouw*, **76**, 163-182.

Dunlop, D.J. & Özdemir, Ö., 1997. *Rock magnetism, fundamentals and frontiers*, Cambridge University Press, 573 p.

Emiliani, C., 1955. Pleistocene temperatures, *J. Geol*., **63**, 538-578.

Evans, M.E. & Heller, F., 2003. *Environmental Magnetism: Principles and Applications of Enviromagnetics*, Academic Press, Elsevier Science, San Diego, London, Burlington, 299 p.

Fischer, G. & Wefer, G., 1999. *Use of Proxies in Paleoceanography: Examples from the South Atlantic*, Springer-Verlag, Berlin, Heidelberg, New York, 735 p.

Frederichs, T., Bleil, U., Däumler, K., von Dobeneck, T. & Schmidt, A.M., 1999. The magnetic view on the marine paleoenvironment: Parameters, techniques, and potentials of rock magnetic studies as a key to paleoclimate and paleoceanographic changes, in *Use of Proxies in Paleoceanography: Examples from the South Atlantic*, pp. 575-599, eds Fischer, G. & Wefer, G., Springer-Verlag, Heidelberg, Berlin, New York.

King, J.W. & Channell, J.E.T., 1991. Sedimentary magnetism, environmental magnetism, and magnetostratigraphy, *Rev. Geophys*., **29**, 358-370.

Imbrie, J. & Kipp, N.G., 1971. A new micropaleontological method for quantitative paleoclimatology: Application to a Late Pleistocene Caribbean core, in *The Late Cenozoic Glacial Ages*, pp. 71-181, ed. Turekian, K., Yale Univ. Press, New Haven, Conn.

Lund, S.P. & Karlin, R., 1990. Introduction to the special section on physical and biogeochemical processes responsible for the magnetization of sediments, *J. Geophys. Res.*, **90**, 4353-4354.

Oldfield, F., 1991. Environmental Magnetism: a personal perspective, *Quat. Sci. Rev*., **10**, 73-85.

Ruddiman, W.F., 2001. *Earth's Climate: Past and Future*, W.H Freeman and Company, New York, 465 p.

Shackleton, N.J. & Opdyke, N.D.,1973. Oxygen isotope and paleomagnetic stratigraphy of equatorial Pacific core V28-238: Oxygen isotope temperatures and ice volumes on a 10^5 year and 10^6 year scale, *Quat. Res.*, **3**, 39-55.

Soffel, H.C., 1991. *Paläomagnetismus und Archäomagnetismus*, Springer-Verlag, Berlin, Heidelberg, New York, 276 p.

Thompson, R. & Oldfield, F., 1986. *Environmental Magnetism*, Allen and Unwin, London, pp. 1-227.

Verosub, K.L. & Roberts, A.P., 1995. Environmental magnetism: past, present, and future, *J. Geophys. Res*., **100**, 2175-2192

Available online at www.sciencedirect.com
SCIENCE DIRECT®
Physics of the Earth and Planetary Interiors 147 (2004) 285–296
PHYSICS OF THE EARTH AND PLANETARY INTERIORS
www.elsevier.com/locate/pepi

Does lithology influence relative paleointensity records? a statistical analysis on South Atlantic pelagic sediments

Christine Franke[a,b,*], Daniela Hofmann[a], Tilo von Dobeneck[a,b]

[a] *Department of Geosciences, University of Bremen, P.O. Box 330 440, D-28334 Bremen, Germany*
[b] *Paleomagnetic Laboratory 'Fort Hoofddijk', Utrecht University, Budapestlaan 17, 3584 CD Utrecht, The Netherlands*

Received 24 November 2003

Abstract

The relative paleointensity (RPI) method assumes that the intensity of post depositional remanent magnetization (PDRM) depends exclusively on the magnetic field strength and the concentration of the magnetic carriers. Sedimentary remanence is regarded as an equilibrium state between aligning geomagnetic and randomizing interparticle forces. Just how strong these mechanical and electrostatic forces are, depends on many petrophysical factors related to mineralogy, particle size and shape of the matrix constituents. We therefore test the hypothesis that variations in sediment lithology modulate RPI records. For 90 selected Late Quaternary sediment samples from the subtropical and subantarctic South Atlantic Ocean a combined paleomagnetic and sedimentological dataset was established. Misleading alterations of the magnetic mineral fraction were detected by a routine Fe/κ test (Funk, J., von Dobeneck, T., Reitz, A., 2004. Integrated rock magnetic and geochemical quantification of redoxomorphic iron mineral diagenesis in Late Quaternary sediments from the Equatorial Atlantic. In: Wefer, G., Mulitza, S., Ratmeyer, V. (Eds.), The South Atlantic in the Late Quaternary: reconstruction of material budgets and current systems. Springer-Verlag, Berlin/Heidelberg/New York/Tokyo, pp. 239–262). Samples with any indication of suboxic magnetite dissolution were excluded from the dataset. The parameters under study include carbonate, opal and terrigenous content, grain size distribution and clay mineral composition. Their bi- and multivariate correlations with the RPI signal were statistically investigated using standard techniques and criteria. While several of the parameters did not yield significant results, clay grain size and chlorite correlate weakly and opal, illite and kaolinite correlate moderately to the NRM/ARM signal used here as a RPI measure. The most influential single sedimentological factor is the kaolinite/illite ratio with a Pearson's coefficient of 0.51 and 99.9% significance. A three-member regression model suggests that matrix effects can make up over 50% of the observed RPI dynamics.

Keywords: Relative paleointensity; PDRM; Sediment lithology; Statistical analysis; South Atlantic

1. Introduction

High-resolution records of the paleointensity of the Earth's magnetic field have been successfully obtained from marine (Roberts et al., 1997; Valet and

* Corresponding author. Tel.: +49 421 218 8922; fax: +49 421 218 8671.
E-mail address: cfranke@uni-bremen.de (C. Franke).
URL: http://www.geophysik.uni-bremen.de/, http://www.geo.uu.nl/~forth (C. Franke).

0031-9201/$ – see front matter © 2004 Elsevier B.V. All rights reserved.
doi:10.1016/j.pepi.2004.07.004

Meynardier, 1993; Tauxe and Shackleton, 1994) and lacustrine sediment (Creer and Morris, 1996; Nowaczyk et al., 2001) sequences. These so-called 'relative paleointensities' (RPI) are determined by normalizing the natural remanent magnetisation (NRM) by the concentration of the magnetic carriers, quantified by parameters such as anhysteretic remanent magnetization (ARM), isothermal remanent magnetization (IRM) or magnetic susceptibility (κ) (Verosub, 1977; Kent, 1982; Tauxe, 1993).

The most widely accepted relative paleointensity reference for the last 800 kyr is the Sint-800 record (Guyodo and Valet, 1999), a global composite of 33 marine records. The RPI records used for this stack correlate well with each other, but not with paleoclimate, and therefore seem to carry a nearly unbiased paleointensity signal. However, on a global scale, very little sediments show such coherent patterns in RPI. In practice, many RPI records routinely obtained from pelagic sediments deviate partly or fully from Sint-800 for mostly unknown reasons. Regionally confined sets of RPI records with similar lithology typically match considerably well internally, but may correlate poorly to records of different origin and composition (Tauxe and Wu, 1990). In some cases, rock magnetic and diagenetic effects are responsible, but it has also been observed that the lithology of the sediment matrix appears to have an influence on the character of the RPI signal (Creer and Morris, 1996).

Laboratory resedimentation experiments by Lu et al. (1990) and Lu (1992) have shown that clay mineralogy and pore water salinity strongly affect PDRM intensity. Lower RPI values result from higher clay mineral, in particular kaolinite, concentration as well as from higher salinity. The authors explain the influence of mineral-dependent surface charges and interparticle forces on magnetic particle alignment by a so-called 'heterocoagulation model'.

Here, we take an analytical and statistical approach to investigate the importance of such 'matrix effects' under natural conditions. RPI data from various deep-sea sediments that were sampled across the frontal systems of the subtropical and subantarctic South Atlantic are compared. The six sites are regionally so well confined, that they should have experienced the same paleofield history, in particular if a (fairly small) dipole based latitudinal correction is applied. These very continent-far locations on the western slope of the Mid-Atlantic ridge receive mainly eolian magnetic mineral input from Patagonian sources (Schmieder et al., 2000) and therefore carry similar magnetic mineral inventories. A detailed environmental magnetic study of this region by Hofmann and Fabian is in preparation. Characteristic differences between the RPI values should therefore reflect the influence of the sediment matrix on magnetic particle alignment.

Extensive sedimentological data were collected for a total of 90 samples from six Late Quaternary sediment series. The sediment matrix was characterized with respect to lithology and grain size. Using bi- and multi-variate statistics, we challenge the prevailing working (and 'null') hypothesis that the mentioned sediment characteristics have no influence on PDRM intensity. In more mathematical terms, we investigate, whether RPI records can be expressed as a product of paleofield intensity, magnetic carrier concentration and a specific 'lithology factor' introducing the influence of the sediment matrix.

2. Material and methods

The proposed paleomagnetic and sedimentological investigations require undisturbed oxic sediments with differing lithologies, but a common field history, hence a narrow spatial distribution. For the deposits of the selected investigation area, the subtropical and subantarctic South Atlantic, all these conditions are largely fulfilled.

The material originates from the western slope of the Mid-Atlantic Ridge (MAR) between 44–32°S and 25–22°W and was taken by gravity coring during the R/V Meteor Cruise M 46/4 (Collaborative Research Center 261, University of Bremen) in March 2000 (Fig. 1). Six out of 29 recovered sediment cores (Table 1) from water depths of 3500–4300 m were selected on basis of their distinct physical properties (porosity, p-wave velocity, magnetic susceptibility and color reflectance) investigated by shipboard logging techniques (Wefer et al., 2001). According to shipboard core descriptions (Wefer et al., 2001), all sediment series appear to be free from disturbances such as hiati or turbidities. Due to a strong southwards increase in primary productivity, there is a tenfold N–S increase in sedimentation rate (0.43–4.56 cm/kyr) from the olig-

Table 1
Core information

Core	Longitude (S)	Latitude (W)	Water depth (m)	Core length (m)	Sedimentation rate (cm/kyr)
GeoB 6428-1	32°30.60	24°14.91	4015	7.26	0.43
GeoB 6425-2	33°49.51	23°35.24	4352	10.73	1.05
GeoB 6422-1	35°42.45	22°44.01	3972	5.32	1.77
GeoB 6407-1	42°02.70	19°30.00	3384	5.36	1.76
GeoB 6405-6	42°00.00	21°51.19	3862	11.94	4.56
GeoB 6408-4	43°00.00	20°26.46	3817	10.55	3.77

otrophic subtropical to the mesotrophic subantarctic South Atlantic.

The six selected cores fall into three different lithological categories; the two northernmost cores from the oligotrophic subtropics (GeoB 6425-2 and 6428-1) have elevated clay mineral contents. The two cores at the subtropical front (GeoB 6407-1 and 6422-1) mostly contain calcareous nannofossil ooze with some foraminifers due to higher primary productivity. The two southernmost cores (GeoB 6405-6 and 6408-4) are under influence of the subantarctic front and have an additional siliceous component contributed by diatoms. In the following, these three sediment types are called clay bearing, foram bearing, and diatom bearing nannofossil oozes. A total of 90 discrete samples, about 15 per core, were taken from maxima and minima of the marine isotope stages 2–8, always from matching age positions back to 280 ka.

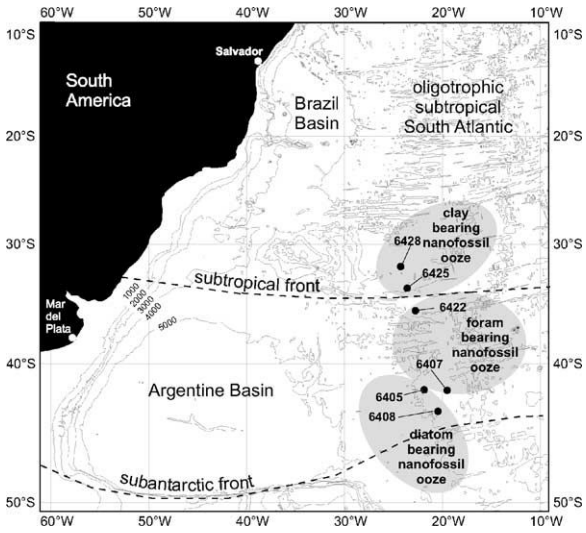

Fig. 1. Core locations in the subtropical and subantarctic South Atlantic on the western slope of the Mid-Atlantic Ridge. Sedimentation conditions are controlled by the frontal systems.

The age models of the two northernmost sediment cores GeoB 6425-2 and GeoB 6428-1 (Schmieder, 2004) were based on a correlation of susceptibility κ to the 'Subtropical South Atlantic Susceptibility Stack' (SUSAS) established by von Dobeneck and Schmieder (1999). The age models of cores GeoB 6405-6, GeoB 6407-1, GeoB 6422-1 and GeoB 6408-4 depend on a multi-parameter correlation (Hofmann et al., in preparation) of κ and element logs, which were tied to the SUSAS and SPECMAP stack (Imbrie et al., 1984). The maxima and minima of the susceptibility signal follow Quaternary climate cycles and correlate very well with available $\delta^{18}O$ isotope records (Donner, unpublished data).

The total carbonate content (Müller, unpublished data) was determined with a Herateus CHN-O-RAPID element analyzer (Weser, 1983). Carbonate content ranges between 6.4 and 86.3 wt.% and is the major matrix component in all investigated sediments. Biogenic opal was analyzed by the automated wet leaching method of Müller and Schneider (1993) and reaches up to 17.7 wt.%. The mineralogy of the clay size fraction of our selected sediment samples was investigated by X-ray powder diffraction. Texture preparations of the centrifuged, decalcified and dried sediment were analyzed in a Phillips PW 1820 diffractometer (Co Kα) and modeled with the Mac Diff 4.2.3 computer program by Petschick (2000). Iron and other element contents were identified with an automated X-ray fluorescence half-core (XRF) scanner (Jansen et al., 1998). Relative element concentrations are given in counts per second with a range from potassium (K) to iron (Fe) (Röhl and Abrams, 2000).

Grain size distribution was analyzed on ultrasonically resuspended wet bulk sediment using a Fritsch Economy Analysette 22 laser particle sizer (Fritsch,

1994). This quick method yields a good representation of the fine sand and silt fraction, but systematically underestimates the submicron clay fraction (Konert and Vandenberghe, 1997). As this effect regards all sediments in a similar way, the obtained grain size fractions should nevertheless be valuable for differentiation.

For a combined paleo- and rock-magnetic analysis (Hofmann and Fabian, in preparation), NRM, IRM and ARM AF demagnetization curves were measured on cubic samples at 5 cm spacing using an automated 2G Enterprises 755 R pass-through cryogenic magnetometer. The issue of the best available NRM standardizer for paleointensity estimates has been widely discussed (Tauxe, 1993; Tauxe, 1995; Levi and Banerjee, 1976). IRM represents the concentration of all magnetic grain sizes. Susceptibility additionally includes the dia- and para-magnetic fraction. ARM, like PDRM, is linked to the fine magnetic particle spectrum as indicated by their similar coercivity spectra. In this study the RPI signals of the sediment samples were calculated by normalizing NRM with ARM after a 20 mT AF treatment to remove viscous overprints. The alternative normalizers yield similar signals except for core GeoB 6407-1.

Early diagenetic magnetite dissolution proceeds even under mildly suboxic conditions (Karlin and Levi, 1983; Canfield, 1989; Leslie et al., 1990). It affects especially the finest magnetite particles, the main carriers of PDRM, and leaves an imprint on the RPI records. Diagenetically affected core sections had to be excluded for the purpose of this study. They were identified by the magnetite dissolution index Fe/κ proposed by Funk et al. (2004). Stable plateau values of Fe/κ throughout the sediment column are indicative of unaltered magnetic mineralogy, while locally elevated values indicate partial magnetite losses due to reductive dissolution. The rationale of this index is the diminution of the magnetic susceptibility κ relative to iron content caused by the diagenetic transformation of (ferric) ferrimagnetic into (ferrous) paramagnetic iron.

The Fe/κ plateau values of the investigated sediment cores increase by a factor of three from North to South (Franke, 2002). Two different Fe/κ levels were therefore applied to a northern (GeoB 6422-1, 6425-1, 6428-1) and southern (GeoB 6405-6, 6407-1, 6408-4) core group (Fig. 2), below which samples are considered as unaffected by reductive diagenesis. According to this criterion, more than one third of originally 90 samples gave subtle to pronounced indication of iron mineral reduction and was excluded from further consideration.

3. Results

The sedimentological characterization of the samples was based on analyses of the major components, grain size distribution and clay mineralogy. Ranges, means and N–S trends of all investigated parameters have been compiled as box-and-whisker plots in Fig. 3a–c. Foraminiferal and coccolithophorid carbonate make up 45–85% of the four northernmost cores and is complemented by terrigenous silicates (Fig. 3a). Temporal downcore variations are related to glacial-interglacial changes of the calcite lysocline (Schmieder et al., 2000). Near the subantarctic front, carbonate contents decrease 20–55% and give way to a much higher terrigenous content and additional siliceous components, mainly diatoms and radiolarians. In terms of the standard grain size classification 55–85% of the sediment falls into the

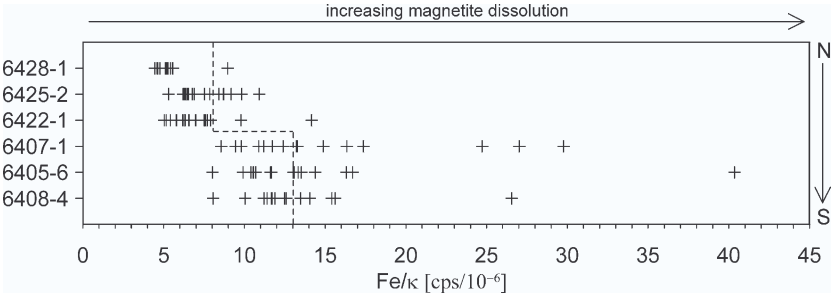

Fig. 2. Sample rejection based upon partial magnetic mineral dissolution according to regional Fe/κ criterion (Funk et al., 2004). Due to increasing Fe/κ plateau values from N to S, two separate threshold values for the northern and southern core group were chosen (dashed line).

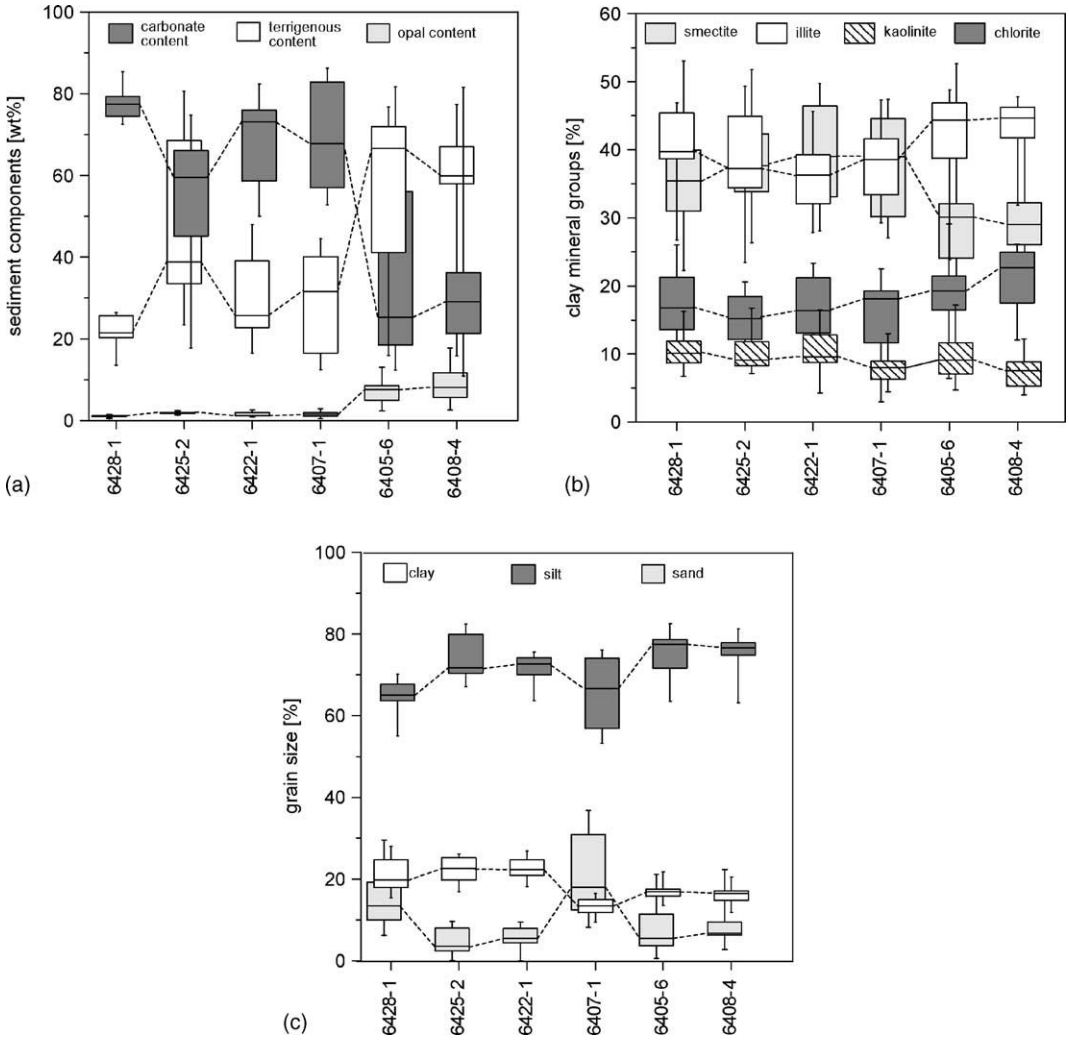

Fig. 3. Univariate box-and-whisker plots of (a) major components, (b) grain size distribution (c) clay mineralogy for the discrete samples from N to S. The boxes represent the median value and interquartile range; the whiskers mark the total data range.

silt fraction (2–63 μm), while sand (>63 μm) and clay (<2 μm) are subordinate (Fig. 3b). The terrigenous clay size fraction is higher in the subtropical than in the subantarctic zone. Winnowing effects explain the relatively high sand content at the shallowest site GeoB 6407-1 exposed to bottom-current erosion. The clay mineral analysis yields relative contents of the clay mineral groups smectite, illite, chlorite and kaolinite. Smectite and illite are the dominant phases and provide some 60–80% of the total content (Fig. 3c). In the subtropical zone, both minerals are nearly equally represented. The subantarctic region is characterized by a lower smectite and higher illite and chlorite content. Chlorite and kaolinite are subordinate, where chlorite is approximately twice as common as kaolinite. A source area and transport pathway of the clay minerals was investigated by Petschick et al. (1996).

All lithological parameters described above contribute to the sedimentary fabric and could be influential on PDRM acquisition. The dependency of the RPI values on each individual parameter was assessed on basis of a linear bivariate correlation analysis (Swan

and Sandilands, 1995). We take the standard approach in geostatistics and use Pearson's product-moment correlation coefficient

$$r_{xy} = \frac{\sum_{i=1}^{n}(x_i - \bar{x})(y_i - \bar{y})}{(N-1)s_x s_y}$$

where x_i are the independent sedimentological parameters, y_i the RPI values, $\bar{x}$ and $\bar{y}$ their respective means, s_x and s_y their standard deviations and N the size of the statistical sample. The significance of any determined r_{xy} value, which may range from 0 (uncorrelated) to ± 1 (strictly linearly dependent), is controlled by the extent of the relationship r and by the number of cases N contributing to the analysis. The test statistics for significance of the correlation coefficient,

$$t = r\sqrt{\frac{N-2}{1-r^2}}$$

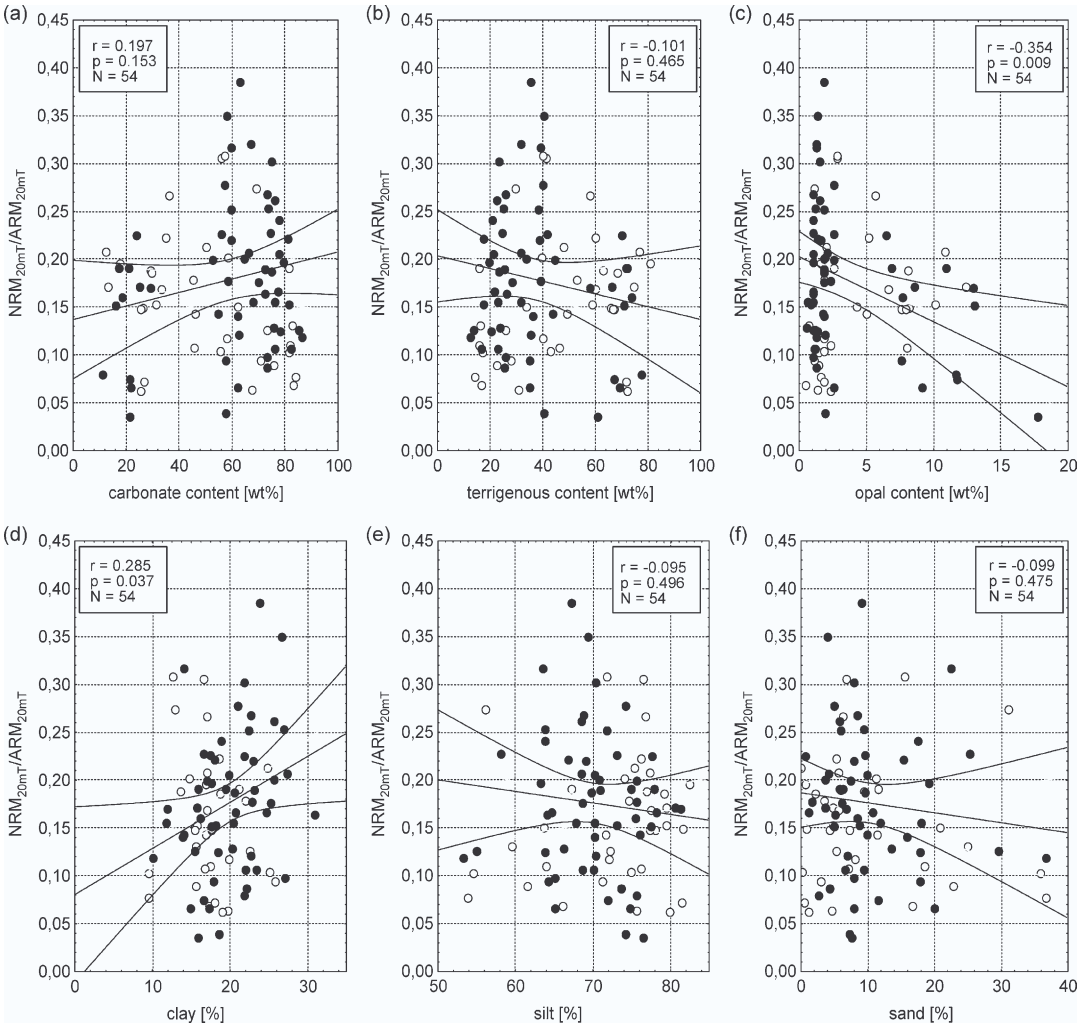

Fig. 4. Biplots of NRM_{20mT}/ARM_{20mT} vs. (a) carbonate, (b) terrigenous, (c) opal, (d) clay, (e) silt and (f) sand content. Pearson's correlation coefficients r, the probabilities p for randomness and samples sizes N are given in the figure headers. The gentle slopes of the regression lines and their broad 95% confidence range are indicative of large bivariate scatter. The correlations were exclusively based on the unaltered samples (solid symbols). The samples rejected by the diagenesis criterion (empty symbols) do not principally fall out of the major trend, but lower correlations and their significance.

leads to a probability measure, p, quantifying the likeliness, that an observed correlation is purely incidental. p-values of 0.05, 0.01 and 0.001 correspond to 95, 99 and 99.9% significance, respectively. Instead of using these fixed significance levels, we state the individual probability for randomness in each analysis.

The probability p is also reflected by the slope and width of the 95% confidence range of the linear regression line shown in the biplots. In contrast to the correlation coefficient r, the linear bivariate regression calculation assumes a causal relationship between lithology and relative paleointensity and therefore minimizes the (squared vertical) deviation of the dependent variable, i.e. NRM_{20mT}/ARM_{20mT}. Because of the impact of geomagnetic field variations and the complexity of lithological controls, each individual sedimentological factor can only exert a partial and rather feeble influence on RPI. We therefore do not present each bivariate regression equation separately and give a multiple regression analysis below.

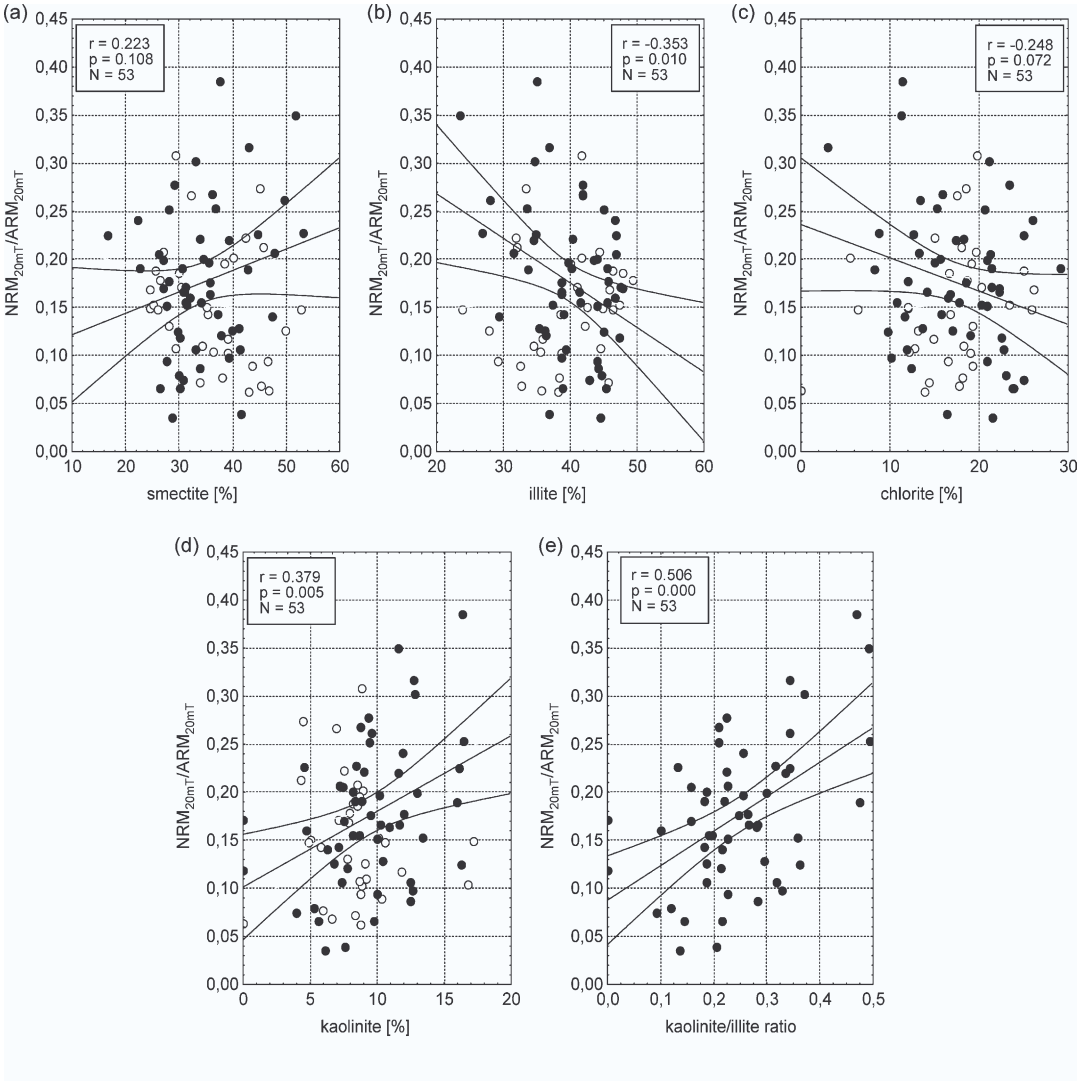

Fig. 5. Biplots of NRM_{20mT}/ARM_{20mT} vs. (a) smectite, (b) illite, (c) chlorite, (d) kaolinite content and (e) kaolinite/illite ratio. For legends and symbols see Fig. 4.

For the following correlation analyses, the data of all 54 samples from the six cores were pooled to encompass a sufficiently large lithological variability and case number. The correlations of major components and grain size fractions with the NRM_{20mT}/ARM_{20mT} ratio are depicted in Fig. 4a–f. In four of the cases, carbonate and terrigenous content, silt and sand content, the correlations are practically insignificant. There is a low ($r = 0.29$) positive correlation with clay at significance level of about 97% and a moderate ($r = -0.35$) negative correlation with opal content at 99% significance level. Fig. 5a–e show the correlations of relative clay mineral contents with the NRM_{20mT}/ARM_{20mT} ratio. In the case of smectite, the correlation is insignificant, while chlorite shows a low ($r = -0.25$) negative correlation at about 93% significance. Illite ($r = -0.35$) and kaolinite ($r = 0.38$) contents are moderately correlated with NRM_{20mT}/ARM_{20mT}, at significance levels of ~99%. Because of the inverse relationships with kaolinite and illite, their ratio is more strongly

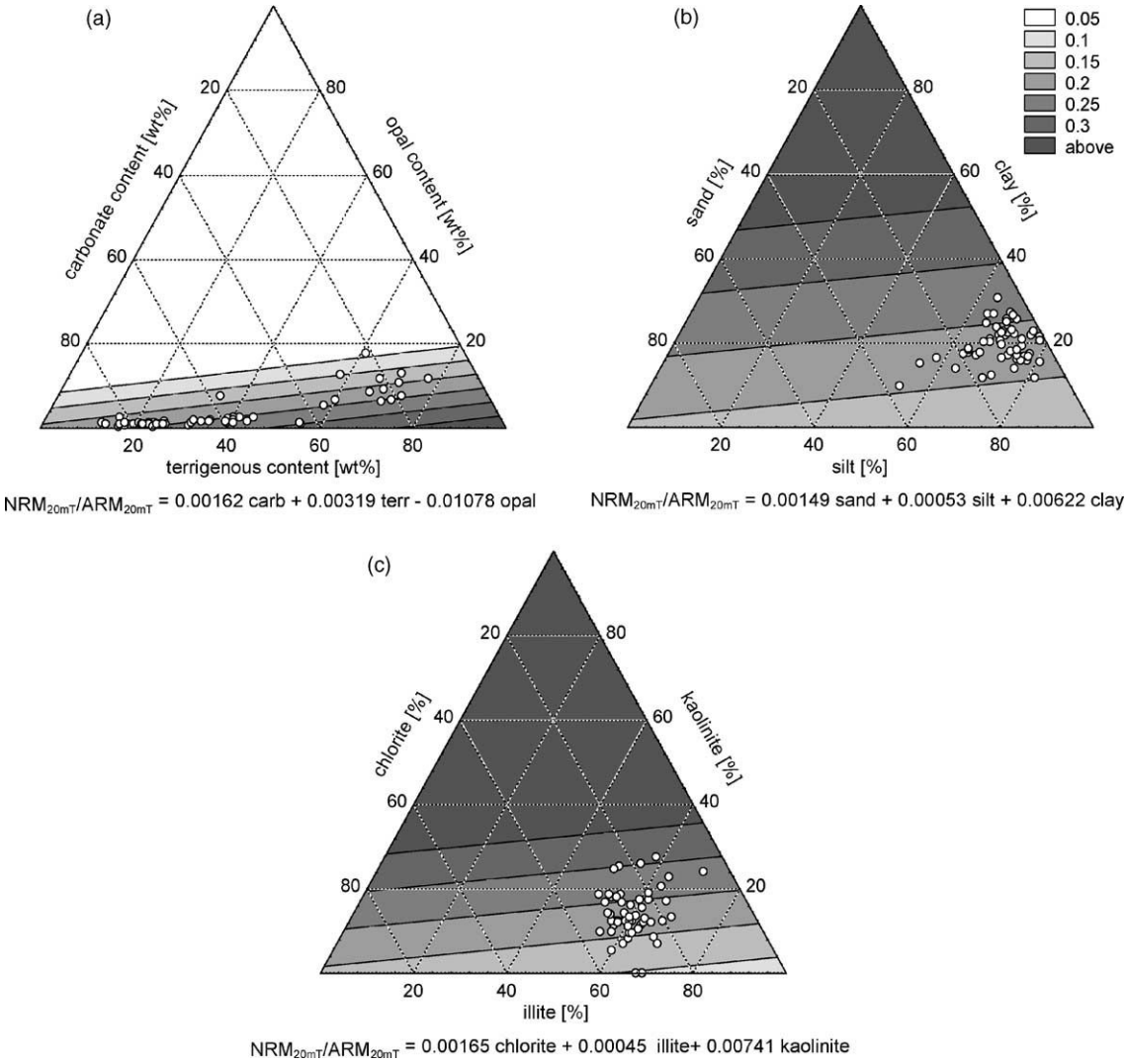

Fig. 6. Trend surface plots of NRM_{20mT}/ARM_{20mT} in the ternary systems of (a) carbonate, opal and terrigenous content, (b) sand, silt and clay percentage, (c) chlorite, illite and kaolinite.

(r = 0.51) and significantly (>99.9%) correlated with NRM_{20mT}/ARM_{20mT} than either single value.

The three lithological parameter groups can be formulated as ternary systems, in which the observed NRM_{20mT}/ARM_{20mT} values are approximated by a regression plane (Fig. 6a–c). In the case of clay mineralogy, the apparently insignificant mineral smectite was excluded and the analysis was performed in the kaolinite–illite–chlorite system. The compilation of all three ternary plots clearly hints at the decisive factors. Rather small opal content seems to lower the RPI signal, while clay content and particularly the relative kaolinite content raise its value. The defining equations of the three ternary planes are given in the diagrams.

The bivariate analyses indicate that several of the investigated sedimentological parameters show a moderate but significant correlation with the RPI signal. Since all of these parameters are to some degree mutually independent, a multiple linear regression model of all factors can be established which quantifies the combined lithological controls on the RPI signal. The difficulty of distinguishing between meaningful and redundant parameters is a well-known problem (Swan and Sandilands, 1995). Here we use the 'backward elimination' method by which an initially overdetermined regression model is successively depleted from regressors with insignificant partial correlation. Multicollinearity is avoided by omitting at least one within a group of complementary parameters from the analysis. With reasonable settings, a multiple regression solution based on the three lithological parameters opal content, terrigenous content and kaolinite/illite ratio was found. The significance level of each individual regressor is equal to or better than 95% (Table 2). The goodness-of-fit R number is 0.59 and the probability of non-randomness exceeds 99.99%. The impact of lithology on RPI is demonstrated in Fig. 7. As the NRM_{20mT}/ARM_{20mT} record doubtlessly holds considerable paleofield information, any better predictability solely based on lithological parameters would seem unrealistic.

Table 2
Summary of multiple linear regression analysis using the 'backward elimination' method

Regressors	Regression coefficient	SD of coefficient	P-Level
Intercept	0.068	±0.034	0.052
opal content	−0.009	±0.004	0.015
Terrigenous content	0.002	±0.001	0.031
Koalinite/illite ratio	0.316	±0.091	0.001

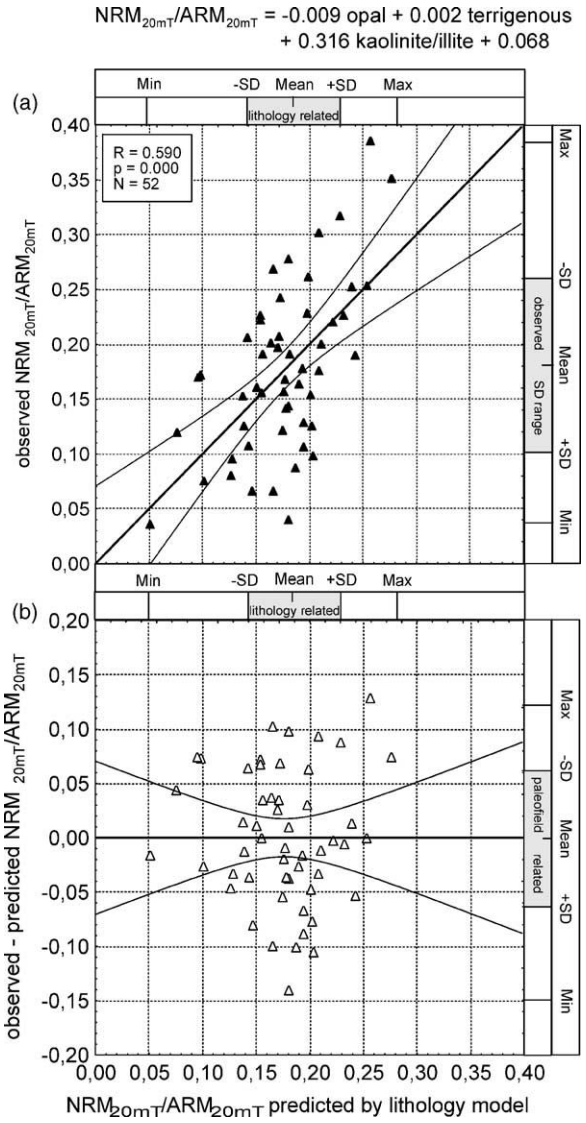

Fig. 7. Biplots of (a) observed and (b) residual NRM_{20mT}/ARM_{20mT} vs. predicted NRM_{20mT}/ARM_{20mT} resulting from the multiple regression model given above. Goodness of fit R, significance level p and sample size N is given in the figure header. All axes are equally scaled. Standard deviation (SD) ranges of the three shown parameters outline the average contributions of lithology and paleofield to the observed RPI signal.

As an alternative approach to quantifying lithology effects, the raw RPI (NRM_{20mT}/ARM_{20mT}) data of the

selected sediment samples were divided by isochronal values of the Sint-800 paleointensity stack. When plotted against the various lithology parameters, these 'paleofield corrected' RPI data show approximately the same scatter as the raw RPI data. It was initially expected, that correlations should be markedly improved by this data treatment. Probable causes for the failure are discrepancies in chronology and temporal resolution of the investigated and reference records.

4. Discussion and conclusions

Current quality requirements of RPI records as established by Levi and Banerjee (1976), King et al. (1983) and Tauxe (1993) are essentially based on rock- and paleomagnetic criteria, namely (1) magnetite as predominant magnetic carrier, homogeneity of (2) concentration and (3) magnetic grain size, as well as absence of (4) inclination errors and (5) magnetic mineral diagenesis. Ongoing analyses indicate, that criteria (1)–(4) are locally fulfilled by groups, the three northern and the three southern cores. Only for the pooled core set, the variations in magnetite concentration exceed the Tauxe (1993) 'one order of magnitude' rule. However, combining diverse lithologies was one basic requirement for the feasibility of this study. Criterion (5) was also respected: By rigorous application of the Fe/κ parameter all samples affected by (mild) chemical overprint, altogether one third of the initial collection, were excluded from the statistical analysis. What else influences paleointensity estimates?

Our statistical results suggest, that the sedimentary magnetic recording process of post-depositional particle alignment is not exclusively an expression of geomagnetic field history, but also controlled by the strong and complex interactions of magnetic carriers with their non-magnetic matrix. These mechanical and electrostatic forces are responsible for the relatively low intensity of PDRM in comparison with laboratory remanences such as ARM. The NRM_{20mT}/ARM_{20mT} ratio of the investigated samples averages at around 0.18 (Table 3). The RPI signal dynamics due to varying matrix effects are considerable; if we compare the standard deviation (SD) range of the RPI data set (±0.077) to the SD range of our lithology-dependent regression model (±0.045) and to the paleofield-dependent residue (±0.063), we find that matrix-related effects could possibly influence signal dynamics to nearly the same extend as geomagnetic field intensity variations.

Of course, the lithological spectrum encountered in our pooled sample set exceeds that of most published RPI records by far and therefore marks an upper limit of matrix-related signal biasing. Nevertheless, any paleointensity record claiming 'high fidelity' should additionally fulfil a criterion (6) related to lithological homogeneity, in particular with respect to clay mineralogy and major components. If RPI data are collected for stratigraphic purposes, we should expect sedimentologically induced patterns at lithological boundaries, e.g. at climate transitions. Our regression equations point towards the possibility of establishing multi-parameter based correction formulas to discard lithological overprint. A broader and more representative database such as the Sint-800 core set would be desirable for this objective. The numerous high-quality records should open the possibility to apply similar regression analyses on singular time slices sharpening the definition of the approach.

It is worth considering, why some of the sedimentological parameters seem to have greater influence on sedimentary magnetic recording than others. Our regionally restricted results indicate an inhibition of magnetic particle alignment by the presence of siliceous microfossils. This could be simply due to the porous structure of diatoms, radiolaria and sponge spicules which favor a high initial porosity followed by extreme postdepositional compaction. In addition, Florindo et al. (2003) suggested that magnetite alteration to authigenic smectite under oxic to suboxic conditions is favored by high silica concentrations. The growth of authigenic smectite directly on diatom

Table 3
Statistical properties of parameters in (Fig. 7)

Variable	Mean	Minimum	Maximum	SD
Observed NRM_{20mT}/ARM_{20mT}	0.183	0.035	0.385	0.077
Predicted NRM_{20mT}/ARM_{20mT}	0.183	0.049	0.281	0.045
Residual NRM_{20mT}/ARM_{20mT}	0.000	−0.153	0.126	0.063

Table 4
Comparative properties of common silicate clay minerals (adapted from Brady and Weil, 1996)

Property	Smectite	Illite	Kaolinite
Size (μm)	0.01–1.0	0.02–2.0	0.5–5.0
Shape	Flakes	Irregular Flakes	Hexagonal Crystals
External surface area (m^2/g)	70–120	70–100	10–30
Internal surface area (m^2/g)	550–650	–	–
Plasticity	High	Medium	Low
Cohesiveness	High	Medium	Low
Swelling capacity	High	Low to None	Low
Unit-layer charge	0.5–0.9	1.0–1.5	0
Interlayer spacing (nm)	1.0–2.0	1.0	0.7
Bonding	Van der Waal's	Potassium Ions	Hydrogen
Net negative charge ($cmol_c/kg$)	80–120	15–40	2–5

frustules has been described by Badaut and Risacher (1983). Clay mineralogy also appears to have a tight grip on magnetic particle orientation. We find that kaolinite has a positive and illite a negative effect on magnetic alignment, while smectite is more indifferent. This is certainly related to the unit-layer charges of the three clay minerals, eventually also to their crystalline versus flaky structure and low versus medium to high plasticity (Table 4). Specific investigations are needed to consolidate these hypotheses. We can nevertheless conclude, that lithology of the sedimentary matrix is an influential and widely underrated factor in the signal formation of relative paleointensity records.

Acknowledgements

Bernhard Diekmann from the Alfred-Wegener-Institute for Marine and Polar Research Bremerhaven/Potsdam was a great support for the clay mineral analyses. Rainer Petschick from Johann–Wolfgang Goethe University, Frankfurt a.M., kindly provided the 'MacDiff 4.2.3.' computer program for XRD analysis. Automated signal correlation for age modelling was performed with the unpublished computer programs 'Automated Signal Correlation, v.07' by Karl Fabian and 'Correlation Tool, v.6' by Thomas Frederichs from University of Bremen, Marine Geophysics group, to whom we owe also thanks for their support of the measurements. Monika Breitzke from GEOMAR Kiel supervised the laser granulometry. We thank Peter Müller for providing unpublished carbonate content data and Barbara Donner for unpublished $\delta^{18}O$ isotopy records. Financial support was provided by the Deutsche Forschungsgemeinschaft (DFG), SPP 1097, in the framework of proposals Do 705/1-1 and Fa 408/1-2. Tilo von Dobeneck acknowledges a visiting research fellowship by the Netherlands Research Centre for Integrated Solid Earth Science (ISES). Christine Franke presently enjoys a stipend of the EUROPROX graduate college (Universities of Bremen, Utrecht and Amsterdam). All data presented in this study are available at the PANGEA database (www.pangea.de, search string: FrankeC).

References

Badaut, D., Risacher, F., 1983. Authigenic smectite on diatom frustules in Bolivian saline lakes. Geochim. Cosmochim. Acta 47, 363–375.

Brady, N.C., Weil, R.R., 1996. The nature and properties of soils, 11th edition. Prentice-Hall International, Inc., New Jersey.

Canfield, D.E., 1989. Reactive iron in marine sediments. Geochim. Cosmochim. Acta 53, 619–632.

Creer, K.M., Morris, A., 1996. Proxy-climate and geomagnetic palaeointensity records extending back to ca. 75,000 BP derived from sediments cored from Largo Grande Di Monticchio. Southern Italy, Quaternary Sci. Rev. 15, 167–188.

Florindo, F., Roberts, A.P., Palmer, M.R., 2003. Magnetite dissolution in siliceous sediments. Geochem. Geophys. Geosyst., 4: 1053. doi: 10.1029/2003GC000516.

Franke, C., 2002. Der Einfluß der Lithologie auf die Rekonstruktion der "relativen Paläointensität" des Erdmagnetfeldes an spätquartären Sedimenten des subtropischen und subantarktischen Südatlantiks, Diploma thesis, Department of Geosciences, University of Bremen, 117 pp.

Fritsch GmbH Laborgerätebau, 1994. Benutzer-Handbuch Laser Particle Sizer Analysette 22, Idar Oberstein, pp. 30–37.

Funk, J., von Dobeneck, T., Reitz, A., 2004. Integrated rock magnetic and geochemical quantification of redoxomorphic iron mineral diagenesis in Late Quaternary sediments from the

Equatorial Atlantic. In: Wefer, G., Mulitza, S., Ratmeyer, V. (Eds.), The South Atlantic in the Late Quaternary: reconstruction of material budgets and current systems. Springer-Verlag, Berlin/Heidelberg/New York/Tokyo, pp. 239–262.

Guyodo, Y., Valet, J.P., 1999. Global changes in intensity of the earth's magnetic field in the past 800 kyr. Nature 399, 249–252.

Hofmann, D., Fabian, K., Schmieder, F., Donner, B., in preparation. A South Atlantic stratigraphic network.

Hofmann, D. and Fabian, K., in preparation. Investigation of the relative paleointensity parameters with respect to lithological influences.

Imbrie, J., Hays, J.D., Martinson, D.G., McIntyre, A., Mix, A.C., Morley, J.J., Pisias, N.G., Prell, W.L., Shackleton, N.J., 1984. The orbital theory of Pleistocene climate: support from a revised chronology of the marine $\delta^{18}O$ record. In: Berger, A.L., Imbrie, J., Hays, G., Kukla, G., Saltzman, B. (Eds.), Milankovitch and climate., 1. D. Reidel Publ. Comp, pp. 269–305.

Jansen, J.H.F., Van der Gaast, S.J., Koster, A.J., 1998. CORTEX, a shipboard XRF-scanner for element analyses in split sediment cores. Marine Geology 151, 143–153.

Karlin, R., Levi, S., 1983. Diagenesis of magnetic minerals in recent haemipelagic sediments. Nature 303, 327–330.

Kent, D.V., 1982. Apparent correlation of paleomagnetic intensity and climate records in deep-sea sediments. Nature 299, 538–539.

King, J.W., Banerjee, S.K., Marvin, J., 1983. A new rock-magnetic approach to selecting sediments for geomagnetic paleointensity studies: application to paleointensity for the last 4000 years. J. Geophys. Res. 88, 5911–5921.

Konert, M., Vandenberghe, J., 1997. Comparisation of laser grain size analysis with pipette and sieve analysis: a solution for the underestimation of the clay fraction. Sedimentology 44, 523–535.

Leslie, B.W., Hammond, D.E., Berelson, W.M., Lund, S.P., 1990. Diagenesis in anoxic sediments from the California Continental Borderland and its influence on iron, sulfur and magnetite behavior. J. Geophys. Res. 95B, 4453–4470.

Levi, S., Banerjee, S.K., 1976. On the possibility of obtaining relative paleointensities from lake sediments. Earth Planet. Sci. Lett. 29, 219–226.

Lu, R., Banerjee, S.K., Marvin, J., 1990. Effects of clay mineralogy and the electrical conductivity of water on the acquisition of depositional remanent magnetization in sediments. J. Geophys. Res. 95B, 4531–4538.

Lu, R., 1992. A study of the effect of matrix properties on postdepositional remanent magnetization (pDRM) acquisition in sediments, Ph.D. thesis, University of Minnesota, 171 pp.

Müller, P.J., Schneider, R., 1993. An automated leaching method for the determination of opal in sediments and particulate matter. Deep-sea Res. 1, 425–444.

Nowaczyk, N.R., Harwart, S., Melles, M., 2001. Impact of early diagenesis and bulk particle grain size distribution on estimates of relative geomagnetic palaeointensity variations in sediments from Lama Lake, northern Central Siberia. Geophys. J. Int. 145, 300–306.

Petschick, R., Kuhn, G., Gingele, F., 1996. Clay mineral distribution in surface sediments of the South Atlantic: sources, transport and relation to oceanography. Marine Geology 130, 203–229.

Petschick, R., 2000. MacDiff 4.2.3, unpublished computer program, Johann-Wolfgang Goethe Universität, Frankfurt a. M.

Roberts, A.P., Lehman, B., Weeks, R.J., Verosub, K.L., Laj, C., 1997. Relative paleointensity of the geomagnetic field over the last 200,000 years from ODP Sites 883 and 884, North Pacific Ocean. Earth Planet Sci. Let. 152, 11–23.

Röhl, U., Abrams, L.J., 2000. High-resolution down hole and nondestructive core measurements from sites 999 and 1001 in the Caribbean Sea: application to the late Paleocene thermal maximum. In: Leckie, R.M., Sigurdsson, H., Acton, G.D., Draper, G. (Eds.), ODP Sci. Res., 165, pp. 191–203.

Swan, A.R.H., Sandilands, M., 1995. Introduction to geological data analysis. Blackwell Science Ltd., Oxford, London.

Schmieder, F., von Dobeneck, T., Bleil, U., 2000. The Mid-Pleistocene climate transition as documented in the deep South Atlantic Ocean: initiation, interim state and terminal event. Earth Planet. Sci. Lett. 179, 539–549.

Schmieder, F., 2004. Magnetic signals in Plio-Pleistocene sediments of the South Atlantic: chronostratigraphic usability and paleoceanographic implications. In: Wefer, G., Mulitza, S., Ratmeyer, V. (Eds.), The South Atlantic in the Late Quaternary: reconstruction of material budgets and current systems. Springer-Verlag, Berlin/Heidelberg/New York/Tokyo, pp. 263–279.

Tauxe, L., Wu, G., 1990. Normalized remanence in sediments of the western equatorial Pacific: relative paleointensity of the geomagnetic field? J. Geophys. Res. 95B, 12.337-12.350.

Tauxe, L., 1993. Sedimentary records of relative paleointensity of the geomagnetic field: theory and practice. Rev. Geophys. 31, 319–354.

Tauxe, L., Shackleton, N.J., 1994. Relative paleointensity records from the Ontong-Java Plateau. Geophys. J. Int. 117, 769–782.

Tauxe, L., 1995. Relative paleointensity in sediments: a pseudo-Thellier approach Geophys. Res. Let. 22, 2885–2888.

Valet, J.-P., Meynardier, L., 1993. Geomagnetic field intensity and reversals during the past four million years. Nautre 366, 234–238.

Verosub, K.L., 1977. Depositional and postdepositional processes in the magnetization of sediments. Geophys. Space Phys. 15, 129–143.

von Dobeneck, T., Schmieder, F., 1999. Using rock magnetic proxy records for orbital tuning and extended time series analysis into the super- and sub-Milankovitch bands. In: Wefer, G., Fischer, G. (Eds.), Use of proxies in paleooceanography: examples from the South Atlantic. Springer-Verlag, Berlin/Heidelberg, pp. 601–633.

Wefer, G. and cruise participants, 2001. Report and preliminary results of Meteor-cruise M 46/4, Mar del Plata (Argentina)—Salvador (Brazil), 10.2-13.3.2000, Reports of the Department of Geosciences, University of Bremen, 173, 136 pp.

Weser, G., 1983. CHN-Elementanalyse im Halbmikromaßstab, Heraeus-Sonderdruck, Leybold-Heraeus GmbH, pp. 14–43.

Chapter 3

The efficiency of heavy liquid separation to concentrate magnetic particles from pelagic sediments demonstrated by low-temperature magnetic measurements

Summary
Low-temperature rock magnetic measurements have distinct diagnostic value. However, in most bulk marine sediments the concentration of ferrimagnetic and antiferromagnetic minerals is that low, that even sensitive instrumentation often senses just the paramagnetic contribution of the silicate matrix in the residual field of the magnetometer. Analysis of magnetic extracts is usually performed to bypass the issue of low magnetic concentrations. Generally, magnetic extracts turn out to be not representative for the entire magnetic inventory. They are biased to components with high spontaneous magnetisation, such as magnetite and titanomagnetite being low coercive magnetic minerals. We show that high coercivity components are rather under-represented in such magnetic extracts. Additionally, classical magnetic extraction generally yields extracts that are coarser grained than the starting bulk sediment material. Therefore, making fully quantified inferences may not be warranted in any case. Here, we test as well heavy liquid separation, using hydrophilic sodium polytungsten solution $Na_6[H_2W_{12}O_{40}]$ and demonstrate its efficiency. Low-temperature cycling of zero-field-cooled, field-cooled and saturation isothermal remanent magnetisation acquired at room temperature were performed on dry bulk sediments, magnetic extracts, and heavy liquid separates, documenting the merit of the latter by showing much more detailed and representative low-temperature remanence measurements.

Key words: heavy liquid separation, magnetic extracts, marine sediments, Equatorial Atlantic Ocean, low-temperature magnetic measurements, Magnetic Properties Measurement System (MPMS)

This chapter is an article in review: Franke, C., Frederichs, T. and Dekkers, M.J., 2006. The efficiency of heavy liquid separation to concentrate magnetic particles from pelagic sediments demonstrated by low-temperature magnetic measurements, *Geophys. J. Int.*

1. Introduction

Rock magnetic investigations of marine sediments aim at unraveling depositional history and diagenetic changes of the magnetic mineralogy for geomagnetic and paleoceanographic investigations. As a rule in marine sediments, variably mixed magnetic components occur in very low concentration, down to the ppm range. In addition, the grain-size range of such particles spans from a few micrometers down to the nm range.

Clay minerals are the most abundant non-ferrimagnetic components in the sediment, besides carbonates and silica. They are important for a proper interpretation of low-temperature magnetic measurements of the bulk sediment, due to their paramagnetic behaviour. Because of their abundance, clay minerals may induce distinct magnetic moments even in the small residual fields prevailing in the magnetometer. Moreover, at temperatures below 25 K, paramagnetic (clay) minerals start to show collective magnetic behaviour that may give rise to appreciable magnetic moments (e.g. Coey 1988). Therefore, they attenuate diagnostic temperature transitions of proportional subordinate ferrimagnetic and antiferromagnetic mineral phases that occur only in trace amounts in almost all sediments. The expression of e.g. the

Verwey-, 34 K-, and Morin-transition of magnetite, pyrrhotite, and hematite respectively, is often below the limit of detection of the instrument used.

The standard tool to enhance the signal of the ferrimagnetic fraction is magnetic extraction. Various existing magnetic extraction techniques are known (e.g. Petersen *et al*. 1986; von Dobeneck 1987; Dekkers 1988; Hounslow & Maher 1999), whether or not combined by leaching the bulk sample material in acetic acid (pH 4 to 5) to dissolve the carbonates. These can be easily applied to wet bulk sediments of marine origin and yield a reasonable amount of extracted magnetic material, that subsequently can be analysed with a sensitive Magnetic Properties Measurement System (MPMS). Nevertheless, the amount of magnetic extract is generally still too low to allow a decent mass determination with a (semi-) microbalance ($d = 10^{-5}$ g). This expounds the problems of true quantification, required for budget calculations (Hounslow & Maher 1999). Comparisons of magnetic extract measurements with the bulk sediment signal, in order to determine how efficient and representative the extract is, are therefore not feasible in practice. Magnetic extraction methods favour strongly ferrimagnetic mineral phases (mainly (titano-) magnetite, maghemite, pyrrhotite and greigite), being magnetically softer, over magnetically harder antiferromagnetic phases (such as hematite or goethite) (Dekkers 1988; Hounslow & Maher 1999).

In this study, we applied heavy liquid separation on marine dry bulk sediments as an alternative extraction method, to achieve a more complete 'magnetic' extract, consisting of the heavy mineral fraction (density > 3.0 g cm^{-3}). This fraction includes all magnetic mineral phases being present in the sample. Hydrophilic sodium polytungsten solution $Na_6[H_2W_{12}O_{40}]$ was applied, providing the possibility to separate the magnetic fraction in very fine grained material, particular in clay-rich samples.

Watery lithium heteropolytungsten solution with a density of 2.85 g cm^{-3} was successfully used by Lagroix *et al.* (2004), to separate the magnetic Fe-Ti oxide fraction from the volcanic glass fraction in their tephra samples. This specific Old Crow tephra occurred intercalated in loess deposits at Halfway House in central Alaska. By classical gravity separation of 24 hours, they managed to divide the magnetic fraction into the lighter volcanic glass (< 2.85 g cm^{-3}) and the rest of the (coarser grained) magnetic Fe-Ti oxides (> 5.0 g cm^{-3}). They claim that their light mineral fraction additionally contains still most of the SP particles and the heavy fraction represents between 1.5 and 0.5% of the bulk sample mass. Certainly the density separation enhanced the possibilities to identify the Fe-Ti oxides in the heavy fraction, but concentrations in the light fraction were still high enough to magnetically identify its composition.The overwhelming amount of para-magnetic components in marine sediments complicates the separation and therefore hydrophilic sodium polytungsten solution with an even higher density of 3.0 g cm^{-3} was used in our study in combination with ultrasonic dispersion and centrifuging techniques to 'purify' the magnetic fraction from the siliceous components in the bulk sediment. The advantage of this non-magnetic separation method is that all magnetic components are extracted regardless their magnetic strength.

2. Sample Material

The chosen sample suite includes six specimens from clay-rich pelagic sediments of three gravity cores of a West-East profile throughout the Equatorial Atlantic. The gravity cores were recovered from the Ceará Rise (GeoB 1523-1, 3°50.8'N and 41°36.6'W), the equatorial Mid-Atlantic Ridge (GeoB 4313-2, 4°02.8'N and 33°26.3'W) and the Sierra Leone Rise (GeoB 2910-1, 4°50.7'N and 21°03.2'W) during *RV Meteor* cruises M16/2, M29/3 and M38/1. This zone in the Equatorial Atlantic is presently oligotrophic (Funk *et al.* 2004b). The pelagic sediments of all

three gravity cores are characterised as clay- and foram-bearing nannofossil oozes. Magnetic particles in these sediments originate from several distinct sources: continental eolian dust (Sahara), fluvial discharge (Amazon River) and submarine weathered ocean ridge basalts (Mid-Atlantic Ridge). Authigenic sources for magnetic particle input constitute the biogenic formation of bacterial magnetosomes and the (inorganic) recrystallisation of previous iron sulphides (Franke *et al*. unpublished data). For further details on gravity core localities and general settings see also Schulz *et al*. (1991), Henrich *et al.* (1994), Fischer *et al*. (1998), Funk *et al*. (2004a, 2004b), and Reitz *et al*. (2004).

Two discrete samples were processed from each of the three gravity cores, one corresponding to Marine Isotope Stage (MIS) 4, i.e. a glacial stage and the other to MIS 5.5 (Eemian), an interglacial stage. These samples, chosen for the detailed studies, represent typical conditions throughout the gravity cores. In glacial conditions a coarser magnetic inventory was found, while interglacial conditions are characterised by a finer magnetic grain-size distributions (Funk *et al*. 2004a, 2004b; Franke *et al.* unpublished data) so the magnetic upgrading procedures can be assessed for contrasting climatic conditions.

3. Upgrading Procedures

3.1 Magnetic Extraction

Magnetic extraction was performed on 10 cm³ of the wet bulk sediment samples using the method of Petersen *et al.* (1986). After the extraction run (8 to 12 hours per sample) the extracted particles were stored in small glass vials filled with ethanol. For MPMS measurements the fluid (containing the magnetic extract) was applied into a gelatine capsule and the sample was dried at room temperature, by evaporating the ethanol in air. Mass determination with a semi-microbalance was not possible, since the typical amount of a magnetic extract is beyond the metering precision of a semi-microbalance ($d = 10^{-5}$ g). Other, more detailed MPMS sample preparation aspects and instrumental settings are outlined in Frederichs *et al.* (2003).

3.2 Heavy Liquid Separation

Heavy liquid separation was performed on typically 0.8 g of the freeze-dried bulk sediments (referred to as dry bulk sediment). After weighing, the samples were dispersed (manually shaking until no obvious clustering was visible anymore, followed by 10 min of ultrasonic bath agitation) in 20 ml hydrophilic sodium polytungsten solution $Na_6[H_2W_{12}O_{40}]$, with a density of exactly 3.0 g cm^{-3}. The 50 ml plastic centrifuge vessels, containing the sediment-fluid suspension, were hereafter directly centrifuged for 5 min using a *Heraeus Minifuge T* at 4000 rps. During this process, the sediment-fluid suspension separates into a floating light sediment fraction (LF) with a density < 3.0 g cm^{-3}, the so-called fluid mirror (= 3.0 g cm^{-3}) in the middle of the centrifuge tube and a heavy sediment fraction (HF) at the bottom, with a density > 3.0 g cm^{-3}. If necessary, the 5 min centrifuge run was repeated without re-homogenising the sample. The LF on top of the fluid mirror and the fluid mirror itself were separated from the HF using a special 10 ml precision pipette, and both fractions were suction filtered separately after separation. For filtration, cellulose acetate filters with 0.1 µm pores were applied. The sediment fractions were dried in air over night (at room temperature), removed from the filters, weighed and filled in gelatine capsules for MPMS measurements.

3.3 Extraction Efficiency

In Table 1, the mass of the starting material of the dry bulk sediment is given, in comparison with the mass of the light and heavy fractions resulting from the density separation. The separated heavy mineral fraction for this sample set ranged from 0.022 to 0.004 g (Table 1), typically 1.4 % of the starting bulk material. The discrepancy between starting material and the sum of light and heavy fractions therefore

Table 1. Heavy liquid separation: masses of starting material, resulting light and heavy fraction, and the material on the filters. The upgrading factor was calculated as the ratio of the mass specific remanences (σ_r) of heavy fraction (HF) to dry bulk sediment (BS) at 300 K, $\frac{\sigma_{r,\,HF\;300K}}{\sigma_{r,\,BS\;300K}}$

Sample	Mass of Starting Material [g]	Total Mass Light Fraction [g]	Rel. Mass Light Fraction [%]	Total Mass Heavy Fraction [g]	Rel. Mass Heavy Fraction [%]	Material on Filters [g]	Material on Filters [%]	Upgrading Factor [ ]
GeoB 1523-1, 160 cm	0.85575	0.81556	95.3	0.0050	0.6	0.0351	4.1	16.3
GeoB 1523-1, 311 cm	0.65728	0.59048	89.8	0.0092	1.4	0.0576	8.6	18.6
GeoB 4313-2, 130 cm	0.68251	0.61931	90.7	0.0096	1.4	0.0536	7.9	14.4
GeoB 4313-2, 245 cm	0.79249	0.70829	89.4	0.0221	2.8	0.0621	7.9	5.2
GeoB 2910-1, 60 cm	0.97421	0.90021	92.4	0.0041	0.4	0.0699	7.2	12.9
GeoB 2910-1, 141 cm	0.87386	0.78406	89.7	0.0145	1.7	0.0753	8.6	11.6

Table 2. Masses of the dry bulk sediment, light and heavy fraction samples used for thermomagnetic measurements. These masses were applied for mass specific normalisation. Measurements on dry bulk sediment were performed on identical material with sample masses given in the second column. Note that only a minor portion of the light fraction was used for MPMS measurements.

Sample	Mass Dry Bulk Sediment [g]	Mass Light Fraction [g]	Mass Heavy Fraction [g]
GeoB 1523-1, 160 cm	0.03153	0.0625	0.0050
GeoB 1523-1, 311 cm	0.02663	0.0609	0.0092
GeoB 4313-2, 130 cm	0.02806	0.0510	0.0096
GeoB 4313-2, 245 cm	0.03429	0.0288	0.0221
GeoB 2910-1, 60 cm	0.02902	0.0491	0.0041
GeoB 2910-1, 141 cm	0.03446	0.0475	0.0145

stems from remaining material on the filters and can be further estimated by weighing the empty and remaining filters after removal of the separated density fractions. The amount of remaining material on the filters is comparable for both density fractions, typically 7.4 %. The amount of magnetic extracts for the same sample set using a much higher amount of starting material (10 cm^3 of wet bulk sediment) results in much lower yields, which cannot be meaningfully mass quantified. In the remainder, all thermomagnetic curves are mass normalised (Table 2), of course except the magnetic extract measurements. An additional advantage of the sodium polytungsten solution as used heavy liquid solution is its non-toxicity. Moreover, the separates can be flushed or washed extensively during filtration, due to the hydrophile character of the sodium polytungsten solution. The upgrading factor of the heavy liquid separation can be quantified in average to 13.2 (Table 1) and allows for control measurements for extraction results of the light and heavy fraction.

4. Thermomagnetic Observations

4.1 Thermomagnetic Measurements

Low-temperature zero-field-cooled (ZFC) and field-cooled (FC) measurements were performed within several weeks after drying the various extracts and separates, using a *Quantum Design XL7 Magnetic Properties Measurement System* (MPMS; noise level ~10^{-11} Am^2), applying a 5 T field at 5 K (for dry bulk sediments at 10 K). Low-temperature warming curves (5 to 300 K) were determined for dry bulk sediments, magnetic extracts, and heavy liquid separates monitored in 2 K increments. For the ZFC measurements, the field was applied at 5 K and was switched off before warming back to 300 K, whereas for the FC measurements, the field was applied at 300 K throughout cooling and switched off before warming back to 300 K. Where appropriate, the first derivatives of both ZFC and FC remanences vs. temperature were cal-culated (in 6 K average value = 3 data points) in order to better visualise changes of the magnetic state during sample warming.

To test for the presence of high coercivity components in the samples (see section 4.3), specific heating experiments were performed. First of all, the pristine dry bulk sediment samples were heated in air up to 340°C. Afterwards, the same procedure for low-temperature ZFC and FC runs in the MPMS was performed on the accordingly heated bulk sediments. The pristine and the heated bulk sediment samples were weighted before performing the low-temperature measurements, therefore the curves are normalised on their respective sample mass and thus the results are directly comparable.

For identification of the high coercivity component(s), additional high-temperature field cycling in the MPMS was performed on the dry bulk sediment samples, applying a 7 T field at room temperature. The samples were run in-field (FH) from 300 to 400 K (heating) and back to room temperature (cooling), followed by a zero-field (ZFH) cycle within the same temperature range. All high-temperature measurements using the MPMS were monitored in 2 K increments. FH curves are corrected for the paramagnetic contribution, which was derived from the linear slope of high-field dependence measured at room temperature between 4 and 7 T.

The room temperature saturation isothermal remanent magnetisation (RT-SIRM) measurements for dry bulk sediments, magnetic extracts, and heavy liquid separates were performed using a 5 T field (applied at RT), before the respective sample was cycled from 300 to 5 K (cooling) and back to room temperature (warming) in zero-field, monitored in 2 K increments.

4.2 Low-Temperature ZFC and FC Results of Dry Bulk Sediments

For all dry bulk sediment measurements, the low-temperature warming curves of ZFC and FC remanence did not show any pronounced remanence transitions (Fig. 1). A rapid decrease in ZFC and FC rema-

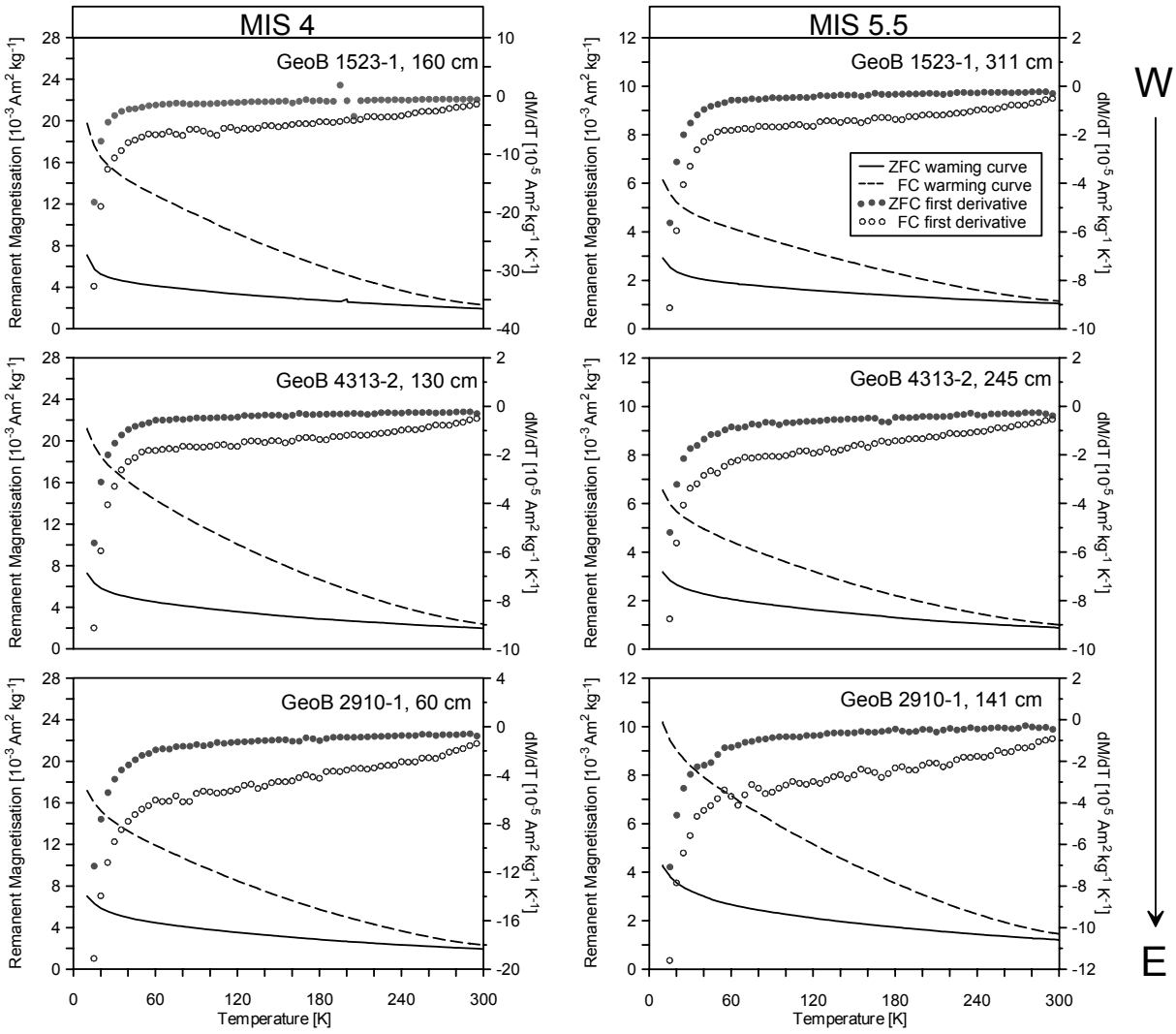

Figure 1. Low-temperature ZFC and FC remanent magnetisation curves for six dry bulk sediment samples (solid line = ZFC, dashed line = FC) along the Equatorial Atlantic West-East profile (from top to bottom). The magnetically coarser samples from glacial stage MIS 4 are shown on the left (scaled to a maximum value of $28 \cdot 10^{-3}$ Am^2 kg^{-1}) and the magnetically finer samples from interglacial stage MIS 5.5 are shown on the right (scaled to a maximum value of $12 \cdot 10^{-3}$ Am^2 kg^{-1}). ZFC and FC warming curves (applied field 5 T) were monitored from 10 to 300 K in 2 K increments. The first derivatives are given in gray, filled symbols for ZFC and open symbols for FC. No evident low-temperature features, such as the Verwey transition, were identified in the dry bulk sediment measurements. All curves are normalised to their respective sample mass.

nence between 10 and 40 K (corresponding to the local minimum in the respective first derivative curves) was observed for all six samples. A similar phenomenon was observed in partially oxidised magnetite of synthetic origin (Özdemir *et al*. 1993) or natural origin (Smirnov & Tarduno 2000). In the latter co-existing ultrafine-grained super-paramagnetic (SP) material is argued to occur. Passier & Dekkers (2002) discussed the possibilities of magnetic interaction, surface effects in very fine grains, or the presence of surface layers around coarser magnetic particles as other possible explanations for such behaviour.

The most important observation of all dry bulk sediment experiments was the remarkable discrepancy between corresponding ZFC and FC curves. These divergences are maximum at 10 K and disappear towards room temperature (Smirnov & Tarduno 2000). Divergences are generally bigger in samples from MIS 4 than in samples from MIS 5.5.

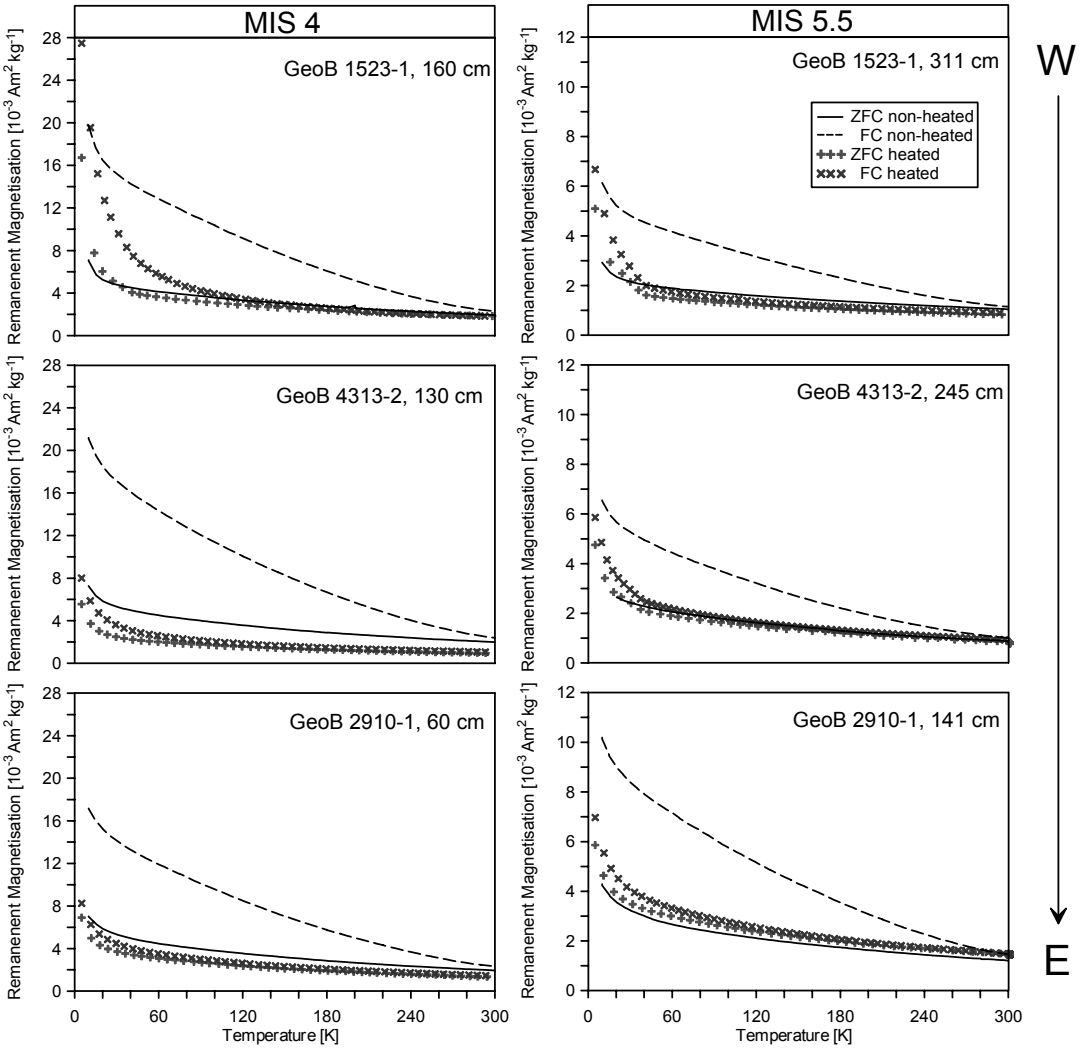

Figure 2. Low-temperature ZFC and FC remanent magnetisation curves for six pristine dry bulk sediment samples (solid line = ZFC, dashed line = FC) from West to East (from top to bottom) in comparison with the cross symbols, which refer to dry bulk sediments previously heated to 340°C; cross symbols for ZFC warming, x-symbols for FC warming curves. Samples from MIS 4 are shown on the left, samples from MIS 5.5 are shown on the right (for scaling compare Fig. 1). ZFC and FC warming curves of the pristine dry bulk sediment were measured from 10 to 300 K in 2 K increments, using an applied field of 5 T, whereas low-temperature ZFC and FC warming curves of the previously heated samples were monitored from 5 to 300 K in 2 K increments, also using an applied field of 5 T. Note the very slight offset at ~300 K of the heated bulk sediment set of curves, which is assumed to originate from an instrumental offset, it can be disregarded here. All curves are normalised to their respective sample mass.

4.3 Heating Experiments of Dry Bulk Sediments

The hypothesis of the presence of goethite was tested by the heating experiments outlined in section 4.1. The discrepancy between ZFC and FC curves decreased dramatically after heating and for most of the samples, ZFC and FC curves merge at temperatures higher than 40 to 60 K (compare Fig. 1 with Fig. 2). The decrease of the low-temperature ZFC-FC divergence after heating to 340°C is interpreted as the absence of the initial goethite signal contribution. This high coercivity component was chemically altered by heating above its Néel point of ~120°C (Dekkers 1989; France & Oldfield 2000; Özdemir & Dunlop 2000).

Further high-temperature remanence measurements (see 4.1) were performed to confirm this interpretation and check for the possibility of thin maghemitised surface layers of magnetite grains (van Velzen & Zijderveld 1992, 1995; van

Velzen & Dekkers 1999a, 1999b). All ZFH and FH curves and their first derivatives(Figs 3 and 4) show a drop at 390 K (~117°C), indicating the Néel point of goethite (e.g. Hedley 1971, Dekkers 1989). During cooling of the ZFH curves (Fig. 3) no new remanence was picked up by the samples, due to the lack of an inducing field. The minor remanence acquisition in some the ZFH cooling curves is caused by a small remaining field (in the order of±150 µT), which is still

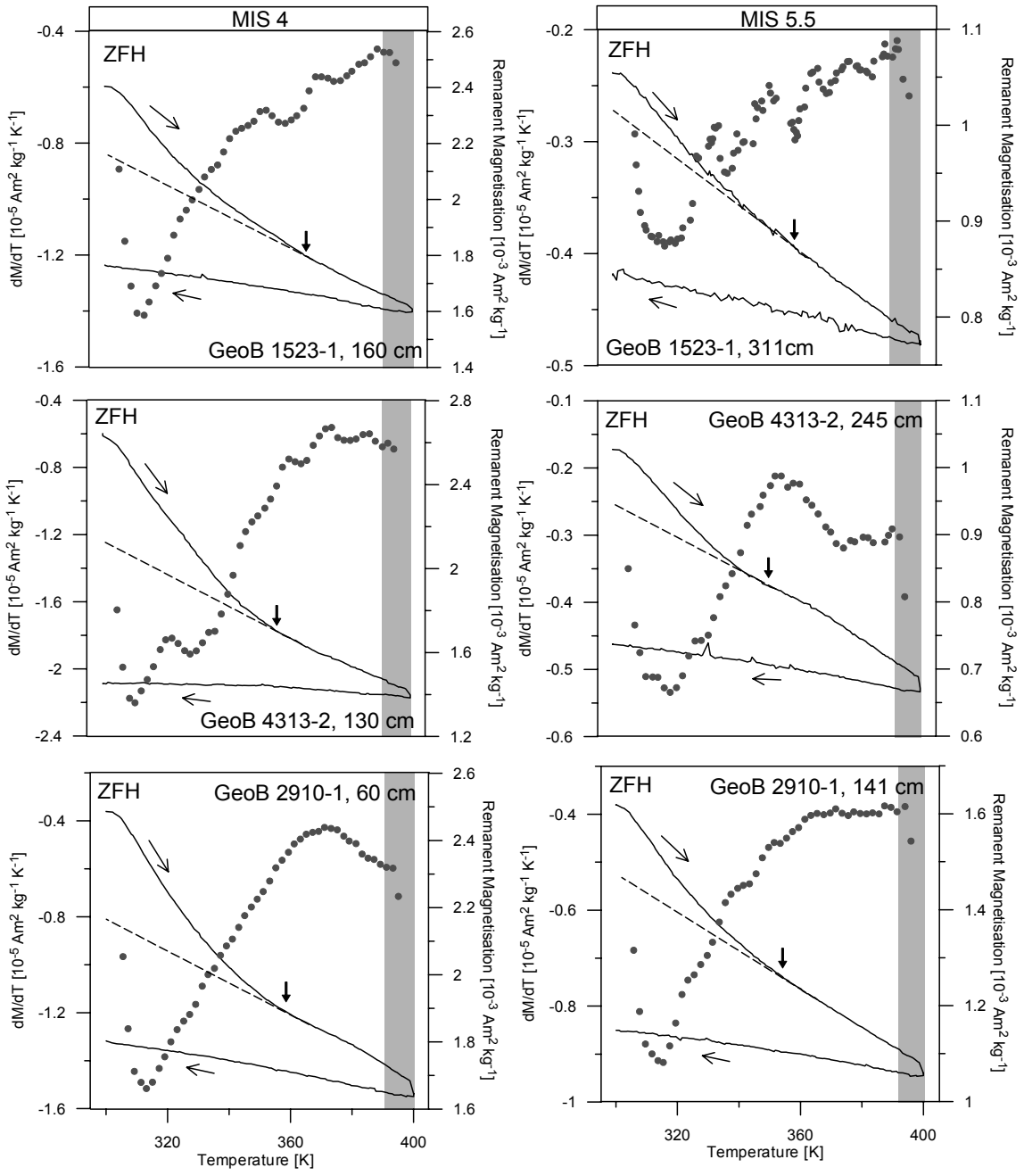

Figure 3. High-temperature cycling of the dry bulk sediments in zero-field (ZFH, solid line), using an applied field of 7 T at 300 K, which was switched off during heating and cooling between 300 and 400 K. The ZFH heating curves show a continuous decrease in remanence, gray shaded areas mark the sharp drop in remanence at 390 to 395 K. Filled symbols show the first derivative of the ZFH heating curve. Note that the ZFH cycle was performed after the FH cycle (compare Fig. 4). All curves are normalised to their respective sample mass. The magnetic non-goethite amount are established by linear extrapolation (dashed lines, after Dekkers 1989) of the decay curve from temperatures above the bending point (vertical bold arrows).

present after the quenching of the MPMS magnet (Kosterov *et al*. 2006).The FH heating curves show a characteristic Hopkinson peak at 360 K (~87°C, e.g. Heller 1978) for most of the samples (Fig. 4).

This feature is even more noticeable in the first derivative curves of the FH of

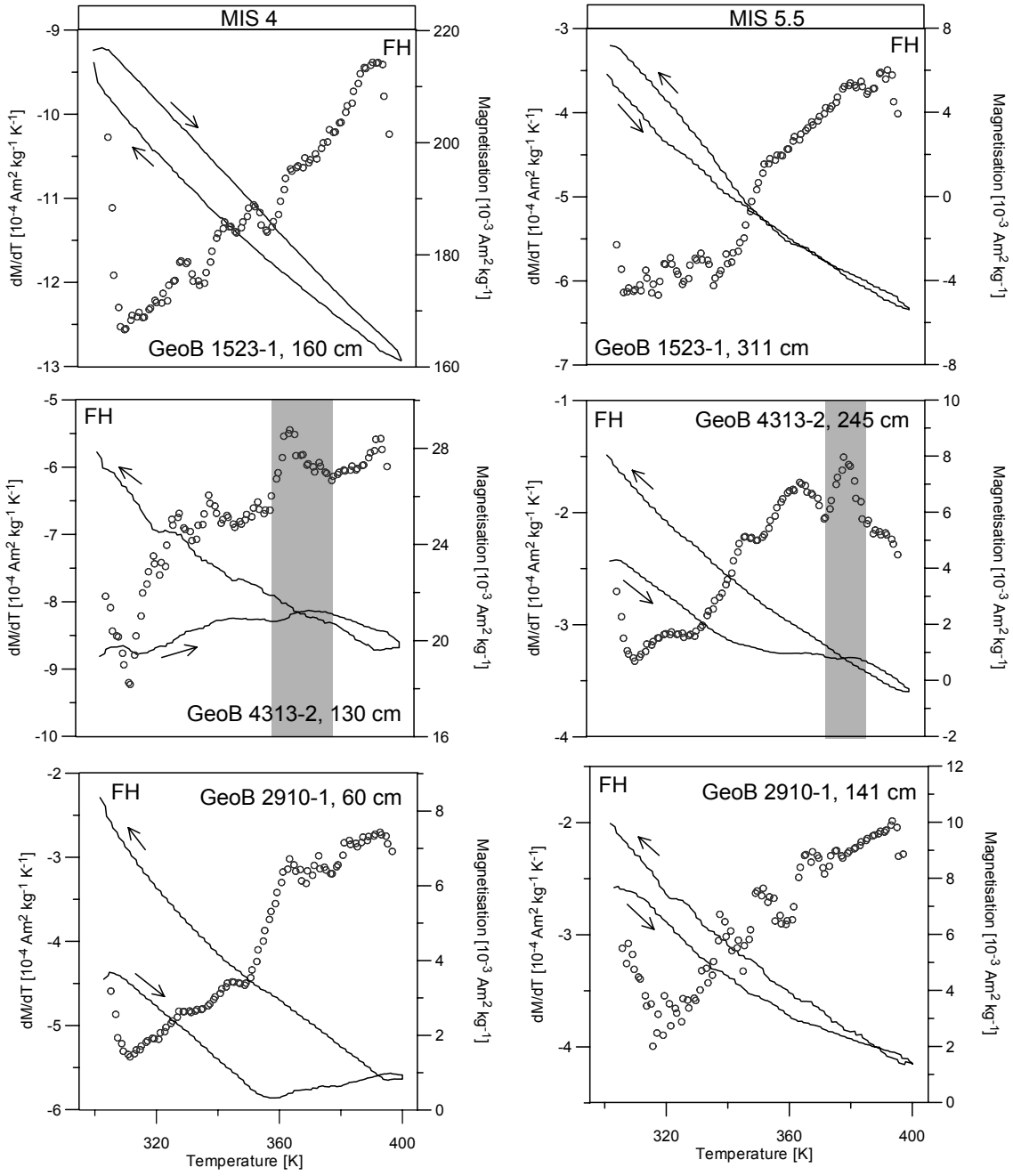

Figure 4. High-temperature cycling of induced magnetisation of pristine dry bulk sediments between 300 and 400 K in an applied field of 7 T (FH, solid line). The FH magnetisation curves were monitored in 2 K increments and are corrected for the paramagnetic contribution. According to the Curie-Weiss-Law, the paramagnetic contribution is assumed to be dependent on 1/T absolute and was achieved by field-depending measurements of the dry bulk sediments between 4 and 7 T at room temperature (not shown here). Open symbols show the first derivatives of the FH heating curves. Grey shaded areas indicate the position of the Hopkinson peak in FH heating curves between 370 and 380 K in samples from core GeoB 4313-2. Cooling curves of the FH measurements show an increase in induced magnetisation at room temperature, except for sample GeoB 1523-1, 160 cm. All curves are normalised to their respective sample mass.

samples from GeoB 4313-2. Note that the intensities of the samples increase after heating above the Néel point of goethite. This is a further indication that indeed most likely a reasonably moderate goethite component is present in these samples.

4.4 Low-Temperature ZFC and FC Results of Magnetic Extracts

The ZFC and FC warming curves for the magnetic extracts (Fig. 5) show four orders of magnitude lower remanence intensities (10^{-7} Am²) than the dry bulk sediments (10^{-4} Am²). Due to the low amount of magnetic extract, the curves (both ZFC and FC) have been simply normalised to the ZFC value at 5 K. The ZFC and FC curves depict a slightly broadened Verwey transition at ~110 K for the samples from the westernmost and the central equatorial sediment cores (GeoB 1523-1 and GeoB 4313-2). No Verwey transition could be observed for GeoB 2910-1, the easternmost site. The shift to slightly lower transition temperatures is indicative of non-stoichiometric slightly oxidised magnetite (Özdemir *et al.* 1993; Kosterov 2003).

The evident discrepancy between ZFC and FC warming curves in the dry bulk sediments was not observed in the magnetic extract data (compare Fig. 1 with Fig. 5). ZFC and FC warming curves of the magnetic extracts diverge only between 5 and 30 K. They are more or less merged at temperatures from ~110 K up to room temperature (see also Smirnov & Tarduno 2000). The substantially reduced ZFC-FC divergence in the magnetic extracts as compared to the bulk material would comply with the (near) absence of goethite in the magnetic extracts, because magnetic separation is biased towards strongly magnetic low coercivity material.

4.5 Low-Temperature ZFC and FC Results of Heavy Liquid Separates

Low-temperature warming curves of ZFC and FC remanence of the separated heavy fraction are overall an order of magnitude higher in intensity than those of the dry bulk sediments (Fig. 6). They show a very distinct steep slope between 5 and 40 K, corresponding to the sharp change of slope in the respective first derivatives. This might be due to the presence of an ultrafine-grained superparamagnetic (SP) phase (Özdemir *et al*. 1993; Smirnov & Tarduno 2000). The Verwey transition at ~110 K was exclusively detected in the westernmost samples of core GeoB 1523-1, it is weakly expressed in the first derivatives of the corresponding ZFC and FC curves.

The discrepancy between ZFC and FC curves mentioned earlier, which is interpreted to be caused by the presence of goethite, is clearly developed in the heavy fractions as compared to the magnetic extracts (compare Fig. 5 and Fig. 6). However, the discrepancy is less strong than in the dry bulk sediment samples. Therefore, the high coercitivity fraction is at least partly successfully extracted during the heavy liquid separation. The significant presence of the high coercivity component might also be the reason for the blurring of the Verwey transition earlier detected in the Mid Atlantic Ridge samples. The heavy liquid separation is not biased for magnetite in comparison to titanomagnetite or goethite, thus the curves of the heavy fraction represent the entire proportion of the magnetic assemblage. The ZFC and FC warming behaviour of the light fractions does not show any characteristic features and is therefore not shown here.

4.6 RT-SIRM Cycling Results

Dry Bulk Sediments compared with Heavy Liquid Separates

Figure 7 shows the RT-SIRM curves of the bulk sediment samples compared to the heavy (HF) and light fraction (LF) derived from heavy liquid separation. The cooling curves of the dry bulk sediments show a gradual increase of remanence from RT down to 10 K for all samples, which is distinctly enhanced below 10 K for most of the samples. On warming, the curves resemble the corresponding cooling curves back to ~150 K. Above 150 K the warming curves proceed below the cooling curves.

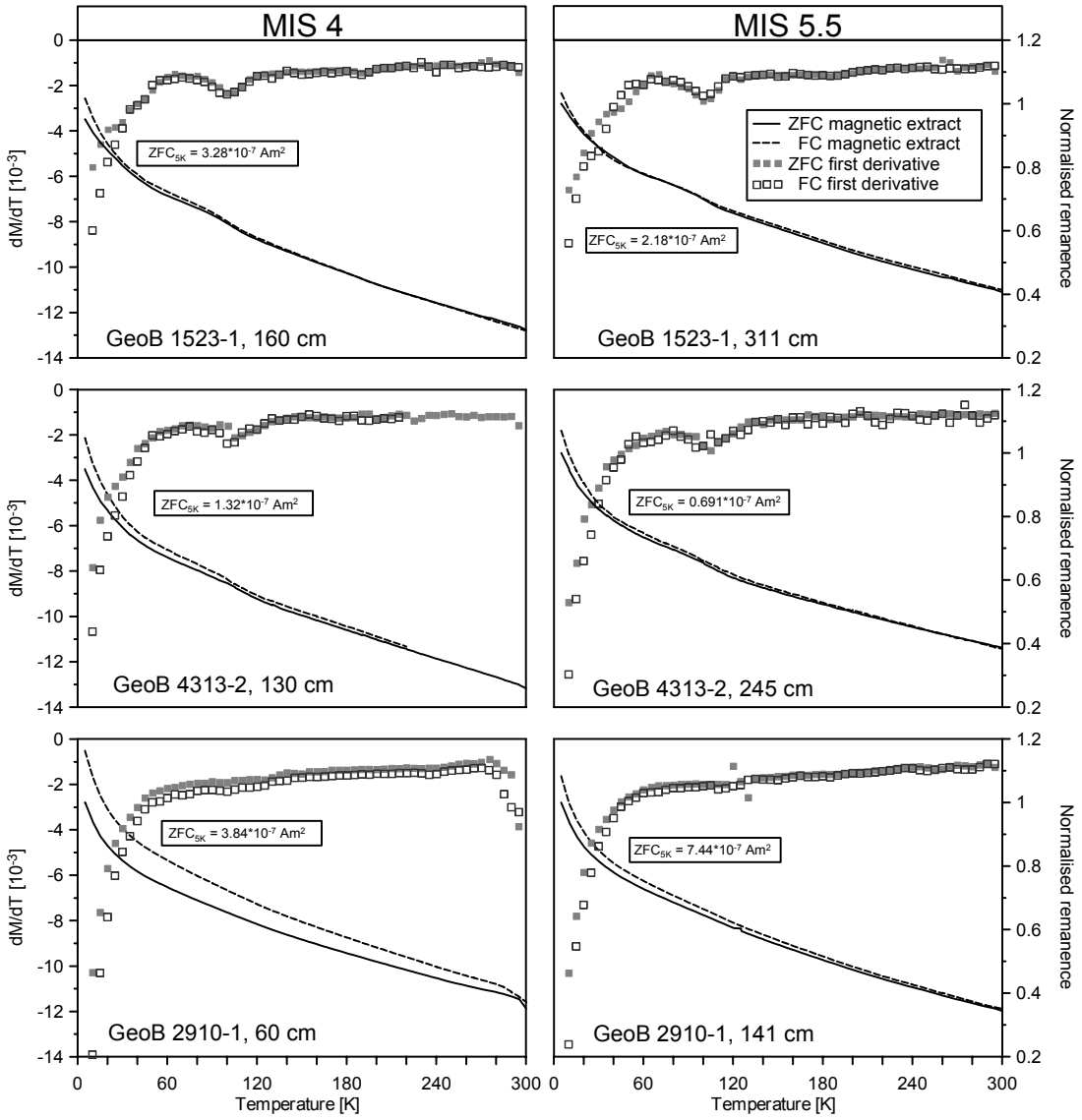

Figure 5. Low-temperature ZFC and FC remanence warming curves for magnetic extracts of all six samples from a West to East profile (from top to bottom).Lines refer to the ZFC and FC warming curves of the magnetic extract (solid line = ZFC, dashed line = FC) between 5 and 300 K in 2 K increments, using an applied field of 5 T. Curves are normalised to the magnitude of the respective ZFC value at 5 K (given for each individual panel). Because of very low yields normalising by mass was not practical in case of the magnetic extracts. Gray squares refer to the first derivatives of the respectively remanence curves (filled symbols = slope of ZFC, open symbols = slope of FC). For samples from GeoB 1523-1, a slightly shifted Verwey transition was detected at ~110 K, which can be also observed in samples from GeoB 4313-2, but is much weaker expressed at this site. No Verwey transition was found for samples of GeoB 2910-1. All ZFC and FC curves have the same ordinate scale.

No specific magnetic transitions were noted in the dry bulk sediment measurements.

The remarkable increase in remanence occurring in the very low temperature range between 10 and 5 K can also be observed in the room temperature SIRM curves of the light fraction (LF). Therefore it is most likely due to low-temperature magnetic ordering of paramagnetic (clay-) minerals (Coey 1988). Because the residual field of the MPMS is very low, this low-temperature ordering of the clay minerals in zero-field could be caused by the SIRM residing in magnetic mineral phases. This would magnetically couple to e.g. clay mineral coatings or ferrihydrite in the direct vicinity of the magnetic particles. Additional transmission electron microscopic (TEM) investigations of the samples

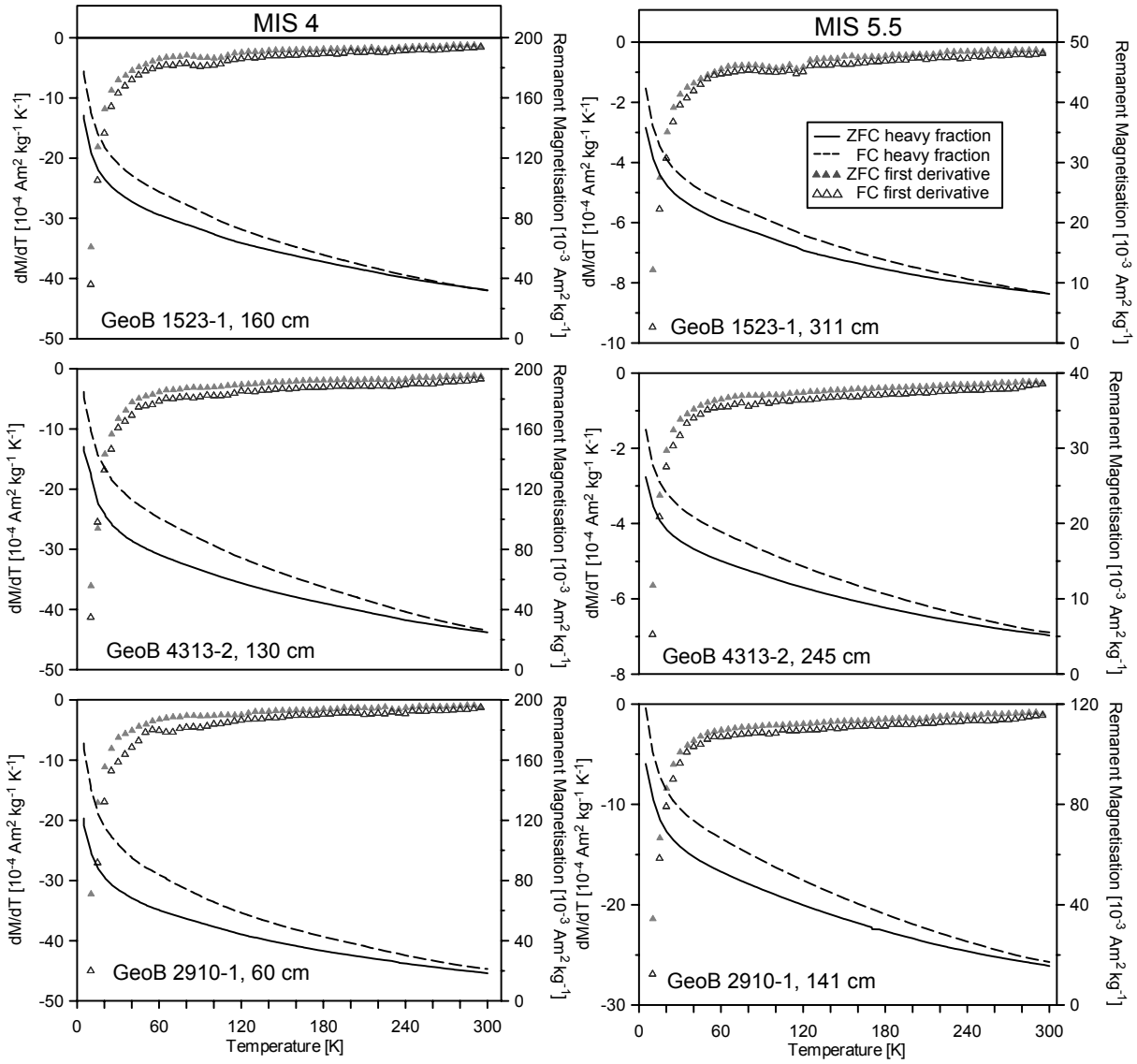

Figure 6. Low-temperature ZFC and FC remanence warming curves for the heavy fractions of the heavy liquid separates of the six samples from a West to East profile (from top to bottom). Lines refer to the ZFC and FC warming curves of the heavy fraction (solid line = ZFC, dashed line = FC), monitored between 5 and 300 K in 2 K increments, using an applied field of 5 T. Gray triangles refer to the first derivative of the respective remanence curves (filled symbols = slope of ZFC, open symbols = slope of FC). For samples from GeoB 1523-1, a weakly expressed Verwey transition was detected at ~110 K. All curves are normalised to their respective sample mass.

support the presence of such suggested mineral phases (Franke *et al*. unpubl. data). On the other hand, this would also suggest that the LF still contains part of the very fine grained SP fraction.

Usually LF curves are quite similar to the dry bulk sediment curves in sense of their general shape and increasing behaviour at very low temperatures. No specific magnetic transitions were detected in the LF measurements. Generally, they show a less steep slope towards lower temperatures and a weaker total intensity. This seems to be reasonable, because the heavy magnetic minerals are present in the HF (and of course in the dry bulk sediments), whereas the LF should be dominated by the lighter non-magnetic mineral fraction, such as clays, silicates, carbonates etc.

If the separation was successful to 100%, the LF would not carry any magnetic remanence and therefore would show a purely paramagnetic low-temperature curve. In practice, the separation seems to be quite efficient, but not abso-

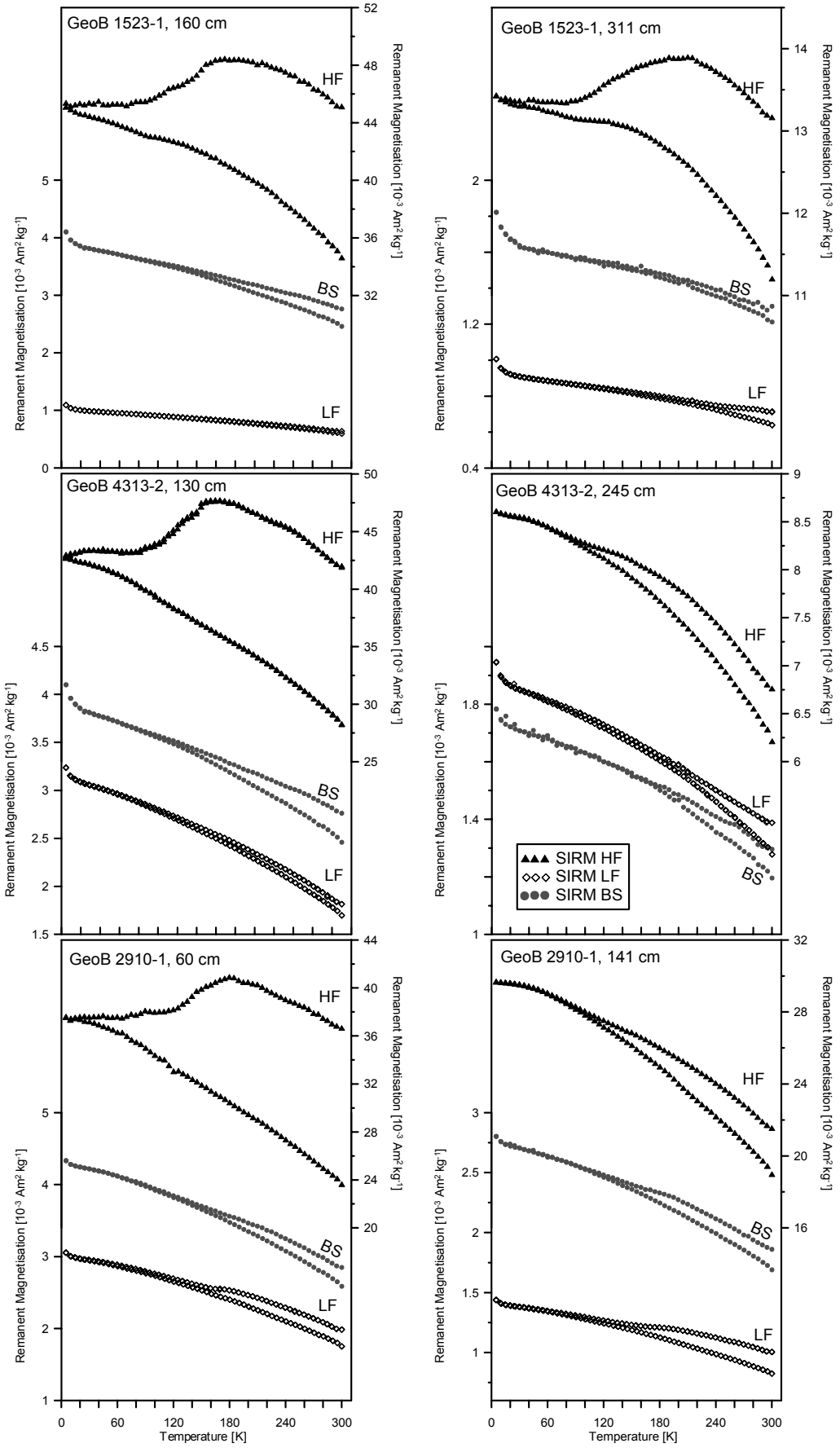
GeoB 1523-1, 160 cm
GeoB 1523-1, 311 cm
GeoB 4313-2, 130 cm
GeoB 4313-2, 245 cm
GeoB 2910-1, 60 cm
GeoB 2910-1, 141 cm
HF
BS
LF
SIRM HF
SIRM LF
SIRM BS
Remanent Magnetisation [10-3 Am2 kg-1]
Temperature [K]

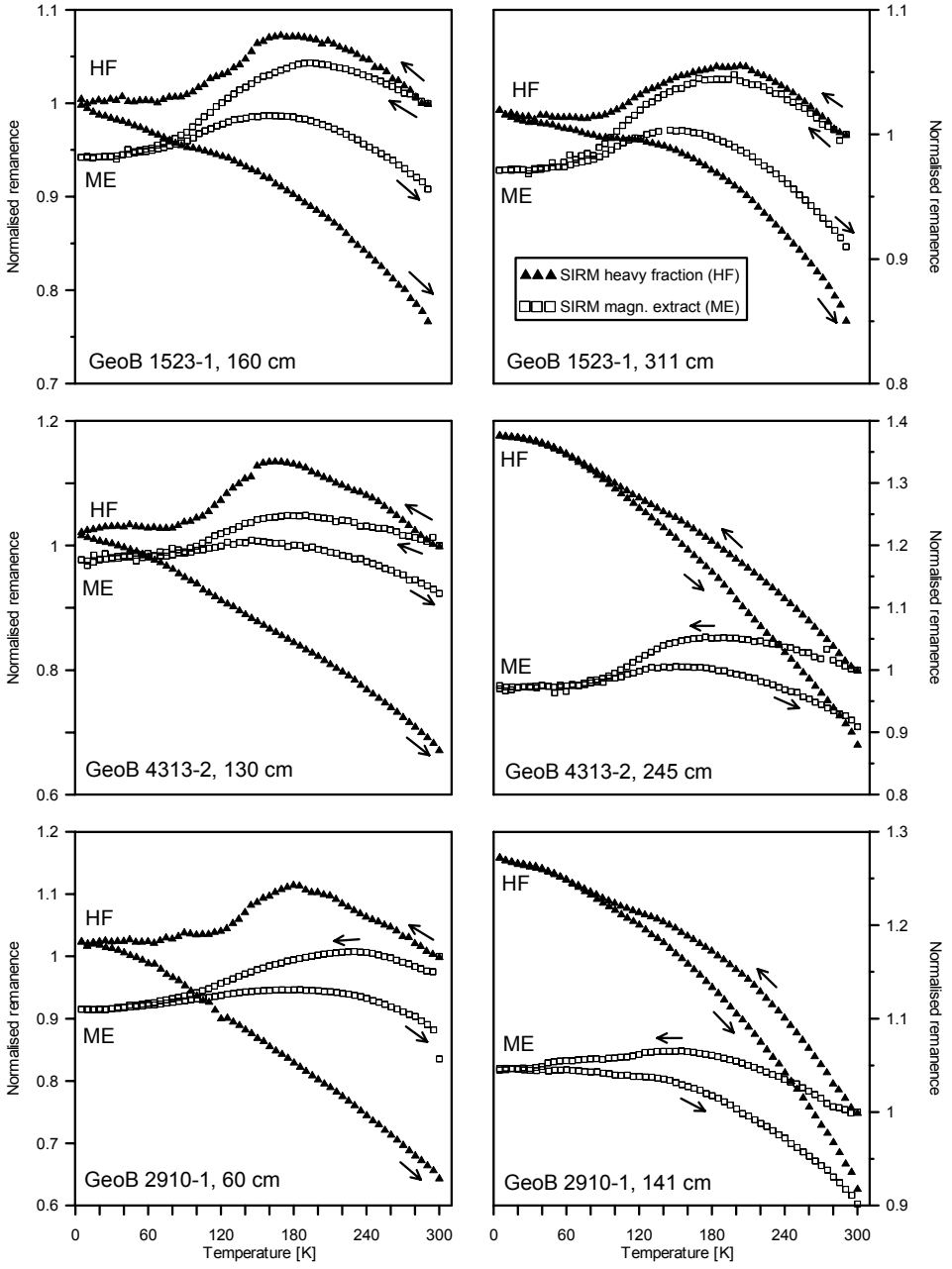

Figure 8. Comparisons of the zero-field cycles of RT-SIRM (applied field 5 T) for the heavy fractions (HF; black triangles) and the magnetic extracts (ME; open squares) of the six samples from a West to East profile (from top to bottom). ME curves are clearly dominated by the soft component magnetite, where as the HF curves show a steeper slope due to the high coercivity component goethite. Further detailed transitions in the temperature range between 240 and 180 K corresponding to the various present Fe-Ti phases. All ME and HF curves are normalised to the value of the respectively ZFC curve at 300 K as weight normalisation was not meaningful in case of the ME samples. The magnetically coarser samples from MIS 4 are shown in the left column and the magnetically finer samples from MIS 5.5 are shown in the right column.

Figure 7, page 37. Zero-field cycles of room temperature SIRM (applied field 5 T at 300 K) curves for the pristine dry bulk sediment samples (BS; gray dots), heavy fractions (HF; black triangles), and light fractions (LF; open diamonds) originating from the heavy liquid separation for the six samples from a West to East profile (from top to bottom). Samples from MIS 4 are shown on the left, samples from MIS 5.5 are shown on the right. The RT-SIRM curves were monitored in 2 K increments and normalised to their respectively sample mass. The BS and LF curves refer to the respective left ordinate axes, HF curves to the respective right ordinate axes. RT-SIRM curves of the HF show generally ten times higher remanence values than the BS samples, the LF curves show lower remanence values, except for sample GeoB 4313-2, 245 cm.

lutely complete and therefore we see a minor antiferromagnetic behaviour of the LF, strongly dominated by the paramagnetic components.

The RT-SIRM curves of the HF show characteristic low-temperature curves for (titano-) magnetite (Özdemir *et al*. 2002; Özdemir & Dunlop 2003; Kosterov 2003; Lagroix *et al*. 2004; Garming *et al*. in rev.), although we realise that RT-SIRM behaviour of (titano-) magnetites is not really well covered in the literature. Comparison of our HF curves with the titanomagnetite results from Özdemir & Dunlop (2003), Lagroix *et al.* (2004) and the RT-SIRM curves of Engelmann *et al*. (unpubl. data) from synthetic Fe-Ti oxide phases of various well defined Ti-content (Lattard *et al*. 2005) confirm the presence of (slightly oxidised) magnetite, various titanomagnetite, and titanohematite components in our samples.

Magnetic Extracts compared with Heavy Liquid Separates

Figure 8 shows the RT-SIRM curves of the magnetic extracts compared to the HF. For the sake of comparison, all curves were normalised to their value at 300 K. The RT-SIRM curves of the magnetic extracts clearly show ferrimagnetic dominated curves, typically of magnetite (Özdemir *et al.* 2002; Kosterov 2003). Comparing the differences between 125 and 105 K for both types of curves – the HF and the magnetic extracts – shows that magnetite is two times overrepresented in the latter. The cooling and warming curves are more or less reversible in the temperature range between 5 and 110 K. The relative changes of the remanence loss during the cooling-warming-cycle are only subtle. Generally samples from the westernmost sediment core show remanence losses of ~9%, the samples from the Mid-Atlantic Ridge site result in ~8% remanence loss and the easternmost samples have the biggest remanence losses of ~13%. The smooth increase with decreasing temperature, caused by the high coercivity component, is not present in the magnetic extract curves.

All RT-SIRM curves of the HF show this continuous increase with decreasing temperatures throughout the whole temperature range. This effect is attributed to the goethite component discussed before (Lowrie & Heller 1982, Dekkers 1989). The general shape of the RT-SIRM curves of the HF were already briefly described above. The occurrence of various Ti-Fe oxides is expressed by several minor changes of the cooling curve slope between 240 and 180 K. The undulations in the cooling curves above ~210 K should document the low-temperature magnetic ordering of present titanohematite phases (Lagroix *et al* 2004; Garming *et al*. in rev.), whereas the undulations detected on cooling below 210 K can be explained as magnetoelastical domain wall pinning postulated for this temperature range by Özdemir & Dunlop (2003). The RT-SIRM cycles of the MIS 5.5 samples of the cores GeoB 4313-2 and GeoB 2910-1 (Fig. 8) rather demonstrate characteristic curves for very Ti-rich oxide phases (Engelmann *et al*. unpubl. data) showing reversal behaviour in cooling and warming between 110 and 5 K. This is also expressed in the remanence loss behaviour of the HF samples: the westernmost sediment core GeoB 1523-1 shows remanence losses of ~13% for both samples, comparable to the remanence loss of ~12% for the MIS 5.5 samples from the Mid Atlantic Ridge (GeoB 4313-2) and the easternmost core (GeoB 2910-1). In contrast, the samples of MIS 4 from cores GeoB 4313-2 and GeoB 2910-1 have the biggest remanence loss of ~35%. This corresponds with findings of Özdemir et al. (2002), who describe an increasing remanence loss for stoichiometric magnetite of increasing grain-size.

5. Discussion

5.1 Further Magnetic Interpretations and Paleoclimatic Implications

The expression of the detected Verwey transition in the ZFC and FC curves of the

magnetic extract samples reflects the changing environmental conditions from West to East throughout the investigated transect in the Equatorial Atlantic. It is well known that the Verwey transition can be totally suppressed either by sufficient oxidation/maghemitisation (e.g. Özdemir *et al.* 1993) or by a fairly high Ti-content of $x \geq 0.4$ (e.g. Kakol *et al.* 1994) of the present magnetite ($Fe_{3-x}Ti_xO_4$). As already mentioned, additional SEM observations, using element dispersive spectroscopy (Goldstein *et al.* 1992), confirm the overall increase of the Ti-content in the magnetic mineral assemblage (Franke *et al.* unpubl. data). The Ti-content is exceedingly expressed by the shape of the RT-SIRM curves of the HF from GeoB 4313-2 and GeoB 2910-1 belonging to MIS 5.5. For the easternmost samples, supplementary Ti-rich titanohematite particles have been identified using electron backscatter diffraction techniques (Franke *et al*. in review). This suggests a (partial) dissolution of the original (titano-) magnetite particles with the concomitant increasing importance of the Ti-rich components, because the Ti-content stabilises the titanomagnetite compounds with regard to dissolution during diagenesis (Karlin 1990; Emiroğlu *et al.* 2004; Garming *et al*. 2005; Dillon & Bleil 2006).

The magnetic extracts do not contain much of a high coercivity component. Therefore they mainly represent the low-temperature behaviour of the low coercivity fraction in the magnetic assembly. The slightly steeper slope in ZFC and FC warming curves of the interglacial samples from MIS 5.5 indicates a finer magnetic grain-size of the low coercivity fraction compared to the glacial samples from MIS 4, which concurs with other magnetic grain-size observations in the dry bulk sediment measurements.

In the heavy liquid extraction procedure high coercivity components, such as goethite, were successfully extracted and contribute distinctly to the characteristics of the magnetic signal. In particular the RT-SIRM curves offer additional mineralogical and grain-size information, which was not detected by the LT-SIRM curves. Therefore low-temperature measurements on marine sediments using the heavy fraction might result in more detailed curves of more complete and quantitative samples. Comparison of the results from the MIS 4 and MIS 5.5 samples showed that the HF distinguished between their coarser and finer magnetic inventory and also showed a clear trend in dependence of the Ti-content of the magnetic assemblage. Funk *et al.* (2004a) described the magnetic grain-sizes of MIS 4 as much coarser as those of MIS 5.5. This does not concur with the reasoning of the coupling of the presence of an (enhanced) SP phase and the increased discrepancy of ZFC and FC curves. Another reasonable explanation of these ZFC and FC curve discrepancies was found in the temperature-dependent behaviour of goethite (Smirnov & Tarduno 2000).

5.2 Advantages of Heavy Liquid Separation

In the present study, we are dealing with natural samples of obviously complex composition and grain-size distributions and therefore our RT-SIRM curves are reflecting features of the various components. The absence in the HF measurements of the above mentioned ferrimagnetic ordering effect of paramagnetic material at very low temperatures confirms the success of the isolation of the dia- and paramagnetic fraction on the one hand and the ferrimagnetic and antiferromagnetic fraction on the other.

Comparisons of both extraction methods illustrate on the differences between the resulting samples. The magnetic extract exclusively represents the soft magnetic components of the dry bulk sediment. Within the range of soft magnetic components, magnetite certainly has the highest spontaneous magnetisation and is therefore preferably extracted by

methods such as described by Petersen *et al.* (1986) or Dekkers (1988). Additionally, the magnetic extraction leads generally to extracts that are coarser grained than the starting bulk sediment material.

Any sample upgrading technique can potentially alter the original material. For marine sediments from suboxic or anoxic environments, this could actually cause subsequent oxidation of iron sulphide mineral phases (e.g. greigite or pyrite). If the samples are suspended in a sediment slurry, the suspension should be deoxygenised by purging with an inert gas. This can be achieved by performing the upgrading in a closed cycle under argon atmosphere and the usage of alcohol instead of water as suspension medium.

In this study, we used non-toxic sodium polytungsten solution $Na_6[H_2W_{12}O_{40}]$. This heavy liquid does not react with the sample material and causes no additional oxidation. Its hydrophilic character allows us to disperse the relatively clay-rich homogenised dry bulk sediment reasonably well without usage of any additional peptiser. No chemical leaching had to be used, so the risk of alteration or even dissolution, particularly of the magnetic nanoparticles can be disregarded. The combination of heavy liquid separation, mechanical (and ultra-sonic) agitation and centrifuging accelerates the classical gravity separation method and leads generally to better results for marine sediment samples, avoiding clustering problems due to high clay content.

The light fraction always serves as a control measure for the success of the separation. Alternatively, as shown in Lagroix *et al* (2004), the specific density of the heavy liquid can be easily adjusted so that distinctly different magnetic fractions can be separated. In case of presence of paramagnetic heavy minerals, such as barite or siderite, these mineral phases are evidently included in the separated heavy fraction and have to be taken into account during low-temperature measurements (Frederichs *et al*. 2003).

The magnetic results for the heavy liquid separates presented here, confirm that the heavy fraction represents the complete range of the magnetic inventory to a reasonable extent. Using this technique, a much lager amount of magnetic material is available for measurements, which can be sufficiently quantified. As always, the success of the separation is generally depending on the grain-size distribution of the magnetic inventory. Especially components such as ultra-fine SP material are difficult to be completely extracted.

6. Conclusions

1. Magnetic extracts are not representative of the magnetic inventory in bulk sediment. Soft ferrimagnetic material is over-represented in the extract. Vice versa, much more weakly magnetic (antiferromagnetic) material, is under-represented. This has to be kept in mind during interpretation of the mineral magnetic data, e.g. low-temperature remanence curves.
2. Heavy liquid separation (with sodium polytungsten solution) is a useful tool to achieve a more complete 'magnetic' extract. It is as straightforward as magnetic extraction, both methods do not demand much experimental time. Heavy liquid separation allows the quantification of the resulting heavy and light mineral fractions and leads to larger yields of 'magnetic' extracts. Applied to fine-grained unconsolidated marine sediments, the combination of a hydrophile heavy liquid (polytungsten) dispersion with ultrasonic waves and subsequent centrifuging was very successful in separating the lighter dia- and paramagnetic mineral fraction from the heavy ferrimagnetic fraction. In sediments with appreciable non-ferrimagnetic heavy minerals, these will be included in the heavy liquid separate as well.
3. Comparison of the samples from MIS 4 and MIS 5.5 showed that the heavy liquid extraction improves in quality with increasing magnetic grain-size. However,

very fine material is still reasonably well extracted.
4. The RT-SIRM curves turned out to be the most indicative measurements for these marine sediment samples. Due to the variable Ti-content of the magnetite particles present those curves are more diagnostic in comparison to LT-ZFC and FC warming curves. Nevertheless, we recommend a combination of both remanence measurements for the sake of completeness and understanding of the low-temperature rock magnetic analysis.

Acknowlegements
The heavy liquid separation was performed at facilities of the Marine Geochemistry group, University of Bremen, we would like to thank particularly Michael Schweizer and Natascha Riedinger for their assistance. TC-Tungsten Compounds enterprises provided advice and heavy liquid solution for test runs. We also owe thanks to the members of the Marine Geophysics group (University of Bremen) and the Paleomagnetic group (Utrecht University) for their support and advice. Financial support of CF was provided by the DFG through the European Graduate College EUROPROX, (Universities of Bremen and Utrecht) and by NWO through the VMSG, Vening Meinesz Research School of Geodynamics (Utrecht University). This investigation is also associated to the Research Center Ocean Margins (RCOM) at the University of Bremen.

References

Coey, J.M.D., 1988. Magnetic properties of iron in soil iron oxides and clay minerals, in *Iron in Soils and Clay Minerals,* pp. 397-466, eds Stucki, J.W., Goodman, B.A. & Schwertmann, U., Reidel Publishing Company, Dortrecht.

Dekkers, M.J., 1988. *Some rockmagnetic parameters for natural goethite, pyrrhotite and fine-grained hematite*, Geologica Ultraiectina, **51**, Ph.D. thesis, Utrecht University, 231 p.

Dekkers, M.J., 1989. Magnetic properties of natural goethite - II. TRM behaviour during thermal and alternating field demagnetization and low-temperature treatment, *Geophys. J.*, **97**, 341-355.

Dillon, M. & Bleil, U., 2006. Rock Magnetic Signatures in Diagenetically Altered Sediments from the Niger Deep-Sea Fan, *J. Geophys. Res*., in press.

Emiroğlu, S., Rey, D. & Petersen, N., 2004. Magnetic properties of sediments in the Ría de Arousa (Spain): dissolution of iron oxides and formation of iron sulphides, *Phys. Chem. Earth*., **29**, 947-959.

Fischer, G. & cruise participants, 1998. Report and preliminary results of Meteor cruise M38/1, Las Palmas – Recife, 25.1.-1.3.1997, *Ber. Fachber. Geowiss. Univ. Bremen*, **94**, 178 p.

France, D.E. & Oldfield, F., 2000. Identifying goethite and hematite from rock magnetic measurements of soil and sediments, *J. Geophys. Res*., **105**, B2, 2781-2795.

Franke, C., Pennock, G.M., Drury, M.R., Lattard, D., Engelmann, R., Garming, J.F.L., von Dobeneck, T. & Dekkers, M.J., in review. Identification of magnetic Fe-Ti oxides by electron backscatter diffraction (EBSD) in scanning electron microscopy, *in review at J. Geophys. Res.*

Frederichs, T., von Dobeneck, T., Bleil, U. & Dekkers, M.J., 2003. Towards the identification of siderite, rhodochrostite and vivianite in sediments by their low-temperature magnetic properties, *Phys. Chem. Earth*, **28**, 669-679.

Funk, J., von Dobeneck, T. & Reitz, A., 2004a. Integrated rock magnetic and geochemical quantification of redoxomorphic iron mineral diagenesis in Late Quaternary sediments from the Equatorial Atlantic, in *The South Atlantic in the Late Quaternary: Reconstruction of Material Budget and Current Systems,* pp. 237-260, eds Wefer, G., Mulitza, S. & Ratmeyer, V., Springer-Verlag, Heidelberg, Berlin, New York.

Funk, J.A., von Dobeneck, T., Wagner, T. & Kasten, S., 2004b. Late Quaternary sedimentation and early diagenesis in the equatorial Atlantic Ocean: Patterns, trends and processes deduced from rock magnetic and geochemical records, in *The South Atlantic in the Late Quaternary: Reconstruction of Material Budget and Current Systems*, pp. 461-497, eds Wefer, G., Mulitza, S. & Ratmeyer, V., Springer-Verlag, Heidelberg, Berlin, New York.

Garming, J.F.L., Bleil, U. & Riedinger N., 2005. Alteration of magnetic mineralogy at the sulphate-methane transition: analysis of sediments from the Argentine continental slope, *Phys. Earth Planet. Inter*., **151**, 290-308.

Garming J.F.L., Bleil, U., Franke, C. & von Dobeneck, T., in review. Low-temperature partial magnetic self-reversal in marine sediments, *Geophys. J. Int.*

Goldstein, J.I., Newbury, D.E., Echlin, P., Joy, D.C., Romig, A.D.Jr., Lyman, C.E., Fiori, C. &

Lifshin, E., 1992. *Scanning electron microscopy and X-Ray microanalysis*, 2nd edition, Plenum Press, New York, 820p.

Hedley, I.G., 1971. The weak ferromagnetism of goethite (α-FeOOH), *Z. Geophy*., **37**, 409-420.

Heller, F., 1978. Rockmagnetic studies of Upper Jurassic limestones from Southern Germany, *J. Geophys*., **44**, 525-543.

Henrich, R. & cruise participants, 1994. Report and preliminary results of Meteor cruise M29/3, Rio de Janeiro - Las Palmas 11.8. - 5.9.1994. *Ber. Fachber. Geowiss. Univ. Bremen*, **60**, 155 p.

Hounslow, M.W. & Maher, B.A., 1999. Laboratory Procedures for Quantitavive Extraction and Analysis of Magnetic Minerals from Sediments, in *Environmental Magnetism, a practical guide*, pp. 139-164, eds Walden, J., Oldfield, F. & Smith, J., *Quaternary Research Association, Technical Guide,* **6**.

Kakol, Z., Sabol, J., Stickler, J., Kozlowski, A. & Honig, J.M., 1994. Influence of titanium doping on the magnetocrystalline anisotropy of magnetite, *Phys. Rev. B*, **49**, 12.767-12.772.

Karlin, R., 1990. Magnetic mineral diagenesis in suboxic sediments at Betis Site N-W, NE Pacific Ocean, *J. Geophys. Res*., **95**, 4421-4436.

Kosterov, A., 2003. Low-temperature magnetization and AC susceptibility of magnetite: effect of thermomagnetic history, *Geophys. J. Int*., **154**, 58-71.

Kosterov, A., Frederichs, T. & von Dobeneck, T., 2006. Low-temperature magnetic properties of rhodochrosite ($MnCO_3$), *Phys. Earth Planet. Inter.*, **154**, 234-242.

Lagroix, F., Banerjee, S.K. & Jackson, M.J., 2004. Magnetic properties of the Old Crow tephra: Identification of a complex iron titanium oxide mineralogy, *J. Geophys. Res*., 109, B01104, doi:10.1029/2003JB002678.

Lattard, D., Sauerzapf, U. & Käsemann, M., 2005. New calibration data for the Fe-Ti oxide thermo-oxybarometers from experiments in the Fe-Ti-O system at 1 bar, 1,000-1,300°C and a large range of oxygen fugacities, *Contrib. Mineral. Petrol*., **149**, 735-754.

Lowrie, W. & Heller, F., 1982. Magnetic properties of marine limestones, *Rev. Geophys. Space. Phys*., **20**, 171-192.

Özdemir, Ö., Dunlop, D.J. & Moskowitz, B.M., 1993. The effect of oxidation on the Verwey transition in magnetite, *Geophys. Res. Lett*., **20**, 1671-1674.

Özdemir, Ö. & Dunlop, D. J., 2000. Intermediate magnetite formation during dehydration of goethite, *Earth Planet. Sci. Lett*., **177**, 59-67.

Özdemir, Ö., Dunlop, D. & Moskowitz, B.M., 2002. Changes in remanence, coercivity and domain sate at low temperature in magnetite, *Earth Planet. Sci. Lett*., **194**, 343-358.

Özdemir, Ö. & Dunlop, D.J., 2003. Low-temperature behaviour and memory of iron-rich titanomagnetites (Mt. Haruna, Japan and Mt. Pinatubo, Philippines), *Earth Plant. Sci. Lett.*, **216**, 193-200.

Passier, H.F. & Dekkers, M.J., 2002. Iron oxide formation in the active oxidation front above sapropel S1 in the eastern Mediterranean Sea as derived from low-temperature magnetism, *Geophys. J. Int*., **150**, 230-240.

Petersen, H., von Dobeneck, T. & Vali, H., 1986. Fossil bacterial magnetite in deep-sea sediments from the South Atlantic Ocean, *Nature*, **320**, 611-615.

Reitz, A., Hensen, C., Kasten, S., Funk, J.A. & de Lange, G.J., 2004. A combined geochemical and rock-magnetic investigation of a redox horizon at the last glacial/interglacial transition, *Phys. Chem. Earth*, **29**, 921-931.

Smirnov, A.V. & Tarduno, J.A., 2000. Low-temperature magnetic properties of pelagic sediments (Ocean Drilling Program Site 805C): Tracers of maghemitization and magnetic mineral reduction, *J. Geophys. Res*., **107**, B7, 16457-16471.

Schulz, H.D. & cruise participants, 1991. Report and preliminary results of Meteor cruise M16/2, Recife – Belem, 28.4.-20.5.1991, *Ber. Fachber. Geowiss. Univ. Bremen,* **19**, 149 p.

Van Velzen, A.J. & Zijderveld, J.D.A., 1992. A method to study alterations of magnetic minerals during thermal demagnetization applied to a fine-grained marine marl (Trubi Formation, Sicily), *Geophys. J. Int*., **110**, 79-90.

Van Velzen, A.J. & Zijderveld, J.D.A., 1995. Effects of weathering on single domain magnetite in early Pliocene marls, *Geophys. J. Int*., **121**, 267-278.

Van Velzen A.J. & Dekkers M.J., 1999a. Low-temperature oxidation of magnetite in loess-paleosol sequences: a correction of rock magnetic parameters, *Studia Geophysica et Geodaetica*, **43**, 4, 357-375.

Van Velzen, A.J. & Dekkers, M.J., 1999b. The incorporation of thermal methods in mineral magnetism of loess-paleosol sequences: a brief overview, *Chin. Sci. Bull*., **44**, Suppl. 1, 53-63.

von Dobeneck, T., Petersen, N. & Vali, H., 1987. Bakterielle Magnetofossilien – paläomagnetische und paläontologische Spuren einer ungewöhnlichen Bakteriengruppe, *Geowissenschaften in unserer Zeit*, **1**, 27-35.

Chapter 4

Identification of magnetic Fe-Ti oxides by electron backscatter diffraction (EBSD) in scanning electron microscopy

Summary
In paleomagnetic and environmental magnetic studies the magneto-mineralogical identification is usually based on a set of rock magnetic parameters, complemented by crystallographic and chemical information retrieved from X-ray diffraction (XRD), (electron) microscopy, or energy dispersive spectroscopy (EDS) of selected samples. While very useful, each of these accessory techniques has its limitations when applied to natural sample material. Identification of the magnetic minerals might be complicated by the limit of detection. Difficulties may also arise for particles of very fine grain-size. For example in marine sediments, concentrations of magnetic particles are typically down to the ppm range and they occur down to the nm range. Therefore, meaningful application of such techniques depends on sample quality.

Electron backscatter diffraction (EBSD) of individual grains in scanning electron microscopy (SEM) enables mineralogical identification of individual grains down to ~0.2 micrometer and is particularly powerful when combined with EDS. EBSD is a relatively commonly used technique in structural geology and petrology. In this study we show the merits of EBSD for rock magnetic investigations by analysing titanomagnetites and hemoilmenites of various compositions and submicron lamella of titanomagnetite-hemoilmenite intergrowths. In natural particles, EDS often has a semi-quantitative character and compositionally similar intergrowths may be difficult to distinguish. With the mineralogical information provided by EBSD unambiguous identification of spinel-type and rhombohedral oxides is obtained. Optimal EBSD patterns are gathered from smooth, polished surfaces but here we show that interpretable EBSD patterns can be obtained as well from loose, so called 'non-embedded' particles from marine sediments.

Key words: titanomagnetite, hemoilmenite, electron backscatter diffraction (EBSD), energy dispersive spectroscopy (EDS), scanning electron microscopy (SEM), rock magnetism

This chapter is an article in review: Franke, C., Pennock, G.M., Drury, M.R., Engelmann, R., Lattard, D., Garming, J.F.L., von Dobeneck, T. and Dekkers, M.J., 2006. Identification of magnetic Fe-Ti oxides by electron backscatter diffraction (EBSD) in scanning electron microscopy, *J. Geophys. Res*

.

1. Introduction

Iron-titanium oxide minerals are fundamental to paleo-, rock, and environmental magnetic purposes because they constitute the most common magnetic particles on Earth. Three Fe-Ti oxide solid solution series are relevant for magnetic studies, the titanomagnetite, the titanomaghemite and the titanohematite-hemoilmenite series (Fig. 1; cf. also O'Reilly 1984; Waychunas 1991; Dunlop & Özdemir, 1997). Titanomagnetite (TM) is the cubic spinel series between the magnetite (Mt, Fe_3O_4) and ulvöspinel (Usp, Fe_2TiO_4) endmembers. The general titanomagnetite formula is $Fe_{3-x}Ti_xO_4$, where x is the mole fraction of the ulvöspinel component. Hereafter, titanomagnetite compositions will be given as 'TMx%', for example TM60 for $x = 0.6$. Phases of the rhombohedral α-oxide series between hematite (Hmt, Fe_2O_3) and ilmenite (Ilm, $FeTiO_3$) are called titanohematite or hemoilmenite, depending on their compositions, and will be here simply abbreviated as Hilm. Their general formula is $Fe_{2-y}Ti_yO_3$, where y is the mole fraction of the ilmenite endmember. Titanomaghemites (Tmh), which are generally formed by oxidation of titanomagnetites at

low temperatures, have a cubic crystal structure related to that of the spinels, but are characterised by variable, mostly high concentrations of cationic vacancies related to the charge-balanced substitution $3Fe^{2+} = 2Fe^{3+} + \square$. Consequently, their compositional field extends over a large range of Fe^{2+}/Fe^{3+} and ΣFe/Ti values (Fig. 1). Although natural Fe-Ti oxides generally contain small amounts of other elements, such as Al, Mg or Cr, the general characteristics listed above are also applicable to those compositions.

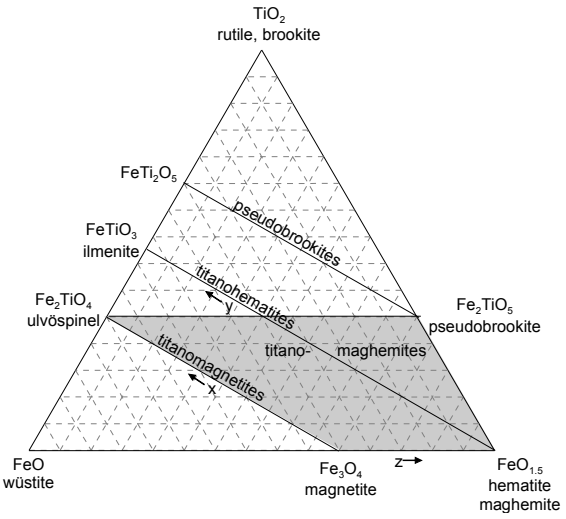

Figure 1. Ternary system of TiO_2-FeO-$FeO_{1.5}$ (modified after Dunlop & Özdemir 1997) showing the titanomagnetite and titanohematite-hemoilmenite solid-solution lines and the titanomaghemite field. The mole per cent of Ti^{4+} is given by the parameter x with respect to the $Fe_{3-x}Ti_xO_4$ substitution along the titanomagnetite solid-solution line, and by the parameter y with respect to the $Fe_{2-y}Ti_yO_3$ substitution along the titanohematite solid-solution line. The degree of oxidation is measured by the parameter z. During oxidation of titanomagnetites, their bulk compositions are shifted to the right, following the horizontal dashed lines. In case of high-temperature oxidation the resulting product is not a single-phase titanomagnetite, but instead a mixture of TM and Hilm. During low-temperature oxidation (< 300°C) single-phase titanomaghemites are formed.

Various rock magnetic techniques and parameters (such as low- and high-temperature magnetic remanence and susceptibility measurements, magnetic hysteresis, first order reversal curve (FORC), anhysteretic (ARM) and isothermal remanent magnetisation (IRM) determination), are available to identify the magnetic Fe-Ti oxide minerals. These magnetic techniques are very sensitive, comparatively rapid and, in suitable combinations, particularly discriminatory for fine, sub-micron sized grains and magnetically contrasting minerals. Rock magnetic parameters are therefore extensively used in stratigraphic correlations and paleoenvironmental proxy studies. However, the mixing of particles from various sources – the rule for marine sediments – complicates the identification of the different magnetic components. After deposition, magnetic minerals may undergo a series of diagenetic reactions altering the concentrations of magnetic particles and adding more complexity to the interpretation of the magnetic signal. Independent information provided by non-magnetic methods is essential to reduce some inherent ambiguities of rock magnetic data and to gain understanding of the state and origin of the different types of magnetic particles.

Powder XRD is not useful for the identification of single magnetic mineral components in marine sediments because concentrations of the complete magnetic assemblage are typically < 1 ‰ by volume. Detailed mineralogical characterisations of magnetic particles by optical microscopic techniques have a long tradition (for example Lindley 1926; Ramdohr 1955; Petersen *et al*. 1979) but have limited spatial resolution. Scanning electron microscopy (SEM) with back scattered electron (BSE) imaging (Lloyd 1985) or EDS (Goldstein *et al*. 1992) are conventional techniques in petrology (Prior *et al*. 1999). Electron microprobe analysis (EMP) is capable to yield the chemical composition of an excitation volume of about 5 µm in diameter. In magnetism studies, SEM is mainly used for secondary electron (SE) and BSE imaging of either polished sections or samples consisting of loose particles, for example magnetic extracts. The elemental composition is normally acquired by (semi-)quantitative EDS. The Fe/Ti ratio can be very similar in titanomagnetite, titanomaghemite and he-

moilmenite (see Fig. 1), as a result these phases can be rather difficult to discriminate (for example Xu *et al*. 1997a). For non-embedded samples consisting of loose particles, quantitative analysis is further hampered by electron beam scattering caused by the irregular grain surfaces.

Analytical transmission electron microscopic (TEM) techniques have been successfully applied in mineral magnetic studies to identify very small magnetic particles in natural samples. For example Xu *et al*. (1994, 1996, 1997a, 1997b), Shau *et al.* (2000) and Zhou *et al*. (1997, 1999a, 1999b, 2001a, 2001b) performed combined rock magnetic and transmission electron microscopic investigations on Fe-Ti oxides of Mid Ocean Ridge Basalts (MORB) using selected area electron diffraction (SAED) or convergent beam electron diffraction (CBED). Unfortunately TEM methods are much more time-consuming in analysis than EBSD for SEM (Kumar *et al*. 2001; Humphreys 2004) and TEM sample preparation is often not as straightforward. Feinberg *et al*. (2004) used EBSD application for rapid and precise determination of lattice orientations (Randle & Engler 2000) of clinopyroxene-hosted magnetite inclusions. They describe EBSD as a significantly less cumbersome and labor intensive as for example TEM and single-crystal XRD methods. EBSD is not yet well established in rock magnetic investigations, but offers a reasonable basis to identify the mineralogy/crystallography of single grains or grain sections within the spatial resolution of the technique (Humphreys *et al.* 1999; Kumar *et al.* 2001; Humphreys 2001, 2004). In principle grains as small as ~200 nm can be analysed by EBSD, as shown by Ohfuji *et al*. (2005). They performed a detailed crystallographic study on microcrystals of natural pyrite framboids.

Here, we test the merits and limitations of the EBSD technique on examples of mineral phase from the Fe-Ti-O system. Several different sample types of synthetic and natural magnetic Fe-Ti oxides have been investigated with EBSD and EDS. Most analyses were performed on polished section samples, but EBSD was also applied to samples consisting of loose particles to achieve crystallographic information of the individual grains.

2. Electron Backscatter Diffraction (EBSD)

2.1 The EBSD Technique

In this study we follow the terminology of Prior *et al.* (1999) using the term EBSD to denote the diffraction technique, which is briefly described below (for further reading see for example Day 1993; Baba-Kishi 2002), and the term EBSP to refer to the individual diffraction pattern. An electron beam is larger (1 nm at the absolute minimum) than the lattice plane spacings of oxides and silicates (~0.3 - 0.1 nm). The incident electrons are scattered over a wide range of angles when penetrating the sample, such that the interaction volume acts as a source for subsequent electron-specimen interactions as the scattered electrons escape from the sample. Incident electrons pass at all possible distances from the atomic nuclei in a specimen: electrons which pass close to a nucleus are scattered through larger angles than those which pass more distantly. Some escaping scattered electrons are diffracted by lattice planes generating cones of diffracted electrons, which have intensities and orientations that depend on the crystal structure and atomic species. Only those electrons that backscatter out of the uppermost layer (± 30nm) of the sample are collected by a detector comprising a phosphor screen and charge-coupled device (CCD) camera (Fig. 2). Diffraction cones of high intensity intersect with the phosphor screen producing a pattern of almost straight bands. The intersection of several bands will give a bright spot on an EBSP. The intensity of these bands and spots is mineral specific and therefore of major importance for identification of the crystallographic structure of the source material. For example EBSPs from two different mineral phases of the same cry-

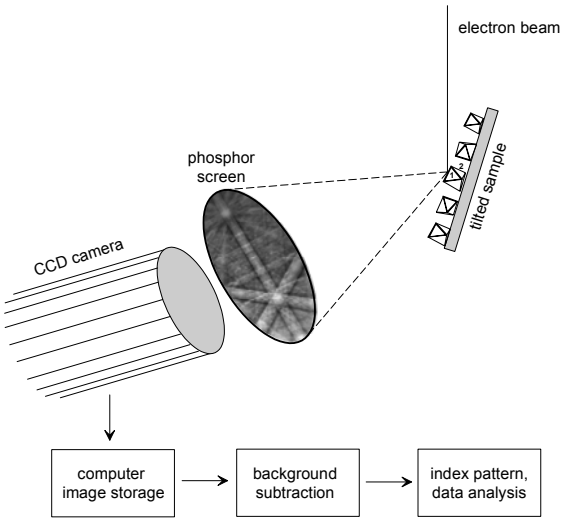

Figure 2. Sketch of the EBSD hardware set up (modified after Prior *et al*. 1999). The EBSD pattern is a projection of the spherical angels between the crystallographic directions onto the flat plain of the phosphor screen. Here we show an schematic sample for non-embedded particles, position 1 is favourable and position 2 is not favourable for obtaining an EBSD signal of the particle. In standard EBSD polished sections with smooth surface are used.

stal class can have close geometric similarities. However, the intensities of these bands vary for each specific mineral, due to the detailed crystallographic configuration (for example space group) and differences in scattering properties of different elements.

The weak EBSD raw signal is processed to improve pattern quality before indexing. Pattern processing involves removal of a non-uniform background signal and is followed by contrast enhancement. The intensity of elastic scattering varies strongly with angle, so the background intensity detected by the phosphor screen is not uniform. This variable background strongly masks the diffraction signal of the EBSP. The background is collected by scanning the beam rapidly over many crystals, so it is an average signal for many different orientations. It is therefore independent of the crystal class, although its intensity depends on differences in individual backscattered coefficients.

Symmetry elements in the EBSP, defined from the relative positions of the bands and spots (Lloyd et al. 1991; Prior et al. 1999) are used to index patterns. This was carried out using *Channel 5* software from *HKL Technology* and can be done by manual or automatic graphical fitting of the observed diffraction bands in the EBSP. The individual graphical fit is then compared (by the software) to EBSPs available from a database. Usually pattern solutions from the database of mineral phases which are considered can be loaded into the software. The crystallographic database used in this study to identify the specific mineral grains originated from the 'American Mineralogic database', provided by HKL Technology, and included magnetite (Mt), titanomagnetites (TM10, TM14) and titanomaghemite (Tmh6), hematite (Hmt), and ilmenite (Ilm) (Blake et al. 1966; Wechsler & Prewitt 1984; Wechsler et al. 1984; Collyer et al. 1988; see Table 1).

In some cases, multiple solutions to an individual EBSP were suggested by the software and a best fit solution was manu-

Table 1. Chemical and crystallographical data of the mineral phases used to generate the simulated EBSD pattern solutions for this study, originating from the 'American Mineralogic database'. References: (1) Blake *et al*. 1966; (2) Collyer *et al*. 1988; (3) Wechsler & Prewitt 1984; (4) Wechsler *et al*. 1984.

Mineral phase	Structural formula	Space group	Ti [at%]	Fe [at%]	O [at%]	Ref.
Mt	Fe_3O_4	$Fd\bar{3}m$	0.0	42.9	57.1	4
Tmh6	$Fe^{3+}_{0.96}\square_{0.04}\left[Fe^{2+}_{0.23}Fe^{3+}_{0.99}Ti^{4+}_{0.42}\square_{0.37}\right]O_4$	$P4_332$	6.3	33.0	60.7	2
TM10	$Fe^{2+}_{1.1}Fe^{3+}_{1.8}Ti^{4+}_{0.1}O_4$	$Fd\bar{3}m$	10.7	32.1	57.1	4
TM14	$Fe^{2+}_{1.14}Fe^{3+}_{1.72}Ti^{4+}_{014}O_4$	$Fd\bar{3}m$	14.3	28.6	57.1	4
Hmt	$\alpha\ Fe_2O_3$	$R\bar{3}c$	0.0	40.0	60.0	1
Ilm	$FeTiO_3$	$R\bar{3}$	20.0	20.0	60.0	3

ally selected by com-paring the geometry, width and relative intensity of diffraction bands in the simulated and observed EBSP. In addition, the goodness of fit between the observed and the indexed EBSPs in the software was given by the mean angular deviation (MAD). A lower MAD value implies a better solution. Typically MAD values < 1.3° are considered acceptable for crystal orientation measurements. Details about software and pattern processing are given by Dingley (1984), Wilkenson & Hirsch (1997), and Day & Quested (1999).

2.2 EBSD Sample Preparation

Smooth sample surfaces are needed to optimise EBSD pattern quality. Therefore all samples (for detailed description of all samples see section 3), except the ones consisting of loose material (extracted magnetic particles from marine sediments), were mechanically polished to a 1 µm finish before chemical-mechanical polishing with colloidal silica (± 0.03 µm; Fynn & Powell 1979). To reduce charging in the SEM, large non-conducting areas (such as the specimen slide) were coated with silver paint. The quality of the EBSP is generally reduced for carbon or gold coated samples, therefore the areas of interest were kept without any coating if possible. The polished section of sample GeoB 6229-6, 655 cm consists of magnetic particles embedded in epoxy resin, and was mechanically polished to a 1 µm finish and coated with a thin layer of carbon. Manually applied silver paint coating was not practical with this kind of sample due to fine grain-sizes of the analysed particles. In comparison to all polished sections, sample GeoB 4313-1, 130 cm was pre-pared as a non-embedded particle sample (see section 3.4 and 3.5). A *FEI XL30 SFEG* scanning electron micros-cope was used, operating acceleration voltages between 12 and 30 kV with a range of currents between 2.11 and 2.41 nA.

2.3 Background Signal

The selection of the appropriate background signal is crucial for achieving a reasonable EBSP (for example Baba-Kishi 2002). The normal approach for polished sections was to collect a background signal on the same sample over many grains. For the non-embedded particle sample (see section 3.5) this method of background collection was not appropriate, because the sample was not flat and the 3D topography of the individual grains produced large variations in the background scattering. Here, a more uniform background signal obtained from the polished synthetic samples was found to be suitable for background subtraction of EBSPs from individual grains of the non-embedded particle sample.

2.4 Adaptation of the Acceleration Voltage

With the natural samples the beam voltage was adapted to the type of mineral grain. For the polished sections of the synthetic samples (see section 3.2), lower voltages around ~12 kV gave already a reasonable EBSP. For critical samples, such as the embedded and non-embedded particle samples, higher beam voltages generally resulted in better EBSP signals. The range of applied beam voltages (12 to 30 kV) had to be chosen individually, balancing on the one hand weak pattern signals and on the other hand charging problems of the sample surface.

3. Sample Material

3.1 Sample Selection Strategy

Different types of samples were selected for this study, ranging from coarse-grained well constrained synthetic materials to extracts of fine-grained magnetic particles from marine sediments (Table 2). Suitable conventional samples for EBSD, with a high quality polish, could be made from synthetic samples and large-grained natural material. Standard sample preparation methods are not easy to apply to fine-grained particles (10 to 0.5 µm in size), so EBSD was conducted directly on particle surfaces, which is problematic because of the variable background scattering.

Table 2. Overview on the samples used in this study, their origin, mineral phases present (identified using EMP and ICP AES see also Table 4), and their sample preparation.

Sample name	Mineral phase	Origin	Sample preparation	Treatments
6F97x2.4	TM8	synthetic	polished section	no coating, colloidal silica polishing (± 0.03µm)
6F92x0.15	TM16 + Hilm42	synthetic	polished section	no coating, colloidal silica polishing (± 0.03µm)
6F72x2.4	TM63 + Hilm76	synthetic	polished section	no coating, colloidal silica polishing (± 0.03µm)
GM	Mt	Green Mill, Maryland, USA	polished section	no coating, colloidal silica polishing (± 0.03µm)
GeoB 6308-4, 625cm	TM, Hilm	Argentine basin, South Atlantic	polished section, embedded particles	mechanically polished to 1 µm finish, carbon coating,
GeoB 4313-2, 160cm	TM, Hilm, Mt	Mid Atlantic Ridge, Central Atlantic	non-embedded loose particles	carbon coating, no polish

3.2 Synthetic Fe-Ti Oxides from the Fe-Ti-O system (polished sections)

Three polycrystalline samples were synthesised at 1300°C in the Fe-Ti-O system, a single phase Fe-rich TM (sample 6F97x2.4) and two TM-Hilm assemblage with intermediate Fe-compositions (sample 6F92x0.15 and 6F72x2.4; Tables 2 and 3). The starting materials for the syntheses were mixtures of Fe_2O_3 (99.9%; Alpha Products) and TiO_2 (99.9%; Aldrich Chemical Comp. Inc.) which were weighed, ground and mixed in an agate mortar under acetone and after drying pressed into pellets. The pellets were fired for 24 hours at 1300°C, that is under sub-solidus conditions in a vertical furnace flowed with a CO/CO_2 gas mixture to control the oxygen fugacity (cf. Deines *et al*. 1974). The synthesis experiments were terminated by drop-quenching into water. More details about the synthesis are given in Lattard *et al.* (2005). All run products were characterised by XRD, SEM and EMP investigations. They consist of polycrystalline, roughly equigranular aggregates, with a mean grain-size between 10 and 50 µm. The modal proportions and the chemical compositions of the Fe-Ti oxide phases within the synthetic samples are given in Table 3. In the two-phase samples (6F92x0.15 and 6F72x2.4) both TM and Hilm have very homogeneous chemical compositions within the crystals and over the whole sample pellet. In the single-phase run product (6F97x2.4), the titanomagnetite crystals have a constant composition in the central part of the pellet (TM8; see Tables 2 and 3), but are slightly richer in Ti within the 200 µm outer zone of the pellet. EBSD measurements have been performed only on crystals from the central part of the pellet. EBSD specimens were small chunks of run products, approximately 2 to 3 mm in diameter, which were embedded in epoxy resin, sectioned and polished.

3.3 Natural Magnetite (polished section)

A sample for testing the EBSD technique on pure Mt was prepared from a greenschist with mm-sized octahedral Mt

single crystals (Martín-Hernández *et al*. 2006), originating from Green Mill (GM), (Maryland, USA; Dekkers, pers. comm.). ICP-AES analyses (method described by Riedinger *et al.* 2005) of theses natural Mt single crystals revealed minor concentrations of Al, Ca, K, Mg and Mn (see Table 4), corresponding to 0.67% non-Fe cations. Ca and K originate most likely from very minor amounts of coatings of the Mt single crystals by surrounding matrix minerals. A standard polished section was prepared (see section 2.2).

3.4 Natural Fe-Ti Oxides (polished section of embedded loose magnetic particles)

For further assessment of the EBSD technique, magnetic particles originating from hemipelagic sediment were chosen. The sediment gravity core GeoB 6229-6 was retrieved from the western Argentine Basin (South Atlantic) during *RV Meteor* cruise M46/2 (Schulz *et al*. 2001). The sediment of 655 cm core depth is characterised by high hydrogen sulphide concentrations in the pore water released by anaerobic oxidation of methane between 4 and 6 meters depth causing diagenetic alteration of reactive iron phases (Riedinger *et al*. 2005). Due to this reducing chemical environment, Fe-Ti oxides, such as TM and Hilm, are dominant in the magnetic assemblage since they are more resistant to dissolution than pure Fe oxides (for example Karlin & Levi 1983; Canfield & Berner 1987; Karlin 1990a, 1990b; Canfield *et al*. 1992). Magnetic mineral grains from this core the section was ground down until grains were exposed at the polished surface. The depth were collected by magnetic extraction (after Petersen *et al.* 1986) and embedded in epoxy resin. After hardening, resulting polished section (Table 2) was coated with carbon for SEM analysis (Garming *et al*. 2005), subsequently EBSD was performed.

3.5 Natural Non-Embedded Sample (consisting of loose magnetic particles)

The fourth sample originated from pelagic sediments of the central Equatorial Atlantic, from gravity core GeoB 4313-2 (Fischer *et al*. 1998). Magnetic extracts (after Dekkers 1988) of the chosen sample (130 cm core depth; Table 2) contained Fe- and Fe-Ti oxides from different sources, such as detritus of the Amazon river, submarine basalt weathering products of Mid-Atlantic Ridge material or eolian dust input from the Sahelian Zone (Funk *et al*. 2004a, 2004b; Franke *et al*. unpubl. data). The preparation of this sample varied from standard EBSD sample preparation. Polished sections only succeed if the single grains are numerous and big enough (≥ 100 µm). Here, the material of interest was available only in very limited quantities and the small grain-size down to a few nm created problems for embedding and polishing. Hence, we tested the EBSD method directly on the non-embedded magnetic grains, which gave reasonable EBSPs considering the non-flat surface topography of the crystals. The extracted material was dispersed in propanol and a drop of this solution was applied to a carbon sticker previously stuck onto the top of a standard SEM stub. After fluid evaporation, the sample was carbon coated.

Table 3. Modal proportions and chemical compositions of the synthetic Fe-Ti oxide phases, results from electron microprobe analyses, vol.% are means over n image analyses, x(Usp) and y(Ilm) are means over N analyses, References: (1) Engelmann *et al.* (unpubl. data); (2) Lattard *et al.* 2005.

			Modal proportions					Chemical compositions					
				TM		Hilm		TM			Hilm		
Sample	Ref.	Phases	n	vol.%	s	vol.%	s	N	x(Usp)	s	N	y(Ilm)	s
6F97x2.4	1	TM	4	100				10	0.083	0.002			
6F92x0.15	2	TM+Hilm	6	86	2	14	2	10	0.161	0.002	10	0.419	0.002
6F72x2.4	1	TM+Hilm	6	79	3	21	3	10	0.628	0.003	10	0.764	0.003

Table 4. Geochemical ICP AES analysis results of magnetite single crystal sample GM (for details concerning the experimental conditions see also *http://www.geochemie.uni-bremen.de*)

(Sub)sample	Al (g/kg)	Ca (g/kg)	Fe (g/kg)	K (g/kg)	Mg (g/kg)	Mn (g/kg)	Ti (g/kg)
GM 1	0.70	1.10	663.0	0.10	0.50	1.00	2.50
GM 2	0.40	0.10	698.0	0.00	0.40	0.70	0.70
Mean	0.55	0.60	680.5	0.05	0.45	0.85	1.60

4. Results

4.1 Discrimination between Titanomagnetite and Hemoilmenite

As shown in Fig. 3, the two mineral phases TM and Hilm present in the synthetic sample 6F92x0.15 can be well discriminated with standard BSE imaging (Fig. 3a) or from their EDS element spectra (Figs 3c and 3d). The reason is that in the simple Fe-Ti-O system TM has always much higher Fe/Ti ratios than the coexisting Hilm (for example Buddington & Lindsley 1964; Lattard *et al*. 2005). Consequently, the intensity ratios of the characteristic Fe K_α and Ti K_α lines are significantly different in the EDS spectra of the respective phases. In standard BSE images, the TM phases display a lighter grey level which reflects the higher mean Z number of this phase compared to that

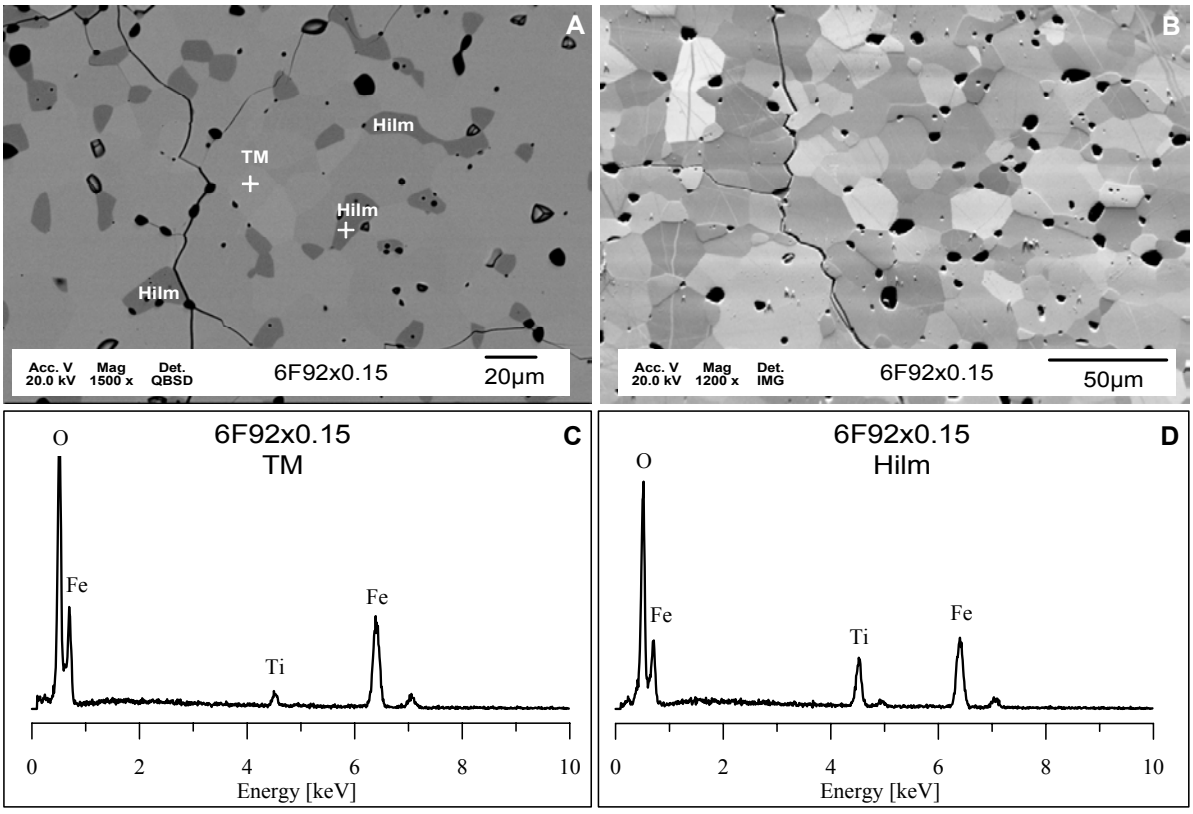

Figure 3. SEM images and EDS element spectrum of two-phase synthetic sample 6F92x0.15 containing 86 vol.% of titanomagnetite (TM16) and a relative small amount (~14 vol.%) of Hilm. (A) Backscatter electron micrograph of part of the sample, obtained on the polished sample surface perpendicular to the electron beam. The grey tones reflect the different chemical compositions of the two phases, with lighter areas corresponding to TM (richer in Fe) and darker areas corresponding to Hilm (poorer in Fe). Black spots and lines are pores and cracks in the sample. (□) Orientation contrast image of forescatter electrons of another part of the same sample surface. The different grey levels show the different orientation of the individual grains. (C) EDS spectrum of the TM phase from the spot marked in A. (D) EDS spectrum of the Hilm phase from the spot marked in A.

imaging of forescatter electrons (Cloete *et al*. 1999) shows the varying orientations of the grains, which have no preferred alignment. In these images, however, TM and Hilm cannot be discriminated (Fig. 3b).Figure 4 shows typical EBSPs acqui-red on both mineral phases of the syn-thetic sample 6F92x0.15. The observed EBSPs from TM grains clearly show spinel pattern (Fig. 4a), those acquired from Hilm grains have rhombohedral patterns (Fig. 4b). Figure 4c shows that the TM solution matches the geometry and width of all observed diffraction bands in the EBSP of Figure 4a. There is no Hilm pattern sol-

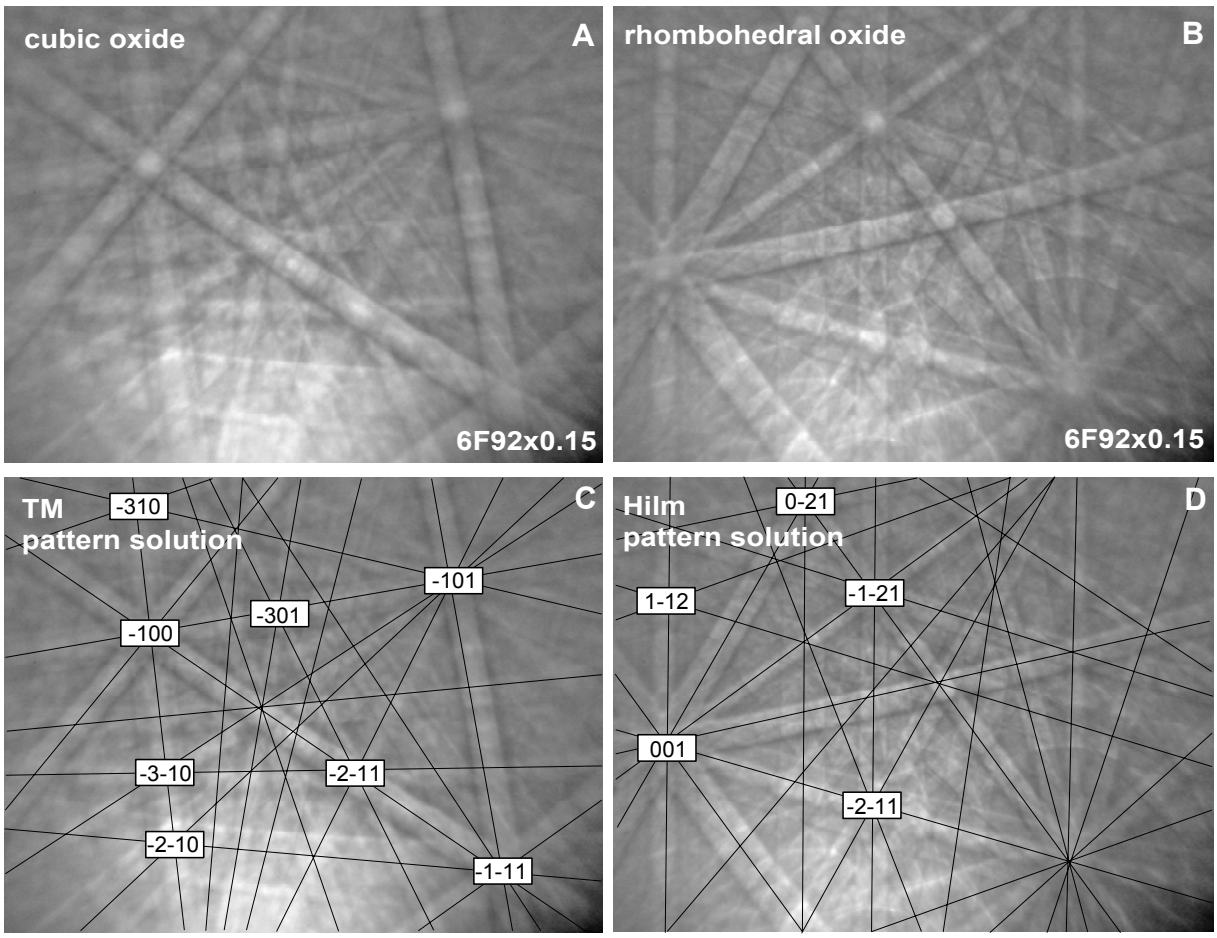

Figure 4. (A) EBSP obtained from the TM phase in the two-phase synthetic sample 6F92x0.15. (B) EBSP obtained from the Hilm phase from the same sample. (C) Indexed EBSP solution of the TM phase. (D) Indexed EBSP solution of the Hilm.

ution, that matches all of the bands in this EBSP. The same applies vice versa for Figure 4d. An indexed solution is acceptable when all observed bands are matched by the solution and the MAD of the detected and calculated bands is within a few degrees.

Figure 5 shows two magnetic Fe-Ti oxide particles, extracted from the marine sediment sample from core GeoB 6229-6 (655 cm), and their respective EDS spectra. The relatively large grains (20 to 35 µm in diameter) contain visible exsolution lamellae in submicron scale. In the grains the TM matrix is either partly or completely dissolved by reductive diagenesis. (compare particle 1 and particle 2). The EDS spectrum of particle 1 (Fig. 5c) was taken from the inner part of the grain, where the mineral matrix seems less dissolved. The element spectrum suggests TM as matrix phase because of the high Fe/Ti intensity ratio (somewhat lower than that of TM16 in sample 6F92x0.15, see Fig 3c). It is clear, however, that the lamellae contribute to

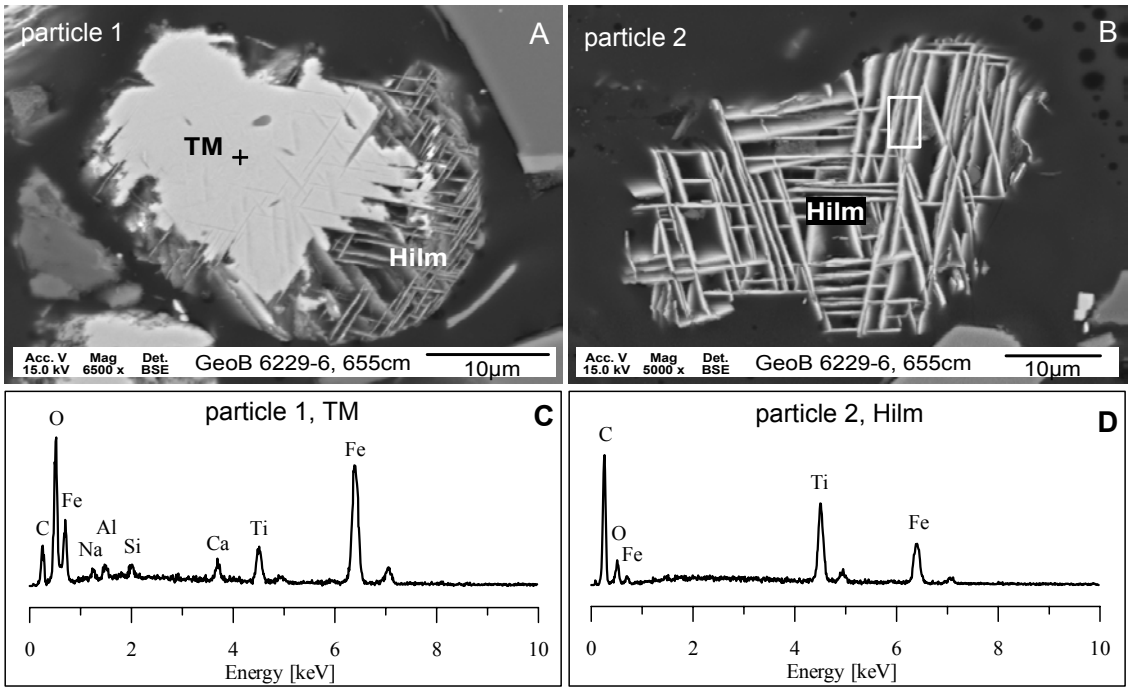

Figure 5. SEM images and EDS element spectra of natural sample GeoB 6229-6, 655 cm, (A) Backscatter electron micrograph of a TM grain (particle 1) with Hilm lamellae (dark background is due to the epoxy resin). The grain experienced partial low-temperature reduction in its sedimentary environment, showing a porous region of thin lamellae and a solid matrix region, in which fine-scale lamellae are also present. Exsolution features within the grain are relicts from former high-temperature oxidation processes in the source rock. (B) Backscatter electron micrograph of Hilm lamellae (particle 2), showing a more advanced stage of reductive diagenesis. (C) EDS spectrum of the spot marked in the TM matrix in particle 1, note that the small amounts of Na, Al, Si, and Ca might be due to minor substitutions or inclusions, C is due to the carbon coating. (D) EDS spectrum of the selected Hilm area marked in particle 2, C is due to the carbon coating.

the EDS signal because they are present in the excitation volume of the electron beam. Since the TM matrix is completely dissolved in particle 2, an EDS analysis could be performed on a small selected area on the residual lamellae, providing an average element spectrum with a low Fe/Ti intensity ratio, which is typical for Hilm (Fig. 5d). However, only the EBSD analysis of both particles gave unambiguous crystallographic evidence of the presence of both, TM and Hilm. Figure 6 shows the observed EBSPs of the Fe-rich matrix phase (Fig. 6a) and the Ti-rich exsolution lamellae (Fig. 6b). Presumably due to the carbon coating, the obtained EBSPs were weaker than from the non coated synthetic samples. Indexing of the observed EBSPs yielded a spinel (TM) pattern solution for the matrix phase and a rhombohedral (Hilm) pattern solution for the lamellae.

4.2 Discrimination between Spinel Phases

The presence of Ti in the Fe-Ti oxides produces subtle changes in the relative intensities of some diffraction bands, because different elements have different scattering properties. As an example Figure 7 shows the effect of Ti-content on the calculated relative intensity of {3-3-5} and {0-4-12} diffraction bands of the pattern solution from the data base. With increasing Ti-content the calculated relative intensity of the {3-3-5} and {0-4-12} bands changes with relative intensities in the range of 8 to 10% of the intensity of the strongest diffraction band. It is important to note that these intensities are calculated from the kinematic (single scattering) theory of electron diffraction. As strong multiple scattering occurs during electron diffraction the actual intensities in observed patterns may deviate significantly from the values calculated from the ki-

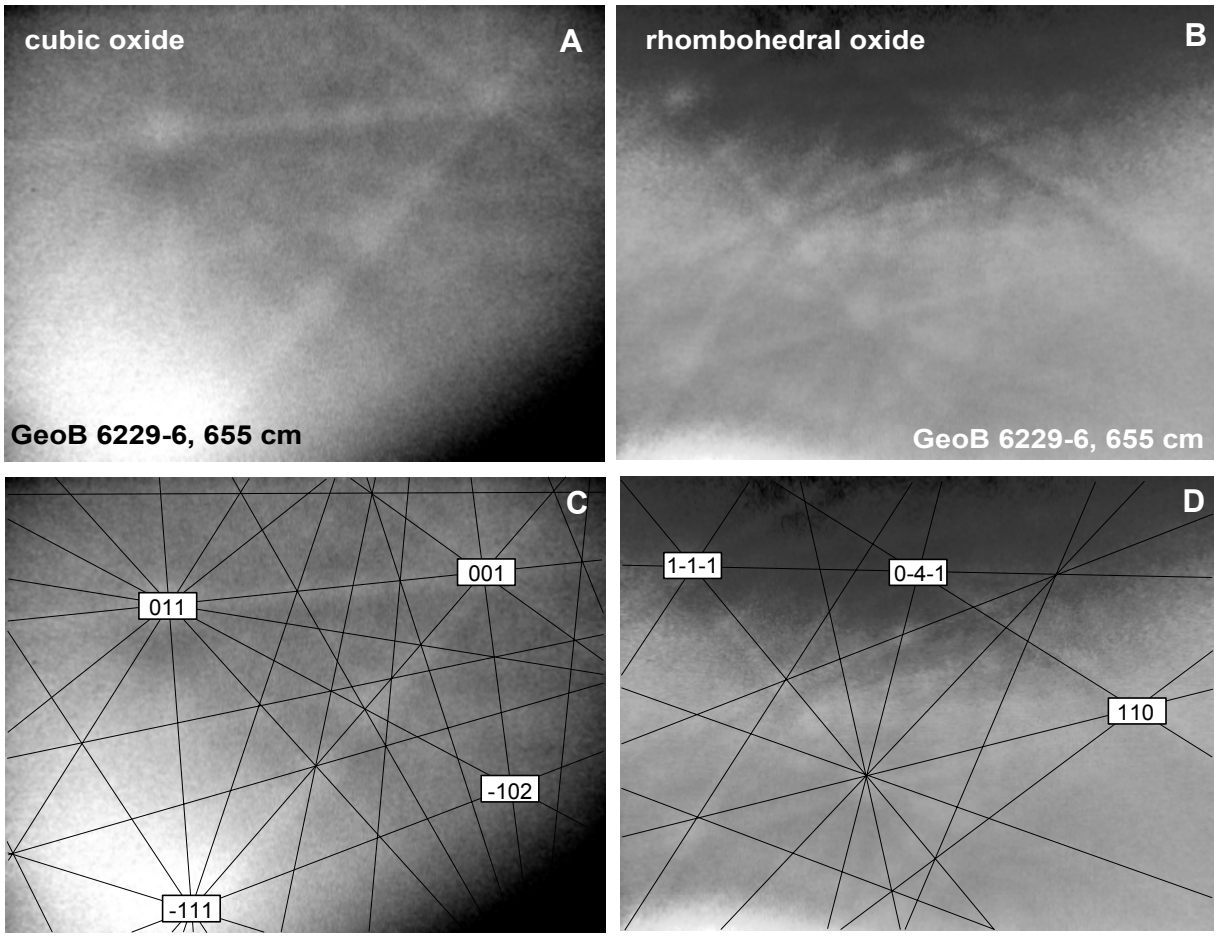

Figure 6. (A) EBSP obtained from the TM matrix phase of particle 1 from the same location as the EDS spectrum (see Fig. 5). (B) EBSP obtained from the lamellae of particle 2 from the same area as the EDS spectrum (see Fig. 5). (C) Indexed EBSP solution for TM. (D) Indexed EBSP solution for Hilm.

nematic theory. These calculated differences are quite small and affect low intensity bands, so very high quality EBSPs would be needed to detect such subtle changes.

Figure 8 shows examples of the EBSPs obtained from Mt and TM. The phases can clearly be distinguished from the EDS spectra (Figs 8c and 8d) yet the EBSPs can be indexed either as Mt or TM. The indexed solution of the 80 strongest diffraction bands (Figs 8e to 8h) does show differences in the presence or absence of some weak diffraction bands but inspection of the patterns in Figures 8a and 8b shows that these weak bands can not be observed, so these patterns can not be used to distinguish between Mt and TM.

The changes in relative diffraction band intensity with Ti content may also produce subtle differences in the geometry of intersecting band edges around the zone axis, similar to the changes observed in convergent beam electron diffraction patterns (CBED) in transmission electron microscopy. We suggest that EBSPs may be used in some limited cases to distinguish between phases with similar structure but different composition, however, this needs to be demonstrated by further work.

4.3 Non-embedded Particle Sample

As already mentioned in section 2.2 to 2.3, the quality of the sample and a sufficient background correction significantly influence the quality of the observed EBSP. Usually the material under study is prepared as a polished section to provide an ideal flat analytical surface. We tested the application of EBSD on non-embedded particles. The individual grains in sample GeoB 4313-2, 130 cm are randomly oriented and dis-

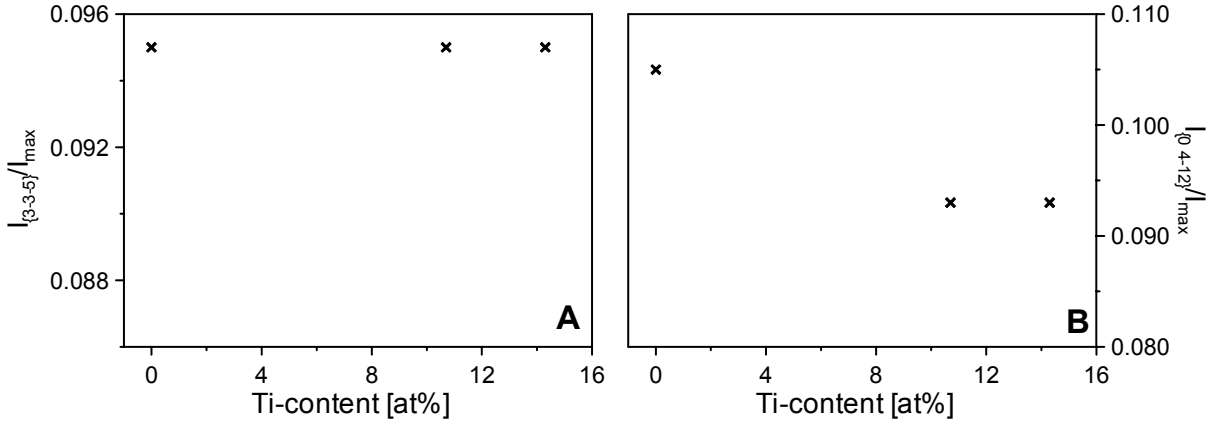

Figure 7. (A) Plot of the ratio of the relative intensity of the {3-3-5} diffraction bands over the total intensity of the brightest diffraction band in titanomagnetites vs. their Ti-content. (B) Analogous plot of the ratio of the relative intensity of the {0-4-12} diffraction bands over the total intensity of the brightest diffraction band. Data originates from the 'American Mineralogic database'. The chemical compositions of the titanomagnetites are given in Table 1.

persed on the SEM stub (Fig. 9a). Therefore they have a significant topography. Nevertheless, it was possible to obtain EBSPs from regions at the edges of flat grain surfaces (Fig. 9b). For successful EBSD, the planes of the crystals/grains have to be oriented towards the EBSD detector (see Fig. 2). Due to the random distribution of the particles, this condition is statistically fulfilled for a certain number of grains. To obtain EBSPs from differently oriented particles, the sample has to be aligned respectively by rotating the sample stage so that the particle surface is in a favourable orienttation for an EBSP to be obtained.

A reasonable background correction has to be provided to obtain EBSPs from the non-embedded particles (here we used the background signal acquired from the synthetic samples; see also section 2.3). The obtained EBSPs were weaker compared to those from the polished sections (Fig. 9c). We assume that this is partly caused by the non-ideal detection of the signal due to the enhanced scattering by the non-flat surface, and partly due to the fact that the sample had to be carbon coated to prevent surface charging. Weaker EBSPs were also obtained from the polished section of sample GeoB 6229-6, 655 cm, providing a flat but carbon coated surface. The quality of the obtained EBSPs from both natural marine particle samples is comparable and therefore we conclude that the weaker signal is mostly due to the carbon coating than to the non-ideal sample surface of the non-embedded particles. Nevertheless, the obtained diffraction patterns were straightforward for indexing with the *HKL* software, because they contained the main bands, which were required for the mineral identification. The best fit for a pattern solution was found for a Ti-poor TM (Fig. 9d). This result is in total agreement with the fact that the particle is obviously an euhedral TM crystal, easy to complete by its specific shape and EDS spectra (Fig. 9e). This particle deals as an example, of course grains of less obvious shape can be identified by the same procedure as well.

5. Discussion and Perspectives

Our results show that EBSD is a reliable tool to discriminate between magnetic spinel and rhombohedral Fe-Ti oxides. This is particularly helpful in combination with EDS analyses. In case of submicron size, single EDS information is often not sufficient enough to identify the mineral phases for certain. The plausible explanation is the very close chemical compositions of the mineral phases and the limited spatial resolution of the EDS. In this study we have obtained meaningful EBSPs from magnetite, titanomagnetite

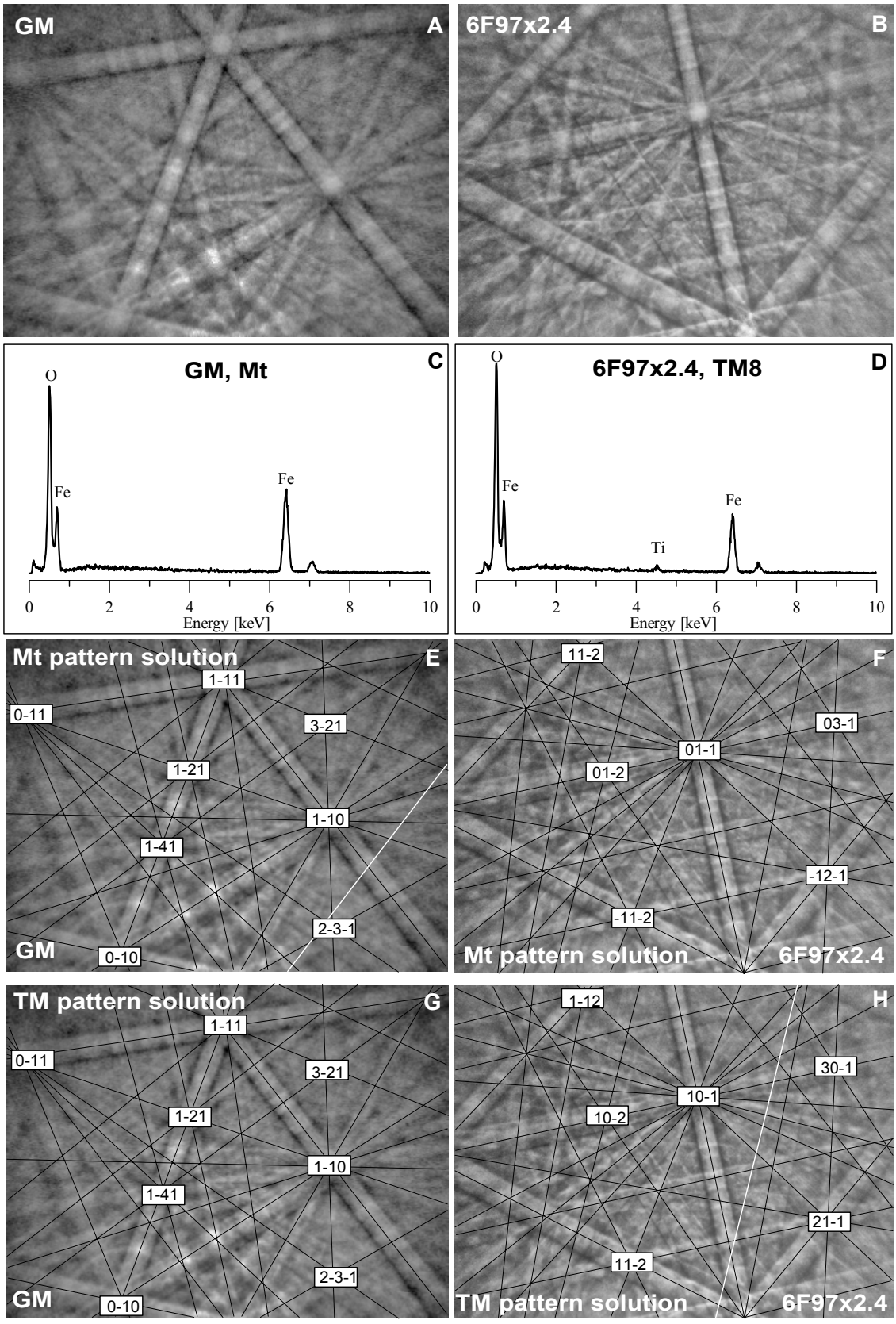

Figure 8. (A) EBSP obtained from sample GM. (B) EBSP obtained from sample 6F97x2.4. (C) representative EDS spectrum of sample GM, confirming the absence of Ti in the element spectrum, the very minor amount of Ti (compare Table 3) is not detectable with EDS. (D) representative EDS spectrum of sample 6F97x2.4, confirming the presence of Ti in the element spectrum. (E) Mt pattern solution for GM, showing the {0-4-12} diffraction band (white line). (F) Mt pattern solution for sample 6F97x2.4, the {3-3-5} diffraction band is absent. (G) TM pattern solution for sample GM, the {0-4-12} diffraction band is absent. (H) TM pattern solution for sample 6F97x2.4, showing the presence of the {3-3-5} diffraction band (white line).

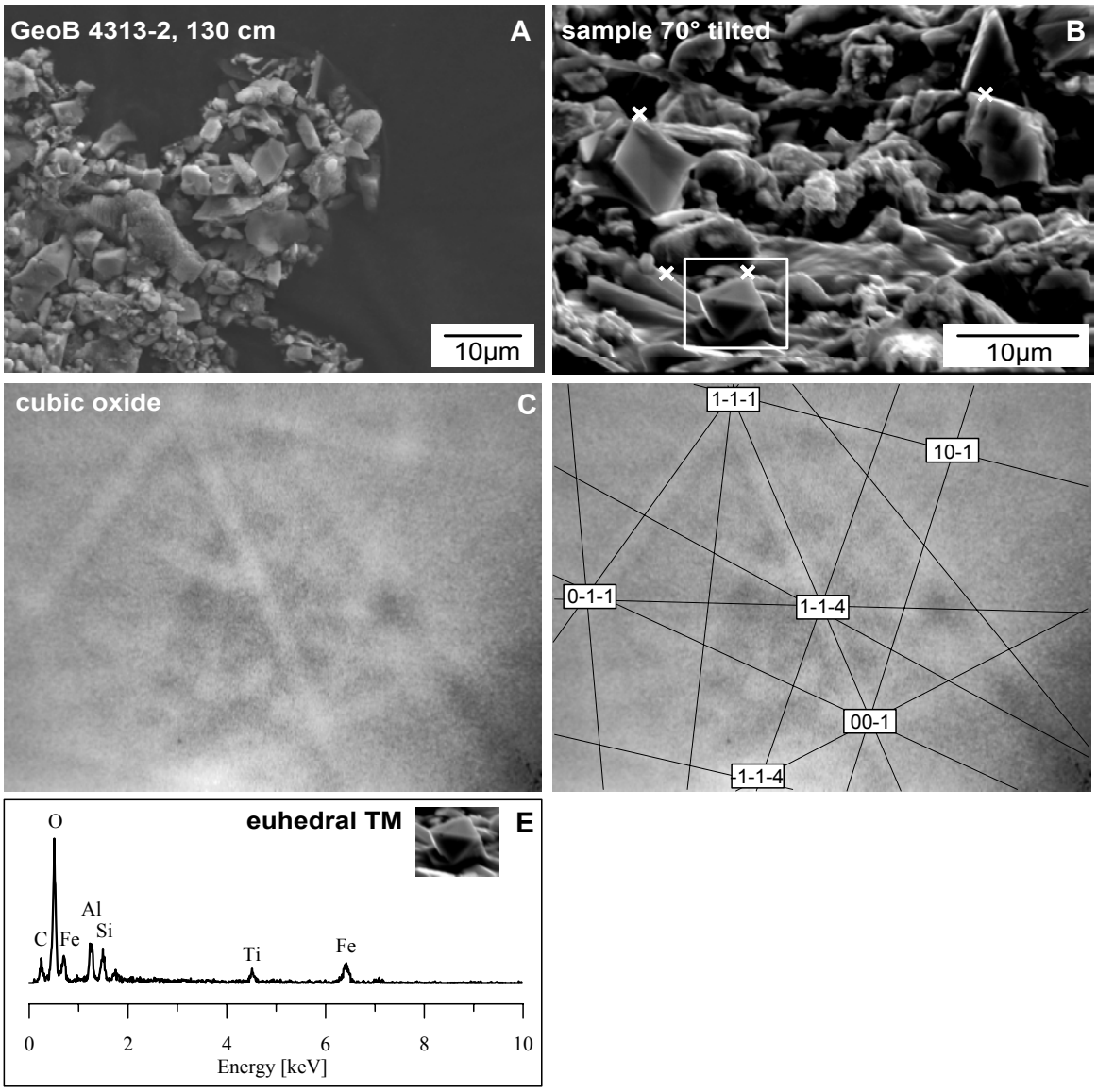

Figure 9. (A) Backscatter electron micrograph overview on the non-tilted and non-embedded particles in sample GeoB 4313-2, 130 cm, carbon coated. (B) Backscatter electron micrograph of the 70°tilted sample surface, EBSD signals could be obtained from marked areas (white cross symbols). (C) EBSP obtained from the euhedral TM crystal. (D) Indexed TM pattern solution of the euhedral crystal. (E) EDS spectrum of the euhedral TM crystal, note that the small amounts of Al and Si, might be due to clay mineral coating of the grain, C is due to the carbon coating.

and hemoilmenite grains in the range of 50 to 1 µm. The analysed Hilm lamellae are even beyond µm-size in width (~500 nm). In principle grains as small as 200 nm can be analysed by EBSD using a FEG scanning electron microscope (Ohfuji *et al*. 2005). For the analysis of smaller magnetic oxide particles TEM diffraction and analysis techniques should be used.

The mineralogical identification of chemically similar Fe-Ti oxide phases using EBSD is important for the interpretation of ambiguous rock magnetic data, for example in identifying exsolution features or paragenesis of different mineral phases, such as in sample GeoB 6229-6, 655 cm. Low-temperature rock magnetic analysis provided a strong indication of a Hilm mineral phase being present in the TM grains of that sample (Garming *et al.* in rev.). Figure 5 shows TM particles, which are most probably derived from the Paraná volcanic province (Garming *et al.* 2005). The intergrowth between TM matrix and Hilm lamellae results from high temperature oxidation. After deposition in

the marine environment, these particles experienced reducing conditions (Riedinger *et al*. 2005). The particles therefore evidently underwent strong reduction during diagenesis resulting in dissolution of the Fe-rich matrix phase (Garming *et al*. 2005). The intergrown Hilm lamellae were obviously more resistant to the Fe reduction. In Figure 5b the original TM matrix has been entirely dissolved and only the Hilm lamellae were left. Both Fe-Ti oxide phases were clearly identified by their EBSD pattern solutions (Fig. 6). Usually the identification of different mineral phases of close chemical compositions within a grain is very difficult. Here a systematical check of EDS and EBSD can provide valuable additional information.

We showed that sample preparation is crucial for the quality of the observed EBSP. The most suitable sample preparation for EBSD and EDS is a well polished section without any additional (carbon) coating. Sometimes, surface charging effects are too strong and a thin carbon coating has to be applied to the polished section, especially when the grain-size is very fine and a manual silver paint coating around the particles is not practical. In samples with a limited abundance of material and very fine (submicron) grain-sizes the EBSD method can also be applied to non-embedded loose particles. This might be suitable for extracts from marine sediments, loess, or anthropogenic samples. In this type of samples different spinel and rhombohedral oxides can be distinguished by EBSD, but the patterns might be too weak to distinguish between for example different spinel phases such as Mt and TM. Additional EDS analysis should be used in combination with EBSD to discriminate between Mt and TM or between Hmt and Ilm grains.

So far, we tested the EBSD technique on a variety of magnetic Fe-Ti oxides. Most likely the application to the most common magnetic sulphides, such as greigite (43 at.% Fe; 57 at.% S) and pyrrhotite (47 at.% Fe; 53 at.% S) should lead to improved discrimination between these compositionally fairly close mineral phases. In marine sediment samples, these magnetic mineral phases are rather fine grained and not always straightforward to identify only by EDS analysis. Sometimes grains occur in different distinguishable morphologies (Roberts & Weaver 2005), but often their grain-sizes are rather just at the edge of the SEM resolution. Additionally, greigite (cubic) and pyrrhotite (monoclinic) are precursors to pyrite and therefore they can occur sequentially next to each other in very similar grain-size distributions and sedimentary settings. So far, EBSD textural and deformation studies have been carried out on micron- to submicron-sized natural pyrite crystals (for example Boyle *et al*. 1998; Freitag *et al*. 2004; Ohfuji *et al*. 2005).

Acknowledgements
The electron microscopy studies were conducted at Electron Microscopy Utrecht (EMU), we thank Pim van Maurik and Hans Meeldijk for their support with the SEM (and EBSD) work. We thank Siska Valke and Otto Stiekema from Utrecht University who supplied valuable help in sample preparation. ICP AES analysis was kindly provided by the Marine Geochemisty group, University of Bremen, we thank in particular Silvana Hessler and Karsten Ennekin. We also owe thanks to the members of the Marine Geophysics group (University of Bremen) and the Paleomagnetic group (Utrecht University) for their support and advice. Financial support of CF was provided by the DFG through the European Graduate College EUROPROX, (Universities of Bremen and Utrecht) and by NWO through the VMSG, Vening Meinesz Research School of Geodynamics (Utrecht University). This investigation is also associated to the Research Center Ocean Margins (RCOM) at the University of Bremen.

References

Baba-Kishi, K.Z., 2002. Electron backscatter Kikuchi diffraction in the scanning electron microscope for crystallographic analysis, *J. Mater. Sci*., **37**, 1715-1746.

Blake, R.L., Hessevick, R.E., Zoltai, T. & Finger, L.W., 1966. Refinement of the hematite structure, *Am. Mineral*., **51**, 123-129.

Boyle, A.P., Prior, D.J., Banham, M.H. & Timms, N.E., 1998. Plastic deformation of metamorphic pyrite: new evidence from electron-back-scatter diffraction and forescatter orientation-contrast imaging, *Mineralium Deposita*, **34**, 71-81.

Buddington, A.F. & Lindsley, D.H., 1964. Iron-titanium oxide minerals and synthetic equivalents, *J. Petrol*., **5**, 310-357.

Canfield, D.E. & Berner, R.A., 1987. Dissolution and pyritization of mag-netite in anoxic marine sediments, *Geochim. Cosmochim. Acta*, **51**, 645-659.

Canfield, D.E., Raiswell, R. & Bottrell, S., 1992. The reactivity of sedimentary iron minerals towards sulfide. *Am. J. Sci*., **292**, 659-683.

Cloete, M., Hart, R.J., Schmid, H.K., Drury, M.R., Demanet, C.M., & Sankar, K.V., 1999. Charaterization of magnetite particles in shocked quartz by means of electron- and magnetic force microscopy: Vredefort, South Africa, *Contrib. Mineral. Petrol.*, **137**, 232-245.

Collyer, S., Grimes, N.W., Vaughan, D.J. & Longworth, G., 1988. Studies of the crystal structure and crystal chemistry of titanomaghemite, *Am. Mineral*., **73**, 153-160.

Day, A., 1993. *Developments in the EBSP Technique and their Application to Grain Imaging*. Ph.D. thesis, University of Bristol, Bristol, 156 p.

Day, A. & Quested, T.E., 1999. A com-parison of grain imaging using HOCI, COCI, EBSD and optical methods, *J. Microscopy*, **195**, 186-196.

Deines, P., Nafziger, R.H., Ulmer, G.C. & Woermann, E.. 1974. Temperature-oxygen fugacity tables for selected gas mixtures in the system C-H-O at one atmosphere total pressure. *Bull. Earth Min. Sci. Exp*., **88**, 129 p.

Dekkers, M.J., 1988. *Some roc kmagnetic parameters for natural goethite, pyrrhotite and fine-grained hematite*, Geologica Ultraiectina, **51**, Ph.D. thesis, Utrecht University, 231 p.

Dingley, D.J., 1984. Diffraction from sub-micron areas using electron back-scattering in a scanning electron microscope, *Scanning Electron Micr-scopy*, **2**, 569-575.

Dunlop, D.J. & Özdemir, Ö., 1997. *Rock magnetism, fundamentals and frontiers*, Cambridge University Press, 573 p.

Feinberg, J.M., Wenk, H.-R., Renne, P.R. & Scott, G.R., 2004. Epiaxial relationship of clinopyroxene-hosted magnetite determined using electron backscatter diffraction (EBSD) technique, *Am. Mineral*., **89**, 462-466.

Fischer, G. & cruise participants, 1998. Report and preliminary results of Meteor cruise M38/1, Las Palmas – Recife, 25.1.-1.3.1997, *Ber. Fachber. Geowiss. Univ. Bremen*, **94**, 178 p.

Freitag, K., Boyle, A.P. & Nelson, E., 2004. The use of electron backscatter diffraction and orientation contrast imaging as tools fro sulphide textural studies: examples from the Greens Creek deposit (Alaska), *Mineralium Deposita*, **39**, 103-113.

Funk, J., von Dobeneck, T. & Reitz, A., 2004. Integrated rock magnetic and geochemical quantification of redoxomorphic iron mineral diagenesis in Late Quaternary sediments from the Equatorial Atlantic, in *The South Atlantic in the Late Quaternary: Reconstruction of Material Budget and Current Systems,* pp. 237-260, eds Wefer, G., Mulitza, S. & Ratmeyer, V., Springer-Verlag, Heidelberg, Berlin, New York.

Fynn, G.W. & Powell, W.J.A., 1979. *The cutting and polishing of electro-optic materials*, Adams Hilger, London, 216 p.

Garming, J.F.L., Bleil, U. & Riedinger N., 2005. Alteration of magnetic mineralogy at the sulphate-methane transition: analysis of sediments from the Argentine continental slope, *Phys. Earth Planet. Inter*., **151**, 290-308.

Garming J.F.L., Bleil, U., Franke, C. & von Dobeneck, T., 2006. Low-temperature partial magnetic self-reversal in marine sediments, *Geophys. J. Int.*, in rev.

Goldstein, J.I., Newbury, D.E., Echlin, P., Joy, D.C., Romig, A.D. Jr., Lyman, C.E., Fiori, C. & Lifshin, E., 1992. *Scanning electron microscopy and X-Ray microanalysis*, 2nd edition, 820 p., Plenum Press., New York.

Henrich, R. & cruise participants, 1994. Report and preliminary results of Meteor cruise M29/3, Rio de Janeiro - Las Palmas 11.8. - 5.9.1994. *Ber. Fachber. Geowiss. Univ. Bremen*, **60**, 155 p.

Humphreys, F.J., Huang Y., Brough, I. & Harris, C., 1999. Electron backscatter diffraction of grain and subgrain structures – Resolution considerations, *J. Microscopy*, **195**, 212-216.

Humphreys, F.J., 2001. Grain and subgrain charaterisation by electron backscatter diffraction, *J. Mater. Sci*., **36**, 3833-3854.

Humphreys, F.J., 2004. Characterisation of fine-scale microstructures by electron backscatter diffraction (EBSD), *Scripta Materialia*, **51**, 771-776.

Karlin, R. & Levi, S., 1983. Diagenesis of magnetic minerals in recent haemi-pelagic sediments, *Nature*, **303**, 327-330.

Karlin, R., 1990a. Magnetite diagenesis in marine sediments from the Oregon continental margin, *J. Geophys. Res*., **95**, 4405-4419.

Karlin, R., 1990b. Magnetic mineral diagenesis in suboxic sediments at Bettis site W-N, NE Pacific Ocean, *J. Geophys. Res*., **95**, 4421-4436.

Kumar, M., Schwartz, A.J. & King, W.E., 2001. Correlating observations of deformation microstructures by TEM and automated EBSD techniques, *Mater. Sci. Eng*., **A309-310**, 78-81.

Lattard, D., Sauerzapf, U. & Käsemann, M., 2005. New calibration data for the Fe-Ti oxide thermo-oxybarometers from experiments in the Fe-Ti-O system at 1 bar, 1,000-1,300°C and a large range of oxygen fugacities, *Contrib. Mineral Petrol*., **149**, 735-754.

Lindley, H.W., 1926. *Mikrographie der Eisenerzmineralien oberhessischer Basalte*, N. Jb. Min. Geol. Paläont., **53**, 324 p.

Lloyd, G.E., 1985. Review of instrumentation, techniques and applications of SEM in mineralo*gy,* in *Applications of electron microscopy in Earth Sciences*, pp. 151-188, ed. White, J. C., Min. Ass. of Canada short courses, **11.**

Lloyd, G.E., Schmidt, N.H., Mainprice, D. & Prior, D.J., 1991. Crystallographic textures. *Mineralogical Magazine*, **55**, 331-345.

Martín-Hernández, F., Bominaar-Silkens, I. ,Dekkers, M.J. & Maan, J.K., 2006. High-field cantilever torque magnetomery as a tool for single cry-stal magnetocrystalline anisotropy determinations, *Tectonophysics*, **418**, 21-30.

Ohfuji, H., Boyle, A.P., Prior, D.J. & Rickard, D., 2005. Structure of framboidal pyrite: An electron back-scatter diffraction study, *Am. Mineral*., **90**, 1693-1704.

O'Reilly, W., 1984. *Rock and mineral magnetism*, Blackie, Glasgow, London, 220 p.

Petersen, N., Eisenach, P. & Bleil, U., 1979. Low temperature alteration of the magnetic minerals in ocean floor basalts, in *Deep Drilling Results in the Atlantic Ocean: Ocean Crust*, pp. 169-209, eds Talwani, M., Harrison, C.G. & Hayes, D.E., Maurice Ewing Series 2, AGU, Washington D.C.

Petersen, H., von Dobeneck, T. & Vali, H., 1986. Fossil bacterial magnetite in deep-sea sediments from the South Atlantic Ocean, *Nature*, **320**, 611-615.

Prior, D.J., Boyle, A.P., Brenker, F., Cheadle, M.C., Day, A., Lopez, G., Peruzzo, L., Potts, G.J., Reddy, S., Spiess, R., Timms, N.E., Trimby, P., Wheeler, J. & Zetterström, L., 1999. The application of electron backscatter diffraction and orientation contrast imaging in the SEM to textural problems in rocks, *Am. Mineral*., **84**, 1741-1750.

Ramdohr, P., 1955. *Die Erzmineralien und ihre Verwachsungen*, Akademie Verlag, Berlin, 875 p.

Randle, V. & Engler, O., 2000. *Introduction to Texture Analysis: Macrotexture, Microtexture and Orientation Mapping*, Gordon and Breach, London, 408 p.

Riedinger, N., Pfeifer, K., Kasten, S., Garming, J.F.L., Vogt, C. & Hensen, C., 2005. Diagenetic alteration of magnetic signals by anaerobic oxidation of methane related to a change in sedimentation rate, *Geochim. Cosmochim. Acta*, **69**, 4117-4126.

Roberts, A.P. & Weaver, R., 2005. Multiple mechanisms of remagnetization involving sedimentary greigite (Fe3S4), *Earth Planet. Sci. Lett*., **231**, 263-277.

Schulz, H.D. & cruise participants, 2001. Report and preliminary results of Meteors Cruise M46/2, Recife (Brazil) – Montevideo (Uruguay), December 2 – December 29, 1999, *Ber. Fachber. Geowiss. Univ. Bremen*, **174**, 107 p.

Shau, Y.-H., Torii, M., Horng, C.-S. & Peacor, D.R., 2000. Subsolidus evolution and alteration of titano-magnetite in ocean ridge basalts from Deep Sea Drilling Project/Ocean Drilling Program Hole 504B, Leg 83: Implications for the timing of magnetization, *J. Geophys. Res*., **105**, 23635-23649.

Waychunas, G.A., 1991. Crystal chemistry of oxides and oxyhydroxides, in *Oxide minerals: Petrologic and magnetic significance*, pp. 11-68, ed. Lindsley, D.H., Reviews in Mineralogy, **25**, Mineral. Soc. Am.

Wechsler, B.A. & Prewitt, C.T., 1984. Crystal structure of ilmenite ($FeTiO_3$) at high temperature and at high pressure, *Am. Mineral*., **69**, 176-185.

Wechsler, B.A., Lindsley, D.H. & Prewitt, C.T., 1984. Crystal structure and cation distribution in titanomagnetites ($Fe_{3-x}Ti_xO_4$), *Am. Mineral*., **69**, 754-770.

Wilkenson, A.J. & Hirsch, P.B., 1997. Electron diffraction based techniques in scanning electron microscopy of bulk materials, *Micron*., **28**, 279-308.

Xu, W., Van der Voo, R. & Peacor, D.R., 1994. Are magnetite spherules capable of carrying stable magnetizations?, *Geophys. Res. Lett*., **21**, 517-520.

Xu, W., Peacor, D.R., Van der Voo, R., Dollase, W. & Beaubouef, R., 1996. Modified lattice parameter/Curie temperature diagrams for titanomag-netite/titanomaghetite within the qua-drilateral Fe_3O_4-Fe_2TiO_4-Fe_2O_3-Fe_2TiO_5, *Geophys. Res. Lett.*, **23**, 2811-2814.

Xu, W., Geissman, J.W., Van der Voo, R. & Peacor, D.R., 1997a. Electron microscopy of iron oxides and implications for the origin of magnetizations and rock magnetic properties of Banded Series rocks of the Stillwater Complex, Montana, *J Geophys, Res.*, **102**, B6, 12139-12157.

Xu, W., Van der Voo, R., Peacor, D.R. & Beaubouef, R.T., 1997b. Alteration and dis-

solution of fine-grained magnetite and ist effects on magnetization of the ocean floor, *Earth Planet. Sci. Lett*., **151**, 279-288.

Zhou, W., Van der Voo, R. & Peacor, D.R., 1997. Single-domain and superparamagentic titanomagnetite with variable Ti content in young ocean-floor basalts: No evidence for rapid alteration, *Earth Planet. Sci. Lett*., **150**, 353-362.

Zhou ,W., Van der Voo, R. & Peacor, D.R., 1999a. Preservation of pristine titanomagnetite in older ocean-floor basalts and its significance for paleointensity studies, *Geology*, **27**, 1043-1046.

Zhou, W., Peacor, D.R., Van der Voo, R. & Mansfield, J., 1999b. Determination of lattice parameter, oxidation state, and composition of individual titano-magnetite / titanomaghemite grains by TEM, *J. Geophys. Res*., **104**, 17689-17702.

Zhou, W., Van der Voo, R., Peacor, D.R., Wang, D. & Zhang, Y., 2001a. Low-temperature oxidation in MORB of titanomagnetite to titanomaghemite: A gradual process with implications for marine magnetic anomaly amplitudes, *J. Geophys. Res*., **106**, 6409-6421.

Zhou, W., Peacor, D.R., Alt, J.C., Van der Voo, R. & Kao, L.-S., 2001b. TEM study of the alteration of interstidal glass in MORB by inorganic processes, *Chem. Geol*., **174**, 365-376.

Chapter 5

Magnetic Petrology of Equatorial Atlantic Sediments: Electron Microscopic Findings and their Environmental Magnetic Implications

Summary

The magnetic micro- and nanoparticle inventories of marine sediments from Equatorial Atlantic sites were investigated by scanning and transmission electron microscopy in order to classify all present detrital and authigenic magnetic species and investigate their regional distribution, origin, transport and preservation. This information is used to establish source-to-sink relations and to constrain environmental magnetic proxy interpretations for this area.

Magnetic extracts were prepared for three supralysoclinal open ocean sediment cores located at the Ceará Rise (GeoB 1523-1), the Mid-Atlantic Ridge (GeoB 4313-2), and the Sierra Leone Rise (GeoB 2910-1) at depths corresponding to marine isotope stages 4 and 5.5. This selection represents characteristic glacial and interglacial conditions of western, central and eastern Equatorial Atlantic sedimentation and avoids inferences by sub-surface and anoxic processes. Crystallographic, elemental, morphological and granulometric data of more than two thousand magnetic particles were collected by electron microscopic analytics. On basis of these properties, nine particle classes could be defined: detrital magnetite, fragmental and euhedral titanomagnetite, titanomagnetite-hemolilmentite intergrowths, silicates with magnetic inclusions, microcristalline hematite, magnetite spherules, bacterial magnetite, goethite needles, and nanoparticle clusters. These particle species can be associated with fluvial, eolian, subaeric and submarine volcanic, biogenic or chemogenic sources and delineate large-scale sedimentation patterns: detrital magnetite is typical for Amazon discharge, fragmental titanomagnetite is a weathering product of mid-ocean ridge basalts, and titanomagnetite-hemoilmenite intergrowths are common magnetic particles in West African dust. This very clear regionalization underlines, that magnetic petrology is an excellent indicator of source-to-sink relations. Hematite encrustations, magnetic spherules and nanoparticle clusters were ubiquitous, while bacterial magnetite and authigenic hematite was only detected at the more oxic western site. At the eastern site surface pits and crevices were seen indicating subtle early diagenetic reductive dissolution.

These results enable us to derive some general implications for Environmental Magnetism. Paleoclimatic signatures of ‘magnetic grain-size’ parameters such as the ratio of anhysteretic and isothermal remanent magnetizations can be formed either by mixing of multiple sources with separate, relatively narrow grain-size ranges (Ceará Rise) or by variable sorting of a single source with a broad grain-size distribution (Sierra Leone Rise). Hematite, goethite and possibly ferrihydrite particles coexist and could have high-coercive or super-paramagnetic properties according to their partly ultra-fine grain-sizes. These two magnetic fractions are generally discussed as separate fractions, but could actually be genetically linked.

***Keywords**:* magnetic particles, electron microscopy, environmental magnetism, marine sediments, Equatorial Atlantic, magnetosomes, titanomagnetite, goethite, hematite.

This chapter is in preparation for submission to *Paleoceanography* as: Franke, C., von Dobeneck, T., Drury, M.R., Meeldijk, J.D. and Dekkers, M.J., Magnetic Petrology of Equatorial Atlantic Sediments: Electron Microscopic Findings and their Environmental Magnetic Implications.

1. Introduction

In the past decades, paleo- and environmental magnetism have contributed significantly to paleoclimatic and paleoceanographic research. Environmental magnetic methods, parameters and applications have been outlined in the textbooks by *Thompson and Oldfield* [1986], *Maher and Thompson* [1999] and *Evans and Heller* [2003] and reviews by *Lund and Karlin* [1990], *Oldfield* [1991], *King and Channell* [1991], *Verosub and Roberts* [1995], and *Dekkers* [1997].

Magnetic studies of marine sediments rely primarily on iron (hydr)oxide and sulfide minerals carrying a wealth of information: Their natural remanent magnetization helps to reconstruct paleofield history, plate tectonics and sediment age (e.g. *Channell et al.*, 2004). Their mineralogy and granulometry help to track sediment sources and transport pathways and to characterize depositional regimes and geochemical environments (e.g. *Frederichs et al.,* 1999). Magnetic proxies delineate past climates, ocean currents, and wind systems (e.g. *Roberts and Turner*, 1993; *deMenocal and Rind*, 1993; *Kissel et al.,* 1997). High-resolution rock magnetic records of marine sedimentary sequences can serve for stratigraphic correlation, orbital tuning and time series analyses (e.g. *von Dobeneck and Schmieder,* 1999).

Bulk magnetic measurements can detect and distinguish sedimentary magnetic minerals, their properties and concentration changes, but their specificity does not suffice to investigate magnetic petrology at the particle level. The current knowledge on genesis and distribution of magnetic mineral species in the marine realm as well as their environmental expression is far from complete; existing assumptions lack 'ground truth' in oceanic key regions (*Dunlop and Özdemir*, 1997).

To advance understanding regarding the regional character of magnetic petrology and proxy parameters, rock magnetic methods have been complemented by particle specific electron microscopic techniques. Scanning (SEM) and transmission (TEM) electron microscopic studies e.g. by *Smith* [1979], *Freeman* [1986], *Petersen et al.* [1986], *Petersen and Vali* [1987], *Vali et al.* [1989], *Roberts* [1995], *Hounslow and Maher* [1996], and *Rey et al.* [2005] described and distinguished numerous litho-, bio- and chemogenic of magnetic particle species by their characteristic compositions, shapes, and grain-sizes.

So far, such investigations have been mainly focused on specific sites and sources. This study takes the particle-oriented approach to a large heterogenic oceanic region, for which detailed environmental magnetic information is already available. The Equatorial Atlantic Ocean appears to be an ideal 'natural laboratory' for this purpose, since the area offers a broad range of climatically driven sedimentation processes accumulating desert dust, fluvial detritus, volcanic ashes, submarine weathering products and biogenic mineral precipitates, while a relatively mild oxic to suboxic milieu (Figure 1) promotes preservation of the primary magnetic mineral assemblage. This study employs SEM and TEM ana-lytics on magnetic and heavy liquid separates (Chapter 3) using electron backscatter diffraction (EBSD) techniques (Chapter 4) to classify magnetic carriers according to their mineralogy, morphology and granulometry. On basis of their characteristics and geographical distri-butions we develop genesis, source, trans-port and diagenesis issues and discuss implications for environmental magnetic proxy methods.

2. Environmental Magnetism in the Equatorial Atlantic

The Equatorial Atlantic is one of the world's geologically best studied open ocean regions, a natural 'marshaling yard' of water masses, heat, nutrient and sediments. Vast eolian fluxes from the North African deserts and savannahs are carried westwards by trade and monsoon winds and an equally important Amazonian sediment load is transported westwards by the North Equatorial Countercurrent. The complexity of marine con-

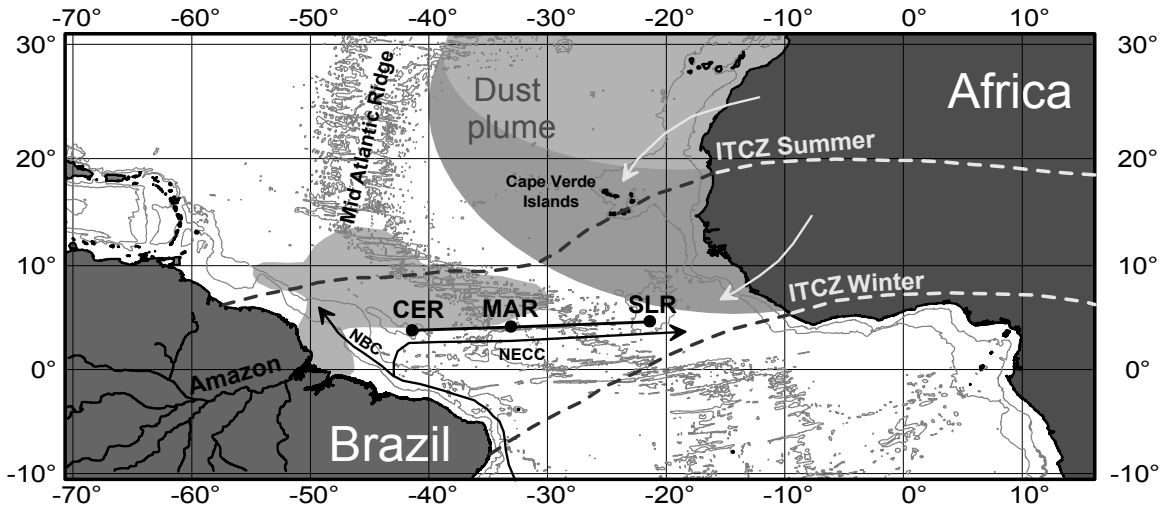

Figure 1. Study area in the Equatorial Atlantic Ocean with locations of the gravity cores at the Ceará Rise (CER = GeoB 1523-1), the Mid-Atlantic Ridge (MAR = GeoB 4313-2), and the Sierra Leone Rise (SLR = GeoB 2910-1) along the West-East profile at ~5°N. Coast lines (black) and Isobaths at 2000 and 4000 m (gray) are given according to *Intergovernmental Oceanographic Commission* [1994]. The average summer and winter positions of the Inter Tropical Convergence Zone (ITCZ) are given as dashed lines (modified after *Ruddiman,* 2001), white arrows mark the major wind directions of the respective areas and black arrows mark the major ocean currents for that area: NBC = North Brazil Current, NECC = North Equatorial Countercurrent. The dust plume from the North Africa is given for approximate summer (upper light grey shaded area) and winter (dark grey shaded area) distribution; the Amazon plume is schematized as lower left grey-checkered area.

ditions is further enhanced by atmospheric and oceanic frontal systems, the Intertropical Convergence (ITCZ) and the Equatorial Divergence Zone creating an equatorial belt of enhanced primary productivity. These interacting sedimentary processes, their glacial-interglacial cycles and early diagenetic consequences have been thoroughly described in the study of *Funk et al.* [2004a] on basis of rock magnetic and geochemical records of 16 Late Quaternary sediment gravity cores.

One of their findings regards the ocean-spanning cyclic variations of magnetic grain-size expressed by the so-called M_{ar}/M_{ir} ratio (Figure 2). Magnetic particles are on average coarser during glacials and finer during interglacials. In the oligotrophic north equatorial belt (5°N) these proxy records carry a mostly primary signature and correlate strongly with low-latitude $\delta^{18}O$ stack by *Bassinot et al.* [1994] lending themselves ideally to cyclostratigraphic purposes. *Funk et al.* observe a systematic West-East trend of magnetic grain-size variations, where the plateau-like glacial signal sections assume low, i.e. 'coarser' levels of 0.04 to 0.05. The interglacial maxima are well developed and reach their largest, thus 'finest' levels of about 0.10 in the western part (Ceará Rise = CER); they take increasingly lower values of 0.07 to 0.08 in the central (Mid-Atlantic Ridge = MAR) and eastern part (Sierra Leone Rise = SLR). The interglacial peaks strongly resemble respective $CaCO_3$ patterns marked by less intense trade winds and hence shallower nutricline and higher productivity in the West contrasted by reduced upwelling and lower productivity in the East. More important to the magnetic fraction, fluvial sediment influx in the West is diminished by higher sea levels and a therefore retreating Amazon plume. Interglacial eolian fluxes in the East are also reduced and finer due to northwards shifting dry winter monsoon and greater humidity in tropical Africa.

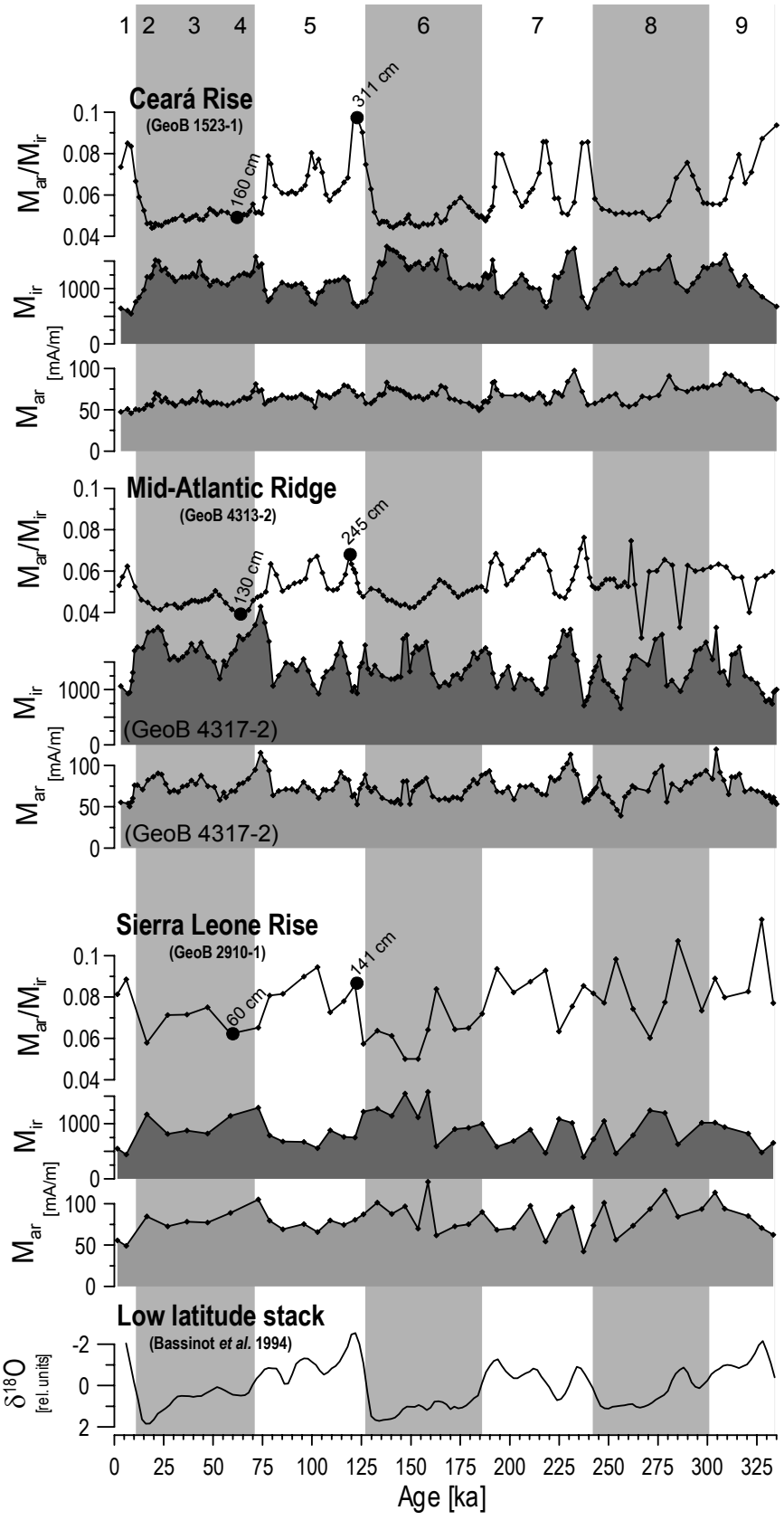

Figure 2. The magnetic grain-size index M_{ar}/M_{ir} (black curves) for the three chosen gravity cores exhibit a uniform signal signature along West-East profile with a high correlation to the $\delta^{18}O$ stack of *Bassinot et al.* [1994] (lowermost curve). Light gray filled curves show the compilation of the single rock magnetic parameters M_{ar} tracking fine-particle (SD) magnetite and dark gray curves show the M_{ir} estimating the total magnetite content (modified after *Funk et al*., 2004a).

Based on comparisons of the relative changes and correlations (Table 1) of the fine, so-called single-domain (SD) magnetic fraction represented by M_{ar} and the coarser, so-called pseudo-single-domain (PSD) and multi-domain (MD) fractions mirrored by M_{ir}, *Funk et al*. [2004a] claim that the increasing variance of fine magnetite and its correlation to coarse magnetite towards the eastern part imply, that the Saharan dust flux progressively contributes and modulates both, coarse and fine magnetite fractions. At the western side, only the coarse magnetite fraction of Amazonian origin shows noticeable climate control, while the fine magnetite fraction barely varies with time. These regional differences in sedimentation conditions and the low correlation of the magnetic SD particles to the climate controlled coarser detrital component in the West are not yet well understood.

In more general terms, these paradox observations raise the important issue, whether magneto-granulometric variations in the marine realm are primarily controlled by mixing of multiple sources with separate, relatively narrow grain-size ranges or rather by variable sorting of a single source with a broad grain-size distribution. *Von Dobeneck* [1998] and *Funk et al.* [2004a] speculate on basis of rock magnetic and statistical data, that the mixing of a relatively constant flux of fine, potentially bacterial magnetite with a sea-level controlled flux of coarser detrital Amazon magnetite may create the first scenario in the western part of the Equatorial Atlantic, while the second scenario is exemplified by a primarily terrigenous and wind-sorted magnetic mineral flux in the eastern part.

Previously, *Schmidt et al.* [1999] presented a comparative rock magnetic study of 194 Equatorial and South Atlantic surface samples extended by multivariate statistics. Their results suggest a reasonable geographical regionalization of magnetic properties in accordance with recent sedimentary regimes. The Equatorial Atlantic peaks out by exceptionally high hematite/magnetite ratios forming a tropical East-West belt at about 5°N. While many other South Atlantic regions show unique magnetic fingerprints, the Amazon and Saharan plumes carry relatively similar magnetic signatures. In a second analyses based exclusively on Equatorial Atlantic sediments and seven instead of five relational rock magnetic parameters (*Frederichs et al*., 1999), the Amazonian sediments differ from the Saharan by their higher paramagnetic mineral (e.g. clay) concentration and higher coercivity.

An environmental magnetic study of seven Western Equatorial sediment series from the CER by *Bleil and von Dobeneck* [2004] established a numerical mixing model discriminating Amazon and Saharan magnetite and hematite/goethite fluxes on basis of zonal accumulation rate gradients. They estimate from these calculations, that about 56% of the hematite, 84% of the magnetite and 79% of the total terrigenous fraction at the CER originate from the Amazon catchments, while the complementary part should be mostly of African origin.

Funk et al. [2004a, 2004b] and *Reitz et al.* [2004] investigated and quantified early diagenetic magnetic mineral dissolution in the Equatorial Atlantic on basis of new specific diagenesis proxies combining rock magnetic and geochemical properties. Over

Table 1. Interparametric Pearson's correlation coefficients (ρ) of the parameters ARM, IRM and HIRM along the West-East transect throughout the Equatorial Atlantic (modified after *Funk et al*., 2004a).

Parameter	**Ceará Rise** (GeoB 1523-1)	**Mid-Atlantic Ridge** (GeoB 4317-1)	**Sierra Leone Rise** (GeoB 2910-1)
ρ(HIRM, IRM)	0.74	0.84	0.90
ρ(ARM, IRM)	0.57	0.83	0.85

the investigated sediment depth range, they excluded important diagenetic influences at the CER site, but found partial magnetite depletion at the MAR and SLR sites within organically enriched layers coincident with cold Marine Isotope Stages (MIS) 6, 10 and 12. SEM micro-graphs of these layers show octahedral and framboidal pyrite aggregates, some with pit marks due partial re-oxidization.

Low-temperature (2 to 400 K) and high-field (5 and 7 T) magnetic remanence studies on dry bulk sediments, magnetic extracts and heavy liquid separates from the three previously mentioned Equatorial Atlantic sites at core positions corresponding to cold MIS 4 and warm MIS 5.5 were performed by the first author (Chapter 3). Zero-field cooled (ZFC) and field cooled (FC) remanent magnetization measurements show a slightly shifted Verwey transition at 110 K indicative of non-stoichiometric, slightly oxidized magnetite for the CER samples. This transition is less pronounced for the MAR samples and not detected for SLR samples (Figure 5 in Chapter 3). In case of the magnetic extracts, low-temperature cycling of the RT-SIRM clearly indicates magnetite for all samples. The heavy mineral fractions (Chapter 3, Figure 8) also show specific features of antiferromagnetic goethite and ferrihydrite as well as ferrimagnetic titanomagnetite (Tmt) and hemoilmenite (Hilm). A characteristic drop in in-field magnetization and zero-field remanence at 120°C indicates considerable amount of goethite in all samples. Hematite could not be detected by lack of diagnostic features in this temperature range.

In summary, the sedimentary regimes and bulk rock magnetic properties of the Equatorial Atlantic are well understood by now. Some assumptions and interpretations still need harder evidence, which can be made available by electron microscopic investigations. Especially for the quantification of the high coercivity components hematite and goethite, the existing data are still insufficient. The contribution of Tmt from weathered mid-ocean ridge basalts (MORB) has not been specified in the equatorial region, but has been described as the dominant magnetic oxide phase further south along the ridge (*Schmidt et al*., 1999). Little is known on the detailed magnetic petrology of the various detrital terrigenous phases, in particular about their morphologies, grain-size distributions, cation compositions, and lattice properties. As shown by fundamental mineral magnetic research (e.g. *Dunlop and Özdemir*, 1997), all these particle characteristics have influence on their magnetic properties. Without consideration of these factors, interpretations of environmental magnetic proxy records remain uncertain or are, in the worst case, misleading. In the positive sense, a better account on magnetic petrology can open new strategies for magnetic proxy development in complex oceanic environments.

3. Sample Selection

The depicted combination of semi-quantitative SEM and TEM studies and specialized rock magnetic analytics are time-consuming therefore only affordable for a small sample suite. Owing to the availability of numerous rock magnetic records and excellent age control in this region, it seemed possible to represent the major spatial and temporal environmental magnetic patterns by selecting just three key positions and two time slices. As for the preceding low-temperature magnetic study (Chapter 3) three Late Quaternary gravity cores (Figure 1) from the northernmost West-East transect of *Funk et al.* [2004a] were chosen all located on submarine heights above the carbonate lysocline: the Ceará Rise (CER, GeoB 1523-1, 3°49.9'N and 41°37.3'W, 3292 m water depth), the equatorial Mid-Atlantic Ridge (MAR, GeoB 4313-2, 4°02.8'N and 33°26.3'W, 3178 m water depth), and the Sierra Leone Rise (SLR, GeoB 2910-1, 4°50.7'N and 21°03.2'W, 2703 m water depth). These cores were recovered during German research vessel *Meteor* cruises M16/2 (*Schulz et al*., 1991),

M29/3 (*Henrich et al*., 1994), and M38/1 (*Fischer et al*., 1998) and dated by correlating their Ca records (*Funk et al.,* 2004a).

From each core, two samples were chosen to represent glacial and interglacial situations. To avoid possible biasing effects by subsurface processes (bioturbation by meiofauna and biomineralization by microfauna) and early diagenesis (reductive dissolution of ferric oxides and precipitation of sulfides) it was decided to systematically sample MIS 4 (glacial) and MIS 5.5 (interglacial), which are distant from both these gradient zones in every core. Sample depths are given in Figure 2. In the following, we will simply refer to these two time slices as 'glacial' and 'interglacial'. As stated earlier, the systematically lower M_{ar}/M_{ir} values during glacial periods indicate coarser magnetic mineral assemblages.

4. Electron Microscopy

For all electron microscopic analyses magnetic extracts were obtained from the wet bulk sediments using a *Frantz magnetic separator* using an extraction procedure of *Dekkers* [1988]. About 10 ml of the sediment were dispersed in demineralized water purged with nitrogen gas by ultra sonic agitation. Sodium polyphosphate [$Na_4 P_2 O_7 \cdot 10H_2O$] was added as a peptizing agent to keep the (clay-)mineral particles in dispersion. The resulting extracts were washed with demineralized water in three steps using a so-called 'magnetic finger' (*von Dobeneck et al.,* 1987) to purify the grains from remaining clay mineral coatings.

For SEM analyses of the microparticle fraction, a drop of the washed magnetic extract was applied onto a carbon sticker, previously stuck on a standard Al stub. A thin carbon coating of a few nm was applied on the dispersed magnetic particles after evaporation of the extraction fluid to prevent surface charging of the sample. Secondary electron (SE) and backscattered electron (BSE) imaging were used for visualizations and energy dispersive X-ray spectroscopy (EDS) for examination of the elemental composition (*Goldstein et al.,* 1992). All recorded elemental spectra were normalized to their respective oxygen maxima. For (semi-) quantification of the obtained elemental spectra, '*EDAX PhiRhoZ Quantification*' software was used. Electron backscattered diffraction (EBSD) yielded additional crystallographic information on the individual magnetic particles (e.g. *Prior et al.,* 1999). All SEM analyses were performed using a *FEI XL30 SFEG* at 12 to 15 kV acceleration voltage. For further instrumental SEM settings, especially concerning the EBSD technique see also Chapter 4.

Systematic grain counting of some few hundreds of the µm-sized particles per sample was performed on the SEM specimens to estimate the abundance of each particle type. These grains were distinguished by their morphology and cation element contents. Crystallographic identification was performed as a spot check on some representative particles.

TEM analyses of the nanoparticle fraction were performed on magnetic extracts. To remove adhering clay mineral coatings, 0.5 ml of the magnetic extracts (in demineralized water) were mixed with 0.25 ml of 0.1 molar ethylenedinitrilotetraacetic acid (EDTA) solution [$C_{10}H_{14}N_2Na_2O_8 \cdot 2\,H_2O$] in a small centrifuge vessel and agitated in an ultra sonic bath for 2 minutes. This mild chemical treatment binds the clay minerals to the EDTA solution and purifies the surfaces of the magnetic particles, but does not alter magnetic particles (*Köster et al.,* 1973). Cleaning techniques by *Mehra and Jackson* [1960] and *Thiel* [1963] can dissolve ferric iron oxide minerals. After mixing and agitation, the solution was centrifuged in a *Eppendorf 5415 C* (centrifuge diameter = 15 cm) for 10 minutes at 14000 rpm. The supernatant (consisting of the EDTA and clay mineral mix) was removed and the concentrate (consisting of the purified magnetic extract) was refilled with 100 µl

of demineralized water. Since the magnetic fraction consists of heavy minerals and the EDTA-clay-solution appears to have a much smaller density, the centrifuging acts as a sort of density separation. After a second agitation in the ultra sonic bath for another 2 minutes to disperse the magnetic concentrate, a discharged carbon coated TEM copper grid was dipped into the extract and subsequently dried in air.

For all TEM analyses a *FEI Tecnai 20 FEG* transmission electron microscope was used at an acceleration voltage of 200 kV in bright field mode, at high resolution (HRTEM), or for recording electron diffraction patterns. In scanning TEM (STEM) mode images were taken using a high angle annular dark field detector (HAADF). Elemental compositions were estimated using energy dispersive spectroscopy (EDS). All shown elemental spectra were normalized to their respective oxygen maxima.

5. Magnetic Particle Classification

SEM and TEM analyses cover separate grain-size ranges and have to be combined to cover the full spectrum from coarse MD (larger than ca. 1 to 10 µm) and PSD (ca. 100 nm to 10 µm) down to SD (ca. 30 to 100 nm) and SP (ca. 1-30 nm) particles. The used SEM instrument resolves grains in the range of a few hundred µm down to a few hundred nm that will be referred to as 'microparticles'. The submicron size range resolved only by TEM is termed 'nanoparticles'. Some particle species such as magnetite fragments, spherules, and Tmt octahedrons are represented in both size fractions, while others like magnetofossils and goethite needles are solely present in the finer fraction. Semi-quantitative grain counts of the dispersed SEM samples yield estimates of the relative abundances of all observed magnetic particle species at the three investigated sites and two time slices (Table 2a).

In the following, we will describe each microscopically distinguishable magnetic species proceeding from coarser to finer grain-size ranges. The electron micrographs have been compiled separately for SEM and TEM. As individual magnetic particle species are frequently associated on single images, it was decided to group the micrographs site-wise from West to East. To avoid repetitious presentations of widely distributed species at every site, we present most types for the westernmost CER site (Figures 4 and 7), where particle preservation is best. For the subsequent sites MAR (Figures 5 and 8) and SLR (Figures 6 and 9), we only show additional symptomatic or diverging observations.

5.1. Detrital Magnetite

One of the most common components present in all samples is detrital magnetite (Mt) (Figures 4a-1, 5a-2, 5b-2, 5b-4, 6a-1, 8b), most likely in various oxidation (maghemitization) states. It occurs in all grain-size ranges from tens of nm to tens of microns corresponding to magnetic domain states from SP to MD (*Butler and Banerjee,* 1975). Detrital Mt grains of terrigenous origin have typically irregular fragmental shapes and knobby, weathered surfaces (e.g. *Freeman*, 1986). They are often coated with clay minerals or encrusted with specular hematite. Only anhedral to subeuhedral forms occur; euhedral crystals were not observed. According to EDS spectra, detrital Mt typically shows minor cation substitutions by the accessory elements Al, Mg and Mn, while Ti was not detected (*Hounslow et al.*, 1995). Si and Al peaks in the spectra relate to the adhering silicates. The worn shapes and surface reflect distant fluvial transport. Pitted or creviced grains document partial reductive magnetite dissolution under suboxic conditions.

Detrital Mt predominates at the western CER site, where it accounts for some 80% of the microparticle fraction. A climate dependence as suggested by rock magnetic data could not be confirmed. However, much lower relative detrital Mt contents of 20-10% at the MAR and SRL

Table 2a. Results of SEM (semi-)quantitative grain counting for the main individual particle components comprising relative amounts of the individual magnetic components, N gives the total number of counted grains.

Sample	Detr. Mt [%]	Diss. Part. [%]	Tmt [%]	Euhedral Tmt [%]	eolian Tmt/Hilm [%]	Spherules [%]	Silicates [%]	other [%]	N
CER glacial	80.3	1.0	8.8	5.0	0.2	0.2	0.7	3.8	408
CER interglacial	75.4	3.8	3.8	6.9	2.3	1.5	3.8	2.3	398
MAR glacial	10.4	8.3	56.3	8.3	2.1	4.2	4.2	4.2	375
MAR interglacial	23.8	7.1	52.4	4.8	2.4	2.4	4.8	2.4	410
SLR glacial	12.7	9.0	36.6	7.5	23.9	6.7	1.5	2.2	363
SLR interglacial	13.6	9.1	24.2	1.5	12.1	6.1	31.8	1.5	390

Table 2b. Results from EDS elemental composition quantification of Tmt ($Fe_{3-x}Ti_xO_4$) and Hilm ($Fe_{2-y}Ti_yO_3$) mineral phases, 'mean TM' and 'mean Hilm' values correspond to the theoretical, average value of all individual quantified compositions, the total amount of Ti-bearing phases is calculated from Table 2a, summarizing the Tmt, euhedral Tmt, and eolian Tmt/Hilm amounts.

Sample	TM Range	mean TM	Hilm Range	mean Hilm	Total amount of Ti-bearing phases [%]
CER glacial	TM3 to TM60	26.8	Hilm45 to Hilm82	56.9	14.0
CER interglacial	TM5 to TM66	28.6	-	58.3	13.0
MAR glacial	TM6 to TM58	23.2	Hilm47 to Hilm96	68.0	66.7
MAR interglacial	TM3 to TM67	31.1	Hilm50 to Hilm83	66.2	59.6
SLR glacial	TM6 to TM50	30.8	Hilm48 to Hilm91	64.2	68.0
SLR interglacial	TM20 to TM65	47.5	Hilm47 to Hilm73	59.5	26.8

sites delineate a marked decline towards the East indicating that this species originates mostly from the Amazon and other South American rivers draining the crystalline hinterland of the South American continent. Dissolution features are most prominent at the organic-richer eastern SLR site (see Figure 6a-1), but are also seen in a milder form at the MAR.

5.2. Fragmental and Euhedral Titanomagnetite

Fragmental titanomagnetite (Tmt) particles are also among the most frequent magnetic particles (Figures 4c-2, 5b-5, 5b-7, 9d-4). They are typically confined by smooth, conchoidal fracture surfaces and have sharp, curved edges. These fractured surfaces were described as 'shrinkage cracks' (*Johnson and Hall,* 1978) caused by submarine low-temperature oxidation of MORB-type Tmt (*Petersen et al.,* 1978); some of the particles are cracked themselves. Their size limits range from tens to tenths of microns and are delimited by the characteristic stress-related average crack distance (*Petersen and Vali*, 1987). From a rock magnetic viewpoint (*Day et al.,* 1977) this size range coincides with SD to PSD domain states (*Vlag et al.*, 1996). According to the semi-quantitative EDS spectra, the Ti content of these particles can reach from 1 to 20% corresponding to a (fresh) Tmt composition of TM3 to TM60 (Figure 3). Averaged over many individual Tmt grains, the mean composition of all sites corresponds approximately to TM30 (Table 2b), which is somewhat lower than to be expected for MORB lithology.

Besides fragmental forms, euhedral Tmt crystals with typical octahedral spinel-type shapes (e.g. *Petersen et al.,* 1978) are found (Figures 4d-4, 6d-5, 8a-1 to 5, 9c-3). They have approximately the

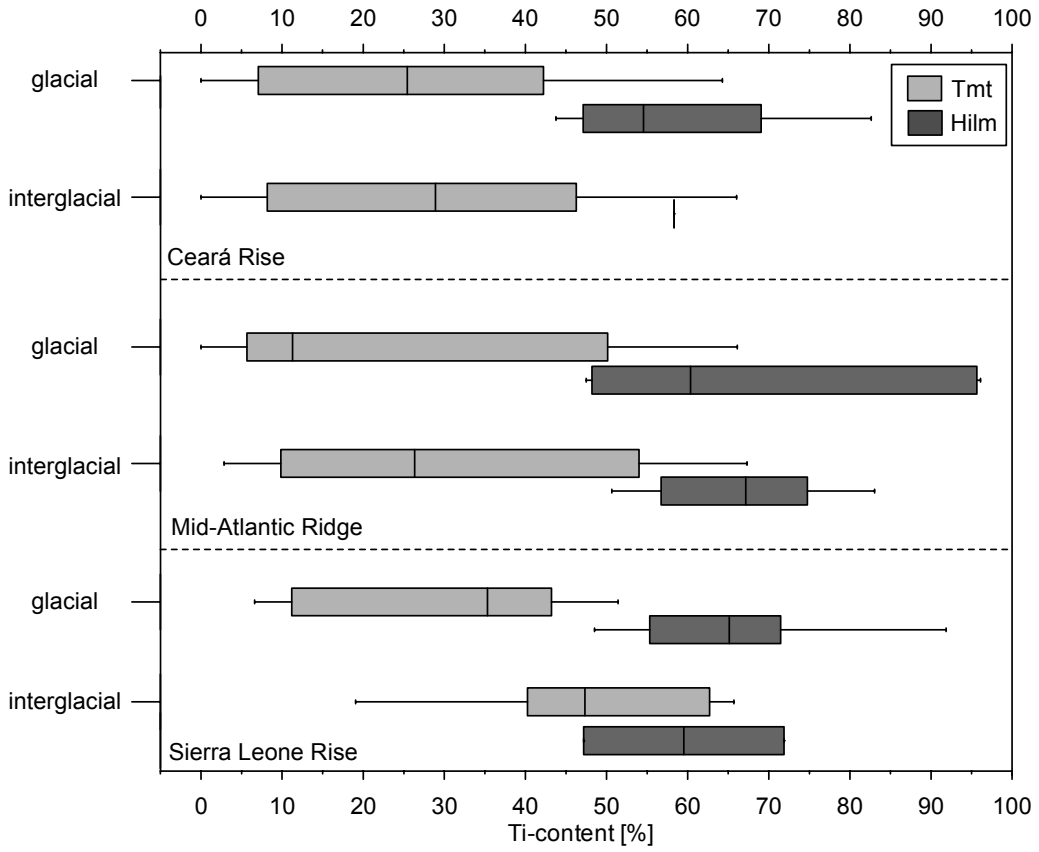

Figure 3. Box-and-whisker-plot for the (semi-)quantification and distribution of the Ti-content in the present Tmt (light gray) and Hilm (dark gray) mineral grains resulting from the elemental dispersive spectroscopy spectra obtained in scanning electron microscopy. Given are the total range, the quartile range, and the median for all identified phases sample-wise.

same composition as the irregular Tmt grains, but may have crystallized under different conditions. The absence of grain rounding or other mechanical transport marks at the CER and MAR sites hint at a proximal basaltic source. In the eastern SLR site, rounded as well as partially dissolved Tmt octahedral were found.

From West to East, fragmental and euhedral Tmt makes up some 10-15% of all microparticles by number at the CER, 60-70% near the MAR, and 25-40% at the SLR showing a strong enhancement towards areas with outcropping crystal rocks. The ratio of fragments and octahedra varies highly along the transect; both shapes occur in nearly equal numbers at the CER, while the octahedral variety represents only one tenth at MAR and one fifth at the SLR. This distinct distribution pattern opens the question, if octahedral Tmt crystals may not have a different origin, for example as former inclusion and submarine halmyrolysis products of larger volcanic or metamorphic silicate rock fragments (e.g. cloudy feldspars).

5.3. Silicates with Magnetic Inclusions

Non-magnetic grains such as detrital blocky feldspar, angular quartz or other weathered silicates were frequently found in the extracts. These silicates extend over the broadest grain-size spectrum among all identified components in the extracts, including the coarsest grains of a few hundred µm down to very fine particles of some ten nm. The compositional range of these non-magnetic host-rocks is equally widespread. Si, O and Al as major elements are accompanied by minor contributions of Na, Mg, Ca, K, S, P, Ti, Mn, Fe and Cr traces. Fe and Ti are frequently the leading minor component. It therefore plausible, that these silicate grains contain submicron magnetic inclusions in form of SD to PSD sized Fe-Ti oxides. Such composites have been found and described in various oceanic sedimentary environments, e.g. in SW Pacific backarc basins (*Vali et al.*, 1989), at Indian Ocean ridges (*Hounslow and Maher*, 1996), and Argentine continental margin (*Garming et al.*, 2005). The contingent of the silicates varies between about 1 to 5% and does not show any particular trend along the West-East transect except in case of the interglacial sample from the SLR, where silicate grains make up ~30% of the magnetic extracts.

5.4. Titanomagnetite-Hemoilmenite Intergrowths

The third major magnetic component are titanomagnetite-hemoilmenite (Tmt-Hilm) particles of angular fractured shape with relatively smooth surfaces (Figures 5a-1, 5a-3, 5b-1, 5b-6, 6a-2, 6b-3, 6c-4, 9c-2), which are frequently intergrown. The intergrowth textures are seen as intersecting ‘exsolution lamellae’ or banded ‘tiger stripes’ (*Carmichael*, 1961). The widths of the lamellae vary from a few microns to submicron. These features are known to originate from high-temperature exsolution, a process occurring during slow cooling of magmatic melt, where thermodynamically instable Ti-rich Tmt separates into a Ti-poor Tmt phase and a Ti-rich Hilm phase (*Buddington and Lindsley*, 1964).

These anhedral to subeuhedral particles were observed in all grain-size ranges from tens of nm to tens of microns (*Hounslow et al.*, 1995; *McEnroe et al.,* 2002). Because of the lamellar character of the ferrimagnetic Tmt phase, the effective magnetic grain-size should be considerably finer than the particle size (*Butler*, 1992). The detrital grains are often partially or entirely covered by specular hematite coatings. The semi-quantitative element analyses (Table 2b, Figure 3) indicate a hemoilmenite compositions between Hilm45 to near the endmember ilmenite (Hilm96) in paragenesis with Tmt phases of reciprocal compositions. Ti-rich Tmt and Hilm crystals were distinguished by a combination of the EDS and EBSD techniques (Chapter 4).

The nearly ‘pure’ Ilm grains are rather

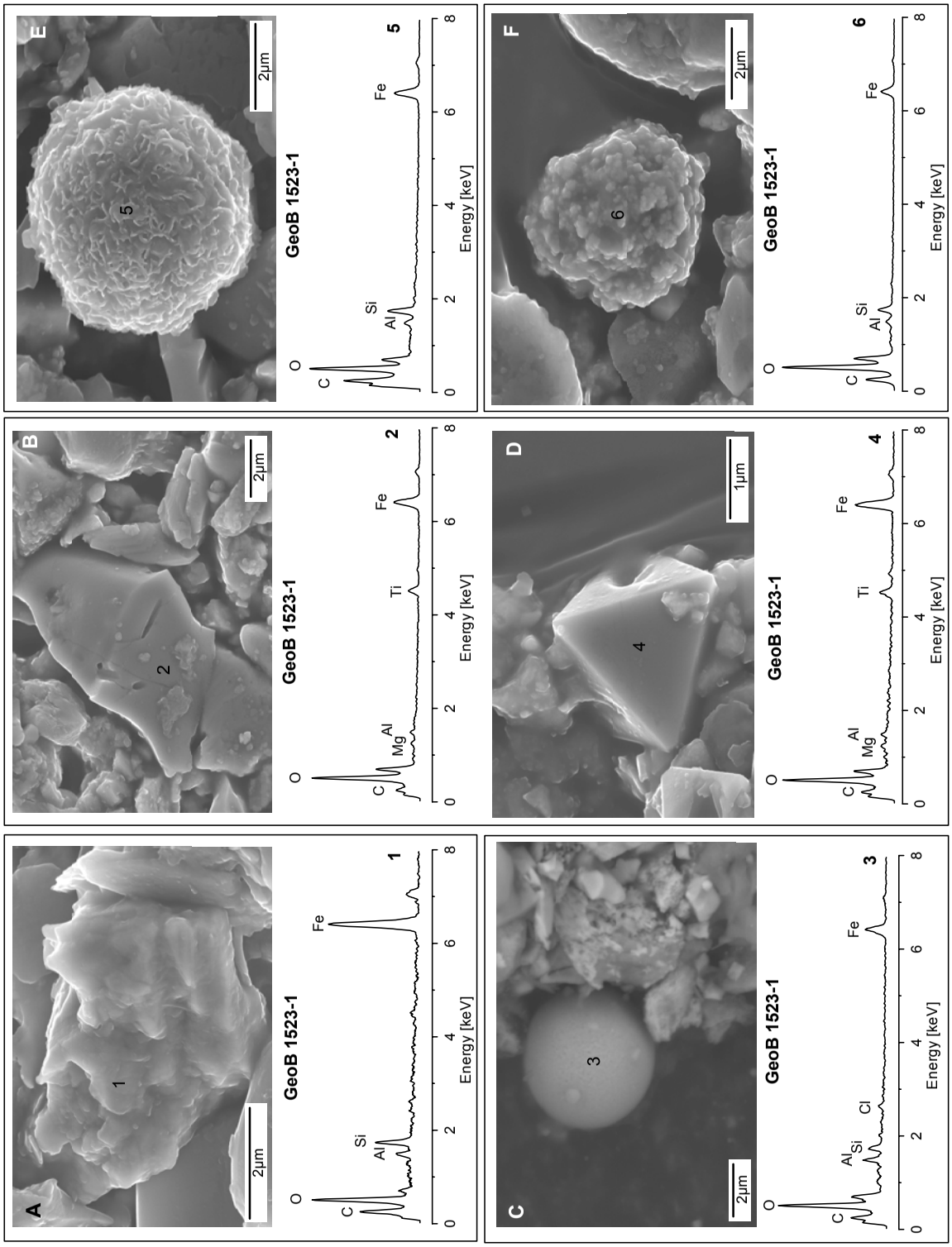

Figure 4. SEM micrographs in secondary electron mode and the respective elemental spectra from representative particles of CER samples (GeoB 1523-1). All EDS spectra are normalized on their respective oxygen maxima, they correspond to spot analyses on the respective numbered particles. (a) Detrital magnetite grain with typical irregular edges and knobby surface. (b) fragmetal Tmt particle of intermediate Ti-content with smooth surface and irregular sharp grain edges. (c) Magnetite spherule with smooth surface. (d) Euhedral titanomagnetite crystal with sharp crystal edges and minor dissolution marks. (e) Spherical cluster of authigenic microcrystalline hematite, a so called 'microrosette'. (f) Typical specular hematite nodules grown as encrusts around detrital magnetite grains.

typical for eolian input of mechanically weathered detritus from the NW African continent (*Stuut et al.,* 2005) and not necessarily of volcanic origin, while the two-phase Fe-Ti oxides are typically volcanic (*Heider et al*., 1993) presumably also transported by wind (*Pye,* 1987). Abundances of these eolian Tmt-Hilm particles at CER and MAR were as low as 2%. The by far higher abundances of 12 to 24% were found at the eastern SLR site. Many particles show signs of grain rounding and/or chemical alteration. The grade of reductive dissolution seems to correlate with Ti content. Ti^{4+}-rich and hence Fe^{3+}-poor Fe-Ti oxides are more resistant to redoxomorphic diagenesis than intermediate Tmt. Shrinkage cracks frequently were observed indicating an earlier low-temperature oxidation (maghemitization) of the respective phase.

5.5. Microcrystalline Hematite

Two species of microcrystalline hematite were identified in the samples. The majority of the observed hematite (Figure 4f-6) occurs as glassy nodular or slightly oblate overgrowths on oxidized detrital magnetite grains. *Walker et al.* [1981] and *Freeman* [1986] describe this type as authigenic specular hematite as conversion product of aged ferrihydrite coatings. The second, scarcer type occurs as spherical to oblate clusters of microcrystals resembling well-developed 'microrosettes' (Figure 4e-5) reaching sizes up to some tens of μm. These are assumed to form as synsedimentary authigenic precipitates in oxidic environments (*Walker et al*., 1981). Both the specular hematite nodules and the sub- to euhedral platy hematite crystals of the microrosette have micron to submicron sizes (cf. crystals shown in *Maher and Thompson,* 1999) and correspond to SD hematite (e.g. *de Boer and Dekkers*, 1998).

Both above described types of microcrystalline hematite were found in sample from the CER. The microrosettes are only present in traces and therefore do not represent a major component in the samples, but they indicate a oxidic sedimentary environment during and after sedimentation. The microrosettes were not present in samples from the MAR or SLR. The specular hematite nodules originate most likely from previous coatings of the detrital magnetite grains. Since fragmental and euhedral Tmt does not seem to show hematite coatings like detrital magnetites, it is likely, that this process was initiated before deposition in the deep sea. Its abundance can be illustrated by the fact that virtually all observed detrital magnetite grains exhibit specular hematite coatings.

5.6. Magnetite Spherules

Another identified component are iron oxide spherules of varying types. They occur in filled or hollow varieties (Figures 4c-3, 5a-4, 5c-1, 6e-6) with smooth (size: 0.5 to 5 μm) or dendritic (size ~10 μm) surface textures. According to *Xu et al*. [1994] who describe very similar magnetite spherules for a Jurassic limestone from Twin Creek, Wyoming USA, such particles have PSD to MD properties. Besides Fe, the spherules contain Mg, Al, Si, Cl and sometimes traces of Ti and Mn; Ni was never detected.

The existence of magnetic spherules in deep-sea sediments has been known since *Murray and Renard's* [1891] H.M.S. Challenger expedition to the Central Pacific. They assigned a cosmic origin to their magnetically extracted round particles - an interpretation which is still accepted (e.g. *Brownlee,* 1981). But spherule shapes are also typical for other types of airborne magnetic particles such as fly ashes from industrial combustion (e.g. *Matzka*, 1997; *Desenfant et al*., 2004), volcanic eruptions and impact events. Volcanic ash particles from major eruption can travel at relatively high altitude and can be transported over greater distances than dust particles (*Pye*, 1987). *Suk et al*. [1990] mention even the possibility of magnetite spherule formation by oxidation of pyrite.

This explanation does not seem to

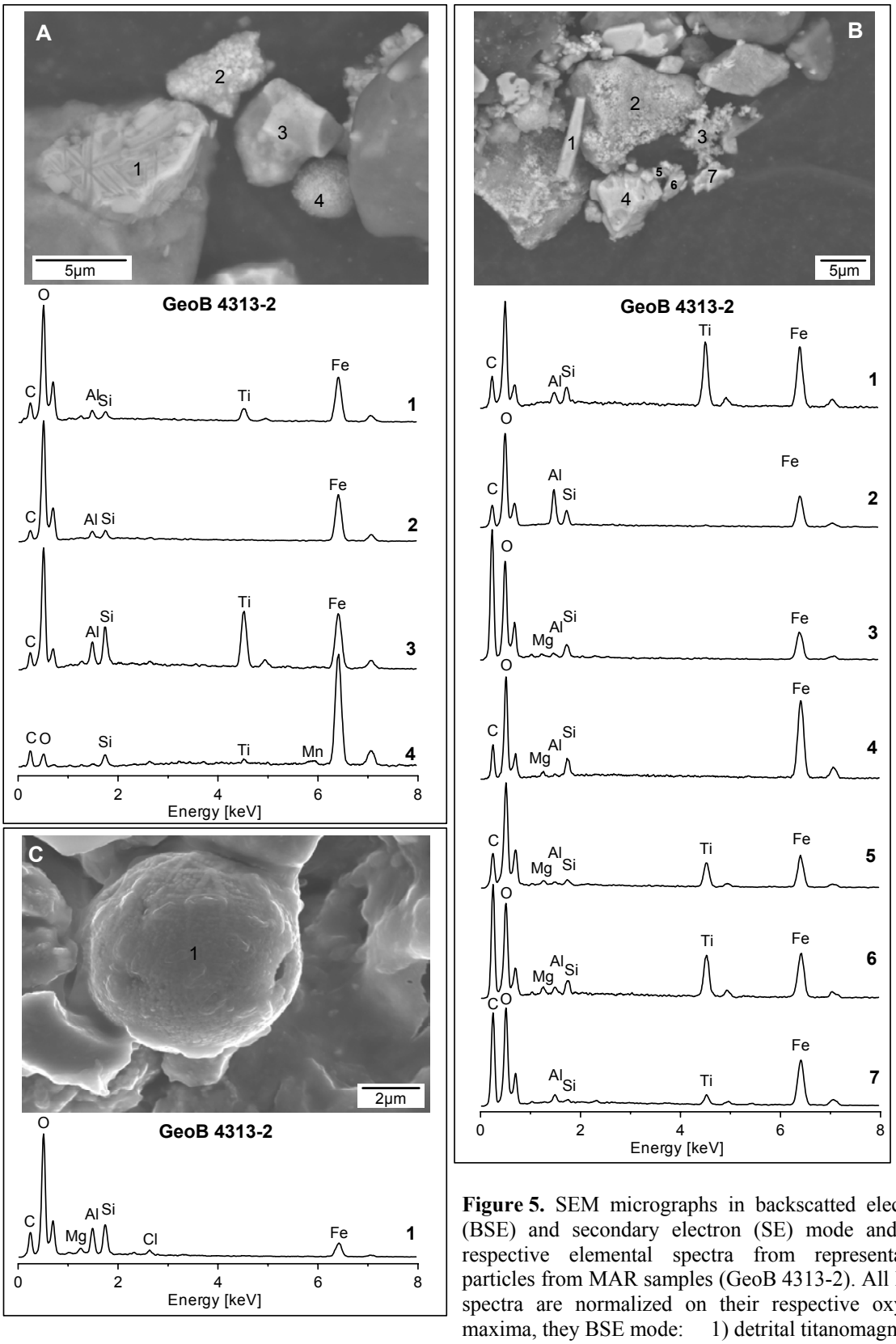

Figure 5. SEM micrographs in backscatted electron (BSE) and secondary electron (SE) mode and the respective elemental spectra from representative particles from MAR samples (GeoB 4313-2). All EDS spectra are normalized on their respective oxygen maxima, they BSE mode: 1) detrital titanomagnetite grain showing weathered correspond to spot analyses on the respective numbered particles. (a) Micrograph obtained in hemoilmenite exsolution lamellae, 2) detrital magnetite grain with irregular surface, 3) hemoilmenite grain, 4) magnetite spherule with minor Ti-content. (b) Micrograph obtained in BSE mode: 1) needle shaped hemoilmenite grain, 2) detrital magnetite grain with hematite encrusted surface, 3) cluster of fine grained iron oxide nanoparticles, 4) smooth surfaced detrital magnetite grain, 5) small euhedral titanomagnetite crystal with relatively high Ti-content, 6) small hemoilmenite grain, 7) fragmental titanomagnetite grain with intermediate Ti-content. (c) Micrograph obtained in SE mode: hollow magnetite spherule with dendritic surface pattern and minor Cl-content.

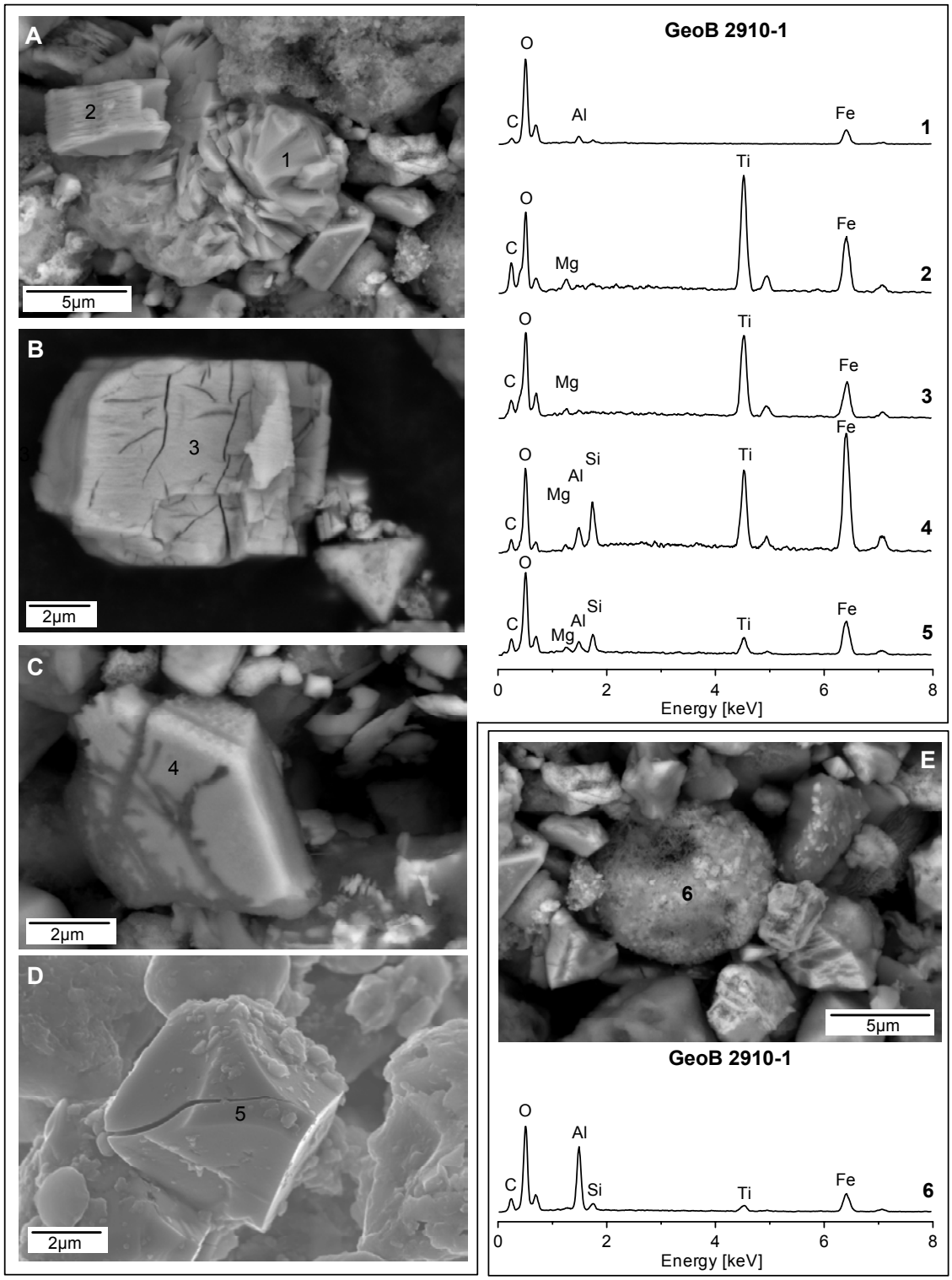

Figure 6. SEM micrographs in backscatted electron (BSE) and secondary electron (SE) mode and the respective elemental spectra from representative particles from SLR samples (GeoB 2910-1). All EDS spectra are normalized on their respective oxygen maxima, they correspond to spot analyses on the respective numbered particles. (a) Micrograph obtained in BSE mode: 1) detrital magnetite grain showing strong reductive diagenetic alteration, 2) detrital titanomagnetite/hemoilmenite grain with 'tiger stripe' pattern. (b) Micrograph obtained in BSE mode: detrital (hemo)ilmenite grain with shrinkage cracks originating from low-temperature oxidation. (c) Micrograph obtained in BSE mode: titanomagnetite grain with high Ti-content showing dissolution marks. (d) Micrograph obtained in SE mode: euhedral titanomagnetite crystal showing rounded grain edges and a shrinkage crack origination from low-temperature oxidation. (e) Micrograph obtained in BSE mode: magnetite spherule with minor Ti-content showing an advanced stage of reductive iron dissolution surrounded by partially dissolved titanomagnetite grains.

apply here since the crystal structures of the spherules do not comply with framboidal pyrite precursors. Since cosmic spherules typically contain at least traces of Ni (e.g. *Brownlow et al*., 1966), which was not seen, we can exclude this possibility as well. Most likely, the magnetite spherules in our samples represent volcanic ash particles, since they contain Al, Si or Cl and sometimes Ti as typical elements of eruptive volcanism (e.g. *Freeman*, 1986). Iron oxide spherules were found at all three Equatorial Atlantic sites, but their abundance increased from ~1% at CER and ~3% at MAR to 6% at SLR. At this easternmost site, the magnetite spherules show signs of reductive dissolution in various stages.

5.7. Bacterial Magnetite

On some TEM micrographs (Figure 7), a fine-grained magnetite species of well constrained grain-size (50 to 100 nm) and specific octahedral, prismatic or bullet

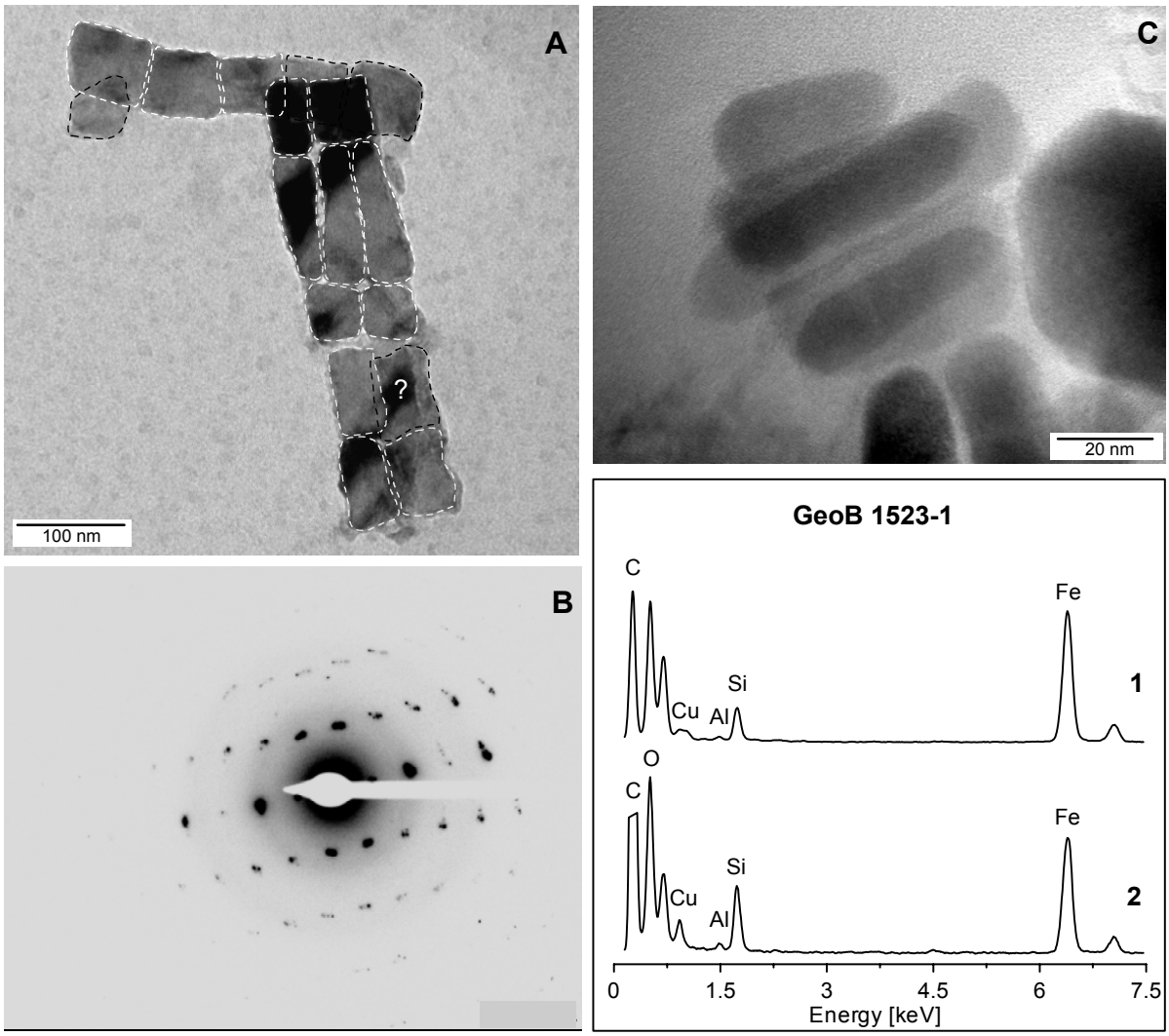

Figure 7. Transmission electron micrographs and the respective EDS spectra obtained on the whole shown area from CER samples (GeoB 1523-1). All EDS spectra are normalized on their respective oxygen maxima. (a) Segments of two individual chains of fossil biogenic magnetite, so called 'bacterial magnetosomes'. Dashed lines show the interpretation of the individual grain edges. The horizontal simple chain consists four single grains of octahedral type, the vertical chain shows two rows of prismatic and bullet shaped grains in a more complicated sequence. The respective transmission electron micrograph was obtained in bright field mode. (b) Electron beam diffraction pattern from the whole area of (a), indicating the approximate <–1 1 2> orientation of the magnetite particles. (c) Individual grains of bullet shaped fossil bacterial magnetosomes obtained in HRTEM mode. The Al and Si-content in the element spectra origins from additionally present clay mineral pollution on the particles, the spectra are normalized on their respective oxygen maxima.

shape can be discerned. These monocrystalline particles are often aggregated in chains or clusters. Their elemental composition corresponds to stoichiometric magnetite or maghemite; faint Al and Si peaks in the spectra result from attached clay particles.

Due to their very specific attributes, these particles can be easily identified as fossil biogenic magnetosomes mineralized by benthic magnetotactic bacteria (e.g. *Petersen et al.,* 1986; *von Dobeneck et al*., 1987; *Petermann and Bleil*, 1993). By their size and shape individual magnetosomes always fall into the stable SD field of the *Butler and Banerjee* [1975] diagram. Because of magnetic interaction within the natural aggregates, bacterial magnetite does often behave PSD-like.

Biogenic magnetite was exclusively

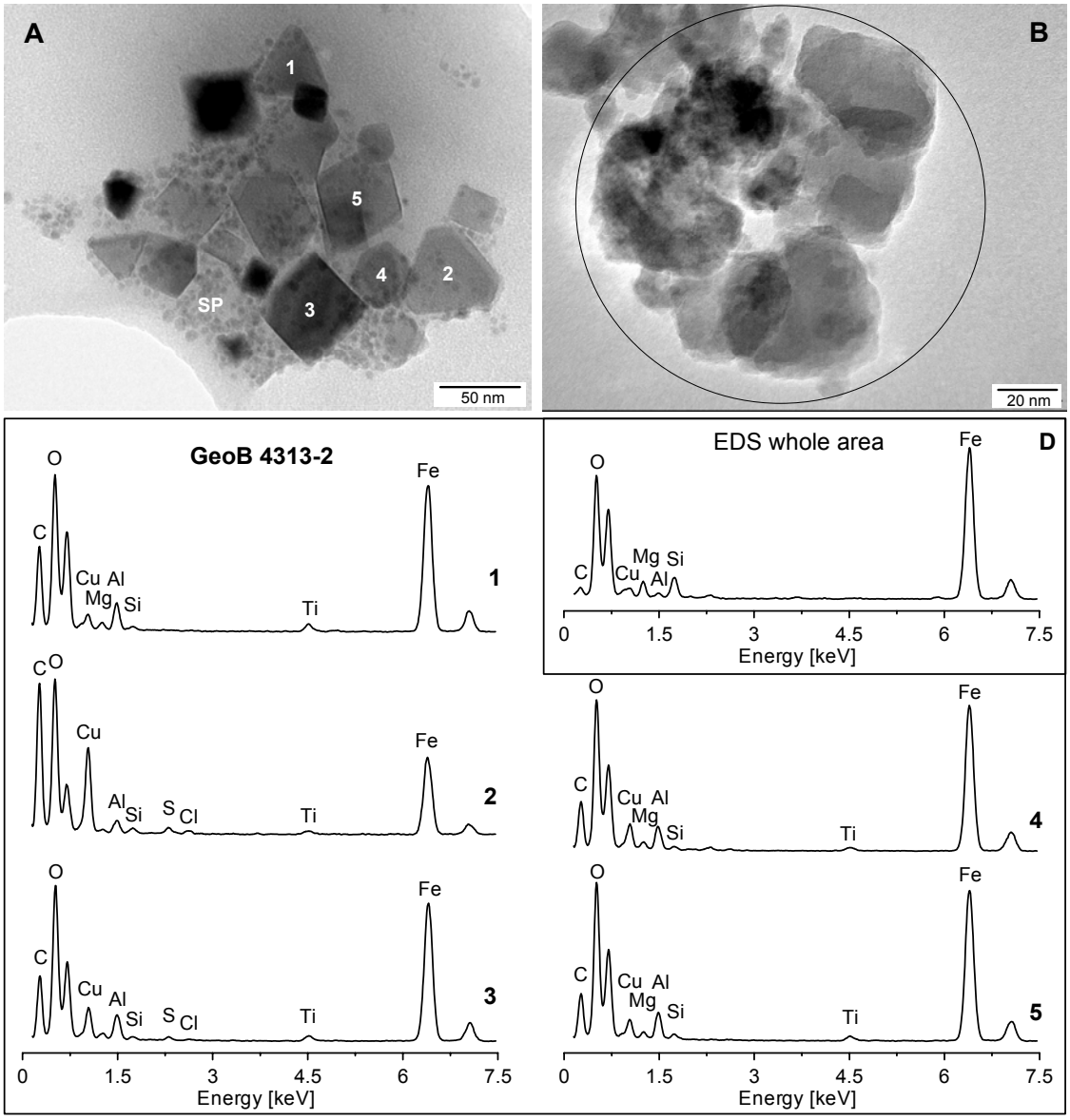

Figure 8. Transmission electron micrographs obtained in bright field mode and the respective EDS spectra from MAR samples (GeoB 4313-2). All EDS spectra are normalized on their respective oxygen maxima. (a) Grains 1-5 show euhedral titanomagnetite crystals of low Ti-content and in different orientations, element spectra are obtained as spot analyses from the individual grains. Note the overall present very fine superparamagnetic (SP) material attached to the bigger titanomagnetite grains. (b) Cluster of detrital magnetite grains with typical irregular grain edges, the element spectrum is obtained from the whole marked area.

found in the two samples from the westernmost CER site. Because of different sample preparation techniques and scales, it is technically impractical to compare abundances of these biogenic nanoparticles relative to the lithogenic microparticles; however, they do not seem rare. The presence of well preserved fossil magnetosomes at sediment depths below 310 cm indicates oxic sedimentary conditions. Bacterial magnetite is rapidly dissolved under suboxic conditions as shown by *Hilgenfeldt* [2000], who described biogenic magnetite depletion within the first few cm of the surface sediment in the Benguela upwelling region.

5.8. Goethite Needles

Another nanophase are ultra-fine needle-shape particles (Figures 9a, 9b-1) arranged in larger aggregates. Their widths range from a 5 to 100 nm, their sizes from 500 to 2500 nm. Whole area EDS spectra were taken as an attempt to estimate the composition of these particles. The quality of these EDS is very limited. Besides Fe and O, small amounts Al, Si and Ti are present, which can be attributed to adhering impurities. These acicular Fe oxide minerals are very characteristic for euhedral 'microgoethite' (*Thiel*, 1963; *Taylor et al.*, 1987). Goethite is antiferromagnetic, but can carry a parasitic ferromagnetic moment increasing with the number of lattice defects; the observed crystals should have SD magnetic grain-size (e.g. *Dekkers*, 1989). The microcrystalline goethite was solely detected at the western SLR site.

5.9. Nanoparticle clusters

The smallest observed magnetic fraction are 1-10 nm sized equant Fe nanoparticles typically arranged in loose, homogenous clusters (Figures 8a-SP, 9a, 9b-1, 9d-SP), which are often attached to larger magnetic Fe-Ti oxides or goethite needles. The absence of a defined crystal shape and lattice fringes suggest a poor crystallinity. This phase occurs frequently in all investigated samples.

Magnetic particles in this size range are superparamagnetic and have been described for various natural and synthetic iron minerals. *Sparks et al.* [1990] discovered anaerobic bacteria precipitating large aggregates of 10-20 nm sized magnetite particles as metabolic byproduct. *Guyodo et al*. [2003] synthesized ultra-fine goethite 'nanodots' (3.5 nm) attaching as 'nanorods' and carrying SP properties. So-called six-line ferrihydrite nanoparticles synthesized by *Guyodo et al*. [2006] have sizes between 3 to 25 nm depending on the reaction temperature. They are superparamagnetic at ambient temperatures, have relatively high susceptibilities and shapes very similar to the particles in our extracts. Ferrihydrite is a typical precursor of goethite with similar origin from e.g. weathering processes (e.g. *Jambor and Dutrizac*, 1998).

On the basis of electron microscopy, these nanoparticles cannot be safely identified with any of the above mentioned SP mineral phases. Our low-temperature magnetics (Chapter 3) and new unpublished Mössbauer data (T.S. Berquó, pers. communication) suggest, that goethite and ferrihydrite are both present and even exceed hematite contents by quantity.

6. Environmental Magnetic Implications

6.1. Regional Character of Magnetic Mineral Assemblages

The electron microscopic results enabled a definition of nine distinct magnetic particle species in Equatorial Atlantic, which can be used to classify and compare site-specific magnetic mineral assemblages. Figure 10 compiles the recognized magnetic micro- and nanoparticle fractions at each of the three investigated sites in the order of their relative grain abundances. Obviously, some components are ubiquitous and others only found locally. Detrital Mt, fragmental and euhedral Tmt, Tmt-Hilm intergrowths are the major microparticle (extending into the nanopar-

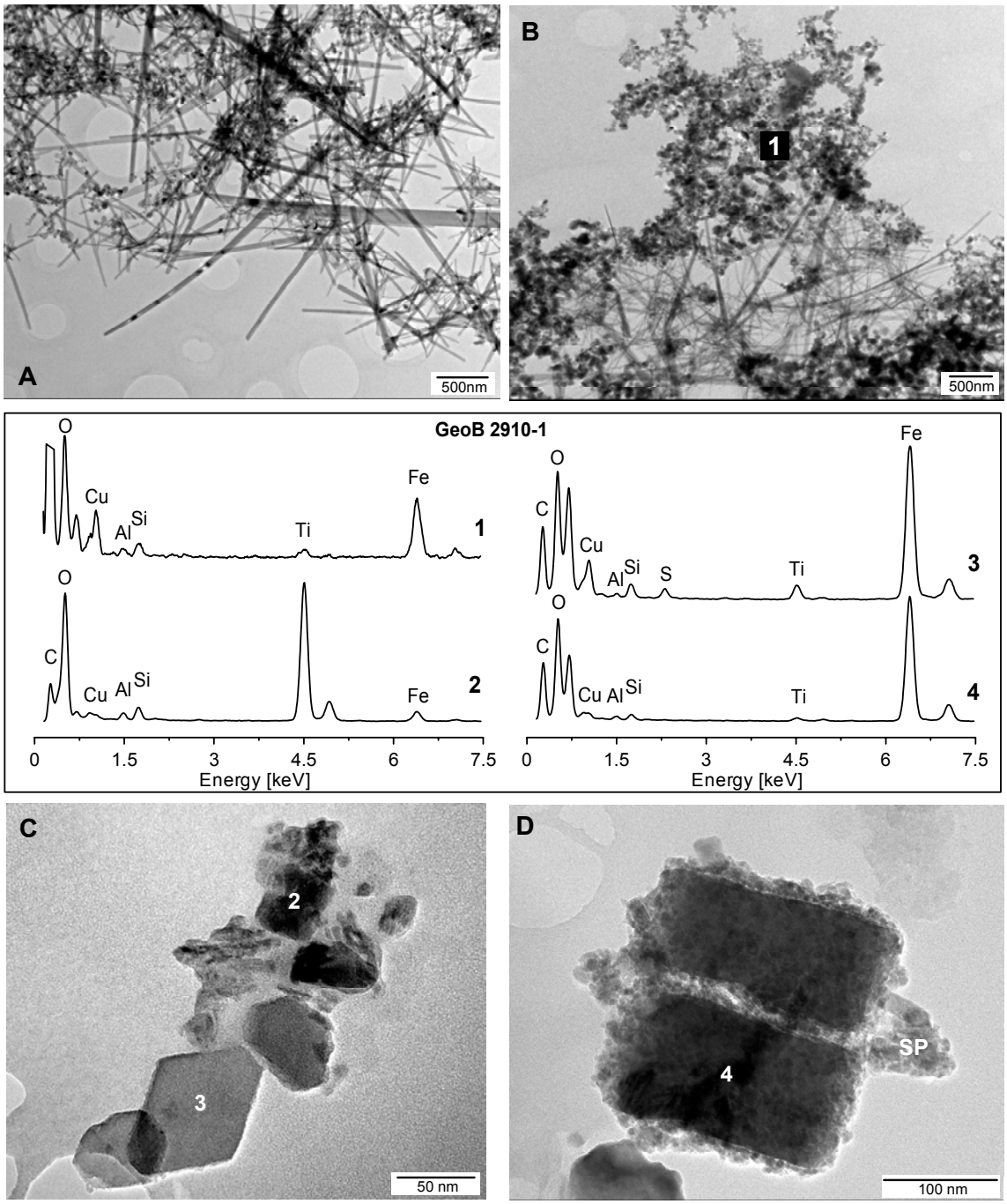

Figure 9. Transmission electron micrographs obtained in bright field mode and the respective EDS spectra from MAR samples (GeoB 2910-1). (a) and (b) show clusters of nanocrystalline needle shaped goethite next to clusters of so called 'nanodots' of presumably either goethite or ferrihydrite. 1) marks the position were an whole area EDS spectrum was obtained for the super fine material, the minor Ti-content might result in a mixture signal with super fine titanomagnetites also being present in the cluster, but detection is rather noisy for this grain-size range. (c) Shows a cluster of detrital 2) hemolimenite and 3) titanomagnetite grains. (d) Relatively big and cracked nanoparticle of titanomagnetite surrounded by nanodot superparamagnetic material (SP) and some needle shaped particles.

ticle range) classes present at all studied sites, yet with strikingly different proportions: Detrital Mt dominates at the CER, fragmental and euhedral Tmt at the MAR and Tmt-Hilm intergrowths at the SLR. Although being generally less common in the extracts, magnetite spherules and silicates with magnetic inclusion are widely distributed. Since the extraction efficiency for silicate rock fragments depends largely on their magnetite content, this fraction is certainly underrepresented

in the extracts and may be more important in the bulk sediment. The same accounts even more for specular and platy hematite, which is probably too weakly magnetic to be extracted quantitatively. For similar reasons, the contribution of hematite coatings on non-magnetic grains and pure detrital hematite grains cannot be specified with our approach.

Interestingly three magnetic mineral species found only locally: bacterial magnetite (only CER), platy hematite (microrosettes; only CER), and goethite needles (only SLR) are all authigenic minerals forming or preserving only under specific geochemical conditions. At the Ceará Rise, oxic conditions promote preservation of bacterial magnetofossils, which may already have been removed by early diagenesis at the other sites in the investigated sediment depths. For the same reason, platy hematite could only precipitate at the CER. The goethite needles at SLR may have formed by reoxidation of reduced and remobilized Fe, eventually during burn-down of the Fe redox boundary (*Kasten et al.,* 1998, 2003; *Funk et al*, 2004b).

As primary productivity and organic carbon burial in the Equatorial Atlantic increase from West to East, the stability of ferric iron minerals is reduced (*Funk et al*, 2004a). This trend is well reflected by the dissolution marks, observed in an initial stage at MAR and in a more advanced state at the SLR. It can be speculated, that the larger proportion of Ti-bearing minerals at SLR vs. CER are due to the fact, that the Ti-content stabilizes Fe-Ti oxides with regard to reductive dissolution (*Karlin,* 1990; *Emiroğlu et al.,* 2004; *Dillon and Bleil,* 2006).

According to the working hypotheses of Environmental Magnetism, the regional character of magnetic mineral assemblages is controlled by sedimentary source-to-sink relations. The validity of this concept is strongly supported by comparison of magnetic and other lithogenic fractions.

The CER site is situated some 700 km north-east off the delta and within the distal particle plume of the Amazon (*Francois and Bacon*, 1991). The terrigenous particle flux is greatly enhanced during sea-level fall, when the sediment depocenters accumulating during high stand are eroded and transported over the shelf break, from where they reach the CER as nepheloid layers at different water depths (*von Dobeneck and Schmieder*, 1999). By tracing clay mineral assemblages, *Petschick et al.* [1996] confirmed an Amazonian particle flux to the CER and MAR. A second, subordinate source of Fe oxides, mostly hematite or goethite, is Saharan and Sahelian dust, in particular during glacial periods of stronger trade winds (*Bleil and von Dobeneck*, 2004). *Prospero et al.* [1981] report on eolian material sampled at Cayenne, French Guiana (4°50'N 52°22'W) in prolongation of our transect. They identified Saharan dust particles under winter and Brazilian dust during summer conditions. The SLR, a volcanic submarine elevation of similar size and origin as the CER, receives large amounts of African, in particular relatively fine-grained dust from the Sahel and savannah zone by NE winter trades (*Sarnthein et al*., 1982; *Stuut et al.,* 2005).

The most common magnetic species at the CER is detrital anhedral magnetite with hematite coatings interpreted as fluvial material. The absence of a comparable fluvial source at the arid Northwest-African margin (*Wynn et al*., 2000; *Holz et al.,* 2004) explains the lack of a similar component at the SLR. Eolian magnetic particles from the West African hinterland dominate here; Mesozoic igneous provinces in Guinea and Southwestern Mali lie within winter trade wind trajectory to the SLR and form a potential source area for coarse and strongly magnetic volcanic detritus.

The distinct source-to-sink relations of magnetic minerals are even more obvious, when total mass budgets and our particle

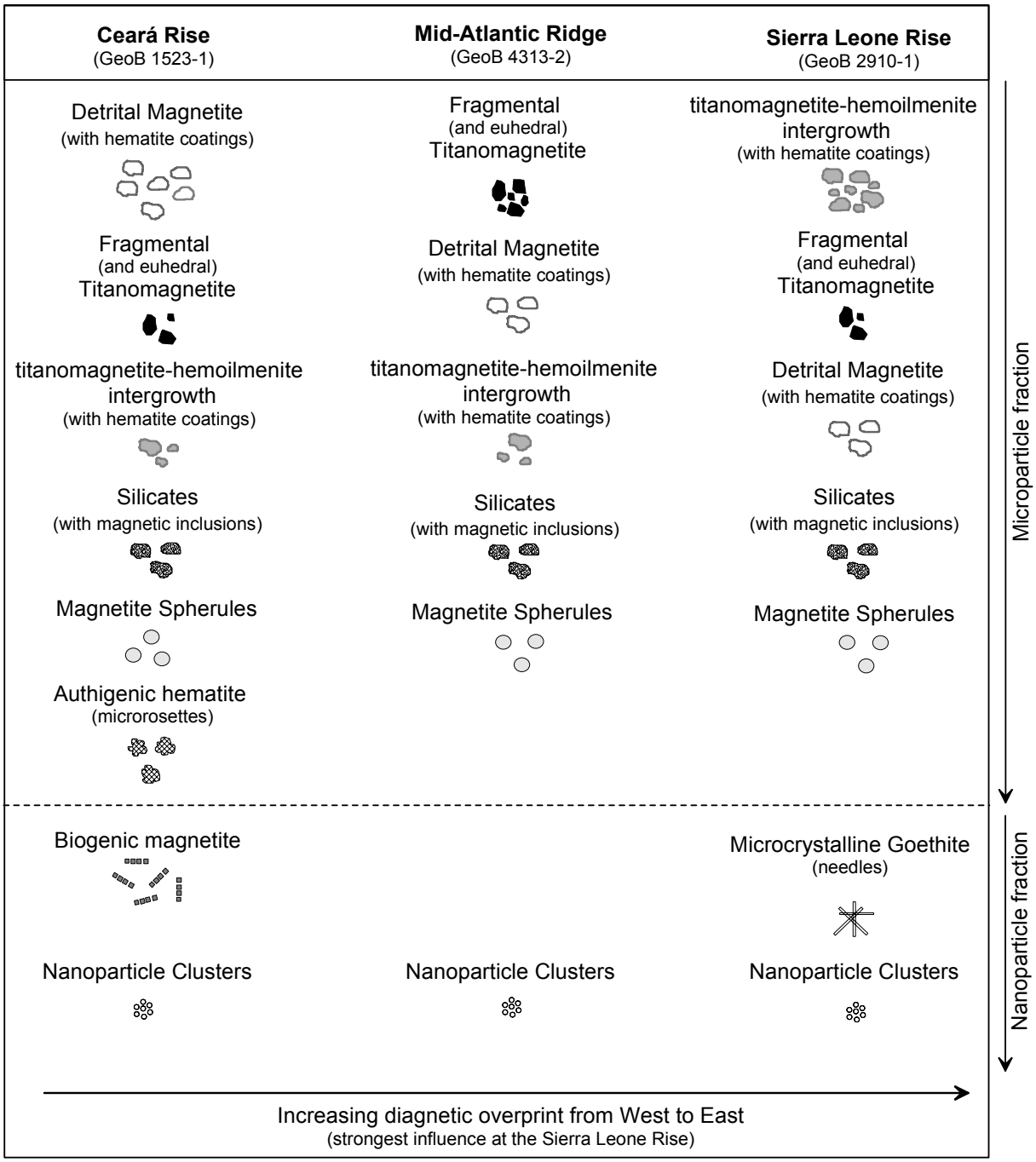

Figure 10. Summary of Electron microscopic results along the West-East profile in the Equatorial Atlantic, all identified magnetic components are given for each investigated site classified by their grain-size, abundance in the samples, and with indications of their sources.

counts are compared. According to calculations of *Funk et al.* [2004a] the interglacial/glacial Fe-Ti oxide accumulation rates (AR_{mag}) in the Equatorial Atlantic, given as magnetite flux equivalents (averaged separately over interglacial MIS 1/5/7 vs. glacial MIS 2-4/6) total 4.38 vs. 5.35 g/m^{2}kyr at the SLR, 6.84 vs. 6.16 g/m^{2}kyr at the MAR, and 6.30 vs. 7.33 g/m^{2}kyr at the CER. These values are apparently similar, but they account for different sources and magnetic minerals. A tenfold higher content of Tmt/Hilm-intergrowths at SLR relative to CER and MAR points at a proximal African source. The Amazonian detrital Mt content is about fivefold higher at CER than at MAR and SLR. At the MAR, fragmental Tmt as a for

some 50% of the magnetic micro-particle some 5% at CER and 30% at SLR (to which northward currents and other local and African sources may also contribute). This little exercise demonstrates that comparing susceptibility-based magnetite accumulation rates without considering magnetic petrology gives no hint to the complex nature of the whole sedimentary system.

6.2. Magnetic Grain-Size: Mixing vs. Sorting

A fundamental issue of marine environmental studies relates to the interpretation of magnetic grain-size records: does an apparent fining or coarsening actually imply a shift of magnetic grain-size due to changing transport intensities ('sorting'), or does it reflect the blending of two or more distinct magnetic species at varying proportions ('mixing')? Our study area provides examples for both scenarios (Figures 2 and 11):

At the CER, we see a mixing of coarser (PSD) detrital Mt and finer (SD) bacterial Mt. The flux of the PSD phase is strongly modulated by the sea-level changes and their control on Amazon discharge to the deep ocean, while the benthic magnetite biomineralization rates depend on carbon rain rates and follow oceanic productivity cycles. While both components do not vary with respect to their grain-size, their changing 'mixing' proportions mimic a cyclic M_{ar}/M_{ir} variation by a factor of two. The change between both states is abrupt and there is little signal variability during sea-level low-stands (e.g. MIS 2 to MIS 4). M_{ar} and M_{ir} curves differ strongly by their signal character and relative amplitudes. This effect was predicted by *Frederichs et al.* [1999] on basis of rock magnetic data of the Western Equatorial sediment core GeoB 1505-1.

At the SLR, bacterial magnetite is practically absent and the magnetic petrology does not seem to change much during Quaternary climate cycles. However, the intensification and south-ward motion of the glacial trade wind system carries coarser particle fractions from the source area to the site. The resulting M_{ar}/M_{ir} changes equally reach a factor of two between peak amplitudes. As more and coarser material transported during glacials M_{ar} and M_{ir} records have similar patterns and amplitudes. The sedimentation conditions at the central MAR seem to represent an intermediate state between the two extremes.

The magnetic mineral assemblage is Compared to CER, the glacial record sections (e.g. MIS 2 to MIS 4) show stronger modulation. In consequence we

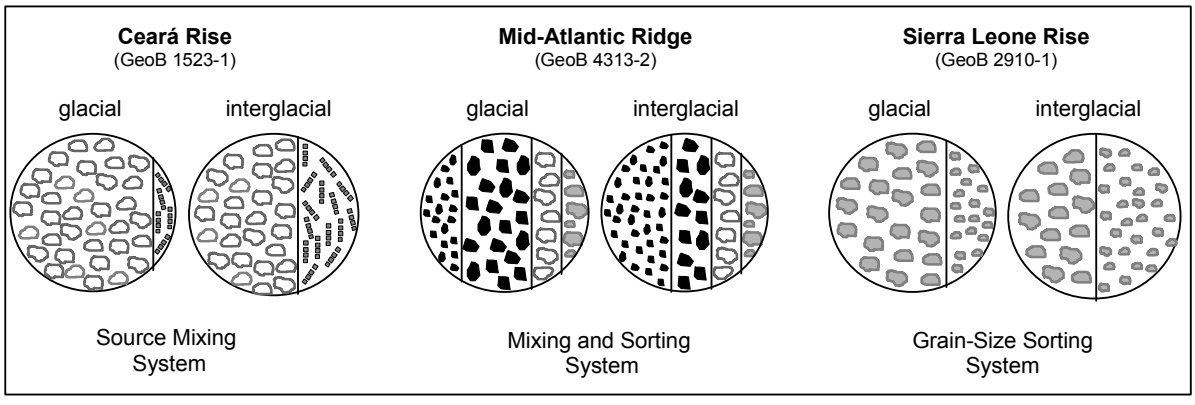

Figure 11. Model for the composition of the magnetic assemblages in the Equatorial Atlantic, at the West relatively detrital magnetite is the dominant magnetic species in the coarse grain-size fraction, where as biogenic magnetite is present in the fine fraction; during interglacials, the dominance of the detrital coarse material decreases. At the central site, the major component is fragmental titanomagnetite varying in grain-size with glacial/interglacial cyclicity. The titanomagnetite component is additionally mixed with the detrital magnetite material from the western source and the eolian material from the eastern source. At the SLR, the eolian input is prevailing, modulated by glacial/interglacial changes of NW-African wind systems.

see rather a grain-size 'sorting' system being fed from local, western and eastern sources. Bottom current variations and changing continental fluxes combine mixing and sorting effects.

6.3. High-Coercive and Superparamagnetic Fractions

In the framework of the Central and South Atlantic Ocean (*Schmidt et al.*, 1999), the northern equatorial belt stands out by particularly low $S_{-0.3T}$ ratios (< 0.90) and high $\kappa_{fd\%}$ values (10-12%), i.e. high hematite/magnetite ratios (estimated > 4:1) and over-proportional contributions of ultrafine (< 30 nm), magnetically superparamagnetic fractions. Without SEM and TEM examination and low temperatures (4 to 400 K) and high field (7 T) magnetic analytics, these environmental magnetic parameters were explained with enhanced fluxes of eolian hematite und ultra-fine magnetite.

This study and Chapter 3 suggests that goethite or other nanocrystalline iron phases, which have seen little attention in marine magnetic studies, should have an important influence on magnetic sediment properties in this region. Their occurrence as nanoparticles and needles and their broad low to ambient temperature unblocking spectra seen in LT warming curves of heavy liquid separates make them prime candidates for both, superparamagnetic and high-coercive magnetic characteristics. Their extreme particle aspect ratios from (finer) equant to (larger) acicular shapes could easily account for these opposed magnetic stability ranges. It would also be very difficult to argue, why detrital Mt should be highly enriched in the < 30 nm fraction, but not in the other particle size ranges. As weathering products Fe oxyhydroxide phases are typically very fine-grained by nature.

7. Discussion and Conclusions

Detailed SEM and TEM investigations on the magnetic petrology of Equatorial Atlantic oxic to suboxic pelagic sediments have delivered important new insights into the mineralogy, granulometry, origin, and characteristics of magnetic carriers in this region.

Magnetic extracts from three key locations (Ceará Rise, Mid-Atlantic Ridge, and Sierra Leone Rise) in the western, central and eastern part sampled at two contrasting climate stages (MIS 4 and MIS 5.5) were found to contain nine well-defined magnetic particle species:

- Detrital magnetite
- Fragmental and euhedral titanomagnetite
- Titanomagnetite-hemolilmentite intergrowths
- Silicates with magnetic inclusions
- Microcristalline hematite
- Magnetite spherules
- Bacterial magnetite
- Goethite needles
- Nanoparticle clusters

The first three species are of detrital, originally magmatic or metamorphic origin. They were found at all sites in varying abundances as dominant ferrimagnetic components and extend over a broad grain-size range from magnetic single- to multi-domain state. Detrital magnetite is associated to the Amazon fluvial source, fragmental titanomagnetite to the weathering of mid-ocean ridge basalts, and titanomagnetite-hemoilmenite intergrowths to eolian distribution of volcanic products from the proximal semi-arid western Africa. The silicates (e.g. quartz and feldspars) with magnetic inclusions are probably of similar provenances. Their contribution was certainly underestimated due to the low extraction efficiency for these mostly non-magnetic particles. The same accounts for specular hematite coatings, which could therefore only be observed on easily extractable magnetite grains. Authigenic hematite microrosettes and presumably pyroclastic magnetite spherules are occasionally found, but of subordinate relevance. Bacterial magnetite in form of fossil magnetosome chains with their typical shapes and narrow size-range restricted to

the single-domain field were only found at one site, eventually due to their low preservation potential. Nanoparticle clusters, partly associated with goethite needles, were however ubiquitous and present in considerable quantities.

The abundances of the various detrital magnetic mineral phases were inversely correlated to source distance (Amazon mouth, Mid-Atlantic Ridge, African dust belt) as to be expected from sedimenttologic considerations. This very clear regionalization underlines, that magnetic petrology is an even better indicator of source-to-sink relations than previously thought (*Schmidt et al.*, 1999). The difficulties of environmental magnetism to distinguish Ti-poor, Ti-rich and exsolved Fe oxides (and maghemitization states) are due to the inability of room-temperature measurements to provide discriminative mineral characteristics. For future work, combined low- and high-temperature sediment analytics should be conceptualized to take more profit from these source attributes. The distinction of fine lithogenic and biogenic magnetite fractions is equally important, e.g. by analyzing coercivity spectra of anhysteretic remanent magnetizations (e.g. *Vali et al.*, 1989; *Egli*, 2004a, 2004b).

An early diagenetic overprint of the magnetic mineral assemblages is seen even under oxic to suboxic, at worst just mildly reducing environments encountered at these sites (and sediment depths). Redox conditions determine, which phases are precipitated, preserved or successively depleted. While hematite is generally described as a magnetic phase of superior chemical stability compared to magnetite, authigenic hematite microrosettes were only found at the most oxic sedimentary environment. Specular hematite encrustations were observed at all sites and may even stabilize the more vulnerable magnetite core. In a similar sense, Ti-rich (and hence Fe^{3+}-poor) hemoilmenite lamellae were found to stabilize intergrown titanomagnetite (Chapter 6). Dissolution pits and crevices on crystal faces rise in number and intensity from West to East as a consequence of increasingly reducing environments. This effect results in preferential depletion of less stable stoichiometric magnetite and relative enrichment of Ti-substituted Fe oxides. However, this mechanism is not thought to explain the above described distribution patterns of the major detrital components since none of the respective remanence (Figure 2) and susceptibility (*Funk et al.*, 2004a) records show signatures of advanced magnetic mineral depletion.

Former interpretations of changes in magneto-granulometric proxies (M_{ar}/M_{ir}, M_{rs}/M_s) as indications of magnetic grain-size shifts caused by climatic variations in transport efficiency (wind or bottom current intensities), hence sorting effects, should be reviewed with attention. Our results suggest, that the mixing of magnetically differing sources may lead to similar results, if their individual fluxes are climate-controlled. Moreover, 'sorting' and 'mixing' regimes are just conceptual endmembers and should generally occur in combination, however with differing tendencies. For sorting systems, we should expect absolute concentration changes of magnetic grain-size fractions to be more strongly correlated than in the case of mixing systems. The same consideration applies principally to all other ratio parameters in Environmental Magnetism: Changing $S_{-0.3T}$ ratios, hence hematite/magnetite ratios, can be a matter of varying humidity and weathering conditions, but equally of mixing of terrestrial (hematite-rich) and marine (hematite-poor) sources – not to speak of the well-known, above mentioned effects of selective dissolution. As in many other fields of paleoceanography, relative changes in sedimentary components can only be understood by looking at the specific particle fluxes, accumulation rates and preservation potentials.

Speaking of S ratios (i.e. simple, coercivity-based proxies for magnetic mineral ratios), this study suggests being more concerned about the nature of the high-

coercive component. This component, which is generally identified with (terrestrial) hematite, could very well be strongly biased by goethite or even ferrihydrite. These secondary Fe minerals are often believed to have much higher coercivity than hematite and to be less relevant for marine than for terrestrial magnetic studies. This may not be the case regarding the sheer abundance and variability of this mineral pointed out by the TEM and low-temperature (Chapter 3) results of this study. Differing crystallinity (nanoparticles vs. needles), cation substitutions and grain-sizes extending into the SP/SD transition region could very well account for uncommonly low goethite coercivity. Goethite may actually strongly bias quantifications of the high-coercive and superparamagnetic magnetic mineral components. In order to detect or reject this possibility, high-field remanence should be cycled across the goethite Néel temperature (120°C) in zero-field. For marine Environmental Magnetism, this finding is rather good than bad news – it opens new perspectives for hematite/goethite proxies.

Acknowledgments

The electron microscopy studies were conducted at Electron Microscopy Utrecht (EMU), we thank Pim van Maurik, Gill Pennock and Prof. J.W. Geus for their support with SEM work. We also owe thanks to all other members of the Marine Geophysics Group (University of Bremen) in particular Melanie Dillon and Thomas Frederichs and of the Paleomagnetic Group (Utrecht University) for their support and advice. Jens Funk generously provided downcore data from previous studies on the investigated sites. Financial support of CF was provided by the DFG through the European Graduate College EUROPROX, (Universities of Bremen and Utrecht) and by NWO through the VMSG, Vening Meinesz Research School of Geodynamics (Utrecht University). This investigation is also associated to the Research Center Ocean Margins (RCOM) at the University of Bremen.

References

Bassinot, F.C., Labeyrie, L.D., Vincent, E., Quidelleur, X., Shakleton, N.J. and Y. Lancelot, The astronomical theory of climate and the age of the Brunhes-Matuyama magnetic reversal, *Earth Planet. Sci. Lett.***,** *126*, 546-559, 1994.

Bleil, U. and von T. Dobeneck, Late Quarternary Terrigenous Sedimentation in the Western Equatorial Atlantic South American versus African Provenance Discriminated by magnetic Mineral Analysis, in *The South Atlantic in the Late Quaternary: Reconstruction of Material Budget and Current Systems,* pp. 213-236, edited by G. Wefer, S., Mulitza, and V. Ratmeyer, Springer-Verlag, Heidelberg, Berlin, New York, 2004.

Brownlee, D.E., Extraterrestrial components, in *The Sea*, pp. 733-762, edited by C. Emiliani, (7), J. Wiley and Sons, New York, 1981.

Brownlow, A.E., Hunter, W. and D.W. Parkin, Cosmic Spherules in a Pacific Core, *Geophys. J. R. Astr. Soc*., *12*, (1-12), 1966.

Buddington, A.F. and D.H. Lindsley, Iron-titanium oxide minerals and synthetic equivalents, *J. Petrol., 5,* 309-357, 1964.

Butler, R.F. and S.K. Banerjee, Theoretical single-domain grain-size range in magnetite and titanomagnetite*, J. Geophys. Res., 80*, 4049-4058, 1975.

Butler, R.F., *Paleomagnetism: Magnetic Domains to Geological Terranes*, Boston, Backwell Scientific Publications, 1992. http://www.geo.arizona.edu/Paleomag/book/

Carmichael, C.M., The magnetic properties of ilmenite-haematite crystals, *Proc. R. Soc.*, *263,* (A), 508 pp., 1961.

Channell, J.E.T, Kent, D.V., Lowrie, W. and J.G. Meert, *Timescales of the Paleomagnetic Field*, 320 pp., American Geophysical Union, Washington D.C., 2004.

Day, R., Fuller, M. and V.A. Schmidt,. Hysteresis properties of titanomagnetites: grain-size and compositional dependence, *Phys. Earth Planet. Inter*., *13*, 260-267, 1977.

de Boer, C.B. and M.J. Dekkers, Thermomagnetic behaviour of haematite and goethite as a function of grain-size in various non-saturating magnetic fields, *Geophys. J. Int., 133*, 541-552, 1998.

Dekkers, M.J., *Some rockmagnetic parameters for natural goethite, pyrrhotite and fine-grained hematite*, Geologica Ultraiectina, 51, Ph.D. thesis, Utrecht University, 231 p., 1988.

Dekkers, M.J., Magnetic properties of natural goethite - I. Grain-size dependence of some low- and high-field related rockmagnetic

parameters measured at room temperature. *Geophys. J., 97,* 323-340*,* 1989.

Dekkers, M.J., Environmental magnetism: an introduction, *Geologie en Mijnbouw*, *76*, 163-182, 1997.

deMenocal, P. and D. Rind, Sensitivity of Asian and African climate to variations in seasonal insolation, glacial ice cover, sea surface temperature and Asian orography, *J. Geophys. Res., 98*, 7265-7287, 1993.

Desenfant, F., Petrovský, E. and P. Rochette, Magnetic signature of industrial pollution of stream sediments and correlation with heavy metals : case study from South France, *Water, Air and Soil Pollution, 152*, 297-312, 2004.

Dillon, M. and U. Bleil, Rock Magnetic Signatures in Diagenetically Altered Sediments from the Niger Deep-Sea Fan, *J. Geophys. Res.*, *111*, B03105, doi:10.1029/2004JB003540., 2006.

Dunlop, D.J. and Ö. Özdemir, *Rock magnetism, fundamentals and frontiers*, Cambridge University Press, 573 p., 1997.

Egli, R., Characterization of Individual Rock Magnetic Components by Analysis of Remanence Curves, 1. Unmixing Natural Sediments, *Studia Geoph. Geod., 48,* (2), 391-446, 2004a.

Egli, R., Characterization of individual rock magnetic components by analysis of remanence curves. 3. Bacterial magnetite and natural processes in lakes, *Phys. Chem. Earth*, *29*, (14), 869-884, 2004b.

Emiroğlu, S., Rey, D. and N. Petersen, Magnetic properties of sediments in the Ría de Arousa (Spain): dissolution of iron oxides and formation of iron sulfides, *Phys. Chem. Earth.*, 29, 947-959, 2004.

Evans, M.E. and F. Heller, *Environmental Magnetism: Principles and Applications of Enviromagnetics*, Academic Press, Elsevier Science, San Diego, London, Burlington, 299 pp., 2003.

Fischer, G. and cruise participants, Report and preliminary results of Meteor cruise M38/1, Las Palmas – Recife, 25.1.-1.3.1997, *Ber. Fachber. Geowiss. Univ. Bremen*, *94*, 178 p., 1998.

Francois, R. and M.P. Bacon, Variations in terrigenous input into the deep Equatorial Atlantic during the past 24,000 years, *Science, 251*, 1473-1475, 1991.

Frederichs, T., Bleil, U., Däumler, K., von Dobeneck, T. and A.M. Schmidt, The magnetic view on the marine paleoenvironment: Parameters, techniques, and potentials of rock magnetic studies as a key to paleoclimate and paleoceanographic changes, in *Use of Proxies in Paleoceanography: Examples from the South Atlantic*, pp. 575-599, edited by G. Fischer and G. Wefer, Springer-Verlag, Heidelberg, Berlin, New York, 1999.

Freeman, R., Magnetic mineralogy of pelagic limestones, *Geophys. J. R. Astr. Soc*., *85*, 433-452, 1986.

Funk, J.A., von Dobeneck, T., Wagner, T. and S. Kasten, Late Quaternary sedimentation and early diagenesis in the equatorial Atlantic Ocean: Patterns, trends and processes deduced from rock magnetic and geochemical records, in *The South Atlantic in the Late Quaternary: Reconstruction of Material Budget and Current Systems*, pp. 461-497, edited by G. Wefer, S., Mulitza and V. Ratmeyer, Springer-Verlag, Heidelberg, Berlin, New York, 2004a.

Funk, J., von Dobeneck, T. and Reitz, A., 2004b. Integrated rock magnetic and geochemical quantification of redoxomorphic iron mineral diagenesis in Late Quaternary sediments from the Equatorial Atlantic, in *The South Atlantic in the Late Quaternary: Reconstruction of Material Budget and Current Systems,* pp. 237-260, edited by G. Wefer, S., Mulitza and V. Ratmeyer, Springer-Verlag, Heidelberg, Berlin, New York, 2004b.

Garming, J.F.L., Bleil, U. and N. Riedinger, Alteration of magnetic mineralogy at the sulphate-methane transition: analysis of sediments from the Argentine continental slope, *Phys. Earth Planet. Inter*., *151*, 290-308, 2005.

Goldstein, J.I., Newbury, D.E., Echlin, P., Joy, D.C., Romig, A.D.Jr., Lyman, C.E., Fiori, C. and E. Lifshin, *Scanning electron microscopy and X-Ray microanalysis*, 2nd edition, Plenum Press, New York, 820 p., 1992.

Guyodo, Y., Mostrom, A., Penn, R.L. and S.K. Banerjee, From Nanodots to Nanorods: Oriented aggregation and magnetic evolution of nanocrystalline goethite, *Geophys. Res. Lett*., *30***,** (10), doi: 10.1029/2003GL17021, 2003.

Guyodo, Y., Banerjee, S.K., Penn, R.L., Burleson, D., Berquo, T.S., Seda, T. and P. Solheid, Magnetic properties of synthetic six-line ferrihydrite nanoparticles, *Phys. Earth Planet. Inter.*, *154*, 222-233, 2006.

Heider, F., Körner; U. and P. Bitschene, Volcanic ash particles as carriers of remanent magnetization in deep-sea sediments from the Kergulen Palteau, *Earth Planet. Sci. Lett*., *118,* 121-134, 1993.

Henrich, R. and cruise participants, Report and preliminary results of Meteor cruise M29/3, Rio de Janeiro - Las Palmas 11.8. - 5.9.1994. *Ber. Fachber. Geowiss. Univ. Bremen*, *60*, 155 p., 1994.

Hilgenfeldt, K., Diagneteic Dissolution of Biogenic Magnetite in Surface Sediments of the Benguela Upwelling System, *Int. J. Earth Sci*., *88*, 630-640. 2000.

Holz, C., Stuut, J.-B.W. and R. Henrich, Terrigenous sedimentation processes along the

continental margin off NW Africa: implications from grain-size analysis of seabed sediments, *Sedimentology*, *51*, 1145-1154, 2004.

Hounslow, M, Maher, B.A. and L. Thistlewood, A Magnetic mineral investigation of polarity reversals in a late Triassic sequence from the Beryl Basin, northern North Sea, in *Application of Paleomagnetism to the Oil Industry*, edited by P. Turner, P. and A. Turner, pp. 119-147, Geological Society of London Special Publications, 98, 1995.

Hounslow, M.W. and B.A. Maher, Quantitative extraction and analysis of carriers of magnetization in sediments, *Geophys. J. Int., 124*, 57-74, 1996.

Intergovernmental Oceanographic Commission, GEBCO Digital Atlas (CD-Rom), *Intergov. Oceanogr. Comm*., Int. Hydrogr. Org., Birkenhead, U.K., 1994.

Jambor, J.L. and J.L. Dutrizac, Occurrence and constitution of natural and synthetic ferrihydrite: a widespread iron oxhydroxide, *Chem. Rev*., *98*, 2549-2585, 1998.

Johnson, H.P. and J.M. Hall, A detailed rock magnetic and opaque mineralogy study of the basalts from the Nazca Plate, *Geophys. J. R. Astr. Soc*., *52*, 45-64, 1978.

Karlin, R., Magnetic mineral diagenesis in suboxic sediments at Betis Site N-W, NE Pacific Ocean, *J. Geophys. Res., 95*, 4421-4436, 1990.

Kasten, S., Freudenthal, T., Gingele, F.X. and H.D. Schulz, Simultaneous formation of iron-rich layers at different redox boundaries in sediments of the Amazon Deep-Sea Fan, *Geochim. Cosmochim. Acta, 62*, 2253-2264, 1998.

Kasten, S., Zabel, M., Heuer, V. and C. Hensen, Processes and signals of nonsteady-state diagenesis in deep-sea sediments and their pore waters, in *The South Atlantic in the Late Quaternary: Reconstruction of Material Budget and Current Systems*, pp. 431-459, edited by G. Wefer, S. Mulitza and V. Ratmeyer, Springer-Verlag, Berlin, Heidelberg, New York, 2003.

King, J.W. and J.E.T. Channell, Sedimentary magnetism, environmental magnetism, and magnetostratigraphy, *Rev. Geophys*., *29*, 358-370, 1991.

Kissel, C., Laj, C., Lehman, B. Labyrie, L. and V. Bout-Roumazeilles, Changes in the strength of the Iceland-Scotland Overflow Water in the last 200,000 years: Evidence from magnetic anisotropy analysis of core SU90-33, *Earth Planet. Sci. Lett., 152*, (1-4), 25-36, 1997.

Köster, H.M., Kohler, E.E., Krahl, J. Kröger, J. and K. Vogt, Veränderungen an Montmorillonit durch Einwirkung von 0,1 m AeDTE-Lösungen, 1 n NaCl-Lösung und 0,1 n Salzsäure, *N. Jb. Miner. Abh*., *119***,** (1), 83-100, 1973.

Lund, S.P. and R. Karlin, Introduction to the special section on physical and biogeochemical processes responsible for the magnetization of sediments, *J. Geophys. Res*., *90*, 4353-4354, 1990.

Maher, B.A. and R. Thompson, *Quarternary Climates*, Environments and Magnetism, 390 pp., Cambridge University Press, Cambridge, 1999.

Matzka, J., *Magnetische, elektronenmikroskopische und lichtmikroskopische Untersuchungen an Stäuben und Aschen sowie and einzelnen Aschepartikeln*, Diploma thesis, University of Munich, Munich, 1997.

McEnroe, S.A., Harrison, R.J., Robinson, P. and F. Langenhorst, Nanoscale haematite-ilmenite lamellae in massive ilmenite rock: an example of 'lamellar magnetism' with implications for planetary magnetic anomalies, *Geophys. J. Int., 151*, 890-912, 2002.

Mehra, O.P., and M.L. Jackson, Iron oxide removal from soils and clays by dithionite-citrate system buffered with sodium bicarbonate, in *Clays and Clay Minerals, Proc. 7th nat. conf. clays and clay minerals*, pp. 317-327, edited by A. Swineford, Washington D.C., 1960.

Murray, S. and A.F. Renard, *Rept. Sci. Results Voyage H.M.S. Challenger*, 3, Neill and Co., Edingbourgh, 1891.

Oldfield, F., Environmental Magnetism: a personal perspective, *Quat. Sci. Rev*., *10*, 73-85, 1991.

Petermann, H and U. Bleil, Detection of live magnetotactic bacteria in South Atlantic deep-sea sediments, *Earth Planet. Sci. Lett., 117*, 223-228, 1993.

Petersen, N., Bleil, U. and P. Eisenach, Low temperature alteration of the magnetic minerals in ocean floor basalts, in *Deep Drilling Results in the Atlantic Ocean: Ocean Crust*, pp. 169-209, eds Talwani, M., Harrison, C.H. and Hayes, D.E., Maurice Ewing Series 2, Am. Geophys. Union, Washington DC, 1978.

Petersen, N., von Dobeneck, T. and H. Vali, Fossil bacterial magnetite in deep-sea sediments from the South Atlantic Ocean, *Nature, 320*, 611-615, 1986.

Petersen, N. and H. Vali, Observation of shrinking cracks in ocean floor titanomagnetites, *Phys. Earth Planet. Inter*., *46*, 197-205, 1987.

Petschick, R., Kuhn, G. and F. Gingele, Clay mineral distribution in surface sediments of the South Atlantic: sources, transport and relation to oceanography, *Mar. Geology*, *130*, 203-229, 1996.

Prior, D.J., Boyle, A.P., Brenker, F., Cheadle, M.C., Day, A., Lopez, G., Peruzzo, L., Potts, G.J., Reddy, S., Spiess, R., Timms, N.E., Trimby, P., Wheeler, J. and L. Zetterström, The application of electron backscatter diffraction and orientation contrast imaging in the SEM to textural problems in rocks, *Am. Mineral., 84*, 1741-1750, 1999.

Prospero, J.M., Glaccum, R.A. and R.T. Nees, Atmospheric transport of soil dust from Africa to South America, *Nature*, *289*, 570-572, 1981.

Pye, K., *Aeolian Dust and Dust Deposits, Academic Press*, Elsevier Science, San Diego, London, Burlington, 334 p., 1987.

Reitz, A., Hensen, C., Kasten, S., Funk, J.A. and G.J. de Lange, A combined geochemical and rock-magnetic investigation of a redox horizon at the last glacial/interglacial transition, *Phys. Chem. Earth, 29*, 921-931, 2004.

Rey, D., Mohamed, K.J., Bernabeu, A., Rubio, B. and F. Vilas, Early diagenesis of magnetic minerals in marine transitional environments: Geochemical signatures of hydrodynamic forcing, *Marine Geology, 215*, (3-4), 215-236, 2005.

Roberts A.P. and G.M. Turner, Diagenetic formation of ferrimagnetic iron sulphide minerals in rapidly deposited marine sediments, South Island, New Zealand, *Earth Planet. Sci. Lett., 115,* (1-4), 257-273, 1993.

Roberts, A., Magnetic properties of sedimentary greigite (Fe3S4), *Earth Planet. Sci. Lett., 134*, (3-4), 227-236, 1995.

Ruddiman, W.F., *Earth's Climate – Past and Future*, 465 pp., W.H. Freeman, New York, 2001.

Sarnthein, M., Thiede, J., Pflaumann, U., Erlenkeuser, H., Fütterer, D., Koopmann, B., Lange, H. and E. Seibold, *Atmospheric and oceanic circulation patterns off Northwest Africa during the past 25 million years, in Geology of the Northwest African Continental Margin*, pp. 545-604, edited by U. Rad, K. Hinz, et al., Springer-Verlag, Berlin, 1982.

Schmidt, A.M., von Dobeneck, T. and U. Bleil, Magnetic characterization of Holocene sedimentation in the South Atlantic, *Paleocean*., *14***,** (4), 465-481, 1999.

Schulz, H.D. and cruise participants, Report and preliminary results of Meteor cruise M16/2, Recife – Belem, 28.4.-20.5.1991, *Ber. Fachber. Geowiss. Univ. Bremen, 19*, 149 p., 1991.

Smith, P.P.K., The identification of single-domain titanomagnetite particles by means of transmission electron microscopy, *Can. J. Earth Sci*., *16*, 375-379, 1979.

Sparks, N.H.C., Mann, S., Bazylinski, D.A., Lovley, D.R., Jannasch, H.W. and R.B. Frankel, Structure and morphology of magnetite anaerobically-produced by a marine magnetotactic bacterium and a dissimilatory iron-reducing bacterium, *Earth Plant. Sci. Lett., 98*, 14-22, 1990.

Suk, D. Peacor, D.R. and R. Van der Voo, Replacement of pyrite framboids by magnetite in limestone and implications for paleomagnetism, *Nature*, *354*, 611-613, 1990.

Stuut, J.-B.W., Zabel, M, Ratmeyer, V. and Helmke, P., Provenance of present-day eolian dust collected off NW Africa, *J. Geophys. Res*., *110*, D04202, doi:10.1029/2004JD005161, 2005.

Taylor, R.M., Maher, B.A. and P.G. Self, Magnetite in Soils: I. The synthesis of single domain and superparamagnetic magnetite, *Clay Min., 22*, 411-422, 1987.

Thiel, R., Zum System α-FeOOH – α-AlOOH, *Z. Anorg. Allg. Chemie*, *326*, 70-78, 1963.

Thompson, R. and F. Oldfield, *Environmental Magnetism*, Allen and Unwin, London, pp. 1-227, 1986.

Vali, H., von Dobeneck, T., Amarantidis, G., Förster, O., Morteani, G., Bachmann, L. and N. Petersen, Biogenic and lithogenic magnetic minerals in Atlantic and Pacific deep sea sediments and their paleomagnetic significance, *Geol. Rundschau*, *78*, 753-764, 1989.

Verosub, K.L. and A.P. Roberts, Environmental magnetism: past, present, and future, *J. Geophys. Res*., *100*, 2175-2192, 1995.

Vlag, P., Rochette, P. and M.J. Dekkers, Some additional hysteresis parameters for a natural (titano)magnetite with known grain-size, *Geophys. Res. Lett., 23*, (20), 2803-2806, 1996.

von Dobeneck, T., Petersen, N. and H. Vali, Bakterielle Magnetofossilien – Paläomagnetische und paläontologische Spuren einer ungewöhnlichen Bakteriengruppe, *Geowissenschaften in unserer Zeit*, *5*, 27-35, 1987.

von Dobeneck, T., The concept of 'partial susceptibilities', *Geol. Carpath., 49*, 228-229, 1998.

von Dobeneck, T. and F. Schmieder, Using rock magnetic proxy records for orbital tuning and extended time series analysis into the super- and sub-Milankovitch bands, in *Use of proxies in paleoceanography: examples from the South Atlantic*, edited by G. Wefer and G. Fischer, pp. 601-633, Springer-Verlag, Berlin, Heidelberg, New York, 1999.

Walker, T.R., Larson, E.E. and R.P. Hoblitt, Nature and origin of hematite in the Moenkopi formation (Triassic), Colorado plateau: a contribution to the origin of magnetism in red beds, *J. Geophys. Res., 86*, 317-333, 1981.

Wynn, R.B., Masson, D.G., Stow, D.A.V. and P.P.E. Weaver, The Northwest African slope apron: a modern analogue for deep-water systems with complex seafloor topography, *Mar. Petrol. Geol*., *17*, 253-265, 2000.

Xu, W., Van der Voo, R. and D.R. Peacor, Are magnetite spherules capable of carrying stable magnetizations? *Geophys. Res. Lett*., *21,* (7), 517-520, 1994.

Chapter 6

Low-Temperature Partial Magnetic Self-Reversal in Marine Sediments

Summary
Various low-temperature experiments were performed on magnetic mineral extracts of marine sediments from the Argentine continental slope near the Rio de la Plata estuary. In these sediments the sulphate-methane transition zone is situated at depths between 4-8 meters. At around this transition, the magnetic mineralogy of the sediments is severely altered by reductive diagenesis. The magnetic mineral assemblage of the extracts, throughout the core, comprises of (titano-)magnetite of varying compositions, titanohematite and ilmenite. In the sulphate-methane transition zone (titano-)magnetite only occurs as inclusions in siliceous matrix and as intergrowths with lamellar titanohematite and ilmenite, originating from high temperature deuteric oxidation within the volcanic host rocks. These relic structures were visualized by scanning electron microscopy and analysed by energy dispersive spectroscopy. While warming of a field-cooled low-temperature saturation remanence (FC-SIRM) only indicates the Verwey transition of magnetite, cooling of a room-temperature saturation remanence (RT-SIRM) shows a marked drop below ~210K, corresponding to the Curie temperature of titanohematite with an approximate composition of $Fe_{1.15}Ti_{0.85}O_3$ (~TH85). The mechanism responsible for this loss of remanence at the moment of ordering is sought in partial magnetic self-reversal caused by magnetostatic interaction of both Fe-Ti-oxides. When titanohematite becomes ferrimagnetic upon cooling, its spontaneous magnetic moments order anti-parallel to the remanence of the RT-SIRM carrying (titano-)magnetite. Low-temperature cycling of RT-SIRM appears to be a valuable low-temperature method for the rock magnetic characterization of certain sedimentary iron-titanium oxides, in particular relic intergrowths of titanomagnetite and titanohematite.

***Keywords*:** self-reversal, marine sediments, titanohematite, titanomagnetite, low-temperature

---

This chapter is an anticle in review: Garming, J.F.L., Bleil, U., Franke, C. and von Dobeneck, T., 2006. Low-Temperature Partial Magnetic Self-Reversal in Marine Sediments, *Geophys. J. Int.*

1. Introduction

Sediments from the Argentine continental slope off the Rio de la Plata estuary have recently been analysed in detail for their geochemical and rock magnetic characteristics by Riedinger *et al*. (2005) and Garming *et al.* (2005), respectively. The principal source of their detrital magnetic mineral fraction is the drainage area of the Rio de la Plata tributaries in the Mesozoic flood basalts of the Paraná Basin (Fig. 1). Carriers of natural remanent magnetisation of these basalts are magnetite and low Ti bearing, slightly maghematised, titanomagnetite (Kosterov *et al.* 1998; Tamrat & Ernesto 1999).

At gravity core location GeoB 6229 (37°12.4'S and 52°39.0'W water depth 3446 m, Schulz *et al.* 2001) suboxic conditions are established close to the sediment surface and anaerobic oxidation of me-thane (AOM) is observed in a few meters sediment depth (Riedinger *et al.* 2005, Fig. 2). In this distinct redox zonation the magnetic iron oxide mineral inventory undergoes a two-stage diagenetic alte-ration. At the iron redox boundary, situated in the first meter, about one quarter of the bulk ferrimagnetic mineral content has been dissolved resulting in a significant coarsening in magnetic grain-size and diminishing of bulk coercivities (Garming *et al.* 2005). Reductive diagenesis in the suboxic zone is a common and frequently studied phenomenon in organic-rich marine sediments (e.g., Karlin and Levi 1983; Canfield & Berner 1987; Karlin 1990a, 1990b; Funk *et al.* 2004a,

2004b). In contrast the diagenetic processes in the intensely reducing environment of the sulphate methane transition (SMT) zone surrounding the AOM have been scarcely investigated so far.

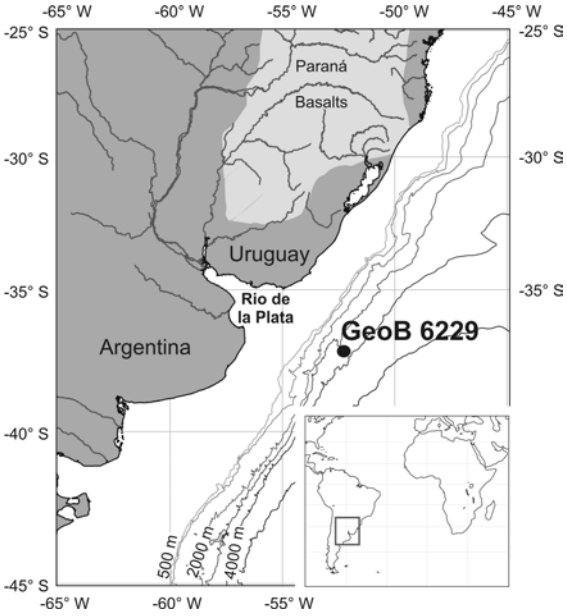

Figure 1. Location of core GeoB 6229 at the South American continental margin off the Rio de la Plata estuary. Grey shading schematically outlines titanium bearing Mesozoic flood basalts of the Paraná Basin (Peate *et al.*, 1992). Isobaths at 1000 m intervals, including the 500 m isobath, are according to GEBCO.

In the present example, only a small fraction below 10 %, of the primary (titano-)magnetite escaped dissolution being protected either as inclusions in a siliceous matrix or as relic intergrowths with high titanium bearing and well-preserved titanohematite lamellae (Garming *et al.* 2005). A greater stability of Ti bearing oxides relative to pure Fe oxides has been frequently observed (e.g., Karlin 1990b; Emiroglu *et al.* 2004). It can be plausibly explained by the fact that every Ti^{4+} substitution in Fe oxides lowers twofold the number of Fe^{3+} cations acting as electron acceptors under anaerobic conditions. In case of substantial Ti^{4+} substitution, the remaining iron is almost entirely in the reduced ferrous (Fe^{2+}) state, rendering the mineral less reactive and vulnerable to reductive dissolution.

To demonstrate the compositional changes of the magnetic mineral fraction during progressive sub- and anoxic diagenesis, various low-temperature cycling experiments were performed on magnetic mineral extracts. Their results are discussed here together with the findings of scanning electron microscopic (SEM) analyses and energy dispersive spectroscopy (EDS).

2. Samples and Measurements

The magnetic extraction technique of Petersen *et al.* (1986) was applied to obtain magnetic separates for five samples located at key positions within the vertical redox zonation of gravity core GeoB 6229 (Fig. 2): (1) The suboxic zone below the iron redox boundary (2.45 m depth), (2) the transitional interval from suboxic to sulphidic conditions of the SMT zone (3.85 m depth), (3) the sulphidic SMT zone (5.85 m depth), (4) the transitional interval between the SMT zone and methanic zone (6.55 m depth) and (5) the methanic zone (8.35 m depth).

For low-temperature measurements with a *Quantum Design* Magnetic Property Measurement System (MPMS XL-7), accurately weighed amounts of these extracts were fixed with vacuum grease in small gelatine capsules. Susceptibility was determined from 5 to 300 K in 5 K steps applying a 110 Hz field of 0.4 mT amplitude. Saturation isothermal remanent magnetization (SIRM) experiments comprised thermal demagnetisation to room temperature of a 5 T LT-SIRM acquired at 5 K after zero field cooling (ZFC) as well as after field cooling (FC), and cycling of a 5 T room temperature (300 K) SIRM down to 5 K and back in zero field. For sample (4) hysteresis loops were determined with peak fields of 2 T at 18 selected temperatures between 275 and 160 K.

SEM observations of polished thin sections were made with a *Phillips* XL20 *SFEG*, equipped with an EDS detector. Element compositions were determined from the EDS spectra using the '*Remote*

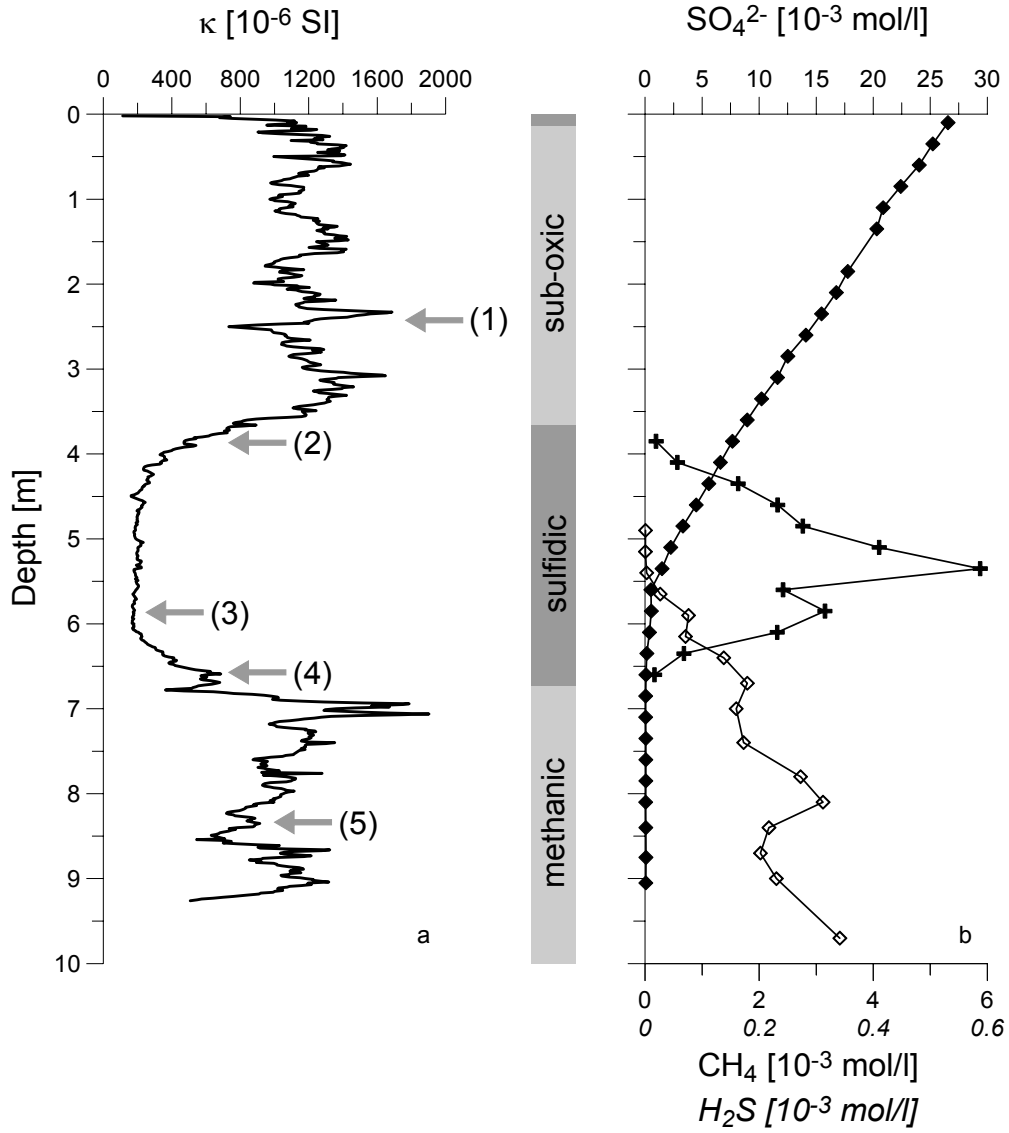

Figure 2. Core GeoB 6229-6 depth profiles of (a) low field magnetic susceptibility κ. (grey arrows indicate the sample positions for the low-temperature studies), and (b) pore water concentrations of sulphate (solid diamonds), methane (open diamonds) and sulphide (crosses) as measured directly after core recovery. Redrawn after Riedinger *et al.* (2005) and Garming *et al.* (2005).

SEM Quant Phiroz' program version 3.4.

3. Results

3.1. Low-Temperature Susceptibilities

The smoothed (5 point average) in-phase susceptibility data (Fig. 3) exhibits generally similar characteristics for all five samples. Increasing gradients above ~30 K and inflections in slope at around 60 K likely hint at the presence of ilmenite (Nagata & Akimoto 1956). A steep rise of susceptibilities above 90 K and a maximum at about 130 K reflect reduced coercivities towards and at the Verwey transition T_V and the isotropic point T_I of magnetite (Dunlop & Özdemir 1997). A third broad maximum around 220 to 230 K is most clearly developed for samples (2) to (4) from the sulphidic SMT zone and its transitional margins to the suboxic and methanic zones. In the suboxic sediment (1) this feature is faint; in the methanic zone it seems to be shifted to higher temperatures (~255 K). Analogous observations at 210 K, for the central Alaskan Old Crow tephra, have also been attributed

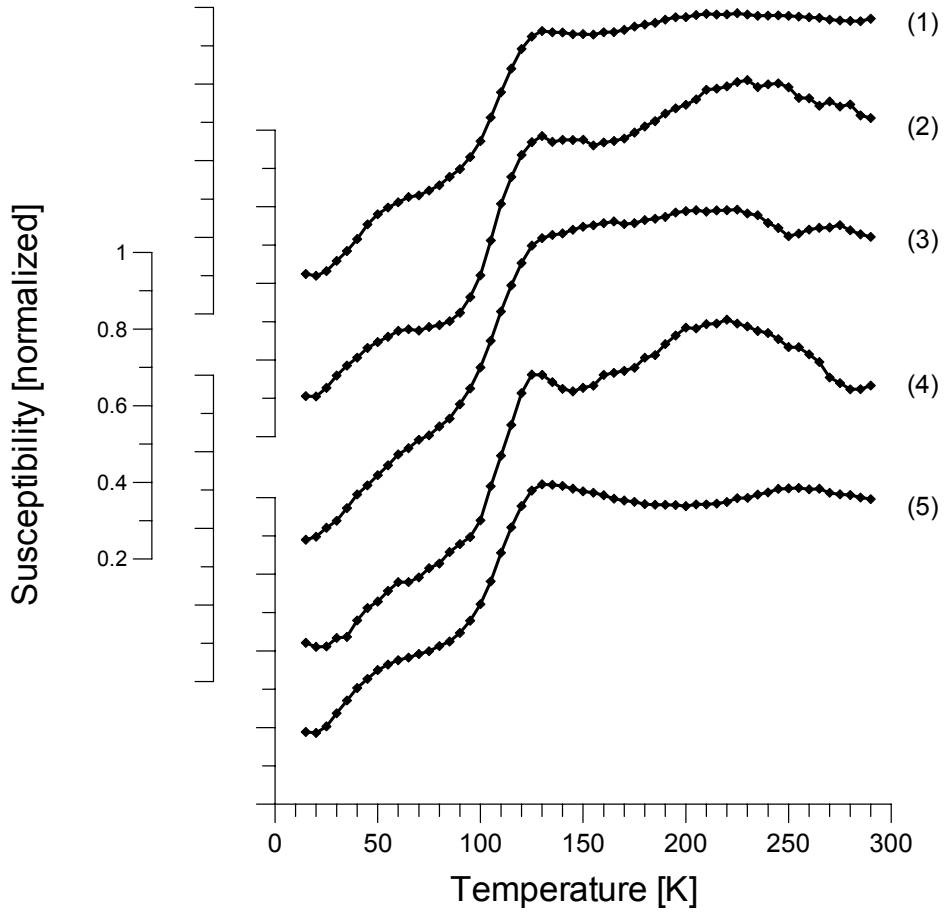

Figure 3. Normalized and smoothed (5 point average) magnetic susceptibilities measured between 5 and 300 K applying a 110 Hz field of 0.4 mT amplitude.

to the transition of a titanohematite phase from the ferrimagnetic to the paramagnetic state (Lagroix *et al.* 2004).

3.2. Low-Temperature SIRM Experiments

Thermal demagnetisation curves of FC- and ZFC-SIRM are shown in Fig. 4. Samples (2) to (4) from the SMT zone acquired 21 to 26 % more remanence by FC than by ZFC, while the difference is noticeably smaller for sample (1) from the suboxic (14 %) and sample (5) from the methanic (8 %) zones, possibly indicating coarser grained magnetic particles. All samples lose ~90 % of their initial 5 K remanence upon warming to 300 K; the remanence loss is largest between 5 and 20 K. The Verwey transition (T_V ~120 K) is broadened, indicating partially oxidized and/or Ti-rich magnetite (Ozdemir *et al.* 1993). Unlike the κ (T) curves, the FC- and ZFC-SIRM warming curves carry no particular features at around 60 K or in the 220 to 255 K interval, not even in their first derivatives (not shown).

Although zero field cooling curves (Fig. 5) also reveal marked slope changes around the Verwey point for all samples, a more prominent remanence loss occurs at higher temperatures. It is most clearly developed in the samples (2) and (4) of the SMT transitional zones, where abrupt breaks in slopes are observed at 210 and 215 K, respectively. Suboxic sample (1) shows a similar kink, whereas the remanence loss of the SMT zone sample (3) extends over a wider temperature range. For methanic zone sample (5) the decline of the RT-SIRM already starts at about 260 K; a faint undulation in gradient can be seen at around 210 K. Overall, these

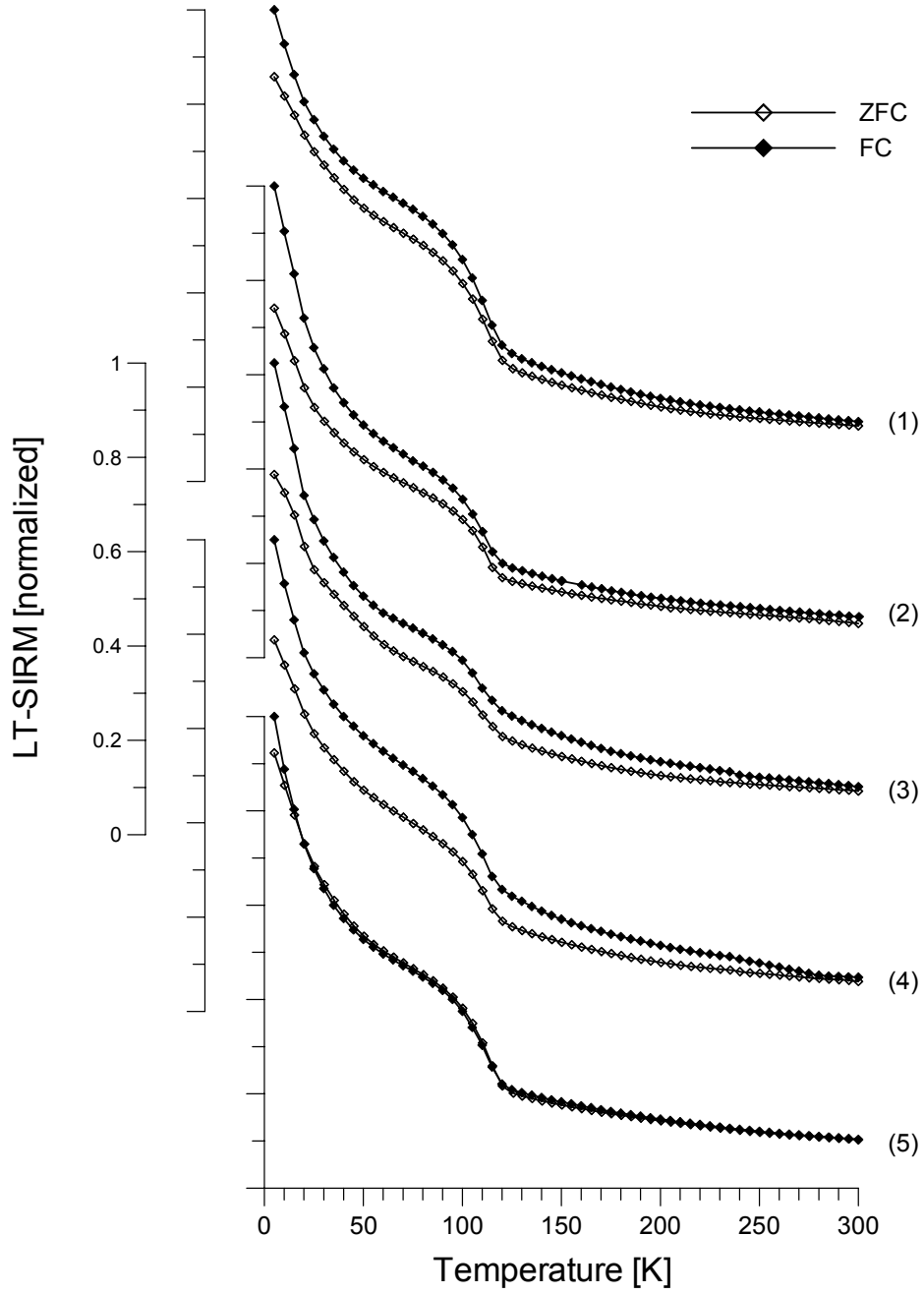

Figure 4. Thermal demagnetisation between 5 and 300 K of normalized 5 T SIRM acquired at 5 K after zero field cooling (open symbols) and 5 T field cooling (solid symbols).

results are fully consistent with the susceptibility data, indicating the presence of a titanohematite phase, with a Curie temperature of about 210 K. At 5 K between 40 to 60 % of the initial RT-SIRM remains, and is reversible up to ~50 K and showing a very limited recovery passing through T_V and in case of sample (4) slightly increases above 235 K. In the other samples the latter effect is restricted to very minor slope changes, (1) to (3), or missing (5).

3.3. Low-Temperature Hysteresis Properties

For transition zone sample (4) the temperature dependence of hysteresis properties has been determined between 160 and 275 K at peak fields of 2 T. Saturation magnetisation (σ_s), saturation

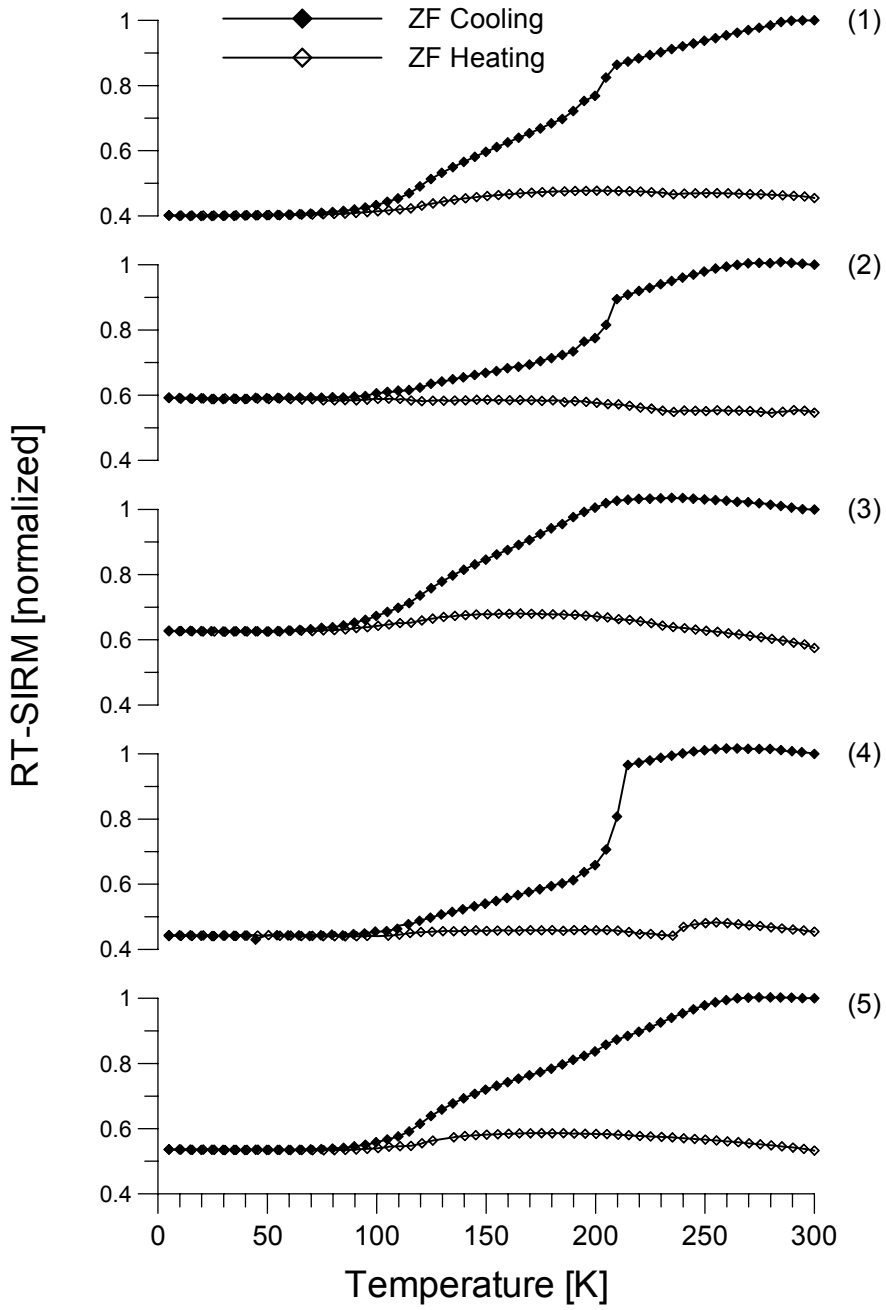

Figure 5. Zero field cooling (300 to 5 K, solid symbols) and warming (5 to 300 K, open symbols) of normalized 5 T room temperature (300 K) SIRM.

remanent magnetisation (σ_{rs}), coercive field (B_c) and domain state index (σ_{rs}/σ_s) were quantified after subtracting para- and diamagnetic components. Saturation magnetization (Fig. 6a) increases linearly by rates of 0.008 and 0.007 (Am^2/kg per Kelvin) when cooling from 275 to 245 K and from 230 to 160 K, respectively. The shift of 8 % between 245 and 230 K suggests that a new magnetic phase is ordering in correspondence to the previous findings (Figs. 3 to 5). A continuous increase with cooling is also observed for saturation remanence (Fig. 6b). The σ_{rs}/σ_s ratio (Fig. 6c) indicates grain-sizes at the multi-domain to pseudo-single-domain boundary, slightly fining towards deeper temperatures. Like the coercive field B_c (Fig. 6d), it reaches a minimum at 230 K. B_c changes at a higher rate (~0.03 mT per

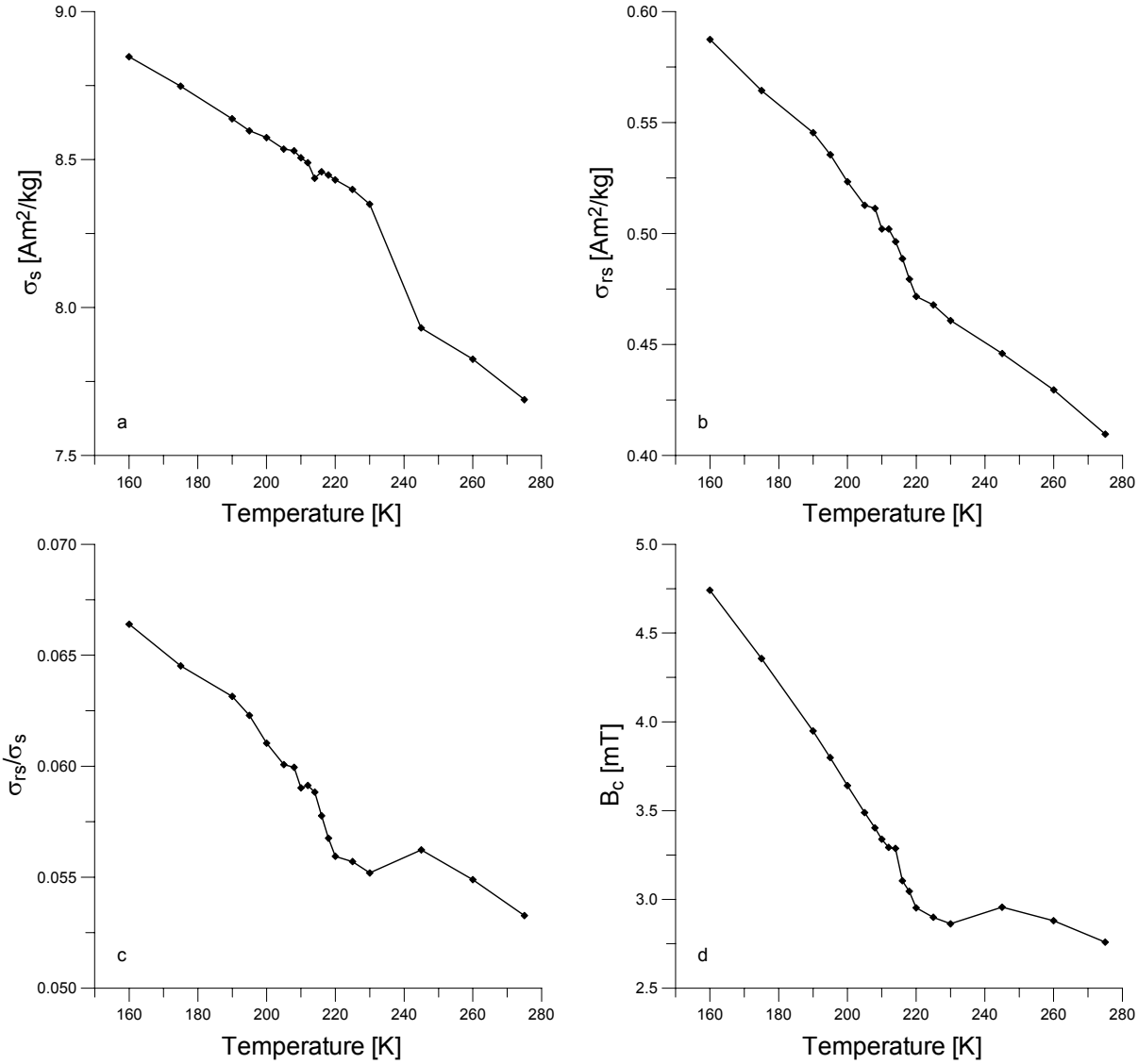

Figure 6. Results of hysteresis measurements for sample (4). Low-temperature dependence of (a) specific saturation magnetisation, σ_s, (b) specific saturation remanent magnetisation, σ_{rs}, (c) magnetic grain-size ratio, σ_{rs}/σ_s, and (d) coercive field, B_c.

Kelvin) below 210 K above 245 K (~0.01 mT per Kelvin).

3.4. Energy Dispersive Spectroscopy (EDS)

Electron optical examination and EDS of polished sections revealed the presence of a variety of iron-titanium-oxide minerals both from the titanomagnetite and the titanohematite solid solution series. According to the EDS analysis, the titanohematite lamellae (Figs. 7a and b), have an approximate composition of 0.85 $FeTiO_3$ · 0.15 Fe_2O_3 (y = 0.85, TH85), but higher Ti contents of up to almost pure ilmenite were also determined. Franke *et al.* (subm.) verified the presence of the titanomagnetite and titanohematite, using an electron backscatter diffraction (EBSD) technique.

Composition estimates for their relic titanomagnetite intergrowths (Fig. 7b), suggest implausibly high Ti contents of 0.40 Fe_2TiO_4 · 0.60 Fe_3O_4 (x = 0.4, TM40). Most likely the analyses were biased by the adjacent and underlying titanohematite lamellae. Almost pure magnetite, positively documented in the low-temperature susceptibility and SIRM records (Figs. 3 to 5), could not be detected else-where in the polished sections, supporting this assumption.

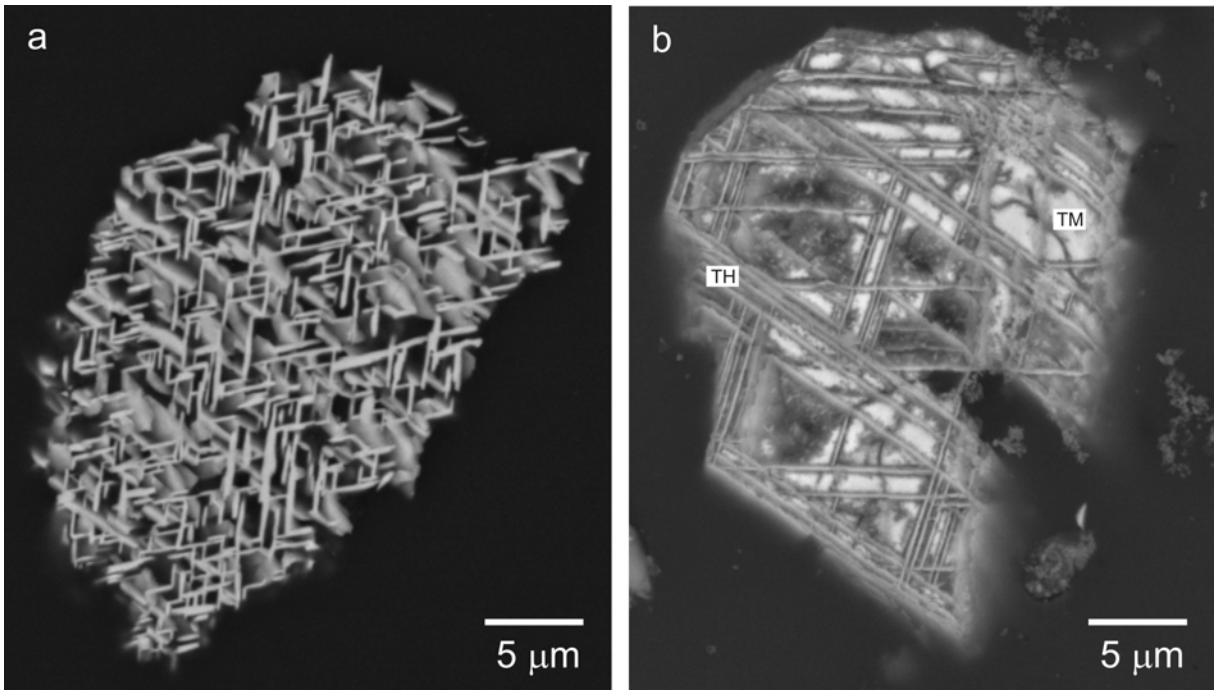

Figure 7. SEM micrograph showing (a) titanohematite lamellae and (b) intergrown titanohematite lamellae (TH) and (titano-)magnetite (TM).

4. Discussion and Conclusions

This study has shown that the magnetic mineral extracts of the continental slope sediments off the Rio de la Plata estuary consist of (titano-)magnetites of various compositions, titanohematite and ilmenite. Garming *et al.* (2005) identified the secondary mineral pyrite in the sulphidic zone surrounding the SMT.

The only plausible magnetic carrier at room temperature is (titano-)magnetite, which is in the sulphidic zone, is either present as inclusions in a siliceous matrix or intergrown with titanohematite lamellae (Fig. 7b). The data indicates compositions from almost pure to up to 40 % Ti-substituted magnetite. Indications for partial low-temperature oxidation of the (titano-)magnetites are present in form of a broad and down-shifted Verwey transitions (Fig. 4; Dunlop & Özdemir, 1997) and shrinking cracks (Fig. 7b; Garming *et al.* 2005).

The titanohematite lamellae have approximate compositions of TH85 and higher and therefore do not contribute to room temperature remanence; they only become ferromagnetic at their Curie temperatures of 210 K and lower (Nagata & Akimoto 1956; Dunlop & Özdemir 1997). Low-temperature hysteresis parameters (Fig. 6a and b) document a gradual transition from a paramagnetic to a superparamagnetic and finally to a stable ferromagnetic state between 190 and 245 K. Grain-size and compositional effects (Fig. 6c) affect the width of this interval. The coercive field minimum at 230 K confirms, in agreement with susceptibility and SIRM data, that the TH phase is predominantly superparamagnetic at this temperature.

Cycling of a RT-SIRM showed that the magnetic moments of the titanohematites order in anti-parallel direction to the RT-SIRM of the intergrown (titano-)magnetite (Fig. 5) on cooling through their Curie and blocking temperature, resulting in an apparent partial SIRM self-reversal. Titanohematites with compositions $y \geq 0.5$ are ferrimagnetic and do show selfreversing properties (Stacey & Banerjee 1974; Dunlop & Özdemir, 1997, and references cited therein). Negative exchange coupling to an intergrown second titanohematite phase of lower Ti content

($y < 0.5$) has often been identified as underlying mechanism. There is no supporting evidence, however, that such a process could be responsible for the drop in RT-SIRM as observed here at around 210 K and higher temperatures (Fig. 5). The host rocks of the detrital sedimentary magnetic mineral assemblage are basalts, that different from felsic volcanics, typically do not contain two phases of intergrown titanohematites. No low Ti titanohematite ($y < 0.5$) was actually detected. Instead, high Ti titanohematite ($y \leq 0.7$), a common product of high temperature titanomagnetite deuteric oxidation, is found intergrown with titanomagnetite (Fig. 7b). Between such physically decoupled magnetic phases magnetostatic interaction seems the only conceivable mechanism for self-reversal (Dunlop & Özdemir 1997). Compared to exchange coupling, magnetostatic interaction is weak. This explains the absence of any anomaly in the critical temperature interval of the LT-SIRM thermal demagnetisation to room temperature (Fig. 4).

The superior stability of Ti-rich titanohematites to reductive diagenesis (e.g., Karlin 1990b; Emiroglu *et al.* 2004) and the relative easy technique of RT-SIRM cycling, can be used as proxy indicator of strongly reducing sedimentary environments by the presence of the shown partial RT-SIRM self-reversal, providing that there are TM/TH intergrowths. The partial self reversal documented here is probably absent in the parent rocks, the Mesozoic flood basalts of the Paraná Basin. The large abundance of titanomagnetite in the unaltered rock would most likely mask the here observed effect.

Acknowledgements

SEM and EDS analyses were performed at the electron microscopy & structural analysis (EMSA) center, Utrecht University, the Netherlands. The Deutsche Forschungsgemeinschaft (DFG) and the Netherlands Organization of Scientific Research (NWO) supported this study as part of the European Graduate College '*Proxies in Earth History*'. This is DFG Research Center Ocean Margins Publication no: RCOM###

References

Canfield, D.E. and Berner, R.A., 1987. Dissolution and pyritization of magnetite in anoxic marine sediments, *Geochim. Cosmochim. Acta*, 51, 645-659.

Dunlop, D.J. and Özdemir, Ö. 1997. *Rock Magnetism: Fundamentals and Frontiers*. pp. 573, Cambridge University Press, Cambridge.

Emiroglu, S., Rey, D. and Petersen, N., 2004. Magnetic properties of sediment in the Ría de Arousa (Spain): dissolution of iron oxides and formation of iron sulphides, *Phys. Chem. Earth*, 29, 947-959.

Franke, C., Pennock, G.M., Drury, M.R., Lattard, D., Engelmann, R., Garming, J.F.L., von Dobeneck, T. and Dekkers, M.J., in review. Identification of magnetic Fe-Ti-oxides by electron backscatter diffraction (EBSD) in scanning electron microscopy, *J. Geophys. Res.*

Funk, J.A., von Dobeneck, T. and Reitz, A., 2004a. Integrated Rock Magnetic and Geochemical Quantification of Redoxomorphic Iron Mineral Diagenesis in Late Quaternary Sediments from the Equatorial Atlantic, *in: The South Atlantic in the Late Quaternary: Reconstruction of Material Budget and Current Systems*, pp. 237-260 Eds. Wefer, G., Mulitza, S. and Ratmeyer, V., Berlin, Springer-Verlag,.

Funk, J.A., von Dobeneck, T., Wagner, T. and Kasten, S., 2004b. Late Quaternary sedimentation and early diagenesis in the Equatorial Atlantic Ocean: patterns, trends and processes deduces from rock magnetic and geochemical records, *in: The South Atlantic in the Late Quaternary: Reconstruction of Material Budgets and Current Systems*, pp. 461-497, Eds. Wefer, G., Mulitza, S. and Ratmeyer, V., Berlin Heidelberg New York Tokyo, Springer-Verlag,.

Garming, J.F.L., Bleil, U. and Riedinger, N., 2005. Alteration of Magnetic Mineralogy at the Sulfate Methane Transition: Analysis of Sediments from the Argentine Continental Slope, *Phys. Earth Planet. Inter.*, 151, 290-308.

Karlin, R., 1990a. Magnetic mineral diagenesis in suboxic sediments at Bettis site W-N, NE Pacific Ocean, *J. Geophys. Res.*, 95, 4421-4436

Karlin, R., 1990b. Magnetite diagenesis in marine sediments from the Oregon continental margin, J. Geophys. Res., 95, 4405–4419.

Karlin, R. and Levi, S., 1983. Diagenesis of magnetic minerals in recent haemipelagic sediments, *Nature*, 303, 327-330.

Kosterov, A.A., Perrin, M., Glen, J.M. and Coe, R.S., 1998. Paleointensity of the Earth's magnetic field in Early Cretaceous time: the Parana Basalt, Brazil, *J. Geophys. Res.*, 103, 9739-53.

Lagroix, F., Banerjee, S.K. and Jackson, M.J., 2004. Magnetic properties of the Old Crow tephra: Identification of a complex iron titanium oxide mineralogy, *J. Geophys. Res.*, 109, doi:10.1029/2003JB002678.

Nagata, T. and Akimoto, S., 1956. Magnetic properties of ferromagnetic ilmenites, *Geofis. Pura Appl.*, 34, 36-50.

Ozdemir, O., Dunlop, D.J. and Moskowitz, B.M., 1993. The effect of oxidation on the verwey transition in magnetite, *Geophys. Res. Lett.*, 20, 1671-1674.

Peate, D.W., Hawkesworth, C.J. and Mantovani, M.S.M., 1992. Chemical stratigraphy of the Paraná lavas (South America): Classification of magma and their spatial distribution, *Bull.Volcanol.*, 55, 119-139.

Petersen, N., von Dobeneck, T. and Vali, H., 1986. Fossil bacterial magnetite in deep-sea sediments from the South Atlantic Ocean, *Nature*, 320, 611-615.

Riedinger, N., Pfeifer, K., Kasten, S., Garming, J.F.L., Vogt, C. and Hensen, C., 2005. Diagenetic Alteration of Magnetic Signals by Anaerobic Oxidation of Methane Related to a Change in Sedimentation Rate, *Geochim. Cosmochim. Acta*, 69, 4117-4126.

Schulz, H.D., and Cruise Participants, 2001. *Report and preliminary results of meteor cruise M 46/2*, pp. 107, Berichte, Fachbereich Geowissenschaften, Universität Bremen, No. 184.

Stacey, F.D. and Banerjee, S.K., 1974. *The Physical Principles of Rock Magnetism*. pp. 195, Elsevier, Amsterdam.

Tamrat, E. and Ernesto, M., 1999. Magnetic fabric and rock-magnetic character of the Mesozoic flood basalts of the Parana Basin, Brazil, *J. Geodynam.*, 28, 419-37

Available online at www.sciencedirect.com
SCIENCE DIRECT®
Earth and Planetary Science Letters 241 (2006) 876–887
EPSL
www.elsevier.com/locate/epsl

Active and buried authigenic barite fronts in sediments from the Eastern Cape Basin

N. Riedinger [a,*], S. Kasten [a,1], J. Gröger [a], C. Franke [a,b], K. Pfeifer [a]

[a] *Fachbereich Geowissenschaften, Universität Bremen, Klagenfurter Straße, 28359 Bremen, Germany*
[b] *Paleomagnetic Laboratory, Fort Hoofddijk', Utrecht University, Budapestlaan 17, 3584 CD Utrecht, The Netherlands*

Received 15 April 2005; received in revised form 19 October 2005; accepted 27 October 2005
Available online 15 December 2005
Editor: H. Elderfield

Abstract

Sediment cores retrieved in the Benguela coastal upwelling system off Namibia show very distinct enrichments of solid phase barium at the sulfate/methane transition (SMT). These barium peaks represent diagenetic barite ($BaSO_4$) fronts which form by the reaction of upwardly diffusing barium with interstitial sulfate. Calculated times needed to produce these barium enrichments indicate a formation time of about 14,000 yr. Barium spikes a few meters below the SMT were observed at one of the investigated sites (GeoB 8455). Although this sulfate-depleted zone is undersaturated with respect to barite, the dominant mineral phase of these buried barium enrichments was identified as barite by scanning electron microscopy (SEM). This is the first study which reports the occurrence/preservation of pronounced barite enrichments in sulfate-depleted sediments buried a few meters below the SMT. At site GeoB 8455 high concentrations of dissolved barium in pore water as well as barium in the solid phase were observed. Modeling the measured barium concentrations at site GeoB 8455 applying the numerical model CoTReM reveals that the dissolution rate of barite directly below the SMT is about one order of magnitude higher than at the barium enrichments deeper in the sediment core. This indicates that the dissolution of barite at these deeper buried fronts must be retarded. Thus, the occurrence of the enrichments in solid phase barium at site GeoB 8455 could be explained by decreased dissolution rates of barite due to the changes in the concentration of barite in the sediment, as well as changes in the saturation state of fluids. Furthermore, the alteration of barite into witherite ($BaCO_3$) via the transient phase barium sulfide could lead to the preservation of a former barite front as $BaCO_3$. The calculations and modeling indicate that a relocation of the barite front to a shallower depth occurred between the last glacial maxium (LGM) and the Pleistocene/Holocene transition. We suggest that an upward shift of the SMT occurred at that time, most likely as a result of an increase in the methanogenesis rates due to the burial of high amounts of organic matter below the SMT.

Keywords: authigenic barite; Benguela upwelling system; anaerobic oxidation of methane (AOM); non-steady state diagenesis; witherite ($BaCO_3$)

1. Introduction

Sediments which underlay areas of high primary productivity are often enriched in barium bearing solid phases [1–5]. The link between productivity and the amount of barium in the sediment is thought to be established by the formation of distinct barite ($BaSO_4$)

* Corresponding author. Current address: Max-Planck-Institute for Marine Microbiology, Celsiusstrasse 1, 28359 Bremen, Germany. Tel.: +49 421 2028 634; fax: +49 421 2028 690.
E-mail address: nar@uni-bremen.de (N. Riedinger).
[1] Current address: Alfred Wegener Institute for Polar and Marine Research, Am Handelshafen 12, 27570 Bremerhaven, Germany.

0012-821X/$ - see front matter © 2005 Elsevier B.V. All rights reserved.
doi:10.1016/j.epsl.2005.10.032

particles in the water column associated with the decay of organic matter or rather the decay of phytoplankton [3,6–8]. Thus, in marine deposits barite is often used as a tracer of paleoproductivity [9–12]. Besides the utilization of excess barium, in particular barite, as a productivity-proxy several other indications can be drawn from barium compounds. Marine barite is often used to reconstruct past Sr isotope compositions of seawater, or for Sr isotope stratigraphy [13,14]. Furthermore it can be applied to reconstruct the former sulfur isotope ratio of marine sulfate [15,16], or to draw conclusions about past changes in the upward flux of methane [17].

However, the use of barium as a proxy (e.g. for paleoproductivity) is clearly limited as shown in several studies [9,12,18]. The alteration of the primary barium signal by diagenetic processes is one of the most important limitations for the application of barium and barium-compounds as a proxy. Generally, barite is relatively resistant to alteration after burial [14,19]. However, in zones of sulfate depletion barite is dissolved and barium is released into the pore water. The upward transport of barium by diffusion into sulfate-bearing pore waters is leading to precipitation of authigenic barite in diagenetic fronts. Thus, barite fronts are mainly found directly above the sulfate penetration depth, at the sulfate/methane transition (SMT) [9,17,20–22]. The formation of authigenic barite fronts is affected by diagenetic alteration due to sulfate reduction and driven by anaerobic oxidation of methane (AOM) [17,23]. Nonsteady-state diagenesis greatly influences authigenic barite precipitation [24]. Drastic decreases in sedimentation rate can fix the barite front at a discrete interval which can lead to the formation of large barite deposits [22]. Moreover, changes in methane flux can shift the SMT and thus the position of the barite front [17]. Thus, barite fronts can be used to reconstruct changes in the upward flux of methane. However, generally only former barite fronts above the current depth of the SMT which formed in association with a downward migration of the SMT can be used. Burial of barite enrichments in sulfate-depleted sediments is assumed to result in their fast dissolution. Up to now, barium enrichments preserved below the SMT have only been described in deeply buried sediments, drilled by the ODP (Ocean Drilling Program). These barium enrichments were mostly described as the result of hydrothermal intrusions or associated with fluid seeps [9,25,26].

In this study we report on barite enrichments at the SMT and in addition we present data of solid phase Ba-enrichments in the sulfate-depleted zone. Scanning electron microscopy (SEM) and energy dispersive spectrometry (EDS) were carried out for identification and semi-quantification of the Ba phases in the sediment. Furthermore, we discuss the mechanisms and/or conditions which lead to the preservation of the barite enrichments below the SMT. To investigate the processes involved, we applied numerical modeling of the geochemical data and we calculated the time needed to produce the barium peaks observed.

2. Materials and methods

2.1. Sampling sites

The gravity cores (Table 1) investigated in this study were retrieved on a down slope transect (T2) on the continental margin off Namibia in the eastern South Atlantic (Fig. 1) during RV *Meteor* expeditions M34/2 and M57/2. The sediments in the Eastern Cape Basin are characterized by low input of terrigenous matter and high biogenic contents. The high amounts of organic matter (up to 12 wt.% at site GeoB 8426, and 9 wt.% at site GeoB 8455) in the sediment are due to the enhanced primary productivity in the surface water [10,27]. The Benguela upwelling system is controlled by the predominant southeasterly trade-winds that drive the coastal upwelling of cold and nutrient-rich water [28,29]. Occasional berg winds, perpendicular to the coast, are the most important means of transport for terrestrial material [29,30]. Minor amounts of terrigenous sediment are supplied by perennial rivers (Orange River) and rivers sporadically carrying water, like the Swakop River [31]. The deposition of river discharge is limited to the shelf, and the slope mainly consists of calcareous ooze [31,32]. Quaternary slumps and slides can only be found close to the Walvis Ridge [27,33] and do not represent important sediment transport processes in the study area.

2.2. Sampling and sample processing

The sampling procedures and analytical techniques are only briefly described below. For detailed infor-

Table 1
Location and water depth of GeoB stations of the investigated gravity cores

Stations	Longitude [E]	Latitude [S]	Water depth [m]
GeoB 3703-8	13°13.8	25°31.1	1369
GeoB 3718-9	13°09.8	24°53.6	1312
GeoB 8426-3	13°21.1	25°28.9	1045
GeoB 8455-2	13°11.0	25°30.4	1503

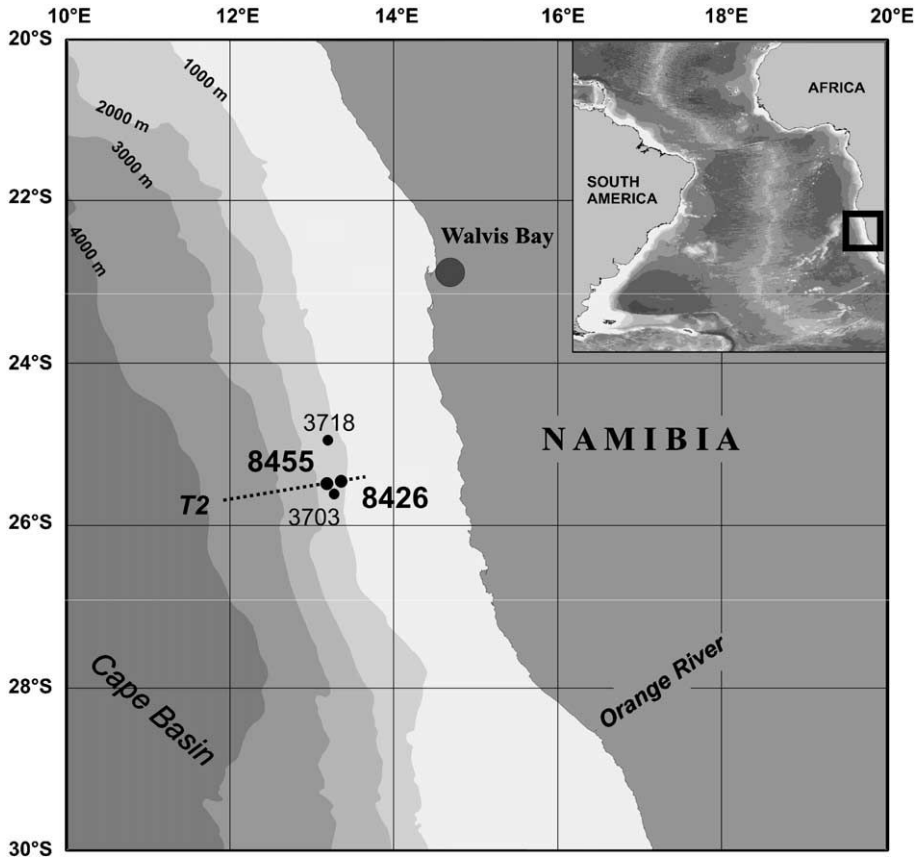

Fig. 1. Map displaying the location of the investigated gravity cores taken at the GeoB stations. The dotted line marks the transect 2 (T2).

mation regarding analytical methods and devices, the reader is referred to Schulz [34] and to the homepage of the geochemistry group http://www.geochemie.uni-bremen.de at the University of Bremen. The set of pore water and solid phase data is available via the geological data network Pangaea (http://www.pangaea.de/PangaVista?query=@Ref26531).

Immediately after retrieval gravity cores were cut into 1 m segments on deck and from the bottom of every segment syringe samples were taken for methane analysis. Syringe samples of 5 mL of sediment were injected into 50 mL septum vials containing 20 mL of seawater, and were stored at −20 °C. To prevent warming of the sediments, all cores were placed in a cooling container and were maintained at a temperature of about 4 °C. Within the first 2 days after recovery, gravity cores were cut lengthwise into two halves and were processed in a glove box under argon atmosphere. Sediment samples were taken every 25 cm for pressure filtration. Solid phase samples for total digestions, sequential extractions and mineralogical analyses were taken at 10 cm intervals and were kept in gas-tight glass bottles under argon atmosphere. To suppress subsequent alteration processes the storage temperature for all sediments was −20 °C. Teflon-squeezers fitted with 0.2 μm cellulose acetate membrane filters were used for pressure filtration (5 bar). For H_2S determination, 1 mL sub samples of the pore water were added to a ZnAc-solution (400 μL) in order to fix all sulfide as ZnS. Sub samples for sulfate determination were diluted 1:20 and stored frozen for ion chromatography (HPLC). All further analyses were carried out at the University of Bremen. Methane was measured with a gas chromatograph (*Varian 3400*) equipped with a splitless injector, by injecting 20 μL of the headspace gas. The concentrations were subsequently corrected for sediment porosity. H_2S was determined using a titration method. Aliquots of the remaining pore water were diluted, and acidified with HNO_3 for determination of cations by atomic absorption spectrometry (AAS, *Unicam Solaar 989 QZ*), and inductively coupled plasma atomic emission spectrometry (ICP-AES, *Perkin Elmer Optima 3000 RL*).

All solid phase analyses were performed on anoxic sub samples. Sample solutions obtained by total acid digestion were analyzed by ICP-AES, with an analytical precision of less than 3%. Solid phase samples from site GeoB 3703 were measured using X-ray fluorescence (XRF). Approximately 4 g of freeze dried and homogenized sediment material was poured into sample cups, and analyzed using the compact benchtop energy-dispersive polarization XRF (EDP-XRF) analysis system *Spectro Xepos*. Total carbon (TC) and total organic carbon (TOC) contents were determined by measuring freeze-dried and homogenized samples using a *LECO CS-300* carbon sulfur analyzer. For organic carbon analysis, the samples were treated with 12.5% HCl, washed two times with Milli Q, and dried at 60 °C. The accuracy, checked by marble standards, was ± 3%. Sediment physical measurements of electrical resistivity, as a measure of porosity and density, were performed at a resolution of 1 cm on board using a *GEOTEK* Multi-Sensor Core Logger (MSCL). Selected dry bulk sediment samples were analyzed by scanning electron microscopy (SEM) using a *Philips XL30 SFEG* (operating between 10 and 12 kV) equipped with an *EDAX* energy dispersive spectrometer (EDS). The non-embedded powder samples were fixed on a carbon sticker, previously stuck onto the top of a standard SEM stub, and coated under argon atmosphere with a 5 nm Pt/Pd layer.

2.3. Geochemical modeling

To simulate the process of barite dissolution and reprecipitation, the column transport and reaction model CoTReM was used. A detailed description of this computer software is given in the CoTReM User Guide [35] and by Adler et al. [36]. The transport mechanism for the solid phase and pore water is the sedimentation rate. The solutes in the pore water are transported by molecular diffusion (D_s). Diffusion coefficients were corrected for tortuosity [37] and temperature (3 °C). The model area, representing the core length of 12 m, was subdivided into cells of 5 cm thickness. The time step to fulfill numerical stability was set to 1×10^{-1} yr. Zero-order kinetics are calculated for the given reaction by defining maximum reaction rates. The calculation of the reaction-specific change in concentration at a specific depth ($\Delta C_{s,d}$) is according to the equation:

$$\Delta C_{s,d} = R_{s,d} \times dt_{num} \times SC_{s,d} \quad (1)$$

Where $R_{s,d}$ [mol L^{-1} yr^{-1}] is the reaction rate, dt_{num} is the time step used in the specific model run, and $SC_{s,d}$ is a stoichiometric factor. The maximum rates are used as long as they can be fulfilled by the available amount of the reactant. If the amount decreases, the rates were automatically reduced to avoid negative concentrations [36]. Sulfate bottom water concentration of 28 mmol L^{-1} and methane concentration of 0.0 mmol L^{-1}, as the major pore water parameters, were defined as the upper boundary condition. To allow diffusion across the boundary, the lower boundary is defined as an open/transmissive boundary. The diffusive flux of methane into the model area from below was defined by using a fixed methane concentration. This methane value was defined to create the gradient necessary to simulate the measured influx of CH_4. All input parameters are given in the respective section below.

3. Results and discussion

3.1. Authigenic barite fronts

In contrast to the non-reactive terrigenous Ba phase, biogenic barium is discussed as the labile Ba phase which is subject to (partial) remobilization in marine sediments due to sulfate depletion (e.g. [22,38]). The biogenic barium fraction is part of excess barium that can be calculated from the total amount of solid phase barium and the ratio of terrigenous Ba/Al or Ba/Ti [4,39,40] or determined by sequential extraction [14,41]. At high productivity area, the main amount of excess Ba in the underlying sediments is composed of barite [42]. Because of the high productivity within the Benguela upwelling area the input of reactive (biogenic) barium into the sediment in this area is high, while the amount of terrigenous barium is low [40,43].

The pore water and solid phase barium profiles at site GeoB 8426 (Fig. 2) display the typical diagenetic cycling of barium as discussed by von Breymann et al. [9]. The reactive solid phase barium is dissolved in the sulfate-depleted zone below the SMT and Ba^{2+} is released into the pore water:

$$Ba^{2+} + SO_4^{2-} \leftrightarrow BaSO_4 \quad (2)$$

The upward migration of the dissolved barium into the sulfate-bearing zone leads to the precipitation of authigenic barite at the SMT which is currently located at about 3.20 mbsf at site GeoB 8426. Just below the SMT, the solid phase profile shows a pronounced Ba peak (Fig. 2). This Ba enrichment contains barite par-

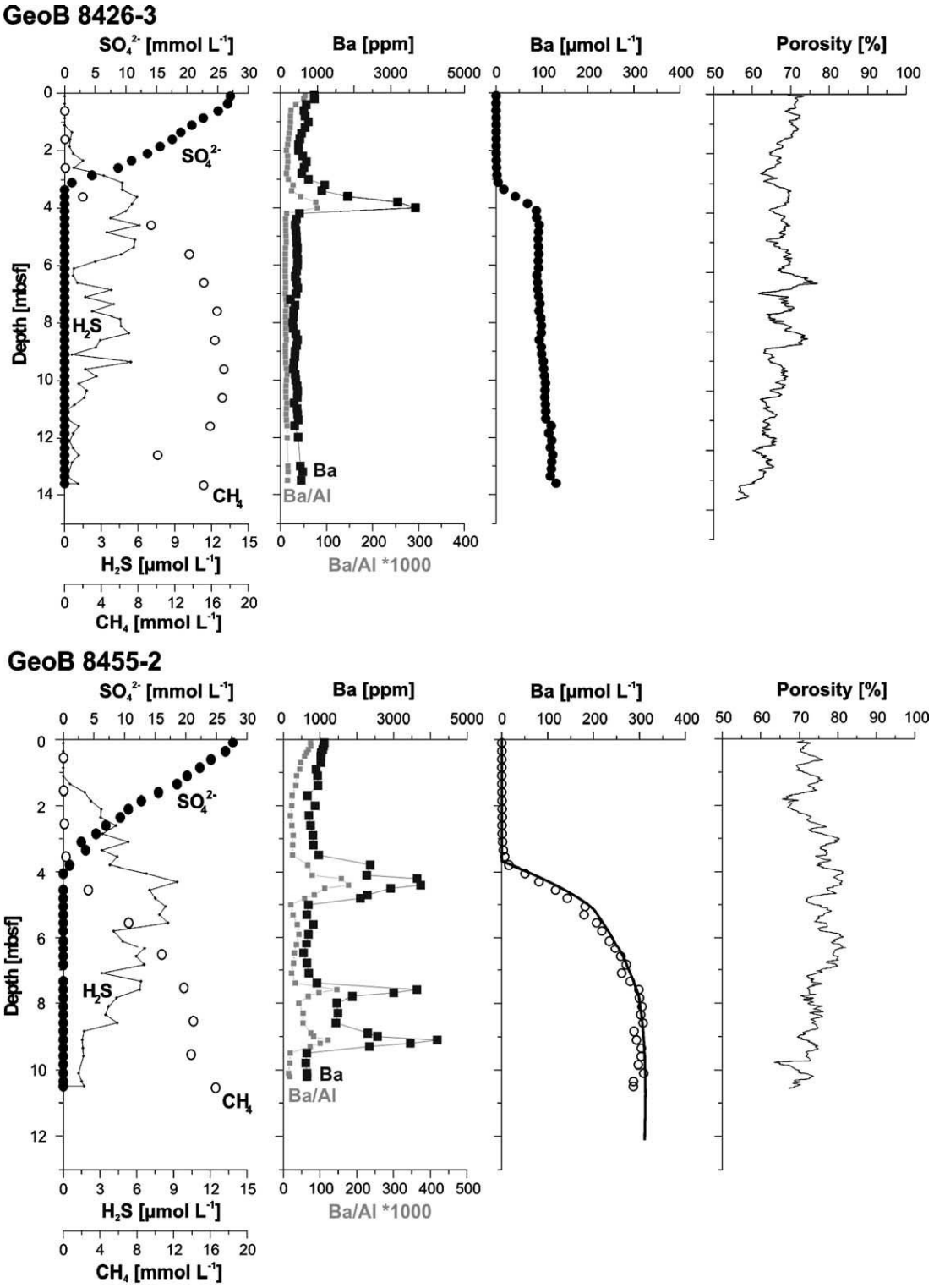

Fig. 2. Profiles of pore water and solid phase at sites GeoB 8426 and GeoB 8455. At both sites barium enrichments occur with a second small peak at the current sulfate/methane transition (SMT). At site GeoB 8455 two further barium enrichments are located a few meters below the SMT, indicating a release of barium into the pore water displayed by the dissolved barium profile. The solid line indicates the modeled pore water profile of barium.

ticles which partially show dissolution structures (Fig. 3A). The "double" barium peak indicates a recent upward shift in the SMT, with the small uppermost peak representing the site of the current/active barite front. Due to the diagenetic cycling of reactive barium, the authigenic barite peak is slowly but constantly growing. The active front slowly moves upward, keeping a constant offset to the sediment surface, corresponding to the SMT.

The penetration depth of sulfate in the study area is controlled by the anaerobic oxidation of methane (AOM) as shown by Niewöhner et al. [44]. At the SMT sulfate is consumed, and hydrogen sulfide is produced due to AOM (e.g. [45,46]):

$$CH_4 + SO_4^{2-} \rightarrow HCO_3^- + H_2O + HS^- \quad (3)$$

The sulfate pore water profiles of the investigated cores GeoB 8426-3 and GeoB 8455-2 show linear decrease with depth (Fig. 2). At site GeoB 8455 the SMT is located at about 3.80 mbsf, where solid phase barium is enriched similar to site GeoB 8426 with a second larger peak slightly below the SMT. In contrast to site GeoB 8426, the barium solid phase profile at site GeoB 8455 is characterized by the occurrence of two further distinct Ba-peaks a few meters below the SMT (Fig. 2). The shape of the barium pore water profile reveals that the deeper buried barium enrichments provide a source of barium to the pore water. This indicates the presence of reactive Ba solid phase. Selected representative samples analyzed by SEM and EDS indicate that the main Ba mineral present in the barium solid phase is barite. Although the deeper buried barite fronts, at depths of about 7.69 and 9.18 mbsf, are dominated by rather small particles, the shape of the barite crystals is similar to those found within the barite peak at the SMT. Some barite crystals from the barite fronts in the sediments of core GeoB 8455-2 are displayed in Fig. 3C–H. In contrast to the displayed barite particles at 4.22 mbsf, the barite grains at 7.69 and 9.18 mbsf show strong dissolution structures.

3.2. Time calculations for the formation of barite enrichments

Under the premise of a constant diffusive upward flux of barium into the sulfate-bearing zone, we calculated the time needed to produce the measured barium enrichment in the solid phase at the SMT. The duration of barium precipitation can be simulated assuming linear diffusive concentration gradients over time (cf. [17]). Similar calculations for the enrichment of iron sulfides were carried out by Kasten et al. [47]. Slight changes in the average porosity have substantial influence on the calculated enrichment periods. It has to be clearly pointed out that the calculated time needed for the formation of each barium enrichment is just an approximation due to these uncertainties. The calculation of the diffusive fluxes was performed according to Fick's first law with a diffusion coefficient in free solution (D_0) for barium of 147.6 $cm^2\ yr^{-1}$ which was corrected for tortuosity [37]. The refractory amount of solid phase barium (the mean concentration of barium in the lowermost core sediments) at sites GeoB 8426 and GeoB 8455 amounts to 500 and 650 ppm, respectively, and the dry density of the bulk sediment averages 2.7 $g\ cm^{-3}$. If we assume an average porosity of 70% for sediments at site GeoB 8426 and 75% for site GeoB 8455, the time needed to produce the observed barium peaks at the SMT would be about 14,000 yr. The variation of the enrichment period due to different porosities is given in Table 2. Assuming a decreasing barium flux with time due to the decreased amount of reactive barite at the deeper buried barium fronts or a decreased dissolution rate, the calculated times would be slightly overestimated. However, the results of the calculation emphasize that the barite enrichments in the deeper sediments at site GeoB 8455 were exposed to a sulfate-depleted environment for at least ten thousand years.

3.3. Numerical modeling

To assess the influence of different mechanisms and/or conditions (e.g. dissolution rates, diffusive barium fluxes, or variations in methane flux or sedimentation rate) on the amount and depth of solid phase barium, we simulated different scenarios by numerical modeling using the transport and reaction model CoTReM.

Dissolution rates for core GeoB 8455-2 were modeled by simulating the measured pore water profile of barium. This computer simulation is based on the assumption that the amount of diagenetic barite which precipitated at the SMT, was primarily supplied by upward diffusion of dissolved barium, resulting from the dissolution of labile barite in the sediment buried below the SMT, and the recycling of input barite at the SMT. The concen-

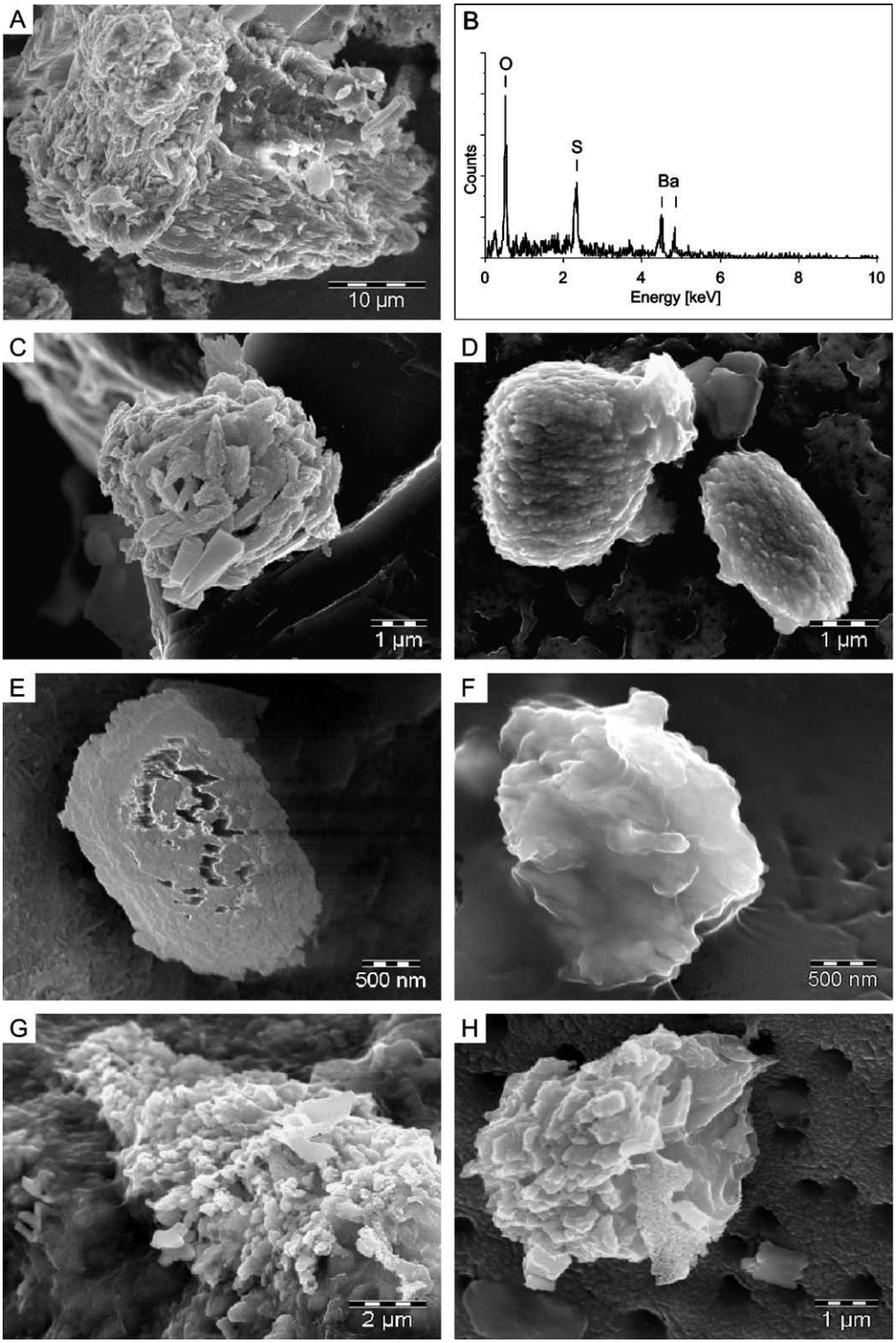

Fig. 3. Scanning electron microscope images of barite crystals. (A) Large barite particle at site GeoB 8426 slightly below the SMT (3.83 mbsf). (B) Energy dispersive spectra (EDS) of the barite particles displayed in (D). Images of barite at site GeoB 8455 at: (C) and (D): 4.22 mbsf. (E) and (F): 7.69 mbsf. (G) and (H): 9.18 mbsf. The barite particles of the last four panels (E–H) show strong dissolution structures.

Table 2
Calculation of the time needed for the formation of barite enrichment at the SMT for different porosities

Core	Ba gradient [mol cm^{-3} cm^{-1}]	Porosity [%]	Period of time [yr]
GeoB 8426-3	9.424 10^{-10}	65	19,905
		70	14,581
		75	10,428
GeoB 8455-2	1.330 10^{-09}	70	19,170
		75	13,709
		80	9439

The Ba flux is assumed to be constant over time, and the sediment dry density averages 2.7 g cm^{-3} .

tration of refractory solid phase barium below the SMT was set to 650 ppm and the mean measured input concentration above the SMT was 1000 ppm. Methane concentration at the lower boundary was set to 36 mmol/L transferred from the current gradient into the zone of SMT. For site GeoB 8455 the porosity of the sediment averages 75% (Fig. 2) and we used a mean sedimentation rate of 10 cm kyr^{-1}, adopted from adjacent sampling sites at similar water depths with sedimentation rates of 8–11 cm kyr^{-1} [48,49].

Modeling of the measured barium pore water profile of site GeoB 8455 (Fig. 2) reveals that the dissolution rate of barite directly below the SMT is higher than at the deeper buried Ba enrichments with rates of 1.1 µmol dm^{-3} yr^{-1}. This rate is similar to the dissolution rate for barite dissolution at methane cold seeps reported by Aloisi et al. [50]. The modeled dissolution rate decreases with depth down to 0.05 µmol dm^{-3} yr^{-1}. This indicates that the dissolution of barite at these deeper fronts is retarded compared to the dissolution rates directly below the SMT. A further interesting outcome of the model is that at steady-state conditions the shape of the barium peak at the SMT (mainly) depends on dissolution rate and sedimentation rate.

At the investigated sites, barite enrichments at the SMT are characterized by a large peak and a second, smaller one on top, representing the current barite front. Thus, there must have been a slight recent upward shift of the SMT, resulting in the formation of the uppermost barite enrichment. To find out whether this process is limited to the investigated sites, we compared barium solid phase data of adjacent coring sites GeoB 3703 and GeoB 3718 (Fig. 4). The occurrence of similar barium profiles with a second larger

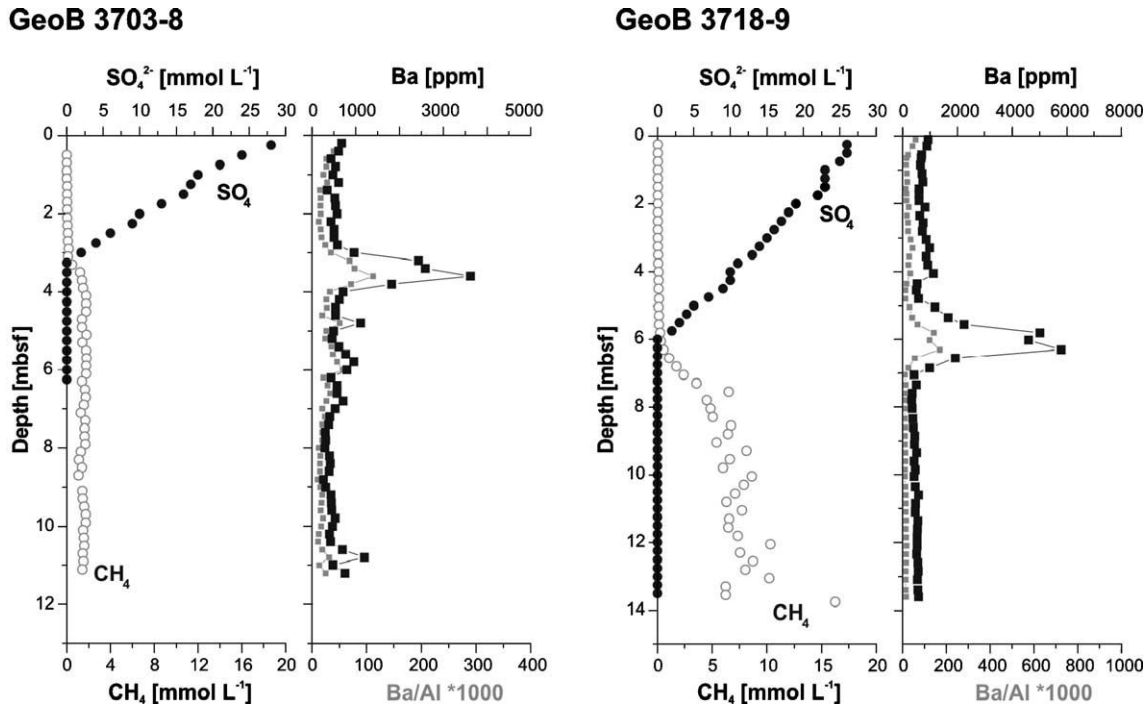

Fig. 4. Pore water and solid phase profiles at sites GeoB 3703 and GeoB 3718. At the current SMT a second smaller peak occurs at both sites. The pore water data of sulfate and methane are taken from Niewöhner et al. [44]. Solid phase data of core GeoB 3718-9 according to Kasten et al. [47].

peak directly below the SMT at all investigated stations reveal that the formation of these enrichments is influenced by more regional process.

Modeling the current positions of the barium peaks in core GeoB 8455-2 indicates enrichment due to nonsteady-state situations. At steady-state conditions only a single barite peak can be modeled. Increasing sedimentation rate or methane flux leads to the formation of a second barite peak. Possible nonsteady-state processes causing the formation of the observed barite fronts could be related to the sediment composition, the depositional dynamics, such as drastic changes in the sedimentation rate, or variations in the upward methane flux. An increase in the upward flux of methane over a larger area can be caused by the degradation of organic matter in deeper sediments, or the decomposition of gas hydrate. High resolution echosounder profiles, as recorded by the PARASOUND shipboard system during the cruises, indicate no depositional irregularities (e.g. caused by gravity mass flows). This is in good agreement with results from previous studies for this area [27]. Thus, the shift of the SMT cannot be explained by such depositional dynamics.

Although the thermodynamic stability criteria for gas hydrate at the sampling sites are fulfilled, chemical indications of their existence were not found in the sediment. An increase in methane concentrations could be also explained by the burial of high amounts of non-refractive organic matter below the SMT and the resulting elevated rates of methanogenesis due to the degradation of the organic matter. This process is likely regional. Regional processes can only account for the recent shift of the SMT leading to the formation of the small current barite peak which was found at both studied sites. In contrast, the finding of additional barium enrichments below the SMT is limited to site GeoB 8455. However, because the sedimentary records do not indicate any sedimentary event (e.g. slumps, slides), we assume that a change in the methane flux is the only process which also explains the prior pronounced shift in the SMT, and thus the preservation of additional barium fronts a few meters below the current SMT.

3.4. Barite enrichments below the SMT

In sulfate-depleted marine sediments, barite is supposed to be unstable. The occurrence of barite enrichments below the SMT at site GeoB 8455 indicates that there are processes or conditions increasing the stability of barite in the sulfate-depleted sediments. One mechanism in this regard could be the strikingly high amount of total barium in the sediment system at site GeoB 8455 (Fig. 2). High concentrations of dissolved barium below the SMT could influence the dissolution rate of barite. Modeling pore water data from site GeoB 8455 at 7.6 mbsf by using PHREEQC 2.10 [51] indicates that for an initial barium concentration of 300 μmol L^{-1} a low sulfate concentration of about 5 μmol L^{-1} would be sufficient to obtain barite saturation (with an equilibrium constant (log KT) of -10.40 at a temperature of 3 °C).

However, sediment volume-normalised dissolution rates are dependent both on the saturation state of fluids and on the concentration of $BaSO_4$ in sediments. Thus, the decrease of the barite dissolution rate with depth that we calculate with the model may be due to changes in the concentration of barite in the sediment, as well as changes in the saturation state of fluids.

Another explanation for the enrichment of barium minerals in the sulfate-depleted zone could be the occurrence of other Ba phases that show oxygen depletion relative to barite. Energy dispersive spectra of barium particles from the deeper buried barium enrichments at site GeoB 8455 reveal that some barium phases have low oxygen concentrations while the amount of sulfur and barium is constant and only the carbon concentration increases (Fig. 5). This suggests that some barite particles were altered, or that primary sulfate-free Ba phases exist. González-Muñoz et al. [52] reported microbially mediated precipitation of barite under laboratory conditions, and found that Ba phases were incorporated into spherical aggregates without sulfate. These spherical aggregates of 0.5 to 1 μm in diameter show a striking similarity to some of the barium particles which are found within the barium enrichments at site GeoB 8455 (Fig. 5C). The observed spherical aggregates described by González-Muñoz et al. [52] mainly contained barium and phosphorus and were supposed to represent an early stage of crystal growth. This does not necessarily imply that the spherical aggregates found in core GeoB 8455-2 were formed by bacterially mediated processes, but that the crystals either are in an early stage of growth or that the growth of the crystals was inhibited at an early stage.

Another process which could explain the occurrence of oxygen-depleted barium phases compared to barite, would be the dissimilatory reduction of sulfate from barite, as investigated by Baldi et al. [53]. Based on laboratory results they discussed the microbial reduc-

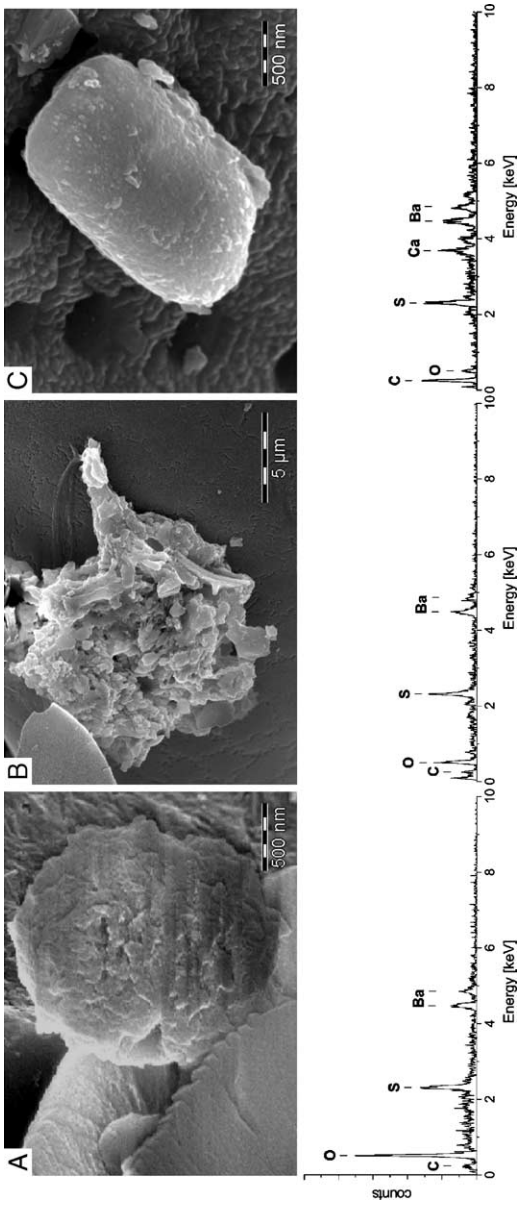

Fig. 5. At site GeoB 8455. (A) Barite crystal at 7.69 mbsf with a characteristic barite ratio of barium, sulfur, and oxygen. (B) Larger barite crystal with strong dissolution structures at 9.18 msbf. The EDS spectrum indicates a decreased oxygen concentration. (C) Barium particle at 9.18 mbsf with calcium incorporations and carbon, but low oxygen concentrations.

tion of barite via the formation of other barium compounds, such as witherite ($BaCO_3$) and the transient species barium sulfide (BaS). These coexisting barium phases were also reported by Malysh et al. [54]. They examined the influence of carbon-containing phases on the reduction of recycled barite in laboratory experiments. The reduction of barite or more precisely the reduction of barium-sulfate, with carbon leads to the formation of witherite via the transient phase barium sulfide:

$$BaSO_4 + 2C \rightarrow BaS + 2CO_2 \quad (4)$$

$$BaS + CO_2 + H_2O \rightarrow BaCO_3 + H_2S \quad (5)$$

This process is accelerated due to the catalyzing effect of the formed barium sulfide particles [54]. Furthermore, the conversion of barite into barium sulfide could lead to a sulfide coating, which can be compared with coatings of ferric iron minerals by iron sulfides in sulfidic sediments (e.g. [55]). This process could shield the barite particle, covered with barium sulfide, from further dissolution. It would also provide a small sink for hydrogen sulfide in deeper sediments. One indication for the process of barite reduction to occur in this environment is the increasing amount of carbon with decreasing oxygen concentrations found in some of the barium particles from the deeper buried barite fronts at site GeoB 8455 (Fig. 5). The sediments of the coring sites are characterized by high concentrations of hydrogen sulfide, high alkalinity (up to 80 mmol(eq) L^{-1}), and high amounts of TOC, and thus would provide a suitable environment for the alteration of barite into witherite (via barium sulfide). However, these processes in marine sediments require further investigations.

4. Conclusions

Sediments of two sites from the Eastern Cape Basin were examined for pore water and solid phase geochemistry. Small uppermost barium enrichments at both sites at the current SMT and large barium peaks slightly below imply a small upward shift of the SMT in the recent past which is likely to be a widespread regional phenomenon in the study area. At one site, distinct solid phase barium enrichments occur a few meters below the SMT in sulfate-depleted sediments which are dominated by small barite particles. These preserved buried barite fronts indicate former positions of the SMT. We assume that the abrupt relocation of the SMT, and thus the formation of

new barite fronts, is most likely triggered by an increase in the upward flux of methane. Calculations of the formation time of these enrichments and numerical modeling suggest that this shift of the SMT occurred between the last glacial maximum (LGM) and the Pleistocene/Holocene transition. High amounts of non-refractive organic matter buried below the SMT which lead to higher rates of methanogenesis, could explain such increases in methane concentrations and fluxes. Furthermore, the detection of barite below the SMT indicates that although being metastable/unstable in the prevailing geochemical environments, such minerals can be preserved/shielded from dissolution by specific processes or mechanisms, and thus be buried into deeper sediments. At such depths barite, for example, could fuel/support AOM to proceed below the SMT. Thus, reactive minerals buried in deeper sediments can have great influence on biogeochemical processes in the deep biosphere by providing terminal electron acceptors.

Acknowledgements

We thank the crew and scientists aboard the RV *Meteor* for their strong support during cruises M34/2 and M57/2. For technical assistance on board and in the home laboratory we are indebted to S. Hessler, S. Hinrichs, and S. Siemer. SEM analyses were carried out at Utrecht University, EMSA. The people there are thanked for their hospitality and cooperation. G. Aloisi, G. Bohrmann, M. Kölling, and M. Zabel are thanked for detailed comments on an earlier version of the manuscript. We thank J. Nüster for reading an earlier draft of this manuscript. Our special appreciation goes to C. Hensen and H.D. Schulz for helpful discussions. The manuscript greatly benefited from detailed comments and corrections of two anonymous reviewers. This research was funded by the Deutsche Forschungsgemeinschaft as part of the Research Center "Ocean Margins" (RCOM) of the University of Bremen, contribution no. RCOM0343.

References

[1] E.D. Goldberg, G.O.S. Arrhenius, Chemistry of Pacific pelagic sediments, Geochim. Cosmochim. Acta 13 (1958) 153–212.
[2] T.M. Church, Marine Barite, in: R.G. Burns (Ed.), Marine Minerals, Rev. Mineral., Miner. Soc. Am., vol. 6, 1979, pp. 175–209.
[3] J.K. Bishop, The barite–opal–organic carbon association in oceanic particular matter, Nature 24 (1988) 341–343.
[4] J. Dymond, E. Suess, M. Lyle, Barium in deep-sea sediment: a geochemical proxy for paleoproductivity, Paleoceanography 7 (1992) 163–181.
[5] T.J. Chow, E.D. Goldberg, On the marine geochemistry of barium, Geochim. Cosmochim. Acta 20 (1960) 192–198.
[6] F. Dehairs, R. Chesselet, J. Jedwab, Discrete suspended particles of barite and the barium cycle in the open ocean, Earth Planet. Sci. Lett. 49 (1980) 915–931.
[7] F. Dehairs, N. Stroobants, L. Goeyens, Suspended barite as a tracer of biological activity in the Southern Ocean, Mar. Chem. 35 (1991) 399–410.
[8] R.S. Ganeshram, R. Franc, J. Commeau, S.L. Brown-Leger, An experimental investigation of barite formation in seawater, Geochim. Cosmochim. Acta 67 (2003) 2599–2605.
[9] M.T. von Breymann, H. Brumsack, K.-C. Emeis, Depositional and diagenetic behavior of barium in the Japan Sea, in: K.A. Pisciotto, J.C. Ingle, M.T. von Breymann, J. Barron, et al., (Eds.), Proc. ODP, Sci. Resul. 127/128, College Station, Texas, USA, 1992, pp. 651–663.
[10] F. Gingele, A. Dahmke, Discrete barite particles and barium as tracers of paleoproductivity in South Atlantic sediments, Paleoceanography 9 (1994) 151–168.
[11] A. Paytan, M. Kastner, F.P. Chavez, Glacial to interglacial fluctuations in productivity in the Equatorial Pacific as indicated by marine barite, Science 274 (1996) 1355–1357.
[12] F.X. Gingele, M. Zabel, S. Kasten, W.J. Bonn, C.C. Nürnberg, Biogenic barium as a proxy for paleoproductivity: methods and limitations of application, in: G. Fischer, G. Wefer (Eds.), Use of Proxies in Paleoceanography: Examples from the South Atlantic, Springer, 1999, pp. 345–364.
[13] S. Mearon, A. Paytan, T.J. Bralower, Cretaceous strontium isotope stratigraphy using marine barite, Geology 31 (2002) 15–18.
[14] A. Paytan, M. Kastner, E.E. Martin, J.D. Macdougall, T. Herbert, Marine barites as a monitor of seawater strontium isotope composition, Nature 366 (1993) 445–449.
[15] G.R. Dickens, Sulfate profiles and barium fronts in sediment on the Blake Ridge: present and past methane fluxes through a large gas hydrate reservoir, Geochim. Cosmochim. Acta 65 (2001) 529–543.
[16] A. Paytan, M. Kastner, D. Campbell, M.H. Thiemens, Sulfur isotope composition of Cenozoic seawater sulfate, Science 282 (1998) 1459–1462.
[17] A. Paytan, M. Kastner, D. Campbell, M.H. Thiemens, Seawater sulfur isotope fluctuations in the cretaceous, Science 304 (2004) 1663–1665.
[18] J. McManus, W.M. Berelson, G.P. Klinkhammer, K.S. Johnson, K.H. Coale, R.F. Anderson, N. Kumar, D.J. Burdige, D.E. Hammond, H.J. Brumsack, D.C. Mccorkle, A. Rushdi, Geochemistry of barium in marine sediments: implications for its use as a paleoproxy, Geochim. Cosmochim. Acta 62 (1998) 3453–3473.
[19] A. Paytan, S. Mearon, K. Cobb, M. Kastner, Origin of marine barite deposits: Sr and S isotope characterization, Geology 30 (2002) 747–750.
[20] D.S. Cronan, Authigenic minerals in deep-sea sediments, in: E.D. Goldberg (Ed.), The Sea, vol. 5, Wiley Interscience, 1974, pp. 491–525.
[21] W.E. Dean, B.C. Schreiber, Authigenic barite, leg 41 deep sea drilling project, in: Y. Lancelot, E. Seibold, et al., (Eds.), Proc. ODP, Init. Repts., vol. 41, U.S. Gov. Off., Washington, D.C., 1978, pp. 915–931.
[22] M.E. Torres, H.J. Brumsack, G. Bohrmann, K.C. Emeis, Barite fronts in continental margin sediments: a new look at barium remobilization in the zone of sulfate reduction and formation of

heavy barites in diagenetic fronts, Chem. Geol. 127 (1996) 125–139.
[23] S. Kasten, B.B. Jørgensen, Sulfate reduction in marine sediments, in: H.D. Schulz, M. Zabel (Eds.), Marine Geochemistry, Springer, 2000, pp. 263–281.
[24] S. Kasten, M. Zabel, V. Heuer, C. Hensen, Processes and signals of nonsteady-state diagenesis in deep-sea sediments and their pore waters, in: G. Wefer, S. Mulitza, V. Ratmeyer (Eds.), The South Atlantic in the Late Quaternary: Reconstruction of Material Budget and Current Systems, Springer, 2003, pp. 431–459.
[25] S.P. Varnavas, Marine barite in sediments from deep sea drilling project sites 424 and 424A (Galapagos hydrothermal mounds field), Mar. Chem. 20 (1987) 245–253.
[26] M.E. Torres, G. Bohrmann, E. Suess, Authigenic barites and fluxes of barium associated with fluid seeps in the Peru subduction zone, Earth Planet. Sci. Lett. 144 (1996) 469–481.
[27] R.W. Embley, J.J. Morley, Quaternary sedimentation and paleoenvironmental studies off Namibia (South-West Africa), Mar. Geol. 36 (1980) 183–204.
[28] L.V. Shannon, The Benguela ecosystem: Part 1. Evolution of the Benguela, physical features and processes, Oceanogr. Mar. Biol. Annu. Rev. 23 (1985) 105–182.
[29] G. Wefer, G. Fischer, Seasonal patterns of vertical flux in equatorial and coastal upwelling areas of the eastern Atlantic, Deep-Sea Res. I 40 (1993) 1613–1645.
[30] L.V. Shannon, G. Nelson, The Benguela: large scale features and processes and system variability, in: G. Wefer, W. Berger, G. Siedler, D. Webb (Eds.), The South Atlantic: Present and Past Circulation, Springer, 1996, pp. 163–210.
[31] J.M. Bremner, J.P. Willis, Mineralogy and geochemistry of the clay fraction of sediments from the Namibian continental margin and the adjacent hinterland, Mar. Geol. 115 (1993) 85–116.
[32] J. Rogers, J.M. Bremner, The Benguela ecosystem: Part VII. Marine-geological aspects, Oceanogr. Mar. Biol. Annu. Rev. 29 (1991) 1–85.
[33] C.P. Summerhayes, B.D. Bornhold, R.W. Embley, Surficial slides and slumps on the continental slope and rise off South-West Africa, Mar. Geol. 31 (1979) 265–277.
[34] H.D. Schulz, Quantification of early diagenesis: dissolved constituents in marine pore water, in: H.D. Schulz, M. Zabel (Eds.), Marine Geochemistry, Springer, 2000, pp. 85–128.
[35] M. Adler, C. Hensen, H.D. Schulz, CoTReM-Column Transport and Reaction Model. http://www.geochemie.uni-bremen.de/downloads/cotrem/index.htm, User Guide, Version 2.3 (2000).
[36] M. Adler, C. Hensen, F. Wenzhöfer, K. Pfeifer, H.D. Schulz, Modeling of subsurface calcite dissolution by oxic respiration in supralysoclinal deep-sea sediments, Mar. Geol. 177 (2001) 167–189.
[37] B.P. Boudreau, Diagenetic Models and Their Implementation: Modeling Transport and Reactions in Aquatic Sediments, Springer, 1997.
[38] J. McManus, W.M. Berelson, G.P. Klinkhammer, T.E. Kilgore, D.E. Hammond, Remobilization of barium in continental margin sediments, Geochim. Cosmochim. Acta 58 (1994) 4899–4907.
[39] K.B. Averyt, A. Paytan, A comparison of multiple proxies for export production in the equatorial Pacific, Paleoceanography 19 (2004) , doi:10.1029/2004PA001005.
[40] A. Reitz, K. Pfeifer, G.J. de Lange, J. Klump, Biogenic barium and the detrital Ba/Al ratio: a comparison of their direct and indirect determination, Mar. Geol. 204 (2004) 289–300.
[41] A. Rutten, G.J. de Lange, A novel selective extraction of barite, and its application to eastern Mediterranean sediments, Earth Planet. Sci. Lett. 198 (2002) 11–24.
[42] M. Eagle, A. Paytan, K.R. Arrigo, G. van Dijken, R.W. Murray, A comparison between excess barium and barite as indicators of carbon export, Paleoceanography 18 (2003) 21–1–21–13.
[43] K. Pfeifer, S. Kasten, C. Hensen, H.D. Schulz, Reconstruction of primary productivity from the barium contents in surface sediments of the Atlantic Ocean, Mar. Geol. 177 (2001) 13–27.
[44] C. Niewöhner, C. Hensen, S. Kasten, M. Zabel, H.D. Schulz, Deep sulfate reduction completely mediated by anaerobic methane oxidation in sediments of the upwelling area off Namibia, Geochim. Cosmochim. Acta 62 (1998) 455–464.
[45] R.O. Barnes, E.D. Goldberg, Methane production and consumption in anoxic marine sediments, Geology 4 (1976) 297–300.
[46] B.B. Bernard, Methane in marine sediments, Deep-Sea Res. 26A (1979) 429–443.
[47] S. Kasten, T. Freudenthal, F.X. Gingele, H.D. Schulz, Simultaneous formation of iron-rich layers at different redox boundaries in sediments of the Amazon deep-sea fan, Geochim. Cosmochim. Acta 62 (1998) 2253–2264.
[48] B. Donner, M. Giese, Stratigraphie und Smear-Slide-Analysen, in: D. Schulz, cruise participants (Eds.), Berichte und erste Ergebnisse über die Meteor-Fahrt M20/2, Abidjan - Dakar, 27.12.1991–2.2.1992, Ber. Fachb. Geowiss. Univ. Bremen, vol. 25, 1992, pp. 51–80.
[49] G. Mollenhauer, R.R. Schneider, P.J. Müller, V. Spieβ, G. Wefer, Glacial/interglacial variability in the Benguela upwelling system: spatial distribution and budgets of organic carbon accumulation, Glob. Biogeochem. Cycles 16 (2002) 1134.
[50] G. Alosi, K. Wallmann, S.M. Bollwerk, A. Derkachev, G. Bohrmann, E. Suess, The effect of dissolved barium on biogeochemical processes at cold seeps, Geochim. Cosmochim. Acta 68 (2004) 1735–1748.
[51] D.L. Parkhurst, C.A.J. Appelo, User's guide to PHREEQC (Version 2.0), U.S. Geol. Surv., Water Resour. Inv. Rep., 1999, pp. 99–4259.
[52] M.T. Gonzáles-Muñoz, B. Fernández-Luque, F. Martínez-Ruiz, K.B. Cheroun, J.M. Arias, M. Rodríguez-Gallego, M. Martínez-Cañamero, C. de Linares, A. Paytan, Precipitation of barite by *Myxococcus xanthus*: possible implications for the biogeochemical cycle of barium, Appl. Environ. Microbiol. 69 (2003) 5722–5725.
[53] F. Baldi, M. Pepi, D. Burrini, G. Kniewald, D. Scali, E. Lanciotti, Dissolution of barium from barite in sewage sludges and cultures of *Desulfovibrio desulfuricans*, Appl. Environ. Microbiol. 62 (1996) 2398–2404.
[54] L.A. Malysh, L.G. Gaisin, M.F. Volkova, A.G. Prokhorov, K.V. Tkachev, Reduction of recycled barium sulfate, Russ. J. Appl. Chem. 75 (2002) 14–17.
[55] J.F.L. Garming, U. Bleil, N. Riedinger, Alteration of magnetic mineralogy at the sulfate methane transition: analysis of sediments from the Argentine continental slope, Phys. Earth Planet. Inter. 151 (2005) 290–308.

8. Epilogue

This study was carried out in the framework of the European Graduate College Europrox and the Vening Meinesz Research School of Geodynamics (VMSG) funded by the German Research Foundation (DFG) and the Netherlands Organisation of Scientific Research (NWO). It underlines the goals of the graduate college, the development and validation of proxy parameters for paleoceanographic purposes.

Within the multidisciplinary proxy research the results of this thesis bring us a step closer towards a full understanding of magnetic proxy parameters delineating Quaternary paleoclimate patterns in marine sedimentary sequences. In this thesis, the merits and pitfalls of several magnetic proxy parameters have been investigated from the viewpoint of sediment and magnetic petrology. The various case studies based on marine sediment sequences from the Equatorial and South Atlantic Ocean link methodological aspects with interpretational issues.

The question why some of the worldwide obtained relative paleointensity records show a high correlation while others don't could be explained to a reasonable extent by a lithological ‘matrix effect’. Among the multiple investigated sedimentologic parameters, clay grain-size, chlorite and opal content, and particularly the ratio of kaolinite and illite yield significant correlations to relative paleointensity signals. It was found that matrix-related effects may possibly influence relative paleointensity signal dynamics to nearly the same extent as geomagnetic field variations. The correction for this matrix effect enhances the correlation of the individual relative paleointensity records to global stacks. An extension of the sample and data set would enable a more generalised definition of lithologic correction coefficients.

Existing extraction and microscopic techniques were adjusted to the specific needs of examining fine-grained magnetic particles. These include the heavy liquid separation using hydrophilic polytungstenate solution, and the adaptation of the electron backscatter diffraction technique in scanning electron microscopy to individual non-embedded particles. The combination of scanning and transmission electron microscopy together with sensitive low-temperature magnetic measurements provided a complete picture of the magnetic inventory along the Equatorial Atlantic transect at 5°N. This area is a so-called ‘natural laboratory’ to study very different climatic input mechanisms and transport pathways of particles that ultimately make up the marine sediment. The results improve the possibilities to link the marine environment with the climatic conditions on the continent.

Paradoxical observations raise the important issues, whether magneto-granulometric variations in the marine realm are primarily controlled by mixing of multiple sources with separate, relatively narrow grain-size ranges or rather by variable sorting of a single source with a broad grain-size distribution. The identification and classification of individual magnetic particles with the help of electron microscopy allow a much more detailed interpretation of routinely applied magnetic proxies. They provided the possibility to distinguish between magnetically similar particle classes from vastly different sources, give information on their relative abundance and elemental compositions, and allowed identification of specific grain morphologies, transport or dissolution marks. The complex

magnetic mineral assemblages in the sediments along the Equatorial Atlantic could be unraveled for representative sites and time slices and highlight that input mechanisms are generally different from East to West, although magnetic accumulation rates might be very similar. Coupling or uncoupling of the coarse and fine magnetic grain-size could be explained along the investigated transect and detrital vs. authigenic magnetic particle sources were traced.

The present work has focused on magnetic iron (oxihydr-)oxides from oxic to suboxic (hemi)pelagic sediments. A logical pursuit would be the extention of the analysis to more reducing conditions that occur often in continental shelf sediments. Electron microscopic techniques, such as electron backscatter diffraction (EBSD) or quantitative particle mapping could be further developed to identify and quantify the individual components, e.g. to be able to judge the chemical composition of titanomagnetites from their EBSD patterns or to distinguish between greigite, and pyrrhotite by their crystallographic structure. Detection of either one or more of these iron sulfides implies paleoenvironmental information. Quantitative particle mapping would provide absolute numbers of each identified (magnetic) particle type and therefore transport pathways could be tracked with absolute flux rates.

Another essential aspect is how 'depositional' the measured magnetic signal is. Therefore potentially present reductive diagenesis and/or lithological differences have to be evaluated before a complete understanding of the environmental setting can be achieved. This study has shown, that the dominant presence of Ti-rich magnetic mineral phases may be related on one hand to a primary source signal or on the other hand to strong dissolution of pure Fe oxides. More specific, some of the newly explored techniques could be used to achieve better 'ground truth' on the magneto-mineral assemblage of reducing sedimentary settings. Typically these sedimentary environments are far from their geochemical equilibrium conditions and depending on source areas, transport mechanisms and alteration processes a whole chain of iron minerals can coexist. The interpretation of the magnetic signal is by no means easy, but a multi-parameter approach linking continents and deep ocean via the continental shelf areas could set the stage for better budget calculations.

Proloog en Samenvatting (in het Nederlands)

In het kader van wereldwijd marien onderzoek vormt de Equatoriale en Zuidelijke Atlantische Oceaan een ideaal 'natuurlijk laboratorium' om het klimaat uit het geologische verleden te bestuderen, omdat deze regio is beinvloed door een grote verscheidenheid aan klimaatgestuurde processen:

Van Noord naar Zuid omvat deze oceaan sterk verschillende klimatologische gebieden: van de tropen tot de polen onderscheiden we achtereenvolgens de intertropische, subtropische en subantarctische frontale systemen met hun zones van hoge primaire productiviteit. Bovendien vindt er uitwisseling plaats van watermassa's uit de Noordelijke Atlantische Oceaan en Zuidelijke Oceaan. In het westen en oosten is de Zuidelijke Atlantische Oceaan begrensd door de Zuid Amerika en Afrika vanwaar grote hoeveelheden terrestrische sedimenten worden aangevoerd via de zogenaamde 'stofzones' van de Sahara, de Sahel en de Patagonische woestijnen. Aanvoer van riviermateriaal wordt verzorgd door grote rivieren zoals de Amazone, de Niger, de Congo en de Rio de la Plata. De Mid-Atlantische Rug met haar actieve spreiding van de oceaanbodem deelt de Zuid-Atlantische Oceaan in een westelijk en oostelijk hoofdbekken, die op hun beurt zelf worden weer onderverdeeld door submariene ruggen zoals de Walvis Rug en de Rio Grande Rise. De grote verscheidenheid van aan elkaar gerelateerde wind-, stromings-, rivier- en primaire productiviteitssystemen, alsmede de morfologie van de zeebodem en stratificatie in de waterkolom, leiden tot een weelde van in elkaar overgaande sedimentaire omgevingen (bv. *Ruddiman* 2001).

De sedimenten uit de Equatoriale en Zuid-Atlantische oceaanbekkens vormen een natuurlijk archief van de complexe geschiedenis van het klimaat en milieu uit deze gehele regio. Verscheidene biologische, chemische en fysische eigenschappen van het sediment bieden bruikbare informatie voor de reconstructie van het paleomilieu, zoals de temperatuur van het oppervlakte water, de primaire productiviteit en de windsterkte. Veel van deze parameters zijn notoir moeilijk te modelleren op basis van fysische wetten. In zulke gevallen is zogenaamde 'proxy' informatie geboden. Proxy parameters zijn meetbare, op het sediment gebaseerde, beschrijvers voor de gezochte (doch niet-observeerbare) variaties in klimaat en/of milieu met hun relatie in ruimte en tijd. Proxy's moeten een nauw, indien mogelijk lineair, verband tot deze variabelen hebben die nu eenmaal aan deze proxy's ten grondslag hebben gelegen. Daarnaast moeten ze over een goed preservatiepotentieel beschikken. In de laatste tientallen jaren zijn een groot aantal proxy's voor het paleomilieu en paleoklimaat ontwikkeld, met name voor het mariene bereik. Om de toepasbaarheid van de proxy parameters te toetsen zijn er vanzelfsprekend talloze case studies uitgevoerd (bv. *Emiliani* 1955; *Imbrie & Kipp* 1971; *Shackleton & Opdyke* 1973; voor de Zuidelijke Atlantische Oceaan bv. *Fischer & Wefer* 1999). Tevens heeft men complementaire proxy's ontwikkeld om bereikte resultaten onafhankelijk te kunnen testen.

De zogenaamde gesteente-, mineraal- of milieumagnetische parameters, verkregen via fysische metingen aan gesteente of sedimentmonsters, vormen een specifieke set van proxy's, die een aanvulling zijn op de beter bekende geochemische of biologische parameters. Ze zijn gebaseerd op verschillen in concentratie en korrelgrootte van ijzeroxides en ijzersulfides en bieden een grote verscheidenheid aan informatie omtrent de geschiedenis van het klimaat, de sedimentatie en diagenese, alsmede aangaande het geomagnetisch veld. Magnetische proxy's zijn algemeen geaccepteerd als chronostratigrafische indicatoren en als cyclostratigrafisch gereedschap; ze zijn echter ook van nut bij

de berekening van massabudgetten en de ontrafeling van de relaties tussen bron- en afzettingsge-bieden (bv. *Thompson & Oldfield* 1986; *Lund & Karlin* 1990, *Oldfield* 1991; *King & Channell* 1991; *Verosub & Roberts* 1995; *Dekkers* 1997; *Frederichs et al.* 1999; *Evans & Heller* 2003).

Het principe van de magnetische proxy's is in theorie eenvoudig, maar complex in realiteit: mariene sedimenten – inclusief hun magnetische mineraalfracties – zijn samengesteld uit verschillende oceanische en terrestrische bronnen; bovendien wordt elke bijdrage nog gemoduleerd door veranderende tektonische, klimatologische en oceanografische omgevingen. De primaire magnetische dragers kunnen verder beinvloed worden door secundaire, zogenaamde 'post-depositionele' processen, die voornamelijk aangedreven zijn door de degradatie van organisch koolstof. De ruimtelijke verdeling van bron- en proces-specifieke types magnetische mineralen in een bepaald sediment-tijdinterval is daarom een samengestelde van alle hierboven beschreven factoren. Bijvoorbeeld rivieraanvoer van detritisch materiaal reflecteert de geologie (bv. de Fe/Ti ratio) en verweringsomstandigheden van het continentale achterland. Afhankelijk van de vochtigheid wisselt de mineralogie van detritische ijzer oxides waarbij hetzij magnetiet (Fe_3O_4), hetzij goethiet (FeOOH), hetzij haematiet (Fe_2O_3) het meest voorkomend kunnen zijn. Korrelgroottes van magnetiet worden bepaald door bron- en transportgerelateerde factoren: aeolische korrelgroottes zijn direct gekoppeld aan windsterkte en transportweglengte. De vorming van authigene fracties zoals bacteriële magnetofossielen alsmede de ijzersulfides greigiet (Fe_3S_4), pyrrhotien (Fe_7S_8) en pyriet (FeS_2) zijn afhankelijk van Eh-pH condities. De identificatie en kwantitatieve beschrijving van deze magnetische componenten biedt dus informatie over veranderingen in massaflux en geochemische omgeving, gerelateerd aan milieuveranderingen (e.g. *Frederichs et al.* 1999).

Mineraalmagnetische proxy's hebben zekere voordelen over andere proxy's: in het algemeen behoeven ze geen tijdrovende monstervoorbereiding, afwegen van het monster volstaat. Ze zijn zo gevoelig dat betekenisvolle informatie normaliter verkregen kan worden uit bulkmonsters van mariene sedimenten. Meestal zijn zeer kleine hoeveelheden afdoende en is de analyse methode niet-destructief, zodat waardevol monstermateriaal ook nog gebruikt kan worden voor vervolganalyse. Maar het belangrijkste voordeel van deze proxy's is hun korrelgrootteïnformatie (en dan vooral voor de kleinste fracties), die moeilijk te verkrijgen is met andere technieken. Gesteente- en milieumagnetische parameters worden onderverdeeld in concentratie-, korrelgrootte- en mineraalspecifieke proxy parameters (bv. *Thompson & Oldfield* 1986; *Butler* 1992; *Dunlop & Özdemir* 1997).

De interpretatie van sommige mineraalmagnetische proxy parameters is helaas niet-uniek. Daarom is deze altijd gebaseerd op een zogeheten multi-parameter aanpak. Tevens dient men het regionale karakter van zo'n interpretatie niet uit het oog te verliezen. Bij voorbeeld: waardes en trends voor een tropisch gebied kunnen niet zondermeer geextrapoleerd worden naar een polair gebied. Specifieke onder-werpen met betrekking tot de betekenis van magnetische proxy's moeten apart worden beschouwd voor elk sedimentair systeem: waarom is er een positieve korrelatie tussen magnetische suscepti-biliteit (een proxy voor magnetische mineraalconcentratie) en het $\delta^{18}O$ signaal (een globale proxy voor ijsvolume en derhalve klimaat) in de ene oceanische regio, en een negatieve, of zelfs helemaal geen korrelatie in een andere? Zijn vari-aties in magnetische korrelgrootte bepaald door verweringscondities, varierende brongebieden of transportmechanismes? Waarom korreleren (relatieve) paleoïntensitieitsgegevens (een proxy voor de sterkte van het aardmagneetveld) wel goed tussen

sommige regio's, maar is er nauwelijks een korrelatie tussen andere gebieden, zelfs wanneer diagenetische overprinting niet belangrijk is? Sommige van dit soort aspecten zijn opgelost, andere staan nog ter discussie, en zijn het onderwerp van dit proefschrift.

Een veelbelovende, maar experimenteel veeleisende strategie om magnetische proxy's te onderzoeken, is het vaststellen van de lithologische eigenschappen van de magnetische dragers en hun sedimentaire matrix. Voor het laatste aspect volstaan gangbare methodes uit de sedimentologie, de analyse van het eerste aspect is gecompliceerder. Om de petrologie van deze ijzerhoudende mineralen – zeer kleine korrelgrootte (micro- en nanometerschaal) en zeer lage concentraties – te onderzoeken, beoogt dit proefschrift specifieke magnetische experimentele technieken en innovatieve extractiemethodes te ontwikkelen. Raster (Scanning) en Transmissie Elektronen Microscopie (SEM en TEM) zijn gebruikt om magnetische proxy interpretaties te ondersteunen en te ijken. Zogenaamde 'electron backscatter diffraction patronen' verkregen met SEM dienen om het onderscheid tussen de verschillende ijzer- en titaniumoxides te vervolmaken. Door de magnetische mineraalassemblages onder de verschillende sedimentologische en geochemische condities nauwgezet te onderzoeken, kunnen we conclusies trekken omtrent de milieumagnetische implicaties van de magnetische petrologie.

Hoofdstuk 2 behandelt de zogenaamde relatieve paleoïntensiteit (RPI). Opnames in hoge resolutie van de paleoïntensiteit van het aardmagneetveld zijn op succesvolle wijze vergaard van vele mariene sedimentopeenvolgingen. Deze zijn vastgesteld door de intensiteit van de natuurlijke remanente magnetisatie (NRM) te normalizeren voor de concen-tratie van de magnetische dragers. Er wordt ingegaan op de vraag waarom sommige wereldwijd vergaarde RPI opnames een sterke korrelatie laten zien, en andere niet. Uit een scala van mogelijke verbanden blijkt de lithologie van de sedimentmatrix met name een invloed te hebben op het karakter van het RPI signaal. In dit hoofdstuk worden zulke 'matrixeffecten' beschouwd middels een sediment-analytische en een statistische aanpak. We vergelijken RPI gegevens van diepzee sedimenten die gemonsterd zijn in een transect over de subtropische en sub-antarctische fronten van de Zuidelijke Atlantische Oceaan. Deze locaties liggen vrij dicht bij elkaar en hebben dus hetzelfde paleomagnetische veld gere-gistreerd, maar hun lithologieën zijn divers. Verschillen in de RPI waardes zouden daarom de invloed van sedimentmatrix op het oplijnen van de magnetische deeltjes moeten weergeven. Uitgebreid sedimentologisch onderzoek is uitgevoerd om de lithologie en korrelgrootte van de sedimentmatrix te karakteriseren. Bi- en multivariate statistiek is toegepast om de hypothese van het 'matrixeffect' te testen. Waar verscheidene parameters geen significante resultaten gaven, is een zwakke korrelatie gevonden tussen de RPI en de deeltjesgrootte in het kleigrootte-bereik en het chlorietgehalte. De RPI toont een redelijke korrelatie met het opaal-, illiet- en kaolinietgehalte. De meest invloedrijke afzonderlijke sedimentologische factor blijkt de kaoliniet/illiet ratio te zijn, met een Pearson's korrelatie coëfficient van 0.51 en een significantie van 99.9%. Het onderzoek laat zien dat de matrix-gerelateerde effecten wellicht een ongeveer evengrote invloed hebben op de RPI signaaldynamiek als de variatie in intensiteit van het aardmagneetveld zelf. De studie biedt voorts een leidraad voor strategieën om voor deze lithologische effecten te corrigeren.

In **Hoofdstuk 3** testen we de efficiëntie van magnetische scheiding en zware vloeistof extractie op mariene sedimenten van de Equatoriale Atlantische Oceaan om de identificatie van magnetische mineralen met behulp van lage-temperatuur gesteentemagnetische techieken te verbeteren. Verrijking van de magnetische deeltjes is noodzakelijk vanwege hun lage con-

centraties in het sediment (gehaltes typisch in de orde van ppm) en om de invloed van de grote paramagnetische bijdrage aan het magnetisch signaal bij lage temperaturen te verwijderen. De toegepaste magnetische extractietechniek is gebaseerd op het circuleren van sediment in suspensie in een sterke magnetische veldgradient, een 'magnetische vinger' waaraan magnetische deeltjes vasthechten. Zware vloeistof scheiding is gebaseerd op verschillende in de soortelijke massa van de individuele mineraalcomponenten in het sediment. De zware vloeistof die gekozen voor deze studie, een natrium polywolframaat oplossing, is vanwege haar hydrofiele karakter geschikt is voor de onderhavige fijn-korrelige mariene sedimenten met een hoog kleimineraal gehalte. De dichtheid was ingesteld op 3 g cm^{-3} om de lichtere niet-magnetische mineralen te scheiden van de zwaardere, magnetisch verrijkte, fractie.

Vervolgens zijn thermomagnetische data vergaard op beide soorten extracten van hetzelfde monstermateriaal om de voordelen en nadelen van elke techniek te laten zien. Zogeheten opwarmcurves vanaf 5 tot 300 Kelvin van 'zero-field' en 'field-cooled' remanente magnetisaties zijn bepaald. Ook zijn monsters met een isothermale remanente magnetisatie ingebracht bij kamertemperatuur, onderworpen aan lage temperatuur cycling. Dit alles om de magneto-mineralogische samenstelling van deze monsters te achterhalen en om de doeltreffendheid van de extracties te quantificeren. Beide extractietechnieken maken het mogelijk om magnetische mineraal fasen, zoals magnetiet, titanomagnetiet, hemoilmeniet, afzonderlijk te identificeren. Eveneens kunnen goethiet en waarschijnlijk ook superparamagnetische ferrihydriet te gedetermineerd worden. Behalve de goethiet, dat ook kan worden getraceerd in metingen aan bulksediment bij temperaturen boven kamertemperatuur, kunnen alle andere magnetische fases alleen geidentificeerd worden in de magnetische en zware vloeistof concentraten. De zware vloeistof methode bleek de magnetische fractie op een efficiëntere manier te extraheren; zwak magnetische mineralen met een hoge coërciviteit en zeer fijnkorrelige materiaal werden veel beter ge-extraheerd dan met behulp van magnetische extractie.

Hoofdstuk 4 illustreert het voordeel van de 'electron backscatter diffraction' (EBSD) techniek bij 'scanning electron microscopy' (SEM) om de verschillende magnetische ijzer-titanium oxides te identificeren. EBSD is in het bijzonder handig in combinatie met 'element dispersive spectroscopy' (EDS) voor monsters die vrijwel dezelfde chemische samenstelling hebben maar een verschillende kristalstruktuur. Een set van synthetische monsters alsmede een aantal natuurlijke monsters van verschillende herkomst, laat zien dat het mogelijk is onderscheid te maken tussen titanomagnetite [$Fe_{3-x}Ti_xO_4$] en hemolimeniet [$Fe_{2-y}Ti_yO_3$]. Tot op heden werd EBSD voornamelijk gebruikt bij gepolijste (dunne) doorsneden met een glad oppervlak. In dit hoofdstuk laten we zien dat het tevens succesvol kan worden toegepast op afzonderlijke deeltjes die slechts met een laagje koolstof zijn bedekt, zogenaamde 'non-embedded' monsters.

Om de implicaties van magnetische proxy data beter te doorgronden is een inventarisatie gemaakt van de magnetische micro- en nanodeeltjes van mariene sedimenten uit de Equatoriale Atlantische Oceaan. Dit is gedaan door analyse met behulp van 'scanning' en 'transmission' electronen microscopie (SEM and TEM) van magnetische extracten, en beschreven in **Hoofdstuk 5**. Alle detritische en authigene magnetische mineralen zijn geclassificeerd naar hun regionale distributie, oorsprong, transport en preservatie. In het bestudeerde west-oost transect zijn heel diverse aanvoerwegen van detritisch materiaal te vinden, zoals rivierdetritus van de Amazone, submariene verwering van de basalten van mid-oceanische-ruggen, en de eolische bijdrage van Saharastof. Deze zijn allemaal traceerbaar met SEM onderzoek. Bovendien zijn authigene bronnen van

chemische precipitatie, biomineralisatie van bacteriële magnetiet, en verschillende stadia van vermoedelijk goethiet in superparamagnetische tot één-domein grootte, geïdentificeerd door TEM. Deze informatie is gebruikt om de relaties tussen het oorsprongs- en afzettingsgebied vast te stellen en om magnetiche proxy interpretaties voor dit gebied te preciseren.

Bij de westelijke locatie (Ceará Rise; 3°49.9'N / 41°37.3'W), werd een 'component mixing system' gevonden, waar ongeveer 80% van de magnetische aanvoer bestond uit relatief grofkorrelige magnetiet van Amazone detritus. De resterende 20% bestaat uit basaltisch titanomagnetiet dat waarschijnlijk een nabije herkomst heeft, eolische input van het Afrikaanse continent, en authigene bacteriële magnetiet. Deze laatste component werd alleen gevonden op deze locatie. Bij de oostelijke locatie (Sierra Leone Rise; 4°50.7'N en 21°03.2'W), is de aanvoer van magnetische componenten voornamelijk beïnvloed door klimaatveranderingen van de heersende passaatwind, met een magnetisch korrelgrootte-sorteringssysteem van de eolische magnetische hoofdcomponent als gevolg (ongeveer 30 tot 60%). De centrale locatie (Mid-Atlantic Ridge; 4°02.8'N en 33°26.3'W) bestond uit een magnetische samenstelling die verklaard kan worden door een combinatie van beide eerder beschreven mechanismes. Hier veroorzaken klimaatgestuurde bodemstromingssystemen de korrelgrootte variaties in de submariene titanomagnetiet fragmenten, die ongeveer 50% beslaan van de magnetiet gevonden bij de Mid-Atlantische Rug. Detritische aanvoer van Amazonemateriaal uit het westen en Saharastof uit het oosten completeren de magnetische inventaris die samen met de titanomagnetiet een drie-componenten systeem vormt. Haematiet, goethiet and mogelijk ferrihydriet komen voor in alle monsters. De eerste twee verklaren de gemeten hoog coërcitieve eigenschappen terwijl het extreem fijnkorrelige deel van de korrelgrootteverdeling in alle drie de mineralen de waargenomen superparamagnetische eigenschappen zou kunnen verklaren. Deze twee magnetische eigenschappen worden in het algemeen beschouwd als gescheiden, maar kunnen hier eigenlijk genetisch gekoppeld zijn.

Hoofdstuk 6 onderzoekt de sterke invloed van reductieve diagenese op de magnetische inventaris van mariene sedimenten die afgezet zijn op de Argentijnse continentale rand vlak bij het Rio de la Plata-estuarium. Alle ijzerrijke magnetische mineralen zijn opgelost behalve als ze voorkomen als insluitsels in silicaten. Gesteentemagnetische metingen, gebruikmakend van een zogeheten 'magnetic-property-measurement-system' (MPMS) in het lage temperatuurbereik (tussen 5 en 300 K), zijn gedaan in combinatie met SEM observaties om de overige meer titaniumrijke magnetische mineralen te karakteriseren. Omdat de dominante aanvoer bestaat uit vulkanische deeltjes van het Paraná Basin, bestaande uit titanomagnetiet en haemoilmeniet, is een magnetische zelfomkering waargenomen tijdens het afkoelen gedurende de lage-temperatuur metingen. Dit is inderdaad een aanwijzing voor de bijna complete afwezigheid van Fe-rijke magnetische mineralen.

De identificatie van de doelgroepmineralen en daaraan gerelateerde proxy parameters is natuurlijk niet beperkt tot de magnetische materialen, maar kan ook van toepassing zijn op andere, niet-magnetische, paleoceanografische indicatoren. In mariene sedimenten wordt bariet vaak gebruikt als een proxy parameter voor paleoproductiviteit. Echter, de bruikbaarheid van deze proxy is gelimiteerd door de mogelijke diagenetische overprinting van het primaire signaal waardoor de originele paleoproductiviteitsinformatie kan veranderen. Daarom is het belangrijk om diagenetische processen in mariene sedimenten te onderzoeken. **Hoofdstuk 7** is gericht op de invloed van 'non-steady-state' diagenetische processen op primaire geochemische signalen. Sedimenten uit het oostelijke Kaap Bekken zijn gebruikt voor deze studie.

Geochemische analyse van porienwater en de vaste fase gecombineerd met numeriek modelleren en elektro-nenmicroscopie, zijn toegepast om het voorkomen van diagenetische barietfronten op en onder de sulfaat-methaan-transitie (SMT) zone te identificeren en te kwantificeren. Barietfronten worden authigeen gevormd door de reactie van opwaarts diffunderend barium met interstitiëel sulfaat. In sulfaatarme sedimenten wordt bariet verondersteld instabiel te zijn. Het voorkomen van barietaanrijkingen onder de SMT zone wordt dus beargumenteerd geassocieerd te zijn met vertraagde oplossing van bariet, wat (onder andere) wordt verklaard door hoge concentraties opgelost barium in het porienwater. Een opwaartse migratie van de SMT zone leidt tot het onstaan van een nieuw actief barietfront. Grote hoeveelheden begraven organisch material onder de SMT zone zullen leiden tot een toename van methanogenese gevolgd door een op-waartse flux van methaan, wat de verschuiving van de SMT zone veroorzaakt. Met zulk gedetailleerd geochemisch onderzoek kunnen onjuiste interpretaties van het paleomilieu met betrekking tot verhoogde paleoproductiviteit verkomen worden.

Het onderzoek beschreven in dit proefschrift illustreert dat magnetische proxy parameters gevalideerd moeten worden, in het ideale geval voor iedere studie van een oceanische regio. Sommige vragen, namelijk de afhankelijkheid van het relatieve paleointensiteitssignaal van de matrixlithologie, het onderscheiden van subtiele verschillen in magnetische dragers in de Equatoriale en Zuidelijke Atlantische Oceaan op een meer regionale schaal, en de oorzaken voor magnetische korrelgrootte variatie, zijn beantwoord of op zijn minst in een gevorderd stadium. De invloed van milde en vergevorderde diagenetische overprinting is onderzocht op microscopische schaal. Het in detail onderzoeken van magnetische proxy's van het milieu met behulp van gesteentemagnetische and 'niet-magnetische' technieken hebben meer inzicht gegeven in de onderliggende processen en het niveau van de interpretaties verder verhoogd. Op zijn beurt vergroot dit de mogelijkheden om de paleoceanografische historie op een regionaal niveau in detail te reconstrueren.

References

Butler, R.F., 1992. Paleomagnetism: Magnetic Domains to Geological Terranes, Boston, Backwell Scientific Publications. http://www.geo.arizona.edu/Paleomag/book/

Dekkers, M.J., 1997. Environmental magnetism: an introduction, *Geologie en Mijnbouw*, **76**, 163-182.

Dunlop, D.J. & Özdemir, Ö., 1997. *Rock magnetism, fundamentals and frontiers*, Cambridge University Press, 573 p.

Emiliani, C., 1955. Pleistocene temperatures, *J. Geol*., **63**, 538-578.

Evans, M.E. & Heller, F., 2003. *Environmental Magnetism: Principles and Applications of Enviromagnetics*, Academic Press, Elsevier Science, San Diego, London, Burlington, 299 p.

Fischer, G. & Wefer, G., 1999. *Use of Proxies in Paleoceanography: Examples from the South Atlantic*, Springer-Verlag, Berlin, Heidelberg, New York, 735 p.

Frederichs, T., Bleil, U., Däumler, K., von Dobeneck, T. & Schmidt, A.M., 1999. The magnetic view on the marine paleoenvironment: Parameters, techniques, and potentials of rock magnetic studies as a key to paleoclimate and paleoceanographic changes, in *Use of Proxies in Paleoceanography: Examples from the South Atlantic*, pp. 575-599, eds Fischer, G. & Wefer, G., Springer-Verlag, Heidelberg, Berlin, New York.

King, J.W. & Channell, J.E.T., 1991. Sedimentary magnetism, environmental magnetism, and magnetostratigraphy, *Rev. Geophys*., **29**, 358-370.

Imbrie, J. & Kipp, N.G., 1971. A new micropaleontological method for quantitative paleoclimatology: Application to a Late Pleistocene Caribbean core, in *The Late Cenozoic Glacial Ages*, pp. 71-181, ed. Turekian, K., Yale Univ. Press, New Haven, Conn.

Lund, S.P. & Karlin, R., 1990. Introduction to the special section on physical and biogeochemical processes responsible for the magnetization of sediments, *J. Geophys. Res.*, **90**, 4353-4354.

Oldfield, F., 1991. Environmental Magnetism: a personal perspective, *Quat. Sci. Rev*., **10**, 73-85.

Ruddiman, W.F., 2001. *Earth's Climate: Past and Future*, W.H Freeman and Company, New York, 465 p.

Shackleton, N.J. & Opdyke, N.D.,1973. Oxygen isotope and paleomagnetic stratigraphy of

equatorial Pacific core V28-238: Oxygen isotope temperatures and ice volumes on a 10^5 year and 10^6 year scale, *Quat. Res.*, **3**, 39-55.

Soffel, H.C., 1991. *Paläomagnetismus und Archäomagnetismus*, Springer-Verlag, Berlin, Heidelberg, New York, 276 p.

Thompson, R. & Oldfield, F., 1986. *Environmental Magnetism*, Allen and Unwin, London, pp. 1-227.

Verosub, K.L. & Roberts, A.P., 1995. Environmental magnetism: past, pre-sent, and future, *J. Geophys. Res*., **100**, 2175-2192

Prolog und Zusammenfassung (in deutscher Sprache)

Im Rahmen der globalen Meeresforschung stellt der Äquatorial- und Südatlantik ein ideales ‚natürliches Laboratorium' zur Untersuchung des Paläoklimas der Erde dar, das durch eine Vielzahl von klimatischen Prozessen gekennzeichnet ist:

Von Nord nach Süd umfaßt dieser Ozean die verschiedensten klimatischen Regionen, angefangen bei den Tropen über das intertropische, subtropische und subantarktische Frontensystem bis hin zur Polarzone. Diese schließen neben den Hochproduktionsgebieten auch den Wassermassenaustausch mit dem Nordatlantik und den südlichen Ozeanen ein. Im Westen und Osten wird der Südatlantik vom südamerikanischen und afrikanischen Kontinent begrenzt, von wo aus große Mengen an terrestrischem Material durch die Sahara-, Sahel- und Patagonien-Staubgürtel eingetragen werden. Die Flußsysteme des Amazonas, Nigers, Kongos und des Rio de la Platas stellen ebenfalls wichtige Zulieferer von detritischem Material dar. Der Mittelatlantische Rücken trennt mit seiner aktiven Ozeanbodenspreizung den Südatlantik in seine westlichen und östlichen Hauptbecken. Eine weiter Unterteilung findet wiederum durch submarine Strukturen wie z.B. den Walfisch Rücken oder den Rio Grande Rise statt. Die komplexen Zusammenhänge von Wind-, Strömungs-, Fluß- und Produktionssystemen bilden zusammen mit der Ozeanbodenmorphologie und Wassermassenstratifizierung eine Vielfalt von sich gegenseitig beeinflussenden Sedimentationssystemen (z.B. *Ruddiman* 2001).

Die Sedimente des Äquatorial- und Südatlantiks stellen ein natürliches Archiv dieser komplexen Klima- und Umweltentwicklung für die gesamte Region dar. Diverse biologische, chemische und physikalische Sedimenteigenschaften liefern hilfreiche Information zur Rekonstruktion von Paläoumweltbedingungen, wie z.B. Oberflächenwassertemperaturen, Primärproduktion oder Windstärken. Viele dieser Parameter sind in erster Näherung schwer zu modellieren. Für solche Fälle wird sogenannte ‚Proxy' Information benötigt; Proxyparameter sind meßbare, sedimentbezogene Deskriptoren der gewünschten (aber nicht beobachtbaren) Umweltvariablen und deren räumlicher und zeitlicher Variabilität. Proxies müssen eine enge, wenn möglich lineare Beziehung zu den Umweltparametern haben, durch die sie geprägt werden. Ein gutes Erhaltungspotential über die Zeit ist außerdem ausschlaggebend. Eine große Anzahl von Paläoumwelt- und paläoklimatischen Proxyparametern wurden im Laufe der letzten Dekaden entwickelt, vor allem für marine Regionen. Zahlreiche Fallstudien (z.B. *Emiliani* 1955; *Imbrie & Kipp* 1971; *Shackleton & Opdyke* 1973; sowie Fallstudien aus dem Südaltantik z.B. in *Fischer & Wefer* 1999) wurden durchgeführt, um die Anwendung von Proxies zu validieren, oder ergänzende Parameter zu entwickeln und damit unabhängige Ergebnisse erzielen zu können.

Die sogenannten gesteins- oder umweltmagnetischen Parameter, die durch physikalische Messungen an Gesteins- oder Sedimentproben gewonnen werden, stellen eine Reihe von spezifischen Proxies dar, das die eventuell besser bekannten geochemischen oder biologischen Ansätze erweitert. Basierend auf der Diversität, Konzentration und Korngröße von Eisenoxiden und –sulfiden ermöglichen sie den Zugang zu Informationen über die Geschichte des Klimas, der Sedimentation, der Diagenese, als auch des geomagnetischen Feldes. Magnetische Proxies sind gut bekannt als chronostratigraphische Marker und zyklostratigraphische Werkzeuge, können aber auch beim Aufstellen von Massenbilanzen oder Beziehungen zwischen Partikelquellen und Senken helfen (z.B. *Thompson & Oldfield* 1986; *Lund & Karlin* 1990; *Oldfield* 1991; *King & Channell* 1991; *Verosub & Roberts* 1995; *Dekkers* 1997; *Frederichs et al.* 1999; *Evans & Heller* 2003).

Die Bildung der magnetischen Proxies

ist theoretisch relativ einfach, aber in der Praxis recht komplex: Marine Sedimente, einschließlich ihrer magnetischen Mineralfraktion, sind normalerweise Kompositionen aus verschiedensten ozeanischen und terrestrischen Quellen. Ihre Zusammensetzung wird durch sich zeitlich verändernde tektonische, klimatische und ozeanographische Gegebenheiten moduliert. Die primären magnetischen Trägerminerale können wiederum durch sekundäre, nach der Ablagerung ablaufende Prozesse, modifiziert werden, die vor allem durch die Degradierung von organischer Materie hervorgerufen werden können. Die räumliche Verteilung von Partikelquellen oder von prozeßspezifischen magnetischen Mineralspezies innerhalb einer bestimmten Zeitscheibe ist demnach ein vielschichtiges Abbild all dieser beschriebenen Faktoren. Detritischer Flußeintrag spiegelt u.a. die Geologie (z.B. durch das Eisen zu Titan Verhältnis) und die Verwitterung auf dem kontinentalen Hinterland wieder. Abhängig von der Feuchtigkeit kann die Mineralogie der detritischen Eisenoxide zwischen Magnetit (Fe_3O_4), Goethit (FeOOH) oder Hämatit (Fe_2O_3) dominierten Szenarien variieren. Magnetische Korngrößen werden wiederum durch quell- und transportabhängige Faktoren kontrolliert: Äolische Korngrößen hängen direkt von den herrschenden Windstärken und der Transportdistanz ab. Die Formation von authigenen Fraktionen, wie z.B. bakterielle Magnetofossilien oder Eisensulfiden wie Greigit (Fe_3S_4), Pyrrhotit (Fe_7S_8) und Pyrit (FeS_2) hängen von den herrschenden Eh und pH Werten ab. Die Identifizierung und quantitative Beschreibung dieser magnetischen Komponenten kann somit Information über Veränderungen im Massenfluß und geochemischen Milieu in Abhängigkeit von Umweltveränderungen geben (z.B. Frederichs *et al*. 1999).

Magnetische Proxies haben einige ganz bestimmte Vorteile gegenüber anderen Proxyparametern: Normalerweise benötigt man keinerlei mühsame Präparation, außer dem Einwiegen einer Probe. Sie sind hochsensible, so daß generell aussagekräftige Information bereits aus Messungen am Gesamtsediment gewonnen werden kann. Außerdem benötigt man normalerweise nur eine recht kleine Menge an Probenmaterial, das zerstörungsfrei gemessen wird und anschließend für weitere Analysen verwendet werden kann. Vor allem aber liefern magnetische Proxies Korngrößeninformation (besonders für die allerfeinste Fraktion), die mit anderen Methoden nur sehr schwierig zu bestimmen ist. Gesteins- und umweltmagnetische Parameter können generell in konzentrations-, korngrößen- und mineralogieabhängige Einflußgrößen unterteilt werden (z.B. *Thompson & Oldfield* 1986; *Butler* 1992; *Dunlop & Özdemir* 1997).

Eine Besonderheit der magnetischen Parameter in bezug auf ihre Interpretation ist ihr regionaler Charakter. Außerdem können Mehrdeutigkeiten von einzelnen Parametern, die aus den physikalischen Prinzipien des Gesteinsmagnetismus resultieren, durch einen Multi-Parameter Ansatz umgangen werden. Gezielte Fragestellungen betreffend der Bedeutung von bestimmten magnetischen Proxies müssen separat für jedes Sedimentationssystem betrachtet werden: Warum z.B. korreliert die magnetische Suszeptibilität (ein weltweiter Proxy für die Konzentration von magnetischen Mineralen) positiv mit sogenannten $\delta^{18}O$ Kurven (ein Proxy für das globale Eisvolumen, und damit fürs Klima) in einigen ozeanischen Regionen und wiederum negativ oder gar nicht in anderen Gebieten? Werden Variationen in der magnetischen Korngröße von den Verwitterungsbedingungen, von unterschiedlichen Herkunftsgebieten oder eher von Transportmechanismen bestimmt? Warum korrelieren (relative) Paläointensitätskurven von Sedimenten (ein Proxy für die Stärke des Erdmagnetfeldes) manchmal gut zwischen verschiedenen Regionen und in anderen Fällen fast gar nicht, sogar wenn der Einfluß von Diagenese ausgeschlossen werden kann? Einige dieser Fragen wurden bereits zum

Teil beantwortet, während andere immer noch offen sind und in dieser Arbeit behandelt werden.

Ein vielversprechender, aber experimentell anspruchsvoller Ansatz, um magnetische Proxies zu untersuchen, ist die lithologische Charakterisierung der umgebenden Sedimentmatrix und der magnetischen Trägerminerale. Während für ersteres die sedimentologische Untersuchungsmethoden meist ausreichen, ist die Identifizierung der magnetischen Trägerminerale eher kompliziert. Um die Petrologie dieser Spurenelemente im Mikro- und Nanometerbereich untersuchen zu können, wurden speziell für dieser Arbeit geeignete magnetische Experimente und Extraktionstechniken entwickelt. Raster- und Transmissionselektronenmikroskopie (REM und TEM) wurden zur Unterstützung und Interpretationen magnetischer Proxies benutzt. Sogenannte im REM erzeugte ‚Electron Backscatter Diffraction' Bilder dienen zur Unterscheidung von unterschiedlichen Fe-Ti-Oxiden. Die genaue Betrachtung der magnetischen Mineralvergesellschaftung unter verschiedenen geochemischen und sedimentologischen Gesichtspunkten läßt Rückschlüsse über die umweltmagnetischen Implikationen der magnetischen Petrologie zu.

Kapitel 2 beschäftigt sich mit der sogenannten relativen Paläointensität (RPI): Hochauflösende Paläointensitätssignale des Erdmagnetfeldes wurden bereits erfolgreich für viele marine Sedimente gewonnen. Diese werden durch die Normierung der natürlichen remanenten Magnetisierung (NRM) auf die Konzentration der magnetischen Träger ermittelt. Die Fragestellung, warum einige dieser insgesamt weltweit verteilten RPI Signale eine hohe Korrelation miteinander zeigen und andere nicht wird in diesem Kapitel behandelt. Unter anderem scheint die Lithologie der Sedimentmatrix Einfluß auf das Signal der RPI zu haben. Solche ‚Matrixeffekte' werden hier mit Hilfe von sedimentologischen und statistischen Methoden untersucht. RPI Daten von Tiefseesedimenten aus dem subtropischen und subantarktischen Frontensystem des Südatlantiks werden hierzu verglichen. Diese Lokalitäten liegen regional relativ eng beieinander und unterlagen demnach dem gleichen Einfluß des Paläomagnetfeldes, wohingegen die Lithologie der einzelnen Kernlokationen recht unterschiedlich ausgeprägt ist. Unterschiede in den RPI Werten sollten demnach den Einfluß der Sedimentmatrix auf die Ausrichtung der magnetischen Partikel im Sediment wiederspiegeln. Ausgiebige sedimentologische Untersuchungen wurden durchgeführt, um die Zusammensetzung und die Korngrößenverteilung eben dieser Sedimentmatrix zu charakterisieren. Bi- und multivariate Statistik wurde zum Test des ‚Matrixeffektes' benutzt. Während manche Parameter keine signifikanten Ergebnisse lieferten, konnte eine schwache Korrelation der Tonkorngröße und des Chloritgehaltes festgestellt. Der Opal-, Illit- und Kaolinitgehalt zeigt moderate Korrelationen mit der RPI. Den einflußreichsten Einzelfaktor stellt das Kaolinit/Illit Verhältnis dar, mit einem Korrelationskoeffizient nach Pearson von 0.51 bei 99,9% Signifikanz. Möglicherweise können die Matrixeffekte die Dynamik des RPI Signals sogar im gleichen Ausmaße beeinflussen, wie die Schwankungen der Intensität des Erdmagnetfeldes selbst. Außerdem zeigt die Studie Strategien zur Korrektur solcher Lithologieeffekte auf.

In **Kapitel 3** wird die Effektivität von magnetischen Extraktions- und Schwereretrennungstechniken an marinen Sedimenten aus dem äquatorialen Atlantik getestet, um magnetische Minerale mit Hilfe von gesteinsmagnetischen Tieftemperatur-Messungen identifizieren zu können. Diese Anreicherung ist aufgrund der sehr niedrigen Konzentration (üblicherweise im ppm Bereich) an magnetischen Partikeln im Sediment notwendig. Außerdem kann so für den erheblichen Einfluß der paramagnetischen Mineralfraktion (vor allem im Tieftemperaturbereich) auf das magnetische Signal

korrigiert werden. Bei der hier verwendeten magnetischen Extraktion wird suspendiertes Sediment nahe eines starken magnetischen Feldgradienten entlang gepumpt. An diesem sogenannten ‚Magnetischen Finger' bleiben dann die magnetischen Partikel aus der Suspension haften. Schweretrennung hingegen basiert auf der spezifischen Dichte der individuellen Mineralkomponenten im Sediment. Die gewählte Schwerelösung (Natriumpolywolframat) ist besonders für feinkörnige marine Sedimente mit hohem Tonmineralanteil geeignet, da sie einen hydrophilen Charakter besitzt. Die Dichte der Lösung wurde auf 3 g cm^{-3} festgesetzt, um die leichteren nicht-magnetische Minerale von der schwereren und magnetisch angereicherten Fraktion abtrennen zu können.

Anschließend wurden thermomagnetische Messungen an beiden Arten von Extrakten aus dem selben Probenmaterial durchgeführt, um die Vorzüge und Nachteile beider Techniken zu verdeutlichen. Tieftemperaturzyklen der remanenten Magnetisierung wurden im Feld und im Nullfeld gemessen. Zusammen mit den ebenfalls durchgeführten Tieftemperaturzyklen der isothermalen remanenten Magnetisierung (erworben bei Raumtemperatur), dienen diese Messungen der Identifizierung der magnetomineralogischen Zusammensetzung der Proben. Außerdem kann anhand dieser Daten die Effizienz der Extraktion quantifiziert werden. Beide Extraktionstechniken erlauben die Identifizierung von magnetischen Mineralphasen wie z.B. Magnetit, Titanomagnetit, Hemoilmenit, Goethit, und wahrscheinlich auch superparamagnetischer Ferrihydrit. Außer Goethit, der auch in den Gesamtsedimentproben nachgewiesen werden konnte, konnten alle anderen Phasen ausschließlich durch die magnetischen Konzentrate identifiziert werden. Es zeigte sich, daß die Schweretrennungsmethode für die magnetische Fraktion weitaus effizienter ist als die magnetische Extraktion, schwachmagnetische / hochkoerzitive Minerale und sehr feine Partikel wurden hierbei viel besser extrahiert.

Kapitel 4 beleuchtet die Vorteile der ‚Electron Backscatter Diffraction' (EBSD) Technik im REM bezogen auf die Identifizierung von verschiedenen magnetischen Eisen-Titanoxiden. EBSD ist besonders hilfreich in Kombination mit der ‚Element Dispersive Spectroscopy' (EDS), vor allem für Proben, die kristallographisch verschiedene Mineralphasen mit sehr ähnlicher elemetarer Zusammensetzung enthalten. An einer Auswahl von synthetischen und natürlichen Proben ganz unterschiedlicher Herkunft wird die Möglichkeit zur Unterscheidung von Titanomagnetit [$Fe_{3-x}Ti_xO_4$] und Hemoilmenit [$Fe_{2-y}Ti_yO_3$] demonstriert. Bislang wurde EBSD hauptsächlich an polierten Schliffen mit ebener Oberfläche angewendet. In diesem Kapitel zeigen wir die Möglichkeit auf, daß auch erfolgreich EBSD Signale von Einzelpartikeln mit unebener Oberfläche gewonnen werden können, eine neue Anwendung an sogenannten ‚nicht-eingebetteten' Proben.

Zum weiteren Verständnis der Implikationen magnetischer Proxyparameter wurde der Bestand an magnetischen Mikro- und Nanopartikeln von Sedimenten aus dem Äquatorialatlantik mit Hilfe von REM und TEM Analysen untersucht. Diese Untersuchungen an magnetischen Extrakten werden in **Kapitel 5** detailliert beschrieben. Alle vorhandenen detritischen und authigenen magnetischen Partikel wurden entsprechend ihrer regionalen Verteilung, ihres Ursprungs, ihres Transportes und ihres Erhaltungszustandes klassifiziert. Der untersuchte West-Ost-Transekt bietet dabei eine Auswahl an unterschiedlichen detritischen Eintragsmechanismen, wie z.B. die Flußfracht des Amazonas, die submarine Verwitterung von mittelozeanischen Basaltrückenmaterial und den äolischen Beitrag von Saharastaub, die rasterelektronenmikroskopisch identifiziert werden konnten. Außerdem wurden mit Hilfe von TEM authigene Quellen wie chemische Ausfällungen, Biomineralisation von bakte-

riellem Magnetit und verschiedene Stadien von superparamagnetischen bis einbereichsteilchengroßem Goethit identifiziert. Diese Informationen wurden verwendet, um Beziehungen zwischen den Quellen und Senken der magnetischen Partikel herzustellen und die Umweltmagnetischen Proxies für dieses Arbeitsgebiet zu interpretieren.

Für die westlichste Lokation am Ceará Rise (3°49.9'N / 41°37.3'W) wurde ein sogenanntes ‚Komponenten-Mischsystem' beobachtet, bei dem 80% des magnetischen Materials aus relativ grobkörnigem Magnetit vom Amazonaseintrag besteht. Die restlichen 20% setzen sich aus Titanomagnetiten aus höchstwahrscheinlich naheliegenden basaltischen Provinzen, äolischem Eintrag vom afrikanischen Kontinent und authigenem bakteriellem Magnetit zusammen. Die zuletzt genannte Komponente wurde ausschließlich in dieses Gebiet gefunden. An der östlichsten Lokation am Sierra Leone Rise (4°50.7'N / 21°03.2'W) wird der Eintrag von magnetischem Material hauptsächlich durch klimatisch bedingte Passatwind-Veränderungen bestimmt, die in einem sogenannten ‚Korngrößen-Sortierungssystem' der äolischen Hauptquelle (30-60% der magnetischen Fraktion) resultieren. Die Lokation am Mittelatlantischen Rücken (4°02.8'N / 33°26.3'W) weist eine Vergesellschaftung der magnetischen Fraktion auf, die am besten durch eine Kombination beider Mechanismen, dem ‚Komponenten-Mischsystem' und dem ‚Korngrößen-Sortierungssystem', erklärt werden kann. Die Schwankungen in der Korngröße der dominierenden Titanomagnetite werden hier durch klimagesteuerte Bodenwasserströmungen getriggert. Sie machen ungefähr 50% der magnetischen Fraktion aus. Zusätzlich gelangen aus dem Westen detritische Partikel aus dem Amazonas in den zentralen äquatorialen Atlantik während aus dem Osten Saharastaub angeliefert wird. Zusammen mit den Titanomagnetiten formen diese Partikelklassen ein ‚Dreikomponentensystem' des magnetischen Inventars. Hämatit, Goethit und eventuell ebenfalls Ferrihydit koexistieren nebeneinander in allen untersuchten Proben und haben entsprechend ihrer Korngröße superparamagnetische oder Einbereichsteilchen-Eigenschaften. Meist werden diese magnetischen Korngrößen als zwei voneinander getrennte Fraktionen angesehen, aber unsere Daten weisen eher darauf hin, daß sie höchstwahrscheinlich stark miteinander verknüpft sein könnten.

Kapitel 6 untersucht den starken Einfluß von reduktiver Diagenese auf das magnetische Signal von marinen Sedimenten, die vom Argentinischen Kontinentalhang nahe des Rio de la Plata stammen. Alle eisenreichen magnetischen Minerale wurden hier weggelöst, solange sie nicht innerhalb einer silikatischen Matrix erhalten bleiben konnten. Gesteinsmagnetische Messungen mit einem sogenannten ‚Magnetic Property Measurement System' (MPMS) im Tieftemperaturbereich zwischen 300 und 5 K wurden mit rasterelektronenmikroskopischen Untersuchungen kombiniert, um die übriggebliebenen titanreichen magnetischen Minerale zu charakterisieren. Da der vorwiegende Eintrag aus vulkanischen Titanomagnetit und Hemoilmenit Partikeln vom Paraná Becken stammt, konnte ein magnetisches Selbstumkehr-Verhalten während der Tieftemperaturmessungen beobachtet werden, das die fast komplette Abwesenheit von eisenreichen magnetischen Mineralphasen bestätigt.

Die Identifikation von spezifischen Mineralen und damit zusammenhängenden Proxyparametern ist natürlich nicht nur auf magnetischen Partikel beschränkt, sondern kann auch für nicht-magnetische paläoozeanographische Tracer angewendet werden. In marinen Sedimenten wird Baryt oft als Proxy für die Paläoproduktivität verwendet. Allerdings kann die Anwendung dieses Proxies durch den Einfluß von reduktiver Diagenese eingeschränkt werden, die das primäre Paläoproduktivitätssignal überprägt. Deswegen ist es wichtig solche Prozesse in marinen Sedimenten zu untersuchen. **Kapitel 7**

befaßt sich mit dem Einfluß von nicht-stationären Diageneseprozessen des geochemischen Primärsignals. Für diese Studie wurden Sedimente aus dem östlichen Kapbecken verwendet. Geochemische Porenwasser- und Festphasenuntersuchungen wurden mit numerischer Modellierung und Rasterelektronenmikroskopie kombiniert, um diagenetische Barytfronten in und unterhalb der Sulfatmethanzone (SMT) zu identifizieren. Barytfronten werde authigen durch die Reaktion von aufsteigendem Barium und Porenwässern gebildet. In sulfatabgereicherten Sedimenten ist Baryt im allgemeinen nicht stabil. Deshalb wird das Vorhandensein von Barytanreicherungen unterhalb der SMT mit der verzögerten Auslösung von Baryt in Zusammenhang gebracht, das unter anderem mit hohen Konzentrationen von gelöstem Barium im Porenwasser erklärt werden kann. Das Aufwärtssteigen der SMT führt zur Einrichtung einer neuen aktiven Barytfront. Ein hohes Aufkommen von organischer Materie unterhalb der SMT zieht einen Anstieg der Methanogenese mit sich. Dieser Prozeß resultiert in einem Aufwärtsfluß von Methan, uns somit einer Verschiebung der SMT. Mit Hilfe von solch detaillierten geochemischen Untersuchungen können Fehlinterpretationen von Paläoumweltbedingungen in Bezug auf die Paläoproduktivität vermieden werden.

Die Studien, die in dieser Arbeit beschrieben werden, verdeutlichen, daß magnetische Proxies idealerweise für jede Fallstudie und jedes Arbeitsgebiet validiert werden müssen. Einige Fragen, wie z.B. die Abhängigkeit der relativen Paläointensität von der Matrixlithologie, die Identifikation von entweder weitverbreiteten oder regional begrenzten magnetischen Trägermineralen sowie die Gründe für die magnetischen Korngrößenvariationen über den äquatorialen Atlantik wurden erklärt oder zumindestens im Verständnis verbessert. Der Einfluß von milder bis starker Diagenese wurde im mikroskopischen Maßstab untersucht. Die Überprüfung von umweltmagnetischen Proxies mit Hilfe von gesteinsmagnetischen und nicht-magnetischen Techniken hat das Verständnis der unterliegenden Prozesse und die Möglichkeiten zur Interpretation erheblich verbessert, dies führt wiederum zu einer verbesserten Rekonstruktion der paläoozeanographischen Geschichte auf regionalem Gebiet.

References

Butler, R.F., 1992. Paleomagnetism: Magnetic Domains to Geological Terranes, Boston, Backwell Scientific Publications. http://www.geo.arizona.edu/Paleomag/book/

Dekkers, M.J., 1997. Environmental magnetism: an introduction, *Geologie en Mijnbouw*, **76**, 163-182.

Dunlop, D.J. & Özdemir, Ö., 1997. *Rock magnetism, fundamentals and frontiers*, Cambridge University Press, 573 p.

Emiliani, C., 1955. Pleistocene temperatures, *J. Geol*., **63**, 538-578.

Evans, M.E. & Heller, F., 2003. *Environmental Magnetism: Principles and Applications of Enviromagnetics*, Academic Press, Elsevier Science, San Diego, London, Burlington, 299 p.

Fischer, G. & Wefer, G., 1999. *Use of Proxies in Paleoceanography: Examples from the South Atlantic*, Springer-Verlag, Berlin, Heidelberg, New York, 735 p.

Frederichs, T., Bleil, U., Däumler, K., von Dobeneck, T. & Schmidt, A.M., 1999. The magnetic view on the marine paleoenvironment: Parameters, techniques, and potentials of rock magnetic studies as a key to paleoclimate and paleoceanographic changes, in *Use of Proxies in Paleoceanography: Examples from the South Atlantic*, pp. 575-599, eds Fischer, G. & Wefer, G., Springer-Verlag, Heidelberg, Berlin, New York.

King, J.W. & Channell, J.E.T., 1991. Sedimentary magnetism, environmental magnetism, and magnetostratigraphy, *Rev. Geophys*., **29**, 358-370.

Imbrie, J. & Kipp, N.G., 1971. A new micropaleontological method for quantitative paleoclimatology: Application to a Late Pleistocene Caribbean core, in *The Late Cenozoic Glacial Ages*, pp. 71-181, ed. Turekian, K., Yale Univ. Press, New Haven, Conn.

Lund, S.P. & Karlin, R., 1990. Introduction to the special section on physical and biogeochemical processes responsible for the magnetization of sediments, *J. Geophys. Res.*, **90**, 4353-4354.

Oldfield, F., 1991. Environmental Mag-netism: a personal perspective, *Quat. Sci. Rev*., **10**, 73-

85.

Ruddiman, W.F., 2001. *Earth's Climate: Past and Future*, W.H Freeman and Company, New York, 465 p.

Shackleton, N.J. & Opdyke, N.D.,1973. Oxygen isotope and paleomagnetic stratigraphy of equatorial Pacific core V28-238: Oxygen isotope temperatures and ice volumes on a 10^5 year and 10^6 year scale, *Quat. Res.*, **3**, 39-55.

Soffel, H.C., 1991. *Paläomagnetismus und Archäomagnetismus*, Springer-Verlag, Berlin, Heidelberg, New York, 276 p.

Thompson, R. & Oldfield, F., 1986. *Environmental Magnetism*, Allen and Unwin, London, pp. 1-227.

Verosub, K.L. & Roberts, A.P., 1995. Environmental magnetism: past, present, and future, *J. Geophys. Res.*, **100**, 2175-2192

Acknowledgements

This study was carried out in the framework of the European Graduate College 'Proxies in Earth History' – Europrox at the Universities of Bremen and Utrecht. Therefore it is a joint project between both institutes, in particular between the Marine Geophysics Group in Bremen and the Paleomagnetic Laboratory 'Fort Hoofddijk' in Utrecht.

First of all, I'd like to thank my promoter and supervisor Tilo von Dobeneck, with whom the whole project started in Bremen and who always supported me throughout the past four years. He told me in the very beginning to develop a scientific 'killer instinct' and although I am still not a very dangerous person, I did take his advise serious and tried my very best!

But what kind of a balance would it have been without my other supervisor and co-promoter Mark Dekkers, who is a never ending source for helpful literature and gave me so much advice in numerous talks. Thank you for always having the time to address my scientific questions, no matter how silly they might have been.

The cooperation within the project would have never been so successful without the support of my promoter Cor Langereis, who always believed in me and treated my as one of his group members from the very first moment. I could not have made it without your know-how.

And through the years another person became particularly important for the success of this project: thanks to Martyn Drury, my co-promoter and electron microscopic specialist! Without his help in microscopic, crystallographic and mineralogic questions this whole study would have simply not been possible.

I thank the members of the dissertation committee, Prof. Dr. Pierre Rochette, Prof. Dr. Barbara Maher, Prof. Dr. Nikolai Petersen, Prof. Dr. Chris Spiers, and Dr. Sabine Kasten, for accepting the responsibility to evaluate this thesis.

I owe thanks to all members of both of my working groups the Marine Geophysics Group in Bremen and the Paleomagnetic Group in Utrecht for their continuous support and help. Especially I'd like to thank Dave, Thomas, Tom, Daniela, Anne, Fatimá, Klaudia, Iuliana, Silja, Yanzhe, Linda, and Ulrich Bleil for their cooperation and help with many questions concerning various aspects of work or life.

For the practical help concerning all electron miscrocopic measurements, I'd like to thank Gill Pennock, Hans Meeldijk, Pim van Maurik, and Prof. Geus from Utrecht University. I thank Natascha Riedinger and the members of the Marine Geochemistry Group at the University of Bremen for their cooperation and aid with all kind of laboratory questions. The cooperation with Dominique Lattard and Ralf Engelmann from University of Heidelberg improved this study in many aspects and I am very grateful for the input they provided. Additionally I'd like to thank the crews and shipboard scientists of the research cruises M57/2 and IODP 308.

As already mentioned above, this study was carried out within 'Europrox' and I am particulary thankful to all members of this graduate college, especially to Maria and Marion, and to Helmut Willems, but also to all recent and former 'Europroxies'.

To my friends and former or recent flat maids, particularly to Maisha (what would I have done without your help?), and to all my friends in Utrecht I'd like to address a special thanks for all the understanding they had during all times, their support and for their contribution to make me feel at home in this lovely dutch town. Of course a special thanks goes to my 'paranymphs' Melanie and Karin, who accompanied me through good and bad times of my (Ph.D.) studies. I thank all my dear friends in Bremen or no matter where they are, for their support and all the moments we shared together.

Besonders meinen Freundinnen Nina und Pamela bin ich zutiefst verbunden, ich weiß daß es nicht immer leicht mit mir als Freundin ist, die nicht immer Zeit für Euch hat dafür aber immer Recht behalten will. Ich bin froh über die vielen Gespräche, Treffen und Emails zwischen uns, die so gar nix mit Geowissenschaften zu tun hatten und trotzdem weiß ich, daß Ihr mich immer unterstützt habt und mich im Grunde genau versteht. Danke!

Ganz besonders danke ich meinen Eltern und meiner Familie. Papa und Mama, Ihr habt mir immer geholfen, mich unterstützt und an mich geglaubt, jeder von Euch auf seine ganz eigene Art. Ich möchte mich an dieser Stelle ganz herzlich bei Euch beiden bedanken für die tolle Ausbildung, die Ihr mir ermöglicht habt und auch für sonst alles, was Ihr für mich getan habt, ich habe Euch sehr lieb! Allen die sonst noch zu meiner bunten Familie gehören und mich immer unterstützt haben sei an dieser Stelle herzlichst gedankt: Ingrid, Rolf, Oma und Opa Graubaum, Opa Franke, Fränzi und Dieter, Ella, Theite, Bernd und Pekka.

Ganz zuletzt aber am allermeisten bedanke ich mich bei Dir, Arne: Du begleitest mich schon so lange durch dick und dünn, ich habe aufgehört die vielen Male zu zählen, die ich mich wirklich oder auch in Gedanken umgedreht habe und Du warst da. Du bist der eine Mensch in meinem Leben, der immer hinter mir steht, ganz egal wann und dafür nix als meine Liebe zurück bekommt. Aber die besitzt Du, das steht jedenfalls fest - ich liebe Dich.

Curriculum Vitae

11th January 1974	Born in Bremerhaven, Germany
1980-1990	Primary and secondary school in Bremerhaven, Germany
1990-1993	Gymnasium School Center Bremerhaven, Germany, Graduation with A-level German high school degree
1993-1994	'Voluntary Social Year' at the General Medical Hospital Eilbek, Hamburg, Germany
Winter 1994/95 until Spring 2002	Studies of Geosciences, major subjects: Marine Geology and Marine Geophysics, University of Bremen, Germany, Graduation Diploma degree
2002-2006	Ph.D. within the framework of the European Graduate College 'Proxies in Earth History' EUROPROX, at the Universities of Bremen and Utrecht, Germany and the Netherlands

Appendices

A. Bibliography

Chapter 2
Franke, C., Hofmann, D. and von Dobeneck, T., 2004. Does lithology influence relative paleointensity records? A statistical analysis on South Atlantic pelagic sediments, *Physics of the Earth and Planeary Interiors*, 147, 285-296.

Chapter 3
Franke, C., Frederichs, T. and Dekkers, M.J., 2006. The efficiency of heavy liquid separation to concentrate magnetic particles from pelagic sediments demonstrated by low-temperature magnetic measurements, *in review at Geophysical Journal International.*

Chapter 4
Franke, C.**,** Pennock, G.M., Drury, M.R., Engelmann, R., Lattard, D., Garming, J.F.L., von Dobeneck, T. and Dekkers, M.J., 2006. Identification of magnetic Fe-Ti-oxides by electron backscatter diffraction (EBSD) in scanning electron microscopy, *in review at Journal of Geophysical Research.*

Chapter 5
Franke, C.**,** von Dobeneck, T., Drury, M.R., Meeldijk, J.D. and Dekkers, M.J. Magnetic Petrology of Equatorial Atlantic Sediments: Electron Microscopic Findings and their Environmental Magnetic Implications, *manuscript in preparation for submission to Paleoceanography.*

Chapter 6
Garming, J.F.L., Bleil, U., Franke, C. & von Dobeneck, T., 2006. Low temperature partial magnetic self-reversal in marine sediments, *in review at Geophysical Journal International.*

Chapter 7
Riedinger, N., Kasten, S., Gröger, J., Franke, C. and Pfeifer, K., 2006. Active and buried authigenic barite fronts in sediments from the Eastern Cape Basin, *Earth and Planetary Science Letters*, 241, 876–887.

B. Greigite as the key recorder of paleomagnetic and paleoenvironmental signals in the Mio-Pliocene sedimentary rocks of the Carpathians foredeep (Romania)

Abstract

During the Mio-Pliocene, the Carpathian region represented the westernmost part of the so-called Eastern Paratethys, a paleo-bioprovince that covered Central and Eastern Europe as well as important parts of southwest Asia. Previous paleomagnetic investigations provided a high-resolution magnetochronology for the sedimentary sequences of the Carpathians foredeep and indicated a marked transition in magnetic carriers from iron oxides to iron sulphides, taking place in chron C3r at an age between 6.0 and 5.5 Ma. Here, we show by detailed rock magnetic investigations and scanning electron microscope (SEM) analyses that the key magnetic iron sulphide is greigite. Thermomagnetic runs show an irreversible decrease in magnetisation with increasing temperature up to 400°C and SEM observations show octahedral grain morphologies and Fe:S ratios indicative for greigite. Hysteresis loops have the socalled "rectangular" shapes, typical of single domain behaviour, and indicate (remanent) coercivity values B_c = 35-45 mT and B_{cr} = 52-67 mT. FORC diagrams furthermore show contours closing around single domain peaks with B_c's of 45-90 mT. IRM component analysis shows a small dispersion for the greigite component (DP ~ 0.15 log units) indicating a narrow grain-size distribution typical of biogenic minerals. We argue that (most of) the greigite was formed under early diagenetic conditions, i.e. within 1000 years of deposition of the sediment in this setting, and that it thus can be considered as a reliable recorder of the paleomagnetic signal. We also performed a similar rock magnetic study on previously well-identified greigite from southwest Taiwan, which clearly exemplifies the high similarity in magnetic properties of early diagenetic greigite from two different sedimentary settings. The sudden appearance of greigite in chron C3r (between 6.0 and 5.5 Ma) in the Carpathians foredeep is most likely related to regional tectonic and/or climatic events that reshaped the basin configuration and consequently drastically influenced the paleo-environmental conditions. It resulted in an increase of sedimentation rates that coincided with a paleoenvironmental change from brackish-marine conditions in the Sarmatian-Meotian (Late Miocene) to dominantly fresh water conditions in the Pontian-Dacian (Late Miocene - Early Pliocene) stages. Since biostratigraphic studies indicate that the bottom layers of the water column remained well ventilated and sufficiently oxygenised throughout the entire succession, we conclude that the anoxic conditions favouring greigite formation could only have been present within the sediments, probably related to high productivity of decomposed organic matter and to good preservation because of huge sedimentation rates.

This is the abstract of a manuscript, which is a separate chapter in the Ph.D. thesis of Mrs. Iuliana Vasiliev and is an article in review: Vasiliev, I., Dekkers, M.J., Krijgsman, W. Franke, C. and Mullender, T.A.T., 2006. Greigite as the key recorder of paleomagnetic and paleoenvironmental signals in the Mio-Pliocene sedimentary rocks of the Carpathians foredeep (Romania), *Geophys. J. Int.*

C. Additional Data

All figures and data shown in this section are supplementary to Chapter 5. They provide additional room- and high-temperature rock magnetic results as well as colour reflectance spectra from the diffusive reflectance spectroscopy for the samples described in Chapter 5.

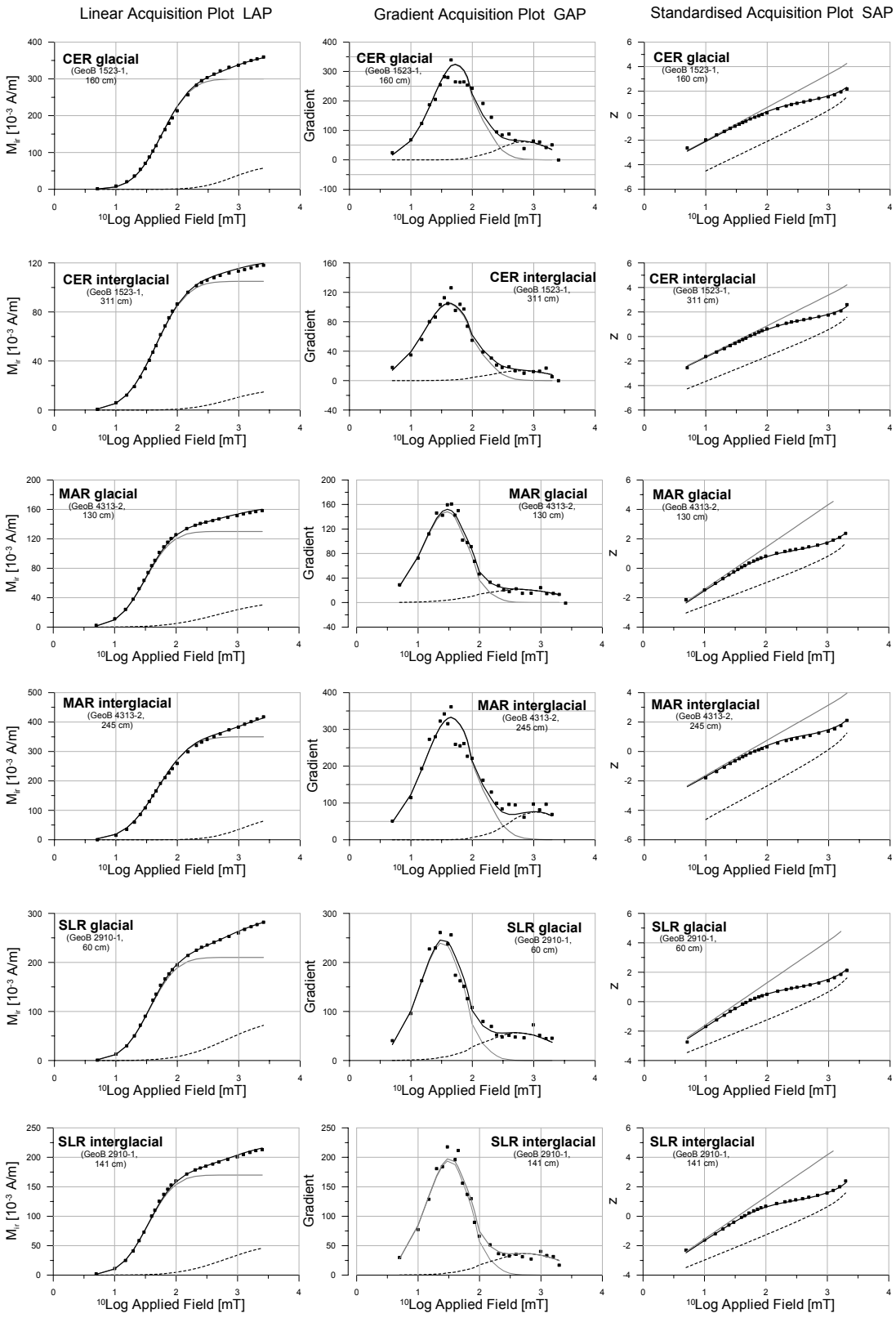

Linear acquisition (LAP), gradient acquisition (GAP) and standardized acquisition plots from isotherman remanent magnetisation component analysis (after *Kruiver et al.* 2001) for two component fitting. Black symbols represent the raw data points, grey solid curves show the contribution of component 1, dashed black curves the contribution of component 2 and black solid lines outline the sum curves of both components. Samples from the Ceará Rise (CER) are shown in the upper two lines, samples from the Mid-Atlantic Ridge (MAR) are shown in the middle two lines, and samples from the Sierra Leone Rise (SLR) are shown in the lower two lines. Note that GAP curves from the CER samples are particularly skewed to the left, indicating reasonable amount of superparamagnetic material.

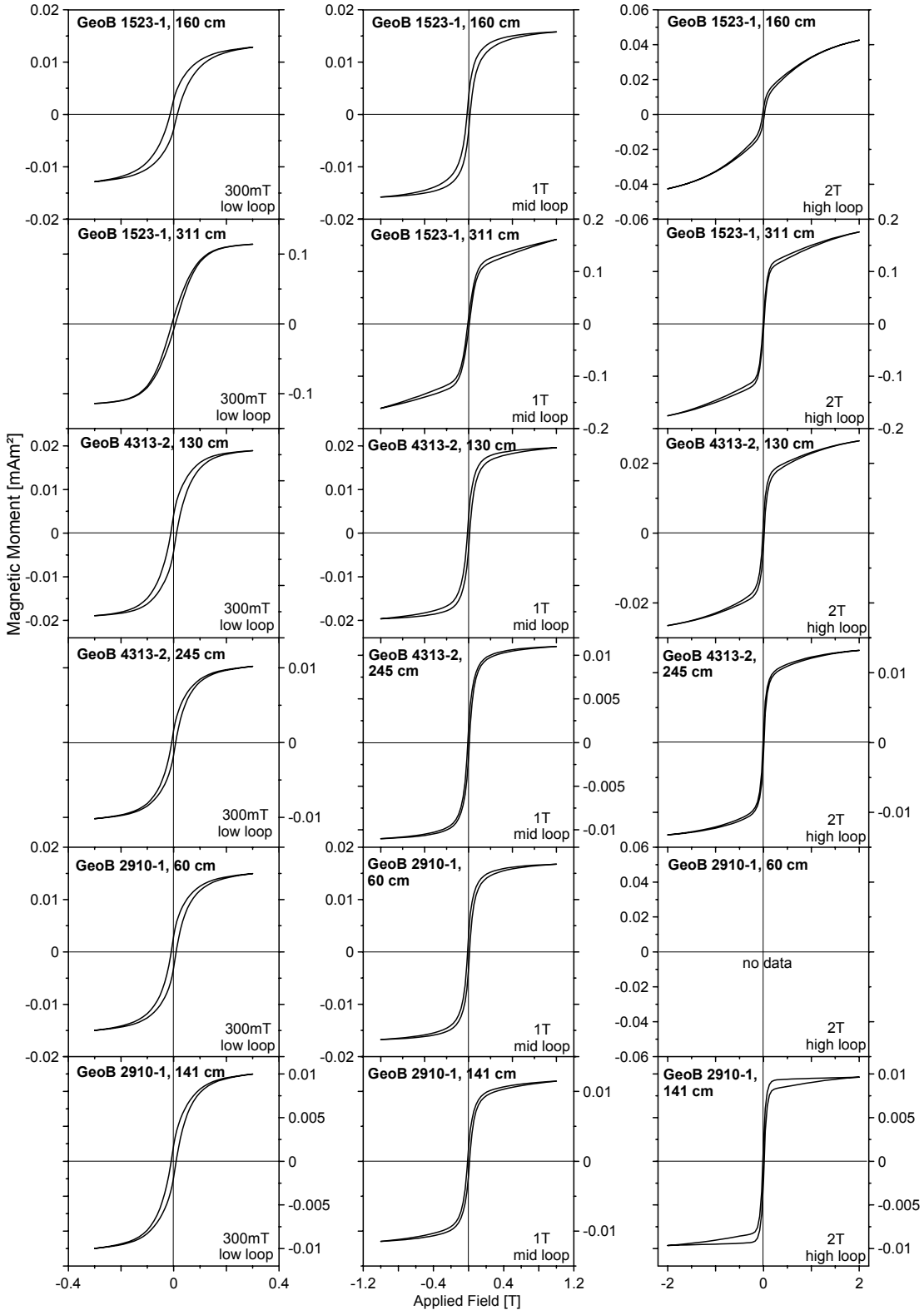

Overview on the hysteresis loops at 300 mT, 1 T, and 2 T, compiled by the 'HYSREAR' software after *von Dobeneck* (1996). Samples from the Ceará Rise (GeoB 1523-1) are shown in the upper two lines, samples from the Mid-Atlantic Ridge (GeoB 4313-2) are shown in the middle two lines, and samples from the Sierra Leone Rise (GeoB 2910-1) are shown in the lower two lines. No complied data available for sample GeoB 2910-1, 60cm.

Results from IRM component analyses after *Kruiver et al*. 2001 using two component fitting; S-ratios are calculated [1]classically using the $IRM_{0.3\ T}/IRM_{1\ T}$ ratio and calculated [2]after Bloemendal *et al*. 1992.

Sample	Calculated S-ratios	Component	Contribution [%]	SIRM [A/m]	log ($B_{1/2}$) [mT]	$B_{1/2}$ [mT]	DP
CER/glacial	0.79[1]	1	82.2	300	1.75	56	0.37
	0.90[2]	2	17.8	65	2.90	794	0.42
CER/interglacial	0.85[1]	1	86.1	105	1.65	45	0.40
	0.93[2]	2	13.9	17	2.85	708	0.50
MAR/glacial	0.85[1]	1	78.8	130	1.50	31	0.35
	0.93[2]	2	21.2	35	2.70	501	0.65
MAR/interglacial	0.80[1]	1	80.0	350	1.68	48	0.42
	0.90[2]	2	19.5	85	3.10	1259	0.45
SLR/glacial	0.78[1]	1	71.2	210	1.55	36	0.35
	0.89[2]	2	28.8	85	2.80	631	0.60
SRL/interglacial	0.81[1]	1	75.6	170	1.54	35	0.35
	0.91[2]	2	24.4	55	2.82	661	0.60

Results from IRM component analyses after *Kruiver et al*. 2001 using three (and four) components; S-ratios are calculated [1]classically using the $IRM_{0.3\ T}/IRM_{1\ T}$ ratio and calculated [2]after *Bloemendal et al*. 1992.

Sample	Calculated S-ratios	Component	Contribution [%]	SIRM [A/m]	log ($B_{1/2}$) [mT]	$B_{1/2}$ [mT]	DP
CER/glacial	0.80[1] 0.90[2]	1	430	165	1.75	56	0.28
		2	37	140	1.85	71	0.50
		3	18	70	3.20	1585	0.50
		4	2	8	1.15	14	0.10
CER/interglacial	0.86[1] 0.93[2]	1	45	55	1.55	36	0.28
		2	45	55	1.85	71	0.50
		3	8	10	3.20	1585	0.40
		4	2	2	1.20	16	0.15
MAR/glacial	0.89[1] 0.94[2]	1	39	65	1.45	28	0.25
		2	52	85	1.70	50	0.50
		3	9	15	3.20	1585	0.40
MAR/interglacial	0.78[1] 0.89[2]	1	13	60	1.45	28	0.28
		2	64	290	1.75	57	0.45
		3	22	100	3.20	1585	0.50
SLR/glacial	0.82[1] 0.91[2]	1	34	100	1.50	32	0.28
		2	52	150	1.75	56	0.50
		3	14	40	3.10	1259	0.30
SLR/interglacial	0.85[1] 0.92[2]	1	41	90	1.50	32	0.28
		2	45	100	1.70	50	0.50
		3	14	30	3.10	1259	0.45

Hysteresis parameters for all six discrete bulk sediment samples (cf. Chapter 5) , Ceará Rise = CER, Mid-Atlantic Ridge = MAR, Sierra Leone Rise = SLR, 300 mt low loop = LPL, 1 T mid loop = LPM, 2 T high loop = LPL.

Sample	Loop	m_{tara} [mg]	m_{dry} [mg]	m_{tot} [mg9	max. field [T]	M_{tot} [Am²/kg]	M_{nf} [Am²/kg]	M_{ferr} [Am²/kg]	M_s [Am²/kg]	M_{rs} [Am²/kg]	M_{rs}/M_{ferr}	M_{rs}/M_s	B_c [T]	B_{cr} [T]	B_{cr}/B_c	χ_{tot} [m³/kg]	χ_{nf} [m³/kg	χ_{ferr} [m³/kg
CER/glacial	LPL	9.88	14.23	19.62	0.3	0.00012	0.00001	0.00011	0.00012	0.00001	0.07393	0.06856	0.00659	0.03313	5.02908	0.00126	0.00002	0.00124
CER/glacial	LPM	9.88	14.23	19.62	1.0	0.15824	-0.00318	0.16142	0.18293	0.01184	0.07333	0.06471	0.00853	-	-	1.32000	-0.00318	1.32318
CER/glacial	LPH	9.88	14.23	19.62	2.0	0.20005	0.02448	0.17557	0.20442	0.01111	0.06330	0.05437	0.00826	-	-	1.26567	0.01224	1.25343
CER/interglacial	LPL	7.21	12.14	19.91	0.3	0.03959	0.02674	0.01284	0.01414	0.00283	0.22003	0.19989	0.01383	0.04133	2.98897	0.28264	0.08915	0.19349
CER/interglacial	LPM	7.21	12.14	19.91	1.0	0.10379	0.08801	0.01578	0.01659	0.00332	0.21028	0.20008	0.01670	-	-	0.26130	0.08801	0.17330
CER/interglacial	LPH	7.21	12.14	19.91	2.0	0.18454	0.14197	0.04256	0.05367	0.00349	0.08199	0.06502	0.01832	-	-	0.23643	0.07099	0.16545
MAR/glacial	LPL	4.68	8.58	14.24	0.3	0.01736	0.00718	0.01018	0.01097	0.00166	0.16291	0.15122	0.00772	0.02381	3.08418	0.22111	0.02393	0.19718
MAR/glacial	LPM	4.68	8.58	14.24	1.0	0.03482	0.02381	0.01101	0.01140	0.00164	0.14903	0.14395	0.00868	-	-	0.18890	0.02381	0.16509
MAR/glacial	LPH	4.68	8.58	14.24	2.0	0.05865	0.04543	0.01322	0.01426	0.00153	0.11551	0.10708	0.00987	-	-	0.15858	0.02271	0.13587
MAR/intergla.	LPL	6.76	9.31	17.43	0.3	0.03967	0.01998	0.01968	0.02115	0.00395	0.20042	0.18651	0.01054	0.03218	3.05297	0.41557	0.06661	0.34896
MAR/intergla.	LPM	6.76	9.31	17.43	1.0	0.08390	0.06428	0.01962	0.02043	0.00372	0.18980	0.18231	0.01235	-	-	0.32631	0.06428	0.26203
MAR/intergla.	LPH	6.76	9.31	17.43	2.0	0.14763	0.12118	0.02645	0.03036	0.00357	0.13512	0.11774	0.01401	-	-	0.28146	0.06059	0.22087
SLR/glacial	LPL	8.97	11.89	21.04	0.3	0.01996	0.00997	0.00999	0.01084	0.00184	0.18405	0.16956	0.00956	0.02905	3.03773	0.21154	0.03323	0.17830
SLR/glacial	LPM	8.97	11.89	21.04	1.0	0.04425	0.03277	0.01148	0.01213	0.00199	0.17360	0.16435	0.01102	-	-	0.18848	0.03277	0.15571
SLR/glacial	LPH	8.97	11.89	21.04	2.0	0.08143	0.07178	0.00965	0.00410	0.00212	0.22031	0.51797	0.01417	-	-	0.16329	0.03589	0.12740
SLR/intergla.	LPL	7.81	12.31	21.40	0.3	0.02818	0.01320	0.01499	0.01623	0.00302	0.20137	0.18590	0.00950	0.02835	2.98598	0.34030	0.04398	0.29632
SLR/intergla.	LPM	7.81	12.31	21.40	1.0	0.05981	0.04307	0.01674	0.01732	0.00319	0.19026	0.18390	0.01082	-	-	0.29678	0.04307	0.25371

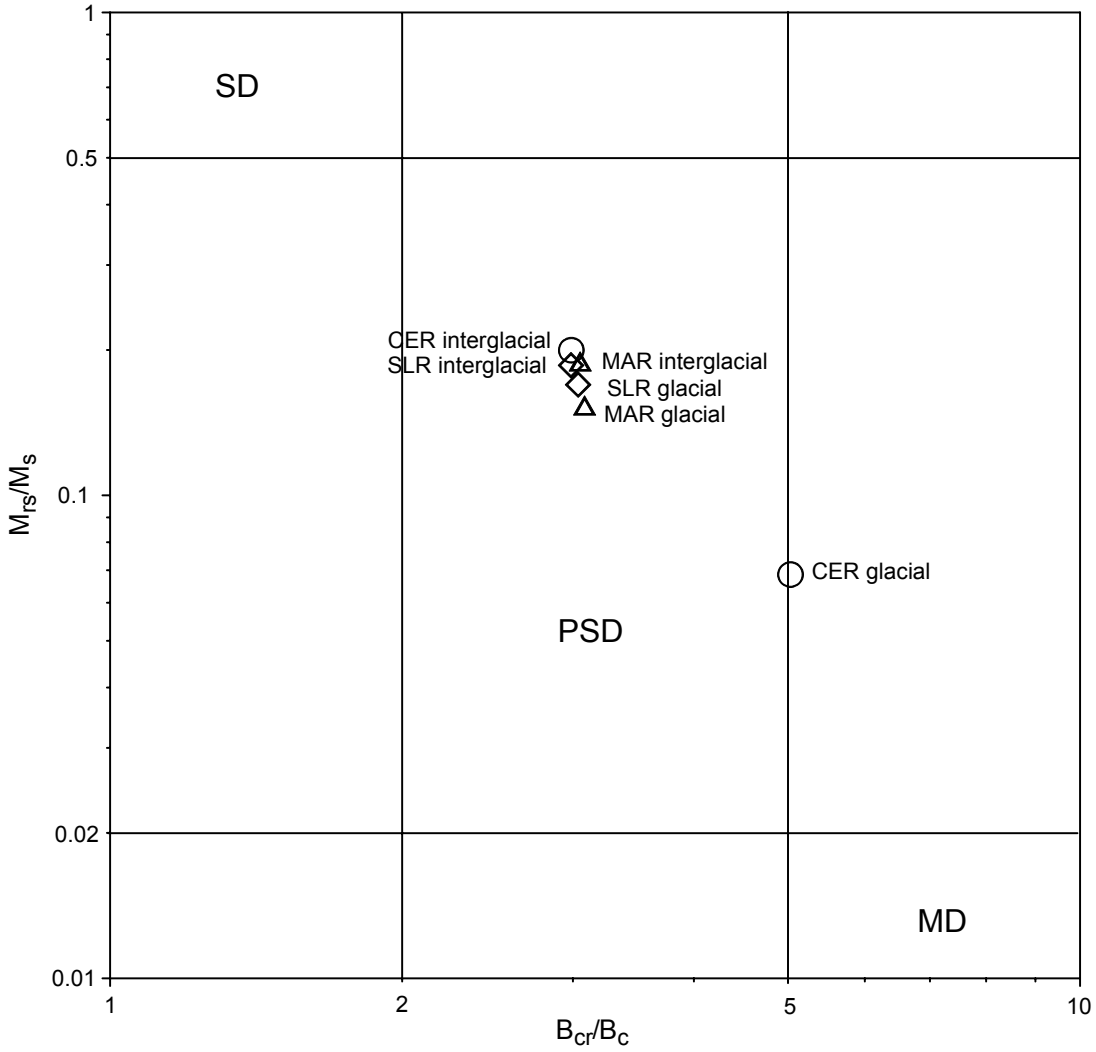

Day plot (double log scale; modified after *Dunlop* 2001a) of the six discrete samples (cf. Chapter 5) indicating the ferromagnetic magnetic grain-size for the 300 mT hysteresis loop data. Samples are indicated as circle symbols (Ceará Rise = CER), triangle symbols (Mid-Atlantic Ridge = MAR) and diamond symbols (Sierra Leone Rise = SLR). Magnetic domain states: single domain = SD, pseudo single domain = PSD, and multi domain = MD.

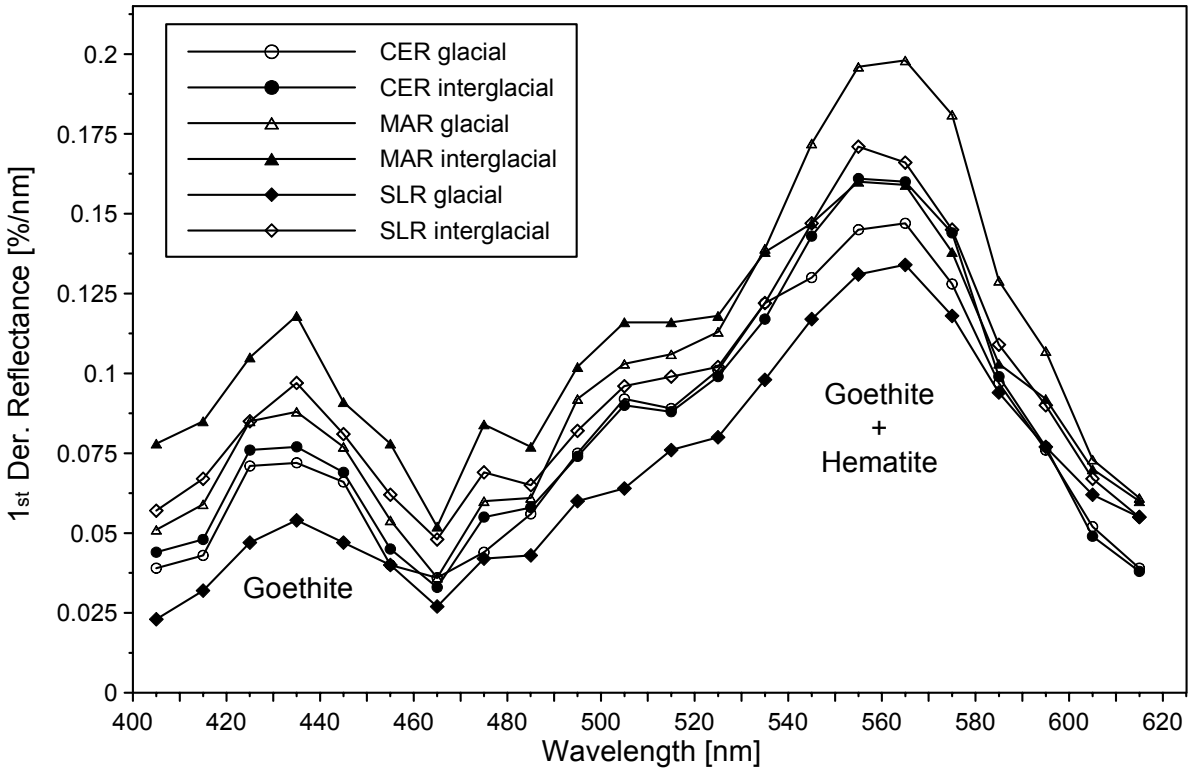

First derivatives of the colour reflectance spectra from the diffusive reflectance spectroscopy (DRS) spot check analysis at all six sample positions (cf. Chapter 5). Circle symbols belong to samples from the Ceará Rise (CER), triangle symbols belonging to samples from the Mid-Atlantic Ridge (MAR), and diamond symbols to samples from the Sierra Leone Rise (SLR). Open symbols represent glacial, filled symbols represent interglacial samples.

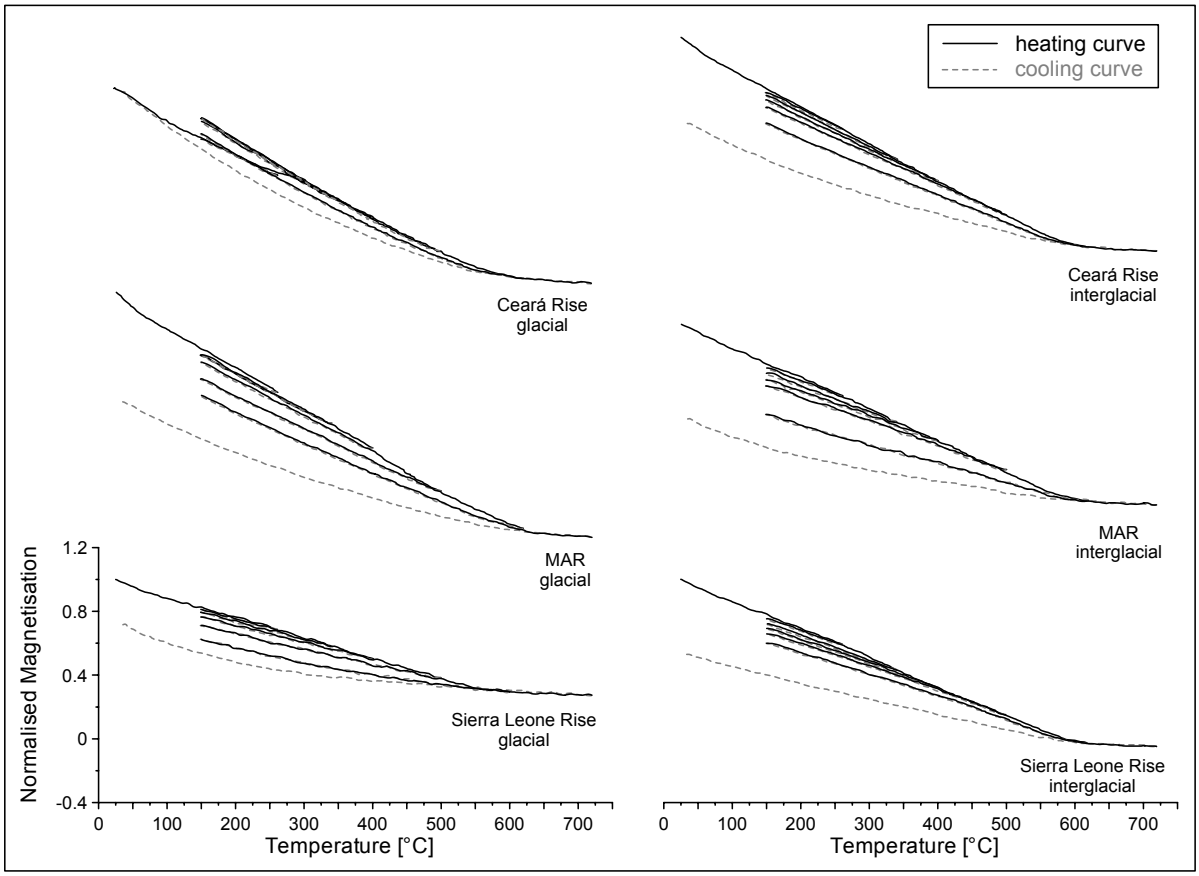

High-temperature thermomagnetic cycles measured on a horizontal translation-type Curie balance (*Mullender et al.* 1993) heating in air and using an oscillating field between 150 and 300 mT. The heating run started at room temperature and was subsequently sub-cycled between 150°C and 260, 340, 400, 500, 600, and 720°C respectively before finally cooling back to room temperature. Heating rates of 5°C per minute (black solid lines) and cooling rates of 10°C per minute (grey dashed lines) were applied. Samples from the Ceará Rise are shown in the upper line, samples from the Mid-Atlantic Ridge are shown in the middle line, samples from the Sierra Leone Rise are shown in the lower line. Glacial samples are shown on the left hand, interglacial samples are show on the right. All curves are normalised on their respective starting value at room temperature.

Appendix References

Bloemendal, J., J. W. King, F. R. Hall, & S.-J. Doh, 1992. Rock magnetism of Late Neogene and Pleistocene deep-sea sediments: Relationship to sediment source, diagenetic processes and sediment lithology, *J. Geophys. Res*., **97**, 4361–4375.

Dunlop, D.J, 2002a. Theory and applications of the Day plot (Mrs/Ms versus Hcr/Hc) 1. Theoretical curves and tests using titanomagnetite data, *J. Geophys. Res*., **107,** B032056, doi: 10.1029/2001JB000486.

Kruiver, P.P., Dekkers, M.J. & Heslop, D., 2001. Quantification of magnetic coercivity components by the analysis of acquisition curves of isothermal remanent magnetisation, *Earth Planet. Sci. Let*., **189**, 269-76.

Mullender , T.A.T., van Velzen, A.J. & Dekkers, M.J., 1993. Continuous drift correction and separate identification of ferrimagnetic and paramagnetic contributions in thermomagnetic runs, *Geophys. J. Int*., **114**, 663-672.

von Dobeneck, T., 1996. A systematic analyses of natural magnetic mineral assemblages based on modeling hysteresis loops with coercivity-related hyperbolic basis functions, *Geophys. J. Int.*, **124**, 675-694.